Advanced Lectures 1988

The climate of the world
Part 2

LONDON, METEOROLOGICAL OFFICE.
Advanced Lectures 1988

The climate of the world. Part II.

00251088 551.583 F62

ORGS UKMO A

National Meteorological Library
FitzRoy Road, Exeter, Devon. EX1 3PB

arters, Bracknell

METEOROLOGICAL OFFICE
152896
23 SEP 1988
LIBRARY

These Lecture Notes have also been produced as Long-Range Forecasting and Climate Research Memoranda Nos 25 to 28.

Advanced Lectures 1988

The climate of the world
Part II

C.K. Folland

D.E. Parker

Permission to quote from this document must be obtained from the Principal, Meteorological Office College, Shinfield Park, Reading RG2 9AU

The climate of the world

Part II

6. **The El Nino Oscillation, the Quasi-biennial oscillation and the 30-60 day variations**
C.K. Folland and D.E. Parker
7. **A review of palaeoclimate from the early Earth to the Pleistocene ice ages**
C.K. Folland and D.E. Parker
8. **Climate from the Late Glacial to the Little Ice Age**
C.K. Folland and D.E. Parker
9. **Climatic change in the instrumental period**
D.E. Parker and C.K. Folland
10. **Carbon dioxide and other greenhouse gases, and climate variations**
D.E. Parker and C.K. Folland

THE EL NINO/SOUTHERN OSCILLATION, THE QUASI-BIENNIAL OSCILLATION, AND THE 30-60 DAY VARIATIONS.

C K FOLLAND AND D E PARKER
MET O 13

SUMMARY

The El Nino-Southern Oscillation phenomenon is a well-known example of ocean-atmosphere interaction, involving not only marked changes of sea-surface temperature and atmospheric circulation and rainfall in the equatorial Pacific, but also related changes in the atmosphere and ocean throughout the remainder of the tropics, and in higher latitudes particularly in the Pacific-North America section. A review is given of observational and numerical modelling studies of El Nino-Southern Oscillation, and the mechanisms involved are discussed. Recent attempts to predict its oceanographic component are included. A briefer consideration is given to the Quasi-biennial Oscillation of winds and temperatures in the equatorial lower stratosphere. Theoretical models, which explain the Quasi-biennial Oscillation in terms of absorption of vertically-propagating waves, are described. Finally, we present an account of the variations on the 30-60 day timescale, which are especially important in the tropics.

6.1 - THE EL NINO - SOUTHERN OSCILLATION (ENSO)

6.1.1 Introduction

The term El Nino (The "Christ Child") was originally given to a weak warm coastal current which commences around Christmas and flows southwards along the coast of Ecuador and Peru during each Southern Hemisphere summer. Every few years the near-coastal warming associated with the current becomes particularly intense (4-7°C); during (usually) the following 12 months the surface of the entire Central and Eastern tropical Pacific Ocean is typically 1-3°C warmer than normal. In December 1982, the sea surface temperature in the open ocean near 5°S, 130°W, was almost 6°C above normal, an amount which can usefully be compared with the annual cycle of sea surface temperature for the world shown in Lecture 5, Fig 5.1.

Fig 6.1A shows the observed sea surface temperature in the Pacific and Fig 6.1B the observed sea surface temperature anomaly (SSTA) there during the Northern Hemisphere winter of 1982-83, near the most intense phase of one of these tropical Pacific warmings (Quiroz (1983)). The term 'El Nino' is now generally used by climatologists to describe the widespread oceanic warming and not the local coastal warming. Fig 2.5, Lecture 2, showed mean January SST for 1951-80; it can be seen that the normal east-west gradient of tropical Pacific SST has nearly disappeared in Fig 6.1A and that the absolute maximum SST in the period Dec 1982 to Feb 1983 was placed about 60°E of its normal position. The 1982-83 El Nino will be discussed below; Quiroz gives a very good observational account.

High surface temperatures are only one aspect of the anomalous behaviour of the tropical Pacific Ocean during an El Nino: the entire thermal and dynamic structure of the upper ocean is different from normal (Gill and Rasmusson (1983)). The presence of such a large anomalous heat source at the lower boundary of the tropical atmosphere can also be expected to affect the atmospheric general circulation and it became clear about 20 years ago that a near global scale mean sea-level pressure (PMSL) sea-saw known for over half a century as the Southern Oscillation (SO) is linked to El Nino.

The possible existence of a large-scale interannual PMSL fluctuation was first hinted at by a Swede, Hildebrandsson in 1897 who found an out of phase relationship between PMSL at Sydney, Australia and Buenos Aires, Argentina. In 1902-6 Lockyer and Lockyer uncovered the worldwide scale of the PMSL fluctuation, but Walker and Bliss (1923-37) provided the first detailed analyses of the companion temperature and rainfall fluctuations and were the first to name the phenomenon the "Southern Oscillation". See Rasmusson and Carpenter (RC) (1982) for historical detail. Fig 6.2A shows the correlation between annual PMSL anomalies at Easter Island and many other stations distributed worldwide, produced by Berlage and de Boer (1959), and confirmed several times since Berlage and de Boer's paper. Djakarta, Java and Easter Island are 140° of longitude (15,000 km) apart and all investigations agree on a negative correlation of -0.9 or so between their annual or even seasonal mean PMSL values. Fig 6.2B shows the average January PMSL in the Pacific (1961-76) and the position of some of the "key" stations that will be used in the description. The SO fluctuations are usually monitored by an SO index (SOI) which has been defined in many ways; Fig 6.2A indicates that the simplest and best index might be simultaneous values of (Easter Island - Djakarta) PMSL.

Returning to relationships between the SO and South American climate, Fig 6.3 shows superimposed time-series of the level of the great Parana river and a multi-station SO index about a century ago. The correlation is 0.56. However due to better data quality and availability Tahiti and Darwin PMSL have often, if less satisfactorily, been used to provide an SO index. Fig 6.4 shows the seasonal normalised pressure difference between Tahiti and Darwin for 1935 to 1987, updated from Parker (1983). Ropelewski and Jones (1987) have extended the Tahiti pressure series back to 1876, thus enabling the construction of Tahiti minus Darwin indices back to 1882 when the Darwin data began, but there are occasional missing years in the earlier Tahiti data which are a little less reliable than those for 1935 onwards. Fig 6.5 shows a time series of seasonal SSTA for 1856-1987 (relative to the 1951-80 average) calculated for the tropical East Pacific (170°W to S American coast, 20°N to 20°S), an area of about 45×10^6 km^2. The correlation between 3 month seasonal mean tropical East Pacific SSTA and SO indices between 1935-80 is about -0.65, i.e. warm SSTA is associated with a negative SO index. The tropical East Pacific SSTA variations are (in the main) part of a worldwide fluctuation of SSTA. This is most readily shown in Fig 6.6 which shows the second (correlation matrix) eigenvector (EOF2) of worldwide SSTA calculated for each season and for the available 10° x 10° areas between 1901-80. The time series of the amplitude of EOF2 is shown in Fig 6.7 together with that of the tropical East Pacific SSTA variations; the two time series of EOF2 are strongly correlated (r=0.75). Use of EOF2 does not, however, allow monitoring of systematic changes in the shape of the worldwide SSTA patterns which might occur as "ENSO events" develop, or monitoring of real differences in patterns between events. Despite these limitations, however, a strong, consistent, warming of the Indian Ocean and the northeast Pacific and a similar tendency for simultaneous negative SSTA in the northwest Pacific when the tropical central and eastern Pacific are warm is apparent. Values of the terms of EOF2 of magnitude about 0.6 or over in Fig 6.6 reflect a reasonably consistent relationship with tropical East Pacific SSTA. Fig 6.8 shows spectra of the time-scales of variation of seasonal tropical East and West Pacific SSTA and marine air temperature for 1861-1980 from Folland et al (1985). The East Pacific (basically El Nino) variations occupy the 2.5-16 year time scales. The West Pacific spectrum is distinctly different, being much "whiter".

6.1.2 Global temperature variations associated with El Nino

6.1.2.1 SSTA

Fig. 6.9 shows the evolution of Pacific SSTA during El Nino, as presented by van Loon and Shea (1987), based on eight warm events between 1950 and 1979. The early stages in the development of an El Nino during which the warming is confined to S American coastal waters, are not well represented because the resolution used was too coarse. By April of year (0), the S Pacific near the western coast of South America as far south as 35°S shows a distinct warming. A tongue of positive SSTA extends westwards from the South American coast along the Equator, reaching 130°W in May and 170°W by July (see also Newman (1984). The SSTA pattern intensifies, so by

September a large proportion of the Tropical Pacific is warmer than normal and by up to 2°C in the east. In December the warming is at its peak with maximum mean SSTA of 2°C to 3°C. In year (+1) SSTA decline. Both Indian and tropical Atlantic Oceans warm during El Nino, starting in late summer of year (0) (Pan and Oort (1983)). By March of year (+1) much of the Atlantic from 30°N to 30°S is warmer than normal by between 0.2° and 0.5°C (Newman (1984)). The Indian Ocean exhibits maximum mean SSTA of up to 0.6°C at the end of year (0) and the beginning of year (+1) (Cadet (1985)).

By contrast, in April of year (0) an area in the central N Pacific, centred near 30°N, is weakly cool; then the negative SSTA spread northwards and strengthen, giving mean anomalies of -0.8°C in some areas near 40°N between July and October (Fig. 6.9). From November of year (0) to March of year (+1) negative SSTA persist, but are generally weaker. In the northeast extratropical Pacific an area of anomalous warmth spreads northwards near the North American coast in October. This warm area persists until after March of year (+1) (Newman (1984)). From October to December of year (0), the north east Atlantic, polewards of 35°N, is weakly cool with a suggestion of cool SSTA south of 40°S, common to much of the Southern Ocean (Pan and Oort (1983); Newman (1984)). The data are too sparse to be certain, however.

RC used SSTA measured between 1953 and 1974 along 6 ship routes in the area 20°N to 20°S, 70°W to the dateline, to investigate the growth and movement of tropical Pacific SSTA during El Nino. The most common time scales of SSTA fluctuations associated with El Nino (in the area and for the period defined above) were found to be between 36 and 43 months. Cross spectral analysis of SST data at different longitudes indicated that the large scale positive SSTA which initially appear off the coast of Peru about December (eg at Puerto Chicama, see "PC" on Fig 6.2B), spread westward along the Equator, reaching 170°W in 3-6 months. They also noted that equatorial SSTA near the dateline appeared to increase modestly almost simultaneously with the coastal SSTA (cf Fig 6.9(b)). The average westward propagation of SSTA has a speed of 0.5-1.0 m s^{-1}. RC also noted a warming of the ocean west of Chile in subtropical latitudes in the year (-1) preceding El Nino.

El Ninos vary considerably in character and in the time intervals between them (eg 3 years between 1969 and 1972, but nine years from 1942-51). This variability may prove crucial to our understanding. For example: the Tropical Pacific west of the dateline was markedly warmer in 1976 than in 1972; in the 1982 event the Tropical E Pacific warmed before the S American coast, which warmed most at the end of the ENSO event, in April-June 1983.The Tropical E Pacific remained warm well into autumn 1983, ie year (+1), and widespread warming of the Indian Ocean exceeded 1.5°C. In 1976, the warming of the Indian Ocean area was weak. The period from 1972 to 1982, during which there were 4 El Ninos (3 of them strong), contrasts with the periods 1942-50 and 1879-1887 when there were none while between 1907 and 1938 El Ninos were few or rather weak (Fig 6.5). Deser and Wallace (1987) document differences in timing and duration of coastal and near-coastal S American SSTA between El Nino events. They note that these SSTA are not very tightly coupled with the SO.

6.1.2.2 Atmospheric Temperature Variations

Pan and Oort (1983) have given a latitude-height cross section of zonal mean temperature differences between three pairs of years having warm and cool East Pacific SST respectively (Fig 6.10) for northern winter. The troposphere as far poleward as 45°N and S warmed by up to 1°C at 400 mb, presumably because of increased moist convection in the tropics. Note also the cooling at middle and high latitudes of about -0.5°C in the Northern Hemisphere, which matches the underlying SST changes fairly well. Yasunari (1987a) obtained similar results.

Pan and Oort also showed that specific humidity rose where air temperature rose and also fell slightly in high latitudes. It is interesting that a tropical forcing (warming) from below has warmed the global troposphere as a whole but that the atmospheric circulation has changed so as to provide a weak cooling in high latitudes. This is rather unexpected, perhaps.

Bradley et al (1987) confirmed the warming associated with ENSO using land surface air temperature data for 0°-30°N.

6.1.3 Variations of Atmospheric Circulation

6.1.3.1 General Description

There is now a considerable literature on aspects of the general circulation associated with ENSO or suspected to have a connection with it. The background climatology is described by Horel (1982). RC and Wyrtki (1975) have both shown that ENSO is associated with variations in the Pacific trade wind circulations and the latter author, sea level fluctuations in the Pacific. The tropical easterly jet is weakened and the associated patterns of divergence are weakened and shifted eastward (Chen and van Loon (1987)). Chen (1982) and Horel and Wallace (1981) have indicated links with the Northern Hemisphere mid-latitude circulations; van Loon and Labitzke (1987) describe associations with the stratospheric circulation and Angell (1981) reports associations with ozone over North America and the water vapour content of the low stratosphere; Bacastow and Keeling (1981) note a link with tropospheric CO_2 content. ENSO has been proposed as a long range forecasting tool for the Indian monsoon by Shukla and Paolino (1983) and has been used to help make long range forecasts in the USA and New Zealand. However both the Indian monsoon (Wu and Hastenrath (1986); Elliott and Angell (1987)) and atmospheric pressure around New Zealand (Trenberth and Shea (1987)) have more recently been shown to anticipate Southern Oscillation indices. Tropical Pacific SST variations (now defined separately in the Central and East Pacific) have recently been introduced, usefully, as a factor in a statistical long range forecasting technique used in the Synoptic Climatology Branch of the Meteorological Office (Maryon and Storey, 1985). The contrast between El Nino and "La Nina" (cold east tropical Pacific) is discussed by Philander (1985).

6.1.3.2 Tropical Atmospheric Variations

The tropical atmosphere is perturbed during ENSO in a complex way as indicated by RC and other authors. In the winter and summer (S Hemisphere) preceeding El Nino, the south east trade winds between 120°W and the dateline are usually abnormally strong giving wind stresses over the tropical S Pacific 50-80% above normal. Relaxation of this stress to below normal levels in the tropical W Pacific in the next summer is followed by the start of El Nino - sometimes the wind stress is reversed, i.e. the winds become westerly. The reason for the weakening is not known, though wind stress is usually less in summer in this region. The triggering mechanism probably comes most often from the Southern Hemisphere but may sometimes arise from the Northern Hemisphere or from within the tropics in association with 40-50 day oscillations (Trenberth and Shea (1987); Lau and Chan (1986)). During year (0) of El Nino, the easterly component of wind stress reaches a minimum but increases once more later in year (0). By contrast, near the equator, between 90°W and about 130°W, the E to SE trades increase in strength to reach a peak during year (0).

The spatial distribution of surface wind anomalies reflects changes in the positions of the Inter-Tropical Convergence Zone (ITCZ) and the South Pacific Convergence Zone (SPCZ) (see Lecture 2). The convergence zones are important in determining the areas of active convection and hence areas of latent heating in the middle and upper troposphere and the rain falling on the "desert" islands of the equatorial Pacific (Lecture 2). Changes in the trade wind circulation also reflect changes in the intensity of the Indonesian Low and Easter Island High, which, as described above, are often used to indicate the phase of the SO.

Figs 6.11(A)-(C) show the anomalous mean tropical Pacific surface winds in an El Nino composite study carried out by RC, shown here for August-October (-1), March-May (0) and December (0) to February (+1). In northern autumn of year (-1) surface wind anomalies are generally small except to the north-east of Australia where anomalous northwesterlies tend to occur and the SPCZ is displaced to the southwest of its normal position. This displacement probably results from positive SSTA following anomalous northerlies in the subtropical southwest Pacific during the previous 6 months (van Loon and Shea (1985)). The South Pacific High then weakens but the Indonesian Low changes little (van Loon and Shea (1987)). Wind anomalies increase from November (-1) to March (0) with a strong anomalous westerly component (not always giving absolute westerlies) developing south of the Equator and north of 10°S from 170°E to 170°W, reflecting a reduction in strength of the south-east trades. The Indonesian Low fills while the Easter Island High continues to decline. From March to May (0) the same trends in the pressure field continue. Between 110°W and 170°E, the ITCZ is now displaced south of its normal position with anomalous northerlies on its northern side. The anomalous westerly component just south of the Equator now reaches 160°W and there is a strengthening of the south-south east trades in the latitude band 30°S to 10°S from east of Australia to the dateline.

During the remainder of year (0) the anomalous features noted above intensify. In particular the ITCZ continues to be placed south of its climatological position and the SPCZ now becomes located markedly north east of its usual location, reducing the size of the equatorial dry zone (centred near the dateline) between them. During August-October of year (0) the equatorial westerly anomalies are at their strongest exceeding 2 ms^{-1} over much of the Tropical Pacific west of 160°W and an anomalous surface wind convergence is centred near 150°W close to the equator. The Pacific High begins to build again about July followed by a deepening of the Indonesian Low about November. As the El Nino year progresses, the surface wind convergence maximum moves eastwards to near 130°W, the westerly anomaly decreases and the south east trades strengthen between 140-180°W, ie west of the wind convergence.

Pan and Oort (1983) correlated SST in a key area near 2.5°S, 130°W (assumed to represent the entire Tropical E Pacific, a reasonable assumption in view of SSTA analyses presented in Section 6.1.2.1) with global fields of 850 mb and 200 mb wind components and 500 mb vertical velocity.

They found that warm SST (El Nino) is associated with:-

a. Anomalous ascent of air over the Central and much of the Eastern Equatorial Pacific, with anomalous descent of air east of 120°W, over the western Pacific between 110°E and 150°E, and over the subtropics.

b. An increase in the 200 mb subtropical westerlies in both hemispheres near 25° latitude, with anomalous 200 mb easterlies over the Equatorial Pacific, roughly west of the main SSTA maximum.

c. A weakening of surface and 200 mb westerlies near 60°N.

Pan and Oort note that these observations are consistent with Bjerknes' pioneering (1969) explanation of ENSO. Bjerknes (1969) suggested that the normal nearly east-west equatorial Pacific Walker cell, in which air ascends in the convectively active area around Indonesia and descends over the Eastern Pacific near 90°W, is weakened during El Nino. Fig 6.12A shows this cell in more detail (from Kousky et al (1984)). See Lecture 2 for "Walker" cells.

The warm tropical ocean causes the Hadley cell to intensify, leading to stronger 200 mb subtropical jets (Figure 6.12B). In Section 6.1.2.1 it was noted that all three tropical oceans warm during El Ninos, which is consistent with the intensification of subtropical jets at all longitudes. A decrease in the westerlies at 60°N is seen by Pan and Oort as evidence for a stronger than normal Northern Hemisphere Ferrel cell.

Selkirk (1984) has provided an analysis of the 200 mb flow associated with ENSO. He usefully discusses the fluctuations in the light of predictions made by linear models, eg that of Simmons (1982) which shows how the 200 mb and lower tropospheric winds might respond to an anomalous (here a Central or Eastern Pacific) heat source. Chen and van Loon (1987) have contrasted the behaviour of the tropical easterly jet in El Nino and non El-Nino years (see 6.1.3.1 above).

It is essential to note that the above-mentioned composites of El Nino — Southern Oscillation are not completely representative of any individual El Nino — Southern Oscillation event, because each event differs. Some variations in the SSTA signature of El Ninos were described in section 6.1.2.1. Here we document some variations in the atmospheric signature. Figure 6.13, from Trenberth and Shea (1987) shows sequences of Darwin MSL pressure for events since 1939. There are variations in amplitude, in sequence, and in timing, the latter demonstrating the imperfect anchoring of the phase of the SO to the annual cycle. The 1986 event began particularly late, and continued through 1987 with unusual phasing of anomalies relative to the annual cycle. Figure 6.14, from the same paper, shows that both the phase difference and the covariance of MSL pressure between Darwin and several other stations has varied interdecadally. Between 1920 and the late 1930s the SO was relatively inactive, in agreement with Fig. 6.5. Figure 6.15, from Harrison (1987), contrasts the anomalies of surface winds over the Gilbert and Ellice Islands in the central equatorial Pacific during the El Ninos of 1969 and 1972. Harrison also created a composite using winds from these stations: his results were different from RC's in several respects, such as the absence of the persistent off-equatorial meriodional wind anomalies suggested by RC. The zonal components of Harrison's composite wind anomalies were also stronger than RC's and more closely confined to the equator. One reason for the differences was probably that RC used ship data which, in the area around these islands, were rather sparse (Fig. 6.11), giving less reliable results.

6.1.3.3 Extra Tropical Relationships with El Nino- Southern Oscillation Events

Many authors have found that the El Nino — Southern Oscillation is associated with changes in extratropical circulations, though teleconnections are less well defined than in the tropics.

Chen (1982) correlated seasonal values of the Tahiti-Darwin Southern Oscillation Index (SOI) with Northern Hemisphere 700 mb geopotential height between 1951 and 1979. He also carried out a composite analysis of the 700 mb data stratified according to the SOI. The composites are shown in Figure 6.16. The winter pattern is quite similar to the 'Pacific North America (PNA)' teleconnection pattern found by Horel and Wallace (1981) (Fig 6.12B) with three centres of response situated at 40°N, 145°W, (high positive correlation), Canada near 125°W (large negative correlation) and near Florida extending towards Spain (high positive correlation). These results were confirmed by Rogers (1984) using MSL pressure and 500 mb geopotential height.Correlations between the 700 mb height field and the SOI of later seasons drop sharply as the lag of SOI behind the 700 mb fields increases. By contrast, correlations reach a maximum when the SOI leads the 700 mb fields by one or two seasons, the response pattern staying broadly similar. However, only in winter with the SOI leading the 700 mb data by one or two seasons is statistical significance at the 95% level unequivocably obtained.

Chen's composite analyses enable non-linearity in the Northern Hemisphere 700 mb atmospheric response to variations in the SOI to be studied. Chen finds that 700 mb height anomalies over the Atlantic are more pronounced with high SOI (low E Pacific SST) (Fig 6.16(A), (B)). However, associations between the Southern Oscillation and the North Atlantic Oscillation are weak (Rogers (1984)).

The Northern Hemisphere extratropical response to ENSO varies between events, as might be expected from a consideration of the variability between events in the tropics described above. Hamilton (1988) found that the PNA pattern in winter was pronounced in EL Nino years when the west tropical Pacific sea surface was anomalously warm, but not when it was anomalously cold. These results confirm the findings of Palmer and Mansfield (1986b) in atmospheric general circulation model studies discussed in Section 6.1.4 below.

In the Southern Hemisphere, the land-sea contrast in summer in 500 mb geopotential height and MSL pressure appears to be modulated by the Southern Oscillation (Mo and White (1985)).

The Southern Oscillation was shown by Barnett (1985) to be part of a global-scale propagating feature in the MSL pressure field. In the light of integrations of an atmospheric general circulation model, it was suggested that the SO resulted from the excitation of a natural dynamical mode of variation within the atmosphere, but that local diabatic forcing by precipitation and remote forcing by Eurasian snow cover, as well as forcing by SST anomalies, were also crucial to the dynamics of the SO. Harrison (1987) found eastward propagation of zonal wind anomalies over the central equatorial Pacific, and so did Cadet (1985) and Yasunari (1987b) over the Indian Ocean but Blazejewski et al (1986) failed to find the eastward propagation of zonal wind anomalies over the Indian Ocean that would have been expected from Barnett's analysis. Trenberth and Shea (1987) suggested that the inferred eastward progression depended on the cyclicity implied by Barnett's analysis in the frequency domain. Fig 6.17, taken from van Loon and Shea (1987), indicates that the major MSL pressure anomalies "arise and move within the core area of the SO on the Southern Hemisphere". Yasunari (1987b), however, considered on the basis of composite fields and lag-correlations that a Eurasian—midlatitude North Pacific interaction may be crucial to ENSO.

6.1.3.4 Rainfall Variations

Equatorial rainfall anomalies are an important aspect of El Nino -Southern Oscillation events because of their obvious implications for Pacific 'weather' and because they indicate the position and anomalous intensity of convective activity associated with ENSO. Figure 6.18 shows an annual rainfall series for the central equatorial Pacific; there are very large increases during ENSO events. These local changes may be put in a global context using satellite data as reported by Newman (1984). Figure 6.19 shows the percentage cover of cloud tops with radiative temperatures less than 235K on a 5° x 5° space scale for northern winter and spring seasons between 1980 and 1983. This index is thought to give a good measure of convective activity. The data are not completely homogeneous in time but are probably spatially reasonably homogeneous. The relative minima in convection over the East Pacific in 1980-82 are the result of the descending branch of the Walker cell. However by March-May 1983, highly anomalous heavy rainfall was reported from the semi-desert Galapagos Islands which turned green as a result; high SSTA persisted and even strengthened again in this region after the earlier peak around December/January 1982-3. NASA (1986) have published an atlas of monthly and seasonal fields of outgoing longwave radiation based on NIMBUS-7 satellite data: the results are in agreement with Fig 6.19.

Ropelewski and Halpert (1987) have analysed the relationships between ENSO and global and regional-scale precipitation patterns, using data from 1875 to 1983. Fig 6.20 illustrates their results for the globe. Relationships are strongest in the Australia-Central Pacific region but are also strong in parts of Southern Africa and South America, and are significant in India. Their paper contains a set of detailed maps like Fig 6.20 for individual regions. Hastenrath et al (1987) obtained slightly grater correlations than implied by Ropelewski and Halpert between the SO and rainfall in the Sahel and some other regions in the Atlantic sector: this may be because Hastenrath et al used regional indices rather than values from individual stations. They also used a shorter period of data (1935-1983). Ropelewski and Halpert note that in some regions, such as the western USA, very different rainfall anomalies accompany different ENSO events. Kiladis and Van Loon (1988) have also presented fields of rainfall anomalies over the Indian and Pacific sectors at different stages of warm events (El Nino) and cold events (anti - El Nino or La Nina): their results are in accord with those of Ropelewski and Halpert (1987) but are accompanied by corresponding fields of MSL presure and temperature anomalies (consistent with the above accounts) which aid interpretation.

6.1.4 AGCM Experiments

Is it physically reasonable that the global atmosphere could respond to El Nino? If so, how? Several experiments using AGCM's have been carried out using El Nino SST forcing; their results broadly support the idea of a widespread tropical response like that observed but give much more variable results in the extratropics. Most of the experiments have concentrated on Northern Hemisphere teleconnections. The first Northern Hemisphere winter AGCM experiment, carried out by Rowntree (1972), indicated, like most subsequent experiments, that a pair of low level low pressure anomalies are forced on either side of the equator near the maximum tropical SSTA (probably nearer the local maximum absolute SST) with upper level anticyclonic anomalies overlying the low pressure centres. Further north a nearly equivalent barotropic response occurs with a low anomaly forced at all levels at about 35-50°N. The general result is to strengthen the Aleutian low. Palmer and Mansfield (1986a, b) carried out extensive experiments on El Nino using the Meteorological Office 11-level AGCM for perpetual winter time conditions. Two of their experiments are discussed below.

6.1.4.1 Experiment 1 "Composite" El Nino SSTA

Palmer and Mansfield (1986a) used a composite of the observed tropical central and eastern Pacific SSTA for northern winter associated with several El Ninos, but doubled in magnitude (Fig 6.21A), with climatological SST elsewhere. They carried out an anomaly experiment with this SSTA and a control experiment without it. Each experiment was continued for 540 model days using "perpetual" January radiation. Anomaly and control experiments both started from real atmospheric data for 28 December 1972, and the model incorporated "envelope" orography whereby mountains are enhanced in height to improve the model's winter climatology.

Fig 6.21B shows the average difference in 200 mb height (anomaly minus control) for these experiments. The "PNA" pattern of Horel and Wallace is evident and was found to be present at all levels. Tropical lows were overlain by tropical highs as expected. See Lecture 5 for a description of the effects of this upper level anticyclonic "vorticity" forcing. Tests showed that the extratropical Rossby wave-like response was highly statistically significant.

6.1.4.2 Experiment 2 - December 1982 SSTA

The maximum of this real SSTA was to the east of the maximum of the composite SSTA (Fig 6.21C). Palmer and Mansfield (1986b) used two versions of the 11-level AGCM integrated for perpetual winter conditions as before:

(a) Anomaly and control integrations using "envelope" orography, starting from 28 December 1972 atmospheric data;

(b) Anomaly and control integrations for a model with "standard" orography, with the same starting date.

"Envelope" orography has higher mountains than "standard" orography. Both pairs of experiments were integrated for 540 model days.

Figs 6.21D,E show the difference between the anomaly and control experiments for (a) and (b). Neither figure shows a recognisable PNA pattern, and such a pattern was not in fact observed in 1982-83. Both models show a Rossby wave like anomaly response and in both pairs of experiments the response is highly statistically significant - but nevertheless different. In the "standard" orography experiment the anomaly wavelength is longer and the pattern is distorted compared with the "envelope" orography experiment. This is not surprising as the climatological mean flow of the "standard" orography model is much more westerly than that of the "envelope" model in winter, the "envelope" model being thought more realistic.

In a further experiment with weak positive SSTA ($\simeq 1^{o}C$) in the tropical West Pacific (and envelope orography), Palmer and Mansfield (1986b) obtained a strong PNA pattern, shifted slightly westward relative to that in Fig 6.21B.

We conclude from these experiments that:

(a) The wintertime extratropical response to El Nino may be quite strong but may vary from event to event eg with the longitude or shape of the SSTA or position of the resulting absolute maximum tropical Pacific SST. Palmer and Mansfield found that the responses to different events in their models were too different to be ascribed to the natural atmospheric variability of the models.

(b) The response of an AGCM will depend on its climatology. A realistic local response, as required for long-range forecasting, may demand a realistic representation of the structure of the mean flow.

6.1.5 Oceanographic aspects

Gill and Rasmusson (1983) discussed the oceanographic aspects of the 1982-83 El Nino using a model to simulate the response of the mixed layer of the tropical Pacific Ocean to the observed weakening of the trade winds during 1982-3. They assumed a realistic pre-existing gradient of sea surface topography with higher sea-level in the western Pacific than in the eastern Pacific. The east-west difference is typically observed to be about 1 m before El Nino and results from the wind stress imparted by the preceding strong SE trade winds. Fig 6.22A shows the longitude-time plot of the eastward wind stress anomaly used as forcing in the model experiment, Fig 6.22B shows the computed change of surface elevation of the sea from the pre-existing condition where the height was greater in the west, and Fig 6.22C shows the resulting eastward ocean currents. These tended to oscillate in direction on a time scale of about 9 months in their model as a result of the prediction of an eastward moving oceanic equatorial 'Kelvin' wave which was partially reflected from the S American coast in the form of an equatorially trapped Rossby wave. Such Kelvin waves have been observed by satellite-based altimeters (Miller et al (1988)). The model of Gill and Rasmusson produced a good simulation of the observed change of sea-level topography and ocean currents during the 1982-3 ENSO. Their model results were also consistent with the observation in 1982-83 of eastward propagation of the main warming of SST towards the central Pacific with even later warming near S America (Fig 6.23D). However, this behaviour, though correct for 1982-3, is not always typical (section 6.1.2.1). Graham and White (1988) have collated evidence that ENSO is a natural oscillator involving not only an oceanic equatorial Kelvin wave but also a simultaneous oceanic off-equatorial Rossby wave which is reflected from the western boundary into the equatorial zone as a Kelvin wave of opposite phase from the one further east.

Cane et al (1986) have used a simplified model of the coupled ocean-atmosphere system to make successful hindcasts of El Nino (Fig 6.23). Their model included thermocline depth or heat content of the upper ocean, currents, SST, and surface winds, over the tropical Pacific. The success of hindcasts made starting up to 2 years before El Nino events was taken as evidence that the sub-surface ocean has an active role in the generation of El Nino.

Sperber et al (1987) have succeeded in simulating the SO in a global model of the coupled atmosphere and upper ocean.

Taken as a whole, the model simulations of ENSO clearly show the need for fully detailed coupled ocean-atmosphere models. Development of these is proceeding apace.

6.1.6 Conclusion

The ENSO event represents the most important non-seasonal, if irregularly recurring, event in the climate system on time scales between the annual cycle and the ice ages that has yet been properly identified. The factors that initiate the El Nino/ENSO sequence remain elusive. Some of the physical processes that occur in the ocean and the atmosphere during ENSO have nevertheless been isolated.

6.2 THE QUASI-BIENNIAL OSCILLATION

6.2.1 Introduction

A brief description is given of this curious lower-stratospheric phenomenon which was discovered almost simultaneously by Ebdon (1960) and Reed (1960). The QBO is the only known example in the climate system of a quasi-periodic process of reasonably regular behaviour whose time scale lies between the annual and ice-age time scales. The next most regular process is the ENSO phenomenon discussed in Part I. Although the links between the QBO and surface climate are tenuous, we justify its inclusion here:-

(a) To provide a background to the discussion of volcanic dust and climate in Lecture 3. The QBO affects our ability to detect and interpret the effects of volcanic dust on stratospheric temperature and thus to unravel the physical properties of volcanic dust.

(b) Because of the possibility of links with climatic phenomena such as ENSO and fluctuations of the Indian northern summer monsoon (Quiroz (1983); Bhalme et al (1987)).

6.2.2 Description

The QBO shows up most prominently as a quasi-biennial oscillation of zonal wind and temperature in the tropical lower stratosphere within 15° of the equator. Fig 6.24A shows the monthly mean 30 mb zonal winds above Canton Island (Central Pacific) for 1954-1967, Gan (Central Indian Ocean) for 1967-75, and Singapore for 1976-87. Corresponding 50 mb winds from 1953 are shown in Fig 6.24B. The associated temperature changes over Singapore between 50 mb, and 150 mb where they disappear, for part of the period are shown in Fig 6.25. Temperatures are higher by several °C in the westerly phase. It is possible to form composite time series such as Fig 6.24 from such widely-separated tropical stations because the QBO occurs on a global scale in the tropics with very little phase-lag between different longitudes at a given elevation. The period of the QBO is not constant: it varies from less than 2 years to about 3 years, and averages 2 years and 3 months. The period does not appear to be related to ENSO or (on the basis of Agung and El Chichon) to volcanic eruptions (Angell (1986); Naujokat (1986)). Periods close to either 2 or 3 years tend to be favoured, and there are also favoured seasons for reversal of the 50 mb or 30 mb wind directions (Dunkerton and Delisi (1985)). A downwards phase propagation of the oscillation occurs; for example, changes in the 50 mb wind vector lag several months behind similar changes in the 30 mb wind vector (Fig 6.26). The maximum amplitude is near 20 mb (Naujokat (1986)). Easterlies are generally stronger than westerlies (Fig 6.24), and are of longer duration than westerlies at 10-30 mb but of shorter duration than westerlies at 40-70 mb (Naujokat (1986)), ie the westerly zones propagate downwards faster.

The discovery of the tropical stratospheric QBO has been followed by widespread reports of quasi-biennial behaviour in local tropospheric climate and circulation parameters. Parthasarathy and Mooley (1978) found a quasi-biennial oscillation in Indian northern summer monsoon rainfall, but this was not strong and regular enough to be used for forecasting. Ebdon (1975) documented anomalies in the Northern hemisphere mid-latitude mean sea level pressure and 500 mb geopotential patterns, and in zonal winds aloft, that varied according to the phase of the tropical 30 mb QBO. Figure 6.27 illustrates the mean sea level pressure anomaly in the extratropical Northern Hemisphere for Julys with a westerly tropical QBO wind mode at 30 mb. The anticyclonic anomaly near the British Isles was found to be statistically significant at about the 5% level. In addition, not only Ebdon (1975) but also Angell and Korshover (1977) observed that the circumpolar upper-tropospheric vortex was smaller during the westerly phase of the tropical 50 mb QBO, particularly in winter, with an associated increase of tropospheric temperature of several tenths °C in mid-latitudes. Consequent possible associations with, for example, summer temperature and sunshine in the United Kingdom, were noted by Ebdon and also by Folland (1977). Holton and Tan (1980) (Fig 6.28) have demonstrated that there may be a 50 mb and a 1000 mb quasi-biennial oscillation in the winter geopotential and temperature of the northern polar regions. The two atmospheric levels oscillate in phase but the amplitude is weaker at 1000 mb. The oscillation appears to be in antiphase with the tropical 50 mb QBO. Van Loon and Labitzke (1987) confirmed Holton and Tan's results at 50 mb by comparing winters at opposite phases of the tropical QBO but excluding El Nino or anti-El Nino years because, as they demonstrated, the ENSO also affects the stratospheric circulation. It must, however, be emphasised that observations of QBO outside the tropical stratosphere have been associated only statistically with the tropical stratospheric QBO at this stage. Physical associations have not been established.

6.2.3 Theories

The physical causes of the tropical stratospheric QBO were investigated in a theoretical paper by Holton and Lindzen (1972). The essence of their hypothesis was that transfer of momentum from upward-propagating equatorial Kelvin and Rossby-gravity waves in zones of vertical shear of zonal wind could explain the observed downward-propagating shear zones (Fig 6.29). The waves originated in the troposphere and lost their momentum in the stratosphere because they were absorbed by radiative damping. Westerly momentum was imparted by the decaying Kelvin waves to the stratosphere in the shear zone beneath the downward propagating westerly phase of the QBO, and the Rossby-gravity waves performed a similar function in regard to the easterly phase. Their hypothesis has subsequently been modified by a variety of workers. The processes by which the waves are absorbed may be mechanical (ie turbulent) as well as radiative (Plumb (1984)). Dunkerton (1985) as well as Plumb (1984) and Hamilton (1984) discuss the influence of the circulation in the vertical-meridional plane; and the effects of absorption of solar radiation by ozone may also be important (Dunkerton (1985), as the concentration of ozone is modulated by the QBO. The vertical meridional circulation appears to be responsible for the fact that the downward propagation of westerly zones is faster than that of easterly zones. The one-dimensional model of Tanaka and Yoshizawa (1987) fails to reproduce this feature, whereas the two-dimensional model of Takahashi (1987) succeeds in obtaining this and other observed details of the morphology of the QBO, such as the appearance, at a given level, of westerlies, but not easterlies, on the equator before they appear at other latitudes (Fig. 6.30). The QBO has not yet been reproduced in atmospheric general circulation models because their vertical resolution is too coarse and their damping coefficients are probably too great (Plumb (1984)).

The mechanisms by which the tropical lower stratospheric quasi-biennial oscillation might affect the rest of the atmosphere are completely uncertain. It is just possible that the associated temperature changes near the tropical tropopause (Fig 6.25) may affect the strength of tropical convection where it is most powerful, eg over the tropical West Pacific, and thereby influence the Hadley or Walker cells and subsequently the rest of the circulation. It is known that tropospheric air almost certainly regularly enters the stratosphere in this region (Newell and Gould-Stewart (1981)). Recent work also indicates that the Indian northern summer monsoon rainfall is modulated by the QBO (Bhalme et al (1987)).

6.2.4 Angular momentum considerations

In the Northern Hemisphere summer the difference in the contribution to the axial angular momentum of the Northern Hemisphere atmosphere by a maximum westerly phase of QBO compared with a maximum easterly phase may sometimes be 5%-10% of the total Northern Hemisphere axial angular momentum, allowing for the phase lags of the QBO with height. The development of a westerly phase of the QBO represents an increase in the axial momentum of the atmosphere where it is already by definition a maximum. At all phases, small compensating changes in atmospheric circulation that preserve axial angular momentum should occur somewhere else (in either hemisphere). Note that this momentum cannot be transmitted to the earth's rotation in a direct way as the stratospheric oscillation occurs well above the level of any mountains, though the transfer could occur indirectly through a tropospheric circulation change.

6.3 THE 30- TO 60-DAY VARIATIONS

6.3.1 Discovery

Madden and Julian (1971) appear to have been the first to detect an oscillation of 40- to 50-day time-scale in tropospheric zonal wind and temperature and surface pressure in the tropical Pacific. They found that the upper- and lower-tropospheric zonal winds were in antiphase and that surface pressure was in phase with lower-tropospheric westerlies and in antiphase with temperatures throughout the troposphere. Madden and Julian speculated that the oscillation was a large circulation cell oriented in zonal planes and centred in the mid-Pacific. They could not detect the oscillation further afield at Singapore or in the Panama Canal Zone. Further analysis (Madden and Julian (1972)) suggested that the oscillation resulted from eastward-moving wavenumber 1 or 2 circulation cells oriented in the equatorial plane, originating in the Indian Ocean and propagating to the eastern Pacific.

In the following account, the broad-band nature of the variations is shown by the range of time scales quoted, e.g. 30 to 50 days, 30 to 60 days etc. The variations have sometimes been called the "seven-week fluctuations".

6.3.2 Detailed description

Using 200 mb, 850 mb and surface pressure data for December 1978 to November 1979 obtained during the First GARP Experiment, (FGGE) (which included the Monsoon Experiment (MONEX) in the Indian Ocean-South Asia region), Krishnamurti et al (1985) identified a planetary-scale divergence and pressure wave of 30- to 50-day time-scale traversing the globe eastward at about 8° longitude per day (Fig 6.31). The divergent circulations were thermally direct over the Asian monsoon region and the western tropical Pacific, but were thermally indirect and became weaker over the eastern tropical Pacific and the tropical Atlantic. There was northward propagation in the Indian monsoon region in northern summer (Fig 6.32), modulating the intensity of the monsson and triggering its onset and withdrawal via interactions with a 10- to 20-day westward-propagating pressure perturbation.

Graves and Stanford (1987) found 40- to 50-day atmospheric oscillations over the southern Pacific. These differed from those found by Madden and Julian in that the zonal wind fluctuations were in phase throughout the troposphere. The temperature fluctuations at 100 mb, partly monitored with a satellite-based microwave sounding unit, were found to be out of phase with those at 250 mb to 500 mb. The oscillations were enhanced during the 1982-3 El Nino.

Research into these intraseasonal variations was intensified when fields of outgoing longwave radiation (OLR) data became available from satellites. These data indicate the location of deep convection: when the clouds are thick and their tops high and cold, outgoing longwave radiation is reduced. Lau and Chan (1985, 1986) have performed extensive analyses for northern winter and northern summer respectively. In northern winter, the dominant pattern of tropical convection was found to be an east-west oriented dipole propagating eastward along the equator from the Indian Ocean but stalling and intensifying on reaching the maritime continent and the equatorial central Pacific. There was also southeastward propagation into the monsoonal region of Australasia, and evidence of interactions with the atmosphere over Asia and the subtropical North Pacific. It was suggested that 40- to 50-day wave activity may have triggered the 1982-3 El Nino — Southern Oscillation event. In northern summer, there was still eastward propagation along the equator from the Indian Ocean to the western Pacific, but there was also northward propagation from the Indian Ocean towards the Indian subcontinent (in agreement with Krishnamurti et al (1985)) and northwestward propagation from the western Pacific towards southern China (Fig 6.33). Again the oscillation was found to modulate the Indian monsoon and to be phase-locked to the monsoon onset over India and to the Mei-yu (plum) rains over southern China. It was suggested that the northward propagation arises through interaction between the eastward-propagating equatorial modes and the monsoon cirulations.

Murakami et al (1986) obtained results consistent with those of Lau and Chan but observed that occasionally the 30- to 60-day perturbations exhibited irregular propagation. On such occasions, the teleconnection patterns were weak. A subsequent study (Shrestha and Murakami (1988)), confined to occasions with systematic eastward propagation, found that, in northern summer, surges of southerlies at 850 mb near northern Madagascar on the 30- to 60-day time-scale were followed by intensification of the monsoonal westerlies near south India and eventually by enhancement of convective activity over the Asian monsoon region. Similar surges off western Australia tended to activate convection over the western equatorial Pacific. Transient (< 30 days) disturbances over India and over the subtropical southern Indian Ocean were found to be amplitude-modulated on a 30- to 60-day time-scale, but this was not the case near the equator. Thus transient disturbances over the subtropics could also be an energy source for the 30- to 60-day fluctuations there. Sumathipala and Murakami (1988) found analogous characteristics over the Australia - Indonesia - western Pacific sector in northern winter: in this case surges in the low-level northeasterlies from the Pacific, rather than in the low-level northerlies from Siberia, played the significant role in Australian monsoon activity.

Fig 6.34 is a schematic depiction of the structure of the 40- to 50-day oscillation taken from the seasonal analysis by Madden (1986) of the 40- to 50-day oscillation in the tropics. Madden found that the oscillation was strongest during northern winter and weakest with less regular eastward propagation during northern summer, and confirmed that it was stronger in the Indian Ocean and western Pacific than elsewhere. The upper- and lower-tropospheric zonal winds were most coherently out of phase at near-equatorial stations in the summer hemisphere, suggesting that the oscillation gains its energy from the deep convection associated with the seasonal migration of the intertropical convergence zone. At 150 mb over the Indian Ocean and western Pacific, the zonal and meridional winds were coherent and out of phase in northern winter but in phase in northern summer, consistent with the anticyclone marked in Fig 6.34 and with the hypothesis of fluctuations associated with stronger and weaker convection in the intertropical convergence zone. The greater regularity of the eastward progression in northern winter, when the convective heating is nearer the equator, was taken as an indication, supported by numerical modelling studies, that the oscillation is at least partly a Kelvin-wave response to this heating.

Madden (1986) also includes a discussion of unexplained features of the 40-to 50-day oscillation, including the absence of Rossby waves, which numerical model studies indicate should propagate westward from areas of equatorial convection, and a review of progress in modelling the oscillation.

6.3.3 Conclusion

The importance of the 30- to 60-day variations to the climate of at least the tropics cannot be over-stressed. They appear, from the foregoing discussion, to be linked to both El Nino-Southern Oscillation and to the Asian northern summer monsoon. The Quasi-Biennial Oscillation in the equatorial lower stratosphere is probably driven by transfer of momentum from Kelvin and Rossby-gravity waves propagating upwards from the troposphere (see Section 6.2), and waves of this type seem to be implicated in the 30- to 60-day oscillations. Thus the discovery by Bhalme et at (1987) of links between the Quasi-Biennial Oscillation and the fluctuations of the Indian northern summer monsoon rainfall should, perhaps, come as no surprise.

REFERENCES TO ADVANCED LECTURE 6

6.1 EL NINO/SOUTHERN OSCILLATION

ANGELL, J K (1981) Comparison of variations in atmospheric quantities with sea surface temperature variations in the equatorial eastern Pacific. Mon Weath Rev, 109, 230-243.

BACASTOW, R B and KEELING, C D (1981) Atmospheric CO_2 and the Southern Oscillation; effects associated with recent El Nino events. Proc WMO/ICSU/UNEP Conf on Analysis and Interpretation of Atmospheric CO_2 data, pp 109-112. WCP-14, Geneva.

BARNETT, T P (1985) Variations in near-global sea level pressure. J Atm. Sci., 42, 478-501.

BERLAGE, H P (1966) The Southern Oscillation and world weather. Mededel. Verhandel. 88, Kon Ned Met Inst, 152 pp.

BERLAGE, H P and DE BOER, H J (1959) On the extension of the Southern Oscillation throughout the world during the period July 1 1949-July 1 1957. Geofis Pure Appl, 44, 287-295.

BJERKNES, J (1969) Atmospheric teleconnections from the equatorial Pacific. Mon. Weath. Rev., 97, 163-172.

BLAZEJEWSKI, H, CADET, D L and MARSAL, O (1986) Low-frequency sea surface temperature and wind variations over the Indian and Pacific Oceans. J Geophys. Res., 91, C4, 5129-5132.

BRADLEY, R S, DIAZ, H F, KILADIS, G N and EISCHEID, J K (1987) ENSO signal in continental temperature and precipitation records. Nature, 327, 497-501.

CADET, D L (1985) The Southern Oscillation over the Indian Ocean. J Climatology, 5, 189-212.

CANE, M A, ZEBIAK, S E and DOLAN, S C (1986) Experimental forecasts of El Nino. Nature, 321, 827-832.

CHEN, T-C and van LOON, H (1987) Interannual variations of the tropical easterly jet. Mon. Weath. Rev., 115, 1739-1759.

CHEN, W Y (1982) Fluctuations in northern hemisphere 700 mb height field associated with the Southern Oscillation. Mon Weath Rev, 110, 808-823.

DESER, C and WALLACE, J M (1987) El Nino events and their relation to the Southern Oscillation: 1925-1986. J. Geophys. Res., 92, C13, 14189-14196

ELLIOTT, W P and ANGELL, J K (1987) The relation between Indian Monsoon rainfall, the Southern Oscillation, and hemispheric air and sea temperature: 1884-1984. J. Clim. Appl. Met., 26, 943-948.

FOLLAND, C K, PARKER, D E and NEWMAN, M R (1985) Worldwide marine temperature variations on the season-to-century time scale. Proc 9th Climate Diagnostics Conf, Corvallis, Oregon, 22-26 Oct 1984, pp 70-85. NOAA.

GILL, A E and RASMUSSON, E M (1983) The 1982-83 climate anomaly in the equatorial Pacific. Nature, 306, 229-234.

GODBOLE, R V and SHUKLA, J (1981) Global analysis of January and July sea level pressure. NASA Tech Mem 82097, Goddard Space Flight Center, Greenbelt, Maryland 20771.

GRAHAM, N E and WHITE, W B (1988) The El Nino cycle; a natural oscillator of the Pacific Ocean-atmosphere system. Science, 240, 1293-1302.

HAMILTON, K (1988) A detailed examination of the extratropical response to tropical El Nino/Southern Oscillation events. J. Climatology, 8, 67-86.

HARRISON, D E (1987) Monthly mean island surface winds in the central tropical Pacific and El Nino events. Mon. Weath. Rev., 115, 3133-3145.

HASTENRATH, S., de CASTRO, L C and ACEITUNO, P (1987) The Southern Oscillation in the tropical Atlantic sector. Beitr. Phys. Atm., 60, 447-463.

HILDEBRANDSSON, H H., (1897) Quelques recherches sur les centres d'action de l'atmosphere. K. Svenska Vetens.-Akad. Handl., 29, 33 pp.

HOREL, J D (1982) On the annual cycle of the tropical Pacific atmosphere and ocean. Mon Weath Rev, 110, 1863-1878.

HOREL, J D and WALLACE, J M (1981) Planetary scale atmospheric phenomena associated with the Southern Oscillation. Mon Weath Rev, 109, 813-829.

KILADIS, G N and VAN LOON, H (1988) The Southern Oscillation. Part VII: Meteorological anomalies over the Indian and Pacific sectors associated with the extremes of the oscillation. Mon. Weath. Rev., 116, 120-136.

KOUSKY, V E, KAGANO, M T and CAVALCANTI, I F A (1984) A review of the Southern Oscillation: oceanic-atmospheric circulation changes and related rainfall anomalies. Tellus, 36A, pp 490-504.

LAU, K-M and CHAN, P H (1986) Aspects of the 40-50 day oscillation during the northern summer as inferred from outgoing longwave radiation. Mon. Weath. Rev., 114, 1354-1367.

LOCKYER, N., and LOCKYER, W J S (1902a) On some phenomena which suggest a short period of solar and meteorological changes. Proc. Roy. Soc. London, 70, 500.

LOCKYER, N and LOCKYER W J S (1902b) On the similarity of the short-period pressure variation over large areas. Proc. Roy. Soc. London, 71, 134-135.

LOCKYER, N and LOCKYER W J S (1904) The behaviour of the short-period atmospheric pressure variation over the earth's surface. Proc. Roy. Soc. London, 73, 457-470

LOCKYER, W J S (1906) Barometric variations of long duration over large areas. Proc. Roy. Soc. London, A78, 43-60.

MARYON, R H and STOREY, A M (1985) A multivariate statistical model for forecasting anomalies of half-monthly mean surface pressure. J Climatology, 5, 561-578.

MILLER, L, CHENEY, R E and DOUGLAS, B C (1988) GEOSAT altimeter observations of Kelvin waves and the 1986-87 El Nino. Science, 239, 52-54.

MO, K C and WHITE, G H (1985) Teleconnections in the Southern Hemisphere. Mon. Weath. Rev., 113, 22-37.

MOSSMAN, R C (1924) Indian monsoon rainfall in relation to South American weather, 1875-1914. Mem Indian Met Dept, 23, 157-242.

NATIONAL AERONAUTICS AND SPACE ADMINISTRATION (NASA) (1986) El Nino and outgoing longwave radiation: an atlas of NIMBUS-7 Earth Radiation Budget observations. NASA Ref. Publ. 1163, 92pp.

NEWMAN, M R (1984) Observational aspects of the El Nino and the atmospheric response. Met O 13 Branch Memo 148.

PALMER, T N and MANSFIELD, D A (1986a) A study of wintertime circulation anomalies during past El Nino events using a high resolution general circulation model. I: Influence of model climatology. Quart. J. Roy. Met. Soc., 112, 613-638.

PALMER, T N and MANSFIELD, D A (1986b) A study of wintertime circulation anomalies during past El Nino events using a high resolution general circulation model. II: Variability of the seasonal mean response. Quart. J. Roy. Met. Soc., 112, 639-660.

PAN, Y H and OORT, A H (1983) Global climate variations connected with sea surface temperature anomalies in the eastern equatorial Pacific Ocean for the 1958-73 period. Mon Weath Rev, 111, 1244-1258.

PARKER, D E (1983) Documentation of a Southern Oscillation index. Met Mag, 112, 184-188.

PHILANDER, S G H (1985) El Nino and La Nina. J Atm Sci, 42, 2652-2662.

QUIROZ, R S (1983) The climate of the "El Nino" winter of 1982-83 - a season of extraordinary climatic anomalies. Mon Weath Rev, 11, 1685-1706.

RASMUSSON, E M and CARPENTER, T H (1982) Variations in tropical sea surface temperature and surface wind fields associated with the Southern Oscillation/El Nino. Mon Weath Rev, 110, 354-384.

ROGERS, J C (1984) The association between the North Atlantic Oscillation and the Southern Oscillation in the Northern Hemisphere. Mon. Weath. Rev., 112, 1999-2015.

ROPELEWSKI, C F and HALPERT, M S (1987) Global and regional scale precipitation patterns associated with the El Nino/Southern Oscillation. Mon. Weath. Rev., 115, 1606-1626.

ROPELEWSKI, C F and JONES, P D (1987) An extension of the Tahiti-Darwin Southern Oscillation Index. Mon. Weath. Rev., 115, 2161-2165.

ROWNTREE, P R (1972) The influence of tropical east Pacific Ocean temperatures on the atmosphere. Quart J Roy Met Soc, 98, 290-321.

SELKIRK, R (1984) Seasonally stratified correlations of the 200 mb tropical wind field to the Southern Oscillation. J Climatology, 4, 365-382.

SHUKLA, J and PAOLINO, D A (1983) The Southern Oscillation and long-range forecasting of the summer monsoon rainfall over India. Mon Weath Rev, 111, 1830-1837.

SIMMONS, A J (1982) The forcing of stationary wave motion by tropical diabatic heating. Quart J Roy Met Soc, 108, 503-534.

SPERBER, K R, HAMEED, S, GATES, W L and POTTER, G L (1987) Southern Oscillation simulated in a global climate model. Nature, 329, 140-142.

TRENBERTH, K E and SHEA, D J (1987) On the evolution of the Southern Oscillation. Mon. Weath. Rev., 115, 3078-3096.

VAN LOON, H, and LABITZKE, K (1987) The Southern Oscillation Part V. The anomalies in the lower stratosphere of the Northern Hemisphere in winter and a comparison with the Quasi-Biennial Oscillation. Mon. Weath. Rev., 115, 357-369.

VAN LOON, H and SHEA, D J (1985) The Southern Oscillation Part IV. The precursors south of 15°S to the extremes of the Oscillation. Mon. Weath. Rev., 113, 2063-2074.

VAN LOON, H and SHEA, D J (1987) The Southern Oscillation Part VI. Anomalies of sea level pressure on the Southern Hemisphere and of Pacific sea surface temperature during the development of a warm event. Mon. Weath. Rev., 115, 370-379.

WALKER, G T (1923) Correlation in seasonal variations of weather. VIII: A preliminary study of world weather. Mem. Indian Met. Dept., 24, 75-131.

WALKER, G T (1924) Correlation in seasonal variations of weather. IX: A further study of world weather. Mem. Indian Met. Dept., 24, 275-332.

WALKER, G T (1928) World Weather III. Mem. Roy. Met. Soc., 2, 97-106.

WALKER, G T and BLISS, E W (1930) World Weather IV. Mem. Roy. Met. Soc., 3, 81-95.

WALKER, G T and BLISS, E W (1932) World Weather V. Mem. Roy. Met. Soc., 4, 53-84.

WALKER, G T and BLISS, E W (1937) World Weather VI. Mem. Roy. Met. Soc., 4, 119-139.

WU, M-C and HASTENRATH, S (1986) On the interannual variability of the Indian Monsoon and the Southern Oscillation. Arch. Met. Geoph. Biocl. Ser.B 36, 239-261.

WYRTKI, K (1975) El Nino - the dynamic response of the equatorial Pacific Ocean to atmospheric forcing. J Phys Ocean, 5, 572-584.

YASUNARI, T (1987a) Global structure of the El Nino/Southern Oscillation. Part I El Nino composites. J. Met. Soc. Japan, 65, 67-80.

YASUNARI, T (1987b) Global structure of the El Nino/Southern Oscillation. Part II. Time evolution. J. Met. Soc. Japan 65, 81-102.

6.2 QUASI-BIENNIAL OSCILLATION

ANGELL, J K (1986) On the variation in period and amplitude of the Quasi-Biennial Oscillation in the equatorial stratosphere 1951-85. Mon Weath Rev, 114, 2272-2278.

ANGELL, J K and KORSHOVER, J (1977) Variation in size and location of the 300 mb north circumpolar vortex between 1963 and 1975. Mon Weath Rev, 105, 19-25.

BHALME, H N, RAHALKAR, S S and SIKDER, A B (1987) Tropical quasi-biennial oscillation of the 10-mb wind and Indian monsoon rainfall — implications for forecasting. J Climatology, 7, 345-353.

DUNKERTON, T J (1985) A two-dimensional model of the Quasi-Biennial Oscillation. J Atm Sci, 42, 1151-1160.

DUNKERTON, T J and DELISI, D P (1985) Climatology of the equatorial lower stratosphere. J Atm Sci, 42, 376-396.

EBDON, R A (1960) Notes on the wind flow at 50 mb in tropical and sub-tropical regions in January 1957 and January 1958. Quart J Roy Met Soc, 86, 540-542.

EBDON, R A (1975) The quasi-biennial oscillation and its association with tropospheric circulation patterns. Met Mag, 104, 282-297.

FOLLAND, C K (1977) Recent work on some quasi-cyclic fluctuations of meteorological parameters affecting British climate. Weather, 32, 336-342.

HAMILTON, K (1984) Mean wind evolution through the quasi-biennial cycle in the tropical lower stratosphere. J. Atm. Sci., 41, 2113-2125.

HOLTON, J R AND LINDZEN, R S (1972) An updated theory for the quasi-biennial cycle of the tropical stratosphere. J Atm Sci, 29, 1076-1080.

HOLTON, J R AND TAN, H-C (1980) The influence of the equatorial quasi-biennial oscillation on the global circulation at 50 mb. J Atm Sci, 37, 2200-2208.

NAUJOKAT, B (1986) An update of the observed Quasi-Biennial Oscillation of the stratospheric winds over the tropics. J Atm Sci, 43, 1873-1877.

NEWELL, R E AND GOULD-STEWART, S (1981) A stratospheric fountain? J Atm Sci, 38, 2789-2796.

PARTHASARATHY, B AND MOOLEY, D A (1978) Some features of a long homogeneous series of Indian summer monsoon rainfall. Mon Weath Rev, 106, 771-781.

PLUMB, R A (1984) The Quasi-Biennial Oscillation. In "Dynamics of the Middle Atmosphere", Eds. J R Holton and T Matsuno, Adv. Earth Planet. Sci., Tokyo (Terra) and Dordrecht (D Reidel), pp 217-251.

QUIROZ, R S (1983) Relationships among the stratosphere and tropospheric zonal flows and the Southern Oscillation. Mon Weath Rev, 111, 143-154.

REED, R J (1960) The circulation of the stratosphere. Paper presented at the 40th Annual meeting of the American Met Soc, Boston, Mass.

TAKAHASHI, M (1987) A 2-dimensional numerical model of the Quasi-Biennial Oscillation: Part I. J Met Soc Japan, 65, 523-536.

TANAKA, H and YOSHIZAWA, N (1987) A slowly varying model of the Quasi-Biennial Oscillation involving effects of transience, self-acceleration and saturation of equatorial waves. J Atm Sci, 44, 1427-1436.

VAN LOON, H and LABITZKE, K (1987) The Southern Oscillation. Part V: The anomalies in the lower stratosphere of the Northern Hemisphere in winter and a comparison with the Quasi-Biennial Oscillation. Mon Weath Rev, 115, 357-369.

6.3 30- TO 60-DAY VARIATIONS

BHALME, H N, RAHALKAR, S S and SIKDER, A B (1987) Tropical quasi-biennial oscillation of the 10-mb wind and Indian monsoon rainfall — implications for forecasting. J Climatology, 7, 345-353.

GRAVES, C E and STANFORD, J L (1987) Low-frequency atmospheric oscillations over the southeastern Pacific. J Atm Sci, 44, 260-264.

KRISHNAMURTI, T N, JAYAKUMAR, P K, SHENG, J, SURGI, N and KUMAR, A (1985) Divergent circulations on the 30 to 50 day time scale. J Atm Sci, 42, 364-375.

LAU, K-M and CHAN, P H (1985) Aspects of the 40-50 day oscillation during the northern winter as inferred from outgoing longwave radiation. Mon Weath Rev, 113, 1889-1909.

LAU, K-M and CHAN, P H (1986) Aspects of the 40-50 day oscillation during the northern summer as inferred from outgoing longwave radiation. Mon Weath Rev, 114, 1354-1367.

MADDEN, R A (1986) Seasonal variations of the 40-50 day oscillation in the tropics. J Atm Sci, 43, 3138-3158.

MADDEN, R A and JULIAN, P R (1971) Detection of a 40-50 day oscillation in the zonal wind in the tropical Pacific. J Atm Sci, 28, 702-708.

MADDEN, R A and JULIAN, P R (1972) Description of global-scale circulation cells in the tropics with a 40-50 day period. J Atm Sci, 29, 1109-1123.

MURAKAMI, T, CHEN, L-X, XIE, A and SHRESTHA, M L (1986) Eastward propagation of 30-60 day perturbations as revealed from outgoing longwave radiation data. J Atm Sci, 43, 961-971.

SHRESTHA, M L and MURAKAMI, T (1988) Intraseasonal fluctuations in low-level meridional winds over the Indian Ocean and monsoonal convection over South Asia. Tellus, 40A, 120-132.

SUMATHIPALA, W L and MURAKAMI, T (1988) Intraseasonal fluctuations in low-level meridional winds over the South China Sea and the western Pacific and monsoonal convection over Indonesia and northern Australia. Tellus, 40A, 205-219.

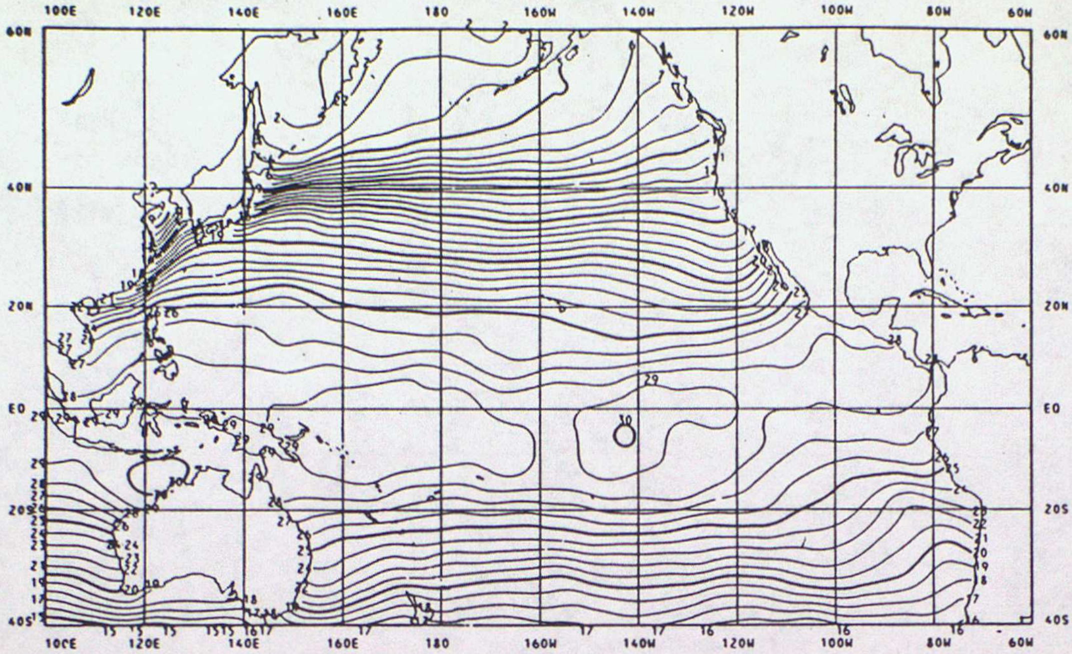
100E
120E
140E
160E
180
160W
140W
120W
100W
80W
60W
60N
40N
20N
EQ
20S
40S
29
30

SEASONAL NMC SST MEAN FIELD (CAC ANALYSIS) DEC JAN FEB 1983

Sea surface temperature over the Pacific Ocean for winter 1982–83.

Figure 6.1A. From Quiroz (1983).

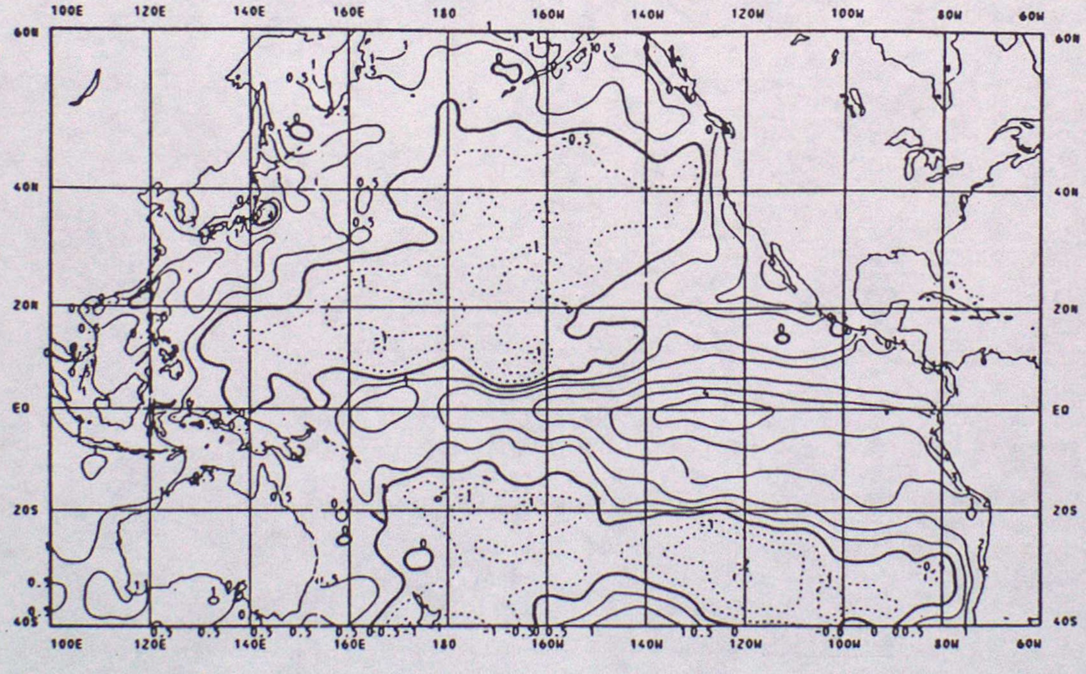
100E
120E
140E
160E
180
160W
140W
120W
100W
80W
60W
60N
40N
20N
EQ
20S
40S

SEASONAL SST ANOMALIES (CAC ANALYSIS, NCC CLIMATE) DEC JAN FEB 1983

Sea surface temperature (°C) for winter 1982–83 over the Pacific Ocean. Dashed lines portray negative anomalies, thin solid lines indicate positive anomalies, and the heavy solid line is the zero line. Anomalous isotherms are at 1°C intervals except for 0.5°C between +1 and −1°C.

Figure 6.1B. From Quiroz (1983).

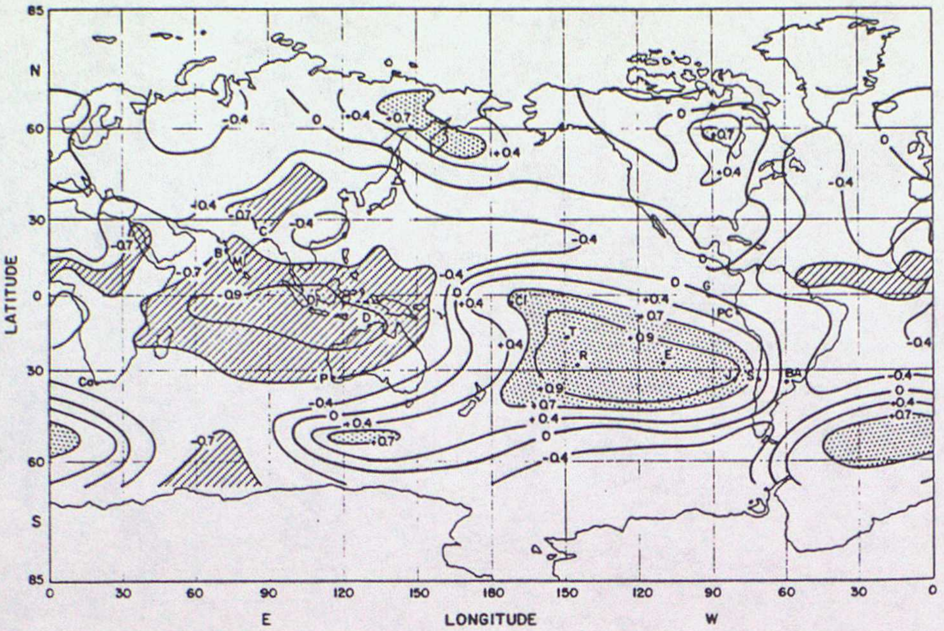
85
N
60
30
0
30
60
S
85
LATITUDE
0
30
60
90
120
150
180
150
120
90
60
30
0
E
LONGITUDE
W
-0.4
0
+0.4
-0.7
+0.7
-0.9
+0.9
B
M
C
Dj
D
P
Co
CI
T
R
E
G
PC
J
S
BA

Figure 6.2A.
From Kousky et al (19

Isolines of correlation coefficients of sea level pressure anomalies using Easter Island (E) as the reference station. Adapted from Berlage and de Boer (1959).

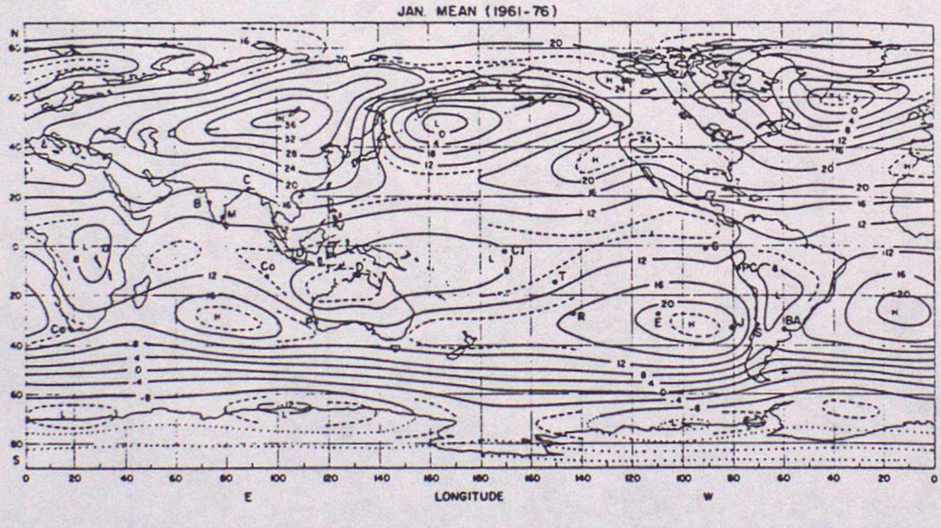
JAN. MEAN (1961-76)
N
S
LATITUDE
0
20
40
60
80
100
120
140
160
180
160
140
120
100
80
60
40
20
0
E
LONGITUDE
W
H
L
Ca
B
M
C
Dj
D
P
Co
CI
T
R
E
J
S
PC
BA

Figure 6.2B.
From Kousky et al (1984

January mean sea level pressure (1961–76). Adapted from Godbole and Shukla (1981). Stations commonly referred to as being key stations in the Southern Oscillation and indicated in the figure are: Capetown (Ca), Bombay (B), Madras (M), Calcutta (C), Djakarta (Dj), Darwin (D), Perth (P), Cocos Island (Co), Canton Island (CI), Papaete, Tahiti (T), Rapa (R), Easter Island (E), Juan Fernandez Island (J), Galapagos Islands (G), Puerto Chicama (PC), Santiago (S) and Buenos Aires (BA).

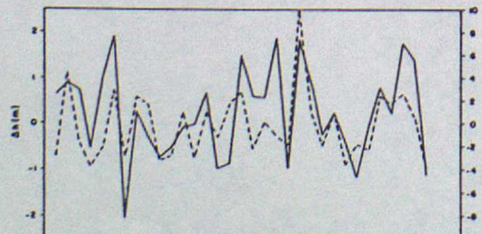

The mean Parana river level anomalies (m), for April–September, at Rosario, Argentina (dashed line) and a Southern Oscillation Index (SOI) (solid line) calculated by taking the sum of the pressure anomalies (mb) at Bombay, Madras, Djakarta, Calcutta, Darwin, Perth and Cape Town for the period of October–March. The SOI values are plotted in the year corresponding to the January–March period, and are taken from Berlage (1966). The Parana river level anomalies are taken from Mossman (1924).

Figure 6.3. From Kousky et al (1984).

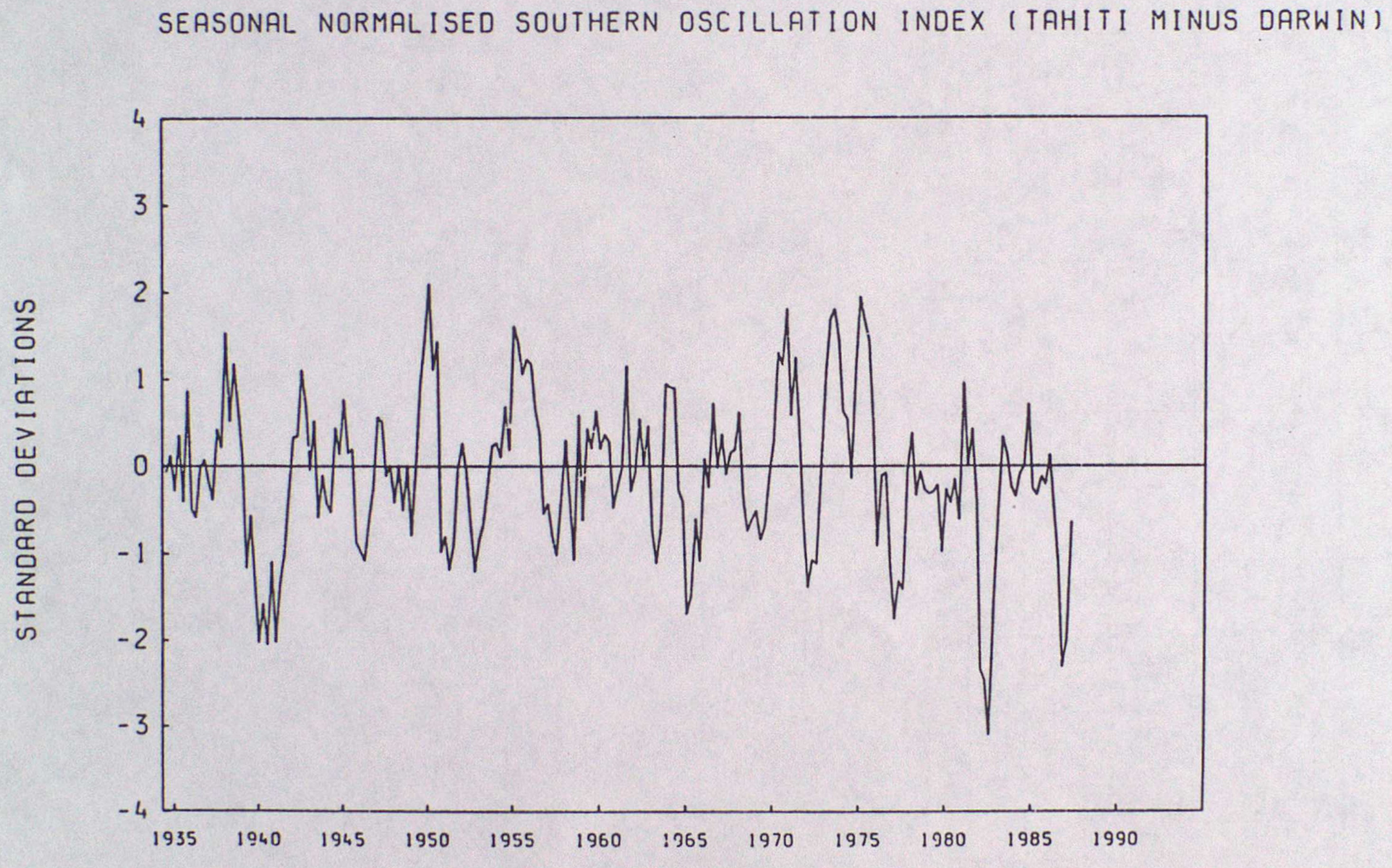
SEASONAL NORMALISED SOUTHERN OSCILLATION INDEX (TAHITI MINUS DARWIN)
STANDARD DEVIATIONS
4
3
2
1
0
-1
-2
-3
-4
1935
1940
1945
1950
1955
1960
1965
1970
1975
1980
1985
1990

Figure 6.4

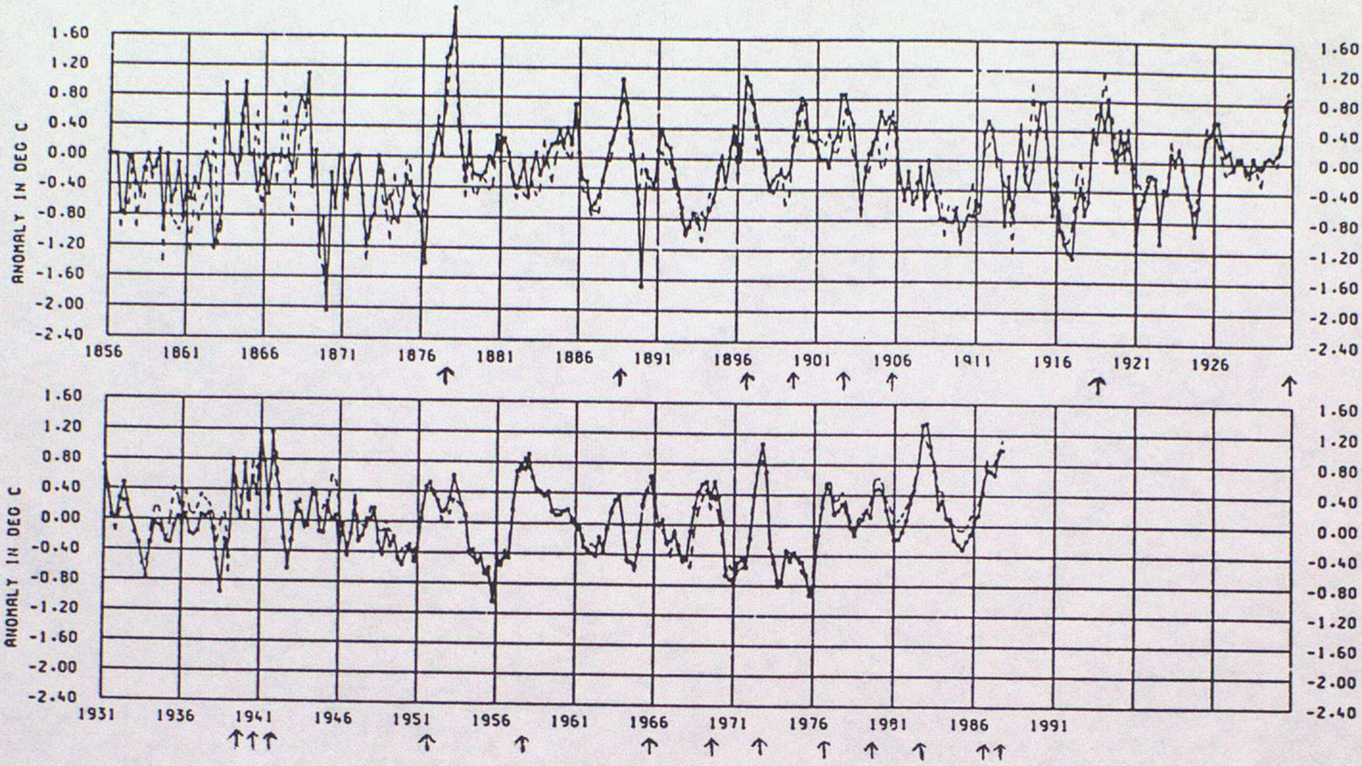

Figure 6.5. Seasonal sea surface temperature (solid) and night marine air temperature (dashed) anomalies (w.r.t. 1951-80) averaged over the tropical East Pacific (20°N to 20°S, east of 170°W) , 1856 to 1987. Arrows mark Oct to Dec of El Nino years.

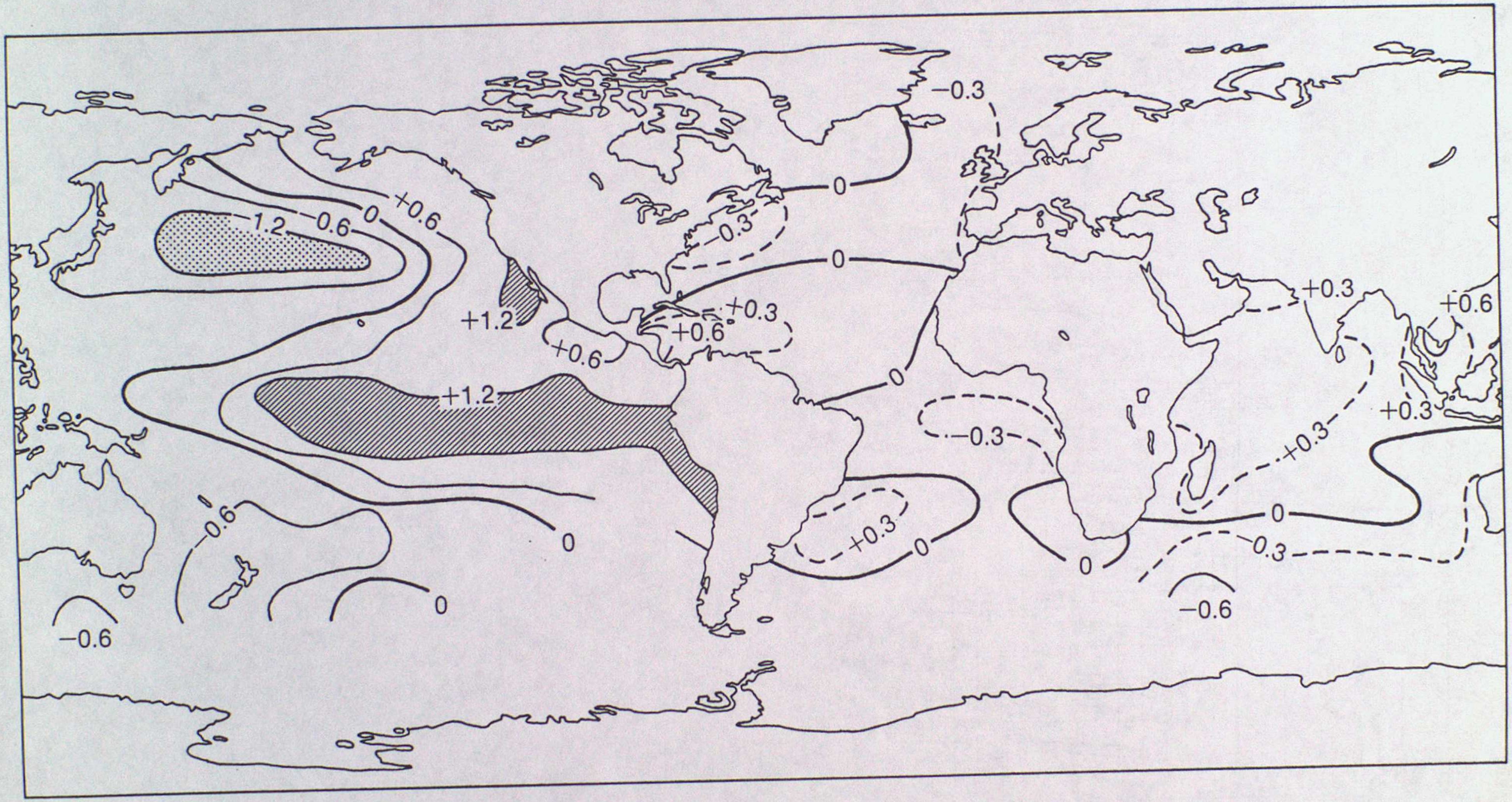
-0.3
0
+0.6
0
-0.6
-1.2
-0.3
0
+1.2
+0.3
+0.6
+0.6
+1.2
0
-0.3
+0.3
+0.6
+0.3
+0.3
-0.6
0
0
+0.3
0
0
-0.3
0
-0.6
-0.6

Figure 6.6 The second covariance matrix eigenvector (EOF2) of worldwide SSTA, 1901-80.
The values are normalised so that the sum of the squares of the values for 10° squares is 100.

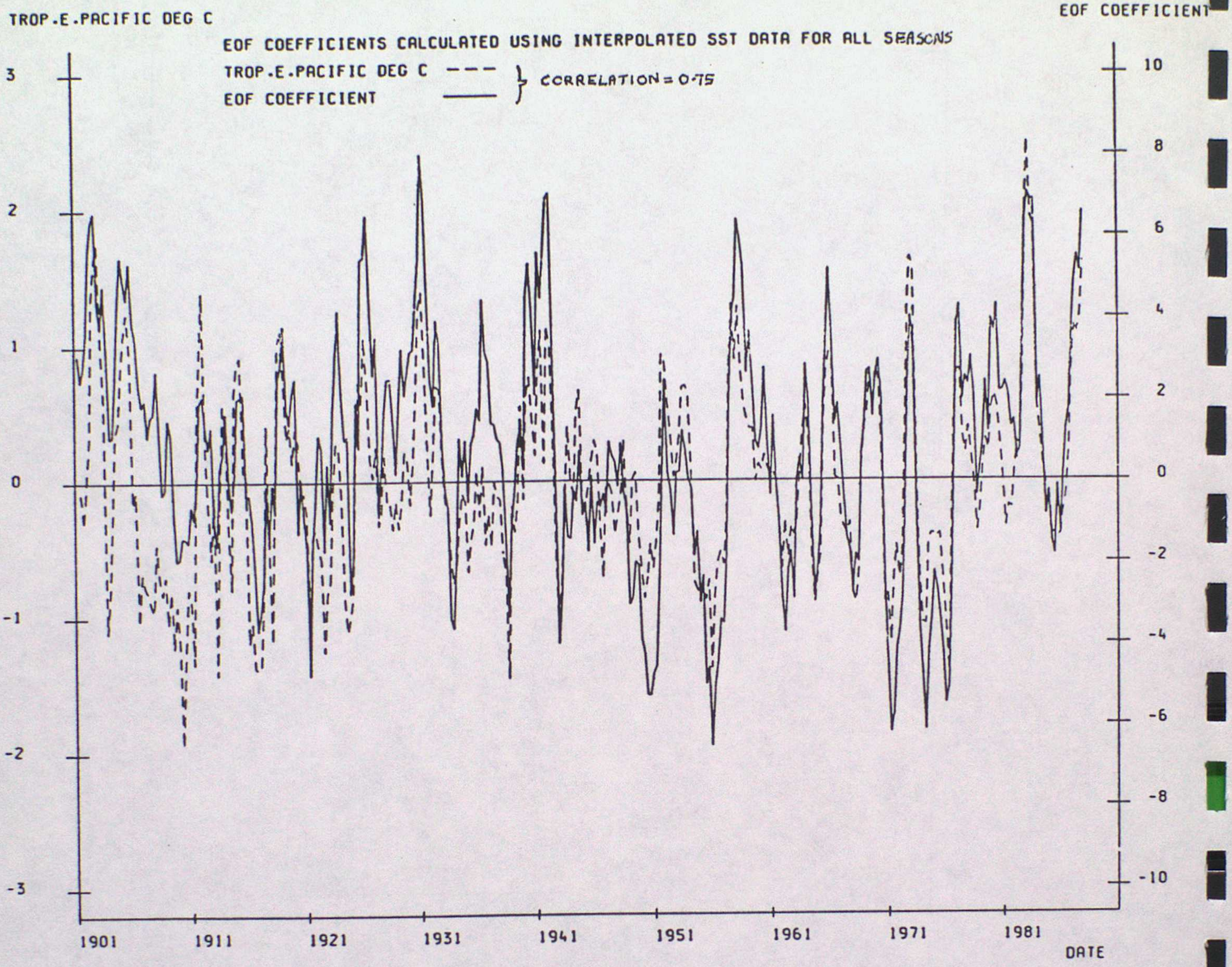

Figure 6.7. Comparison between EOF 2 coefficient and Tropical East Pacific SSTA time serie

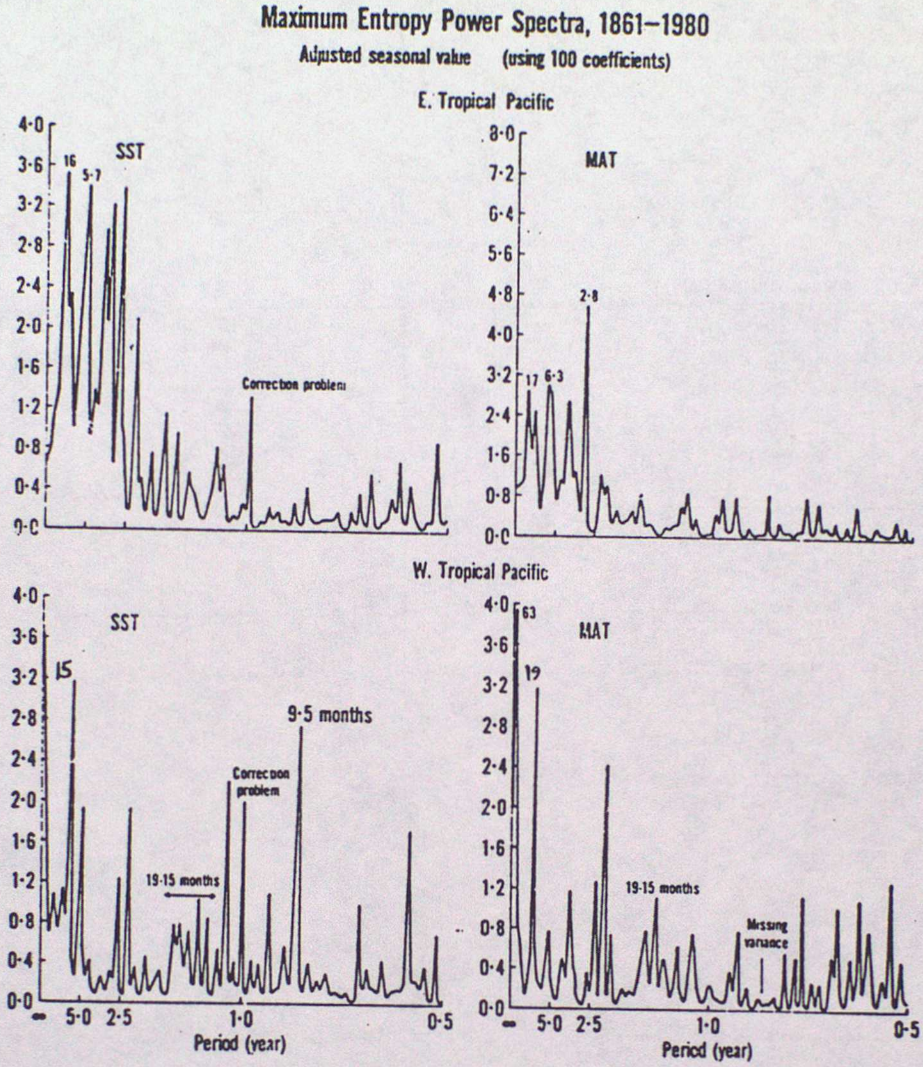

Figure 6.8. From Folland et al (1985).

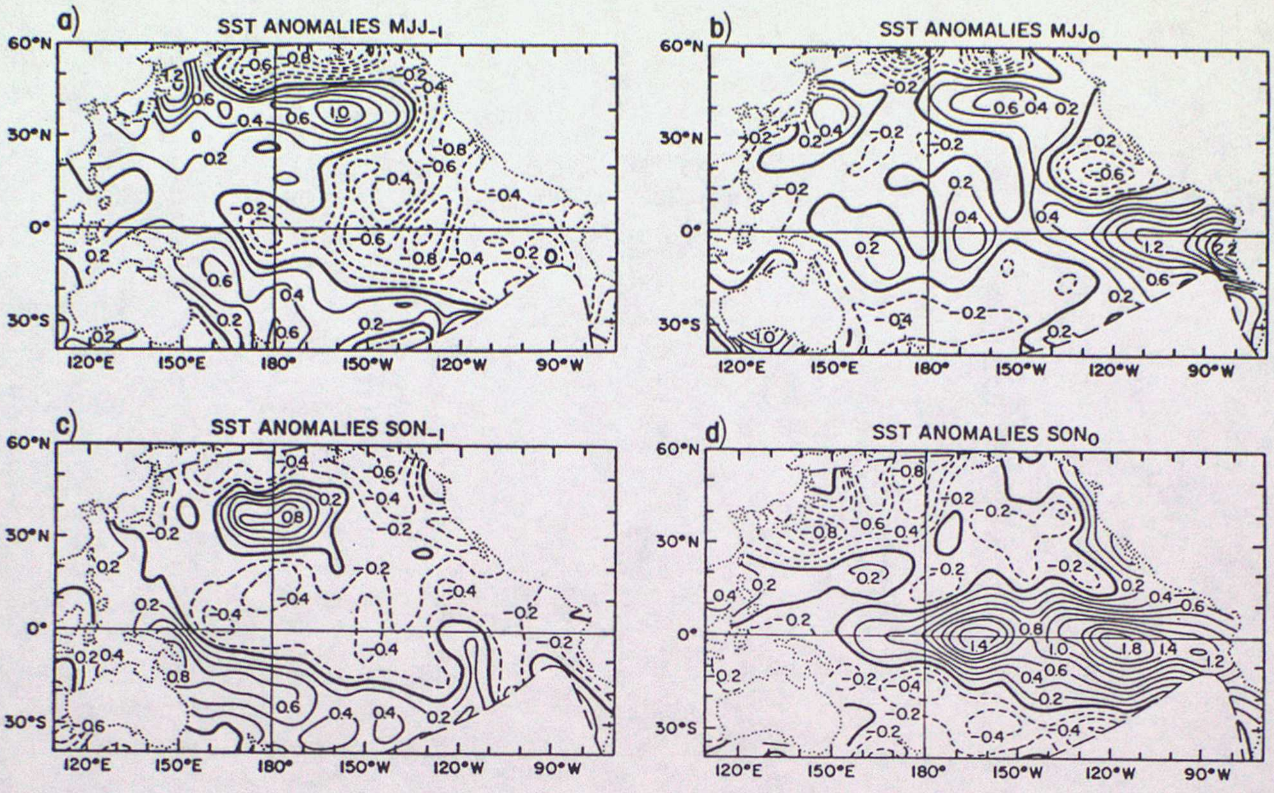
a)
SST ANOMALIES MJJ₋₁
b)
SST ANOMALIES MJJ₀
c)
SST ANOMALIES SON₋₁
d)
SST ANOMALIES SON₀
60°N
30°N
0°
30°S
120°E
150°E
180°
150°W
120°W
90°W

Anomalies of sea surface temperature (°C) in a) May–Jun–Jul$_{-1}$; b) May–Jun–Jul$_0$; c) Sep–Oct–Nov$_{-1}$; d) Sep–Oct–Nov$_0$.

Figure 6.9 From van Loon and Shea (1987).

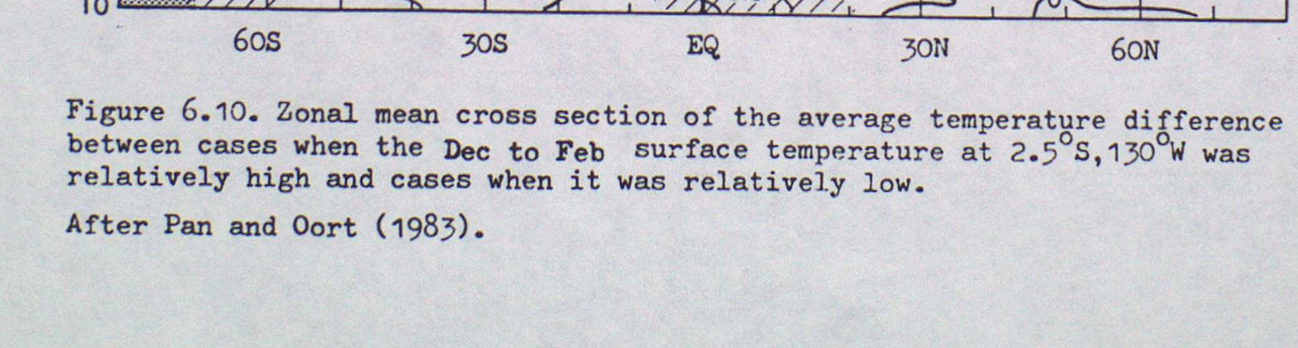

Figure 6.10. Zonal mean cross section of the average temperature difference (°C) between cases when the **Dec to Feb** surface temperature at 2.5°S,130°W was relatively high and cases when it was relatively low.

After Pan and Oort (1983).

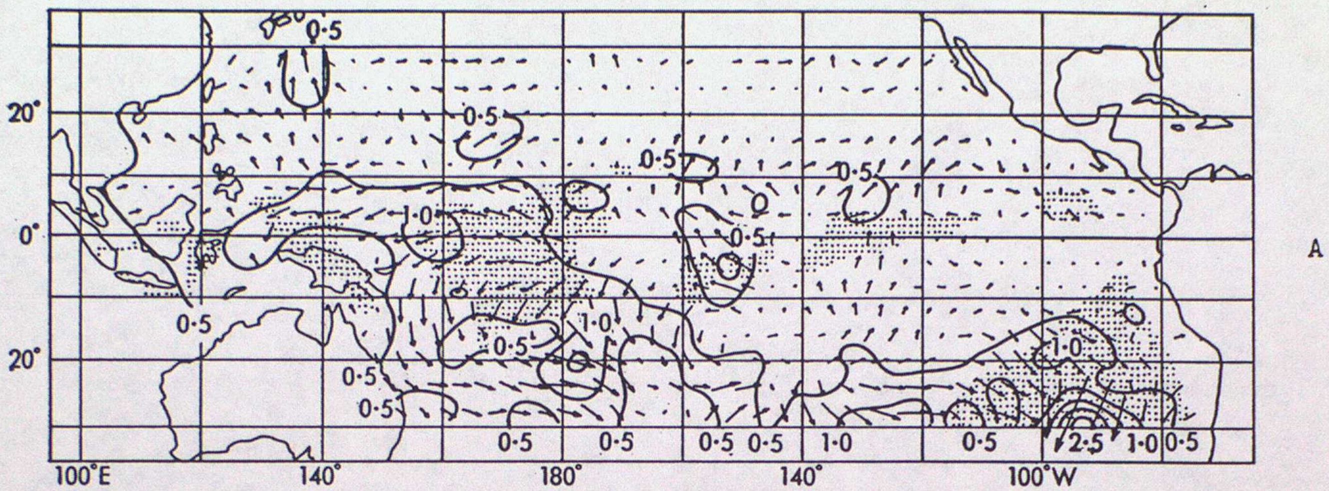
20°
0°
20°
100°E
140°
180°
140°
100°W
0·5
1·0
2·5
A

August—October Year (−1)

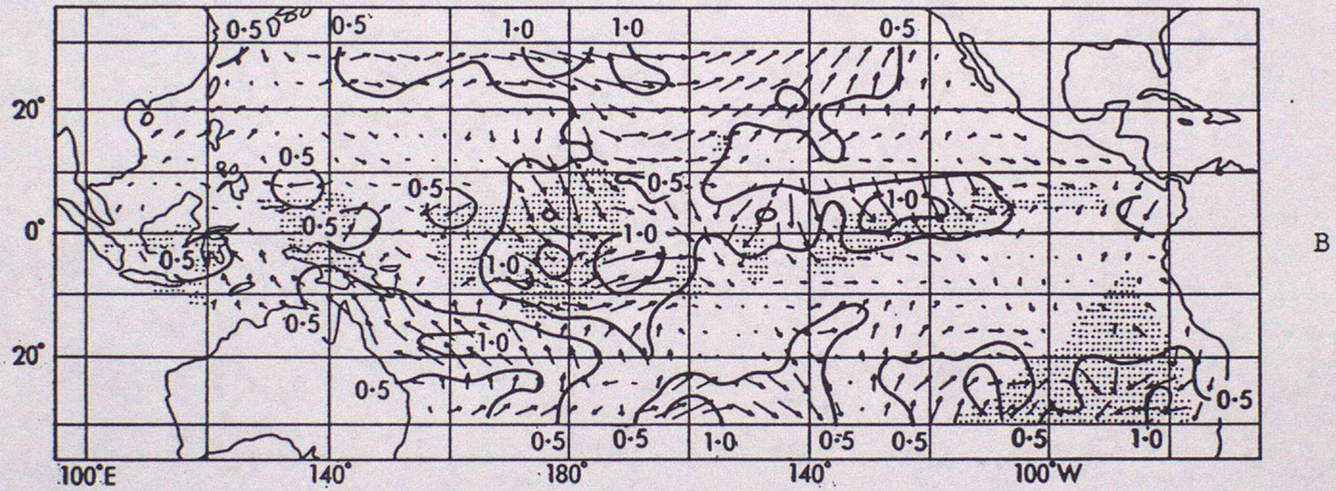
20°
0°
20°
100°E
140°
180°
140°
100°W
0·5
1·0
B

March—May Year (0)

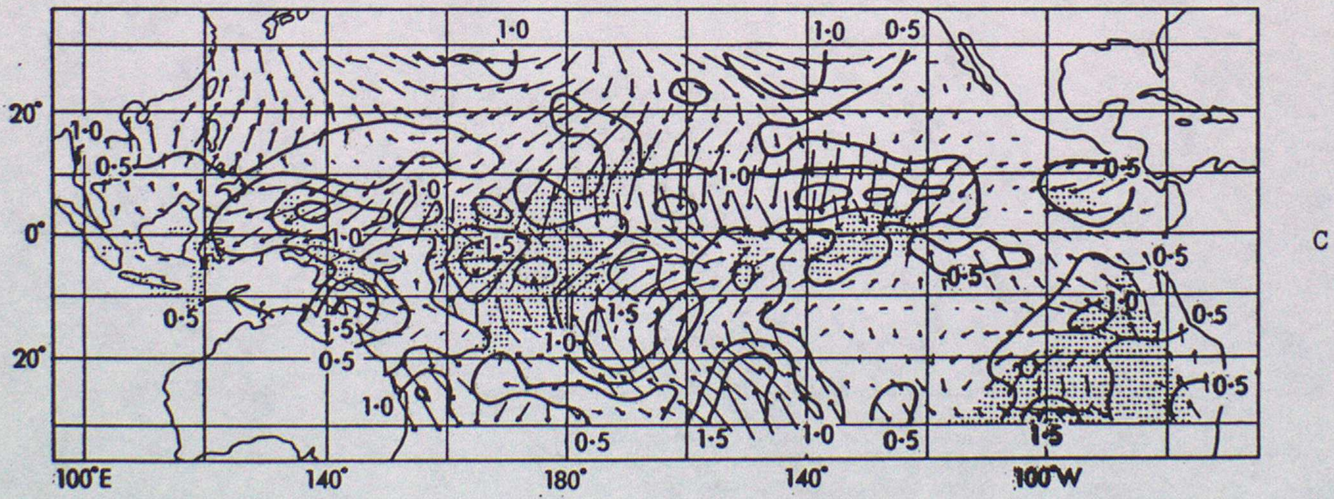
20°
0°
20°
100°E
140°
180°
140°
100°W
0·5
1·0
1·5
C

December Year (0) — February Year (+1)

El-Nino surface wind anomaly composites (units m s^{-1}) .
Areas in which the number of observations average less than 10 in a two degree square are shaded on the wind composite.

Figure 6.11. After Rasmusson and Carpenter (1982).

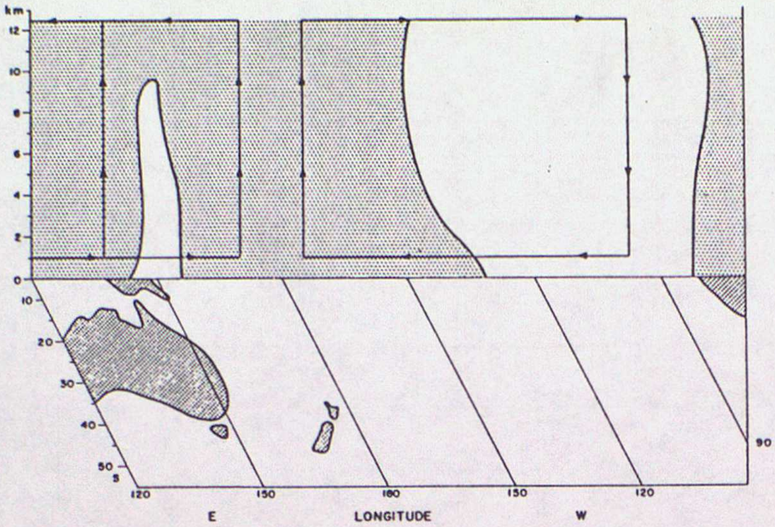

Schematic diagram of the Pacific Walker Circulation. Shaded regions are areas of rising motion. The circulation pattern shown is the January mean for 1979–81.

Figure 6.12A.

From **Kousky** et al (1984).

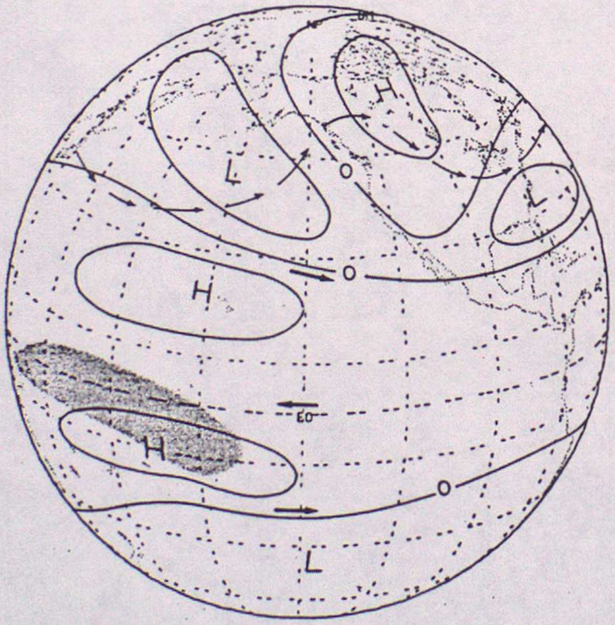

Figure 6.12B.

After Horel and Wallace (1981).

Schematic illustration of the hypothesized global pattern of middle and upper tropospheric geopotential height anomalies (solid lines) during a Northern Hemisphere winter which falls within an episode of warm sea surface temperatures in the equatorial Pacific. The arrows in darker type reflect the strengthening of the subtropical jets in both hemispheres along with stronger easterlies near the equator during warm episodes. The arrows in lighter type depict a mid-tropospheric streamline as distorted by the anomaly pattern, with pronounced "troughing" over the central Pacific and "ridging" over western Canada. Shading indicates regions of enhanced cirriform cloudiness and rainfall.

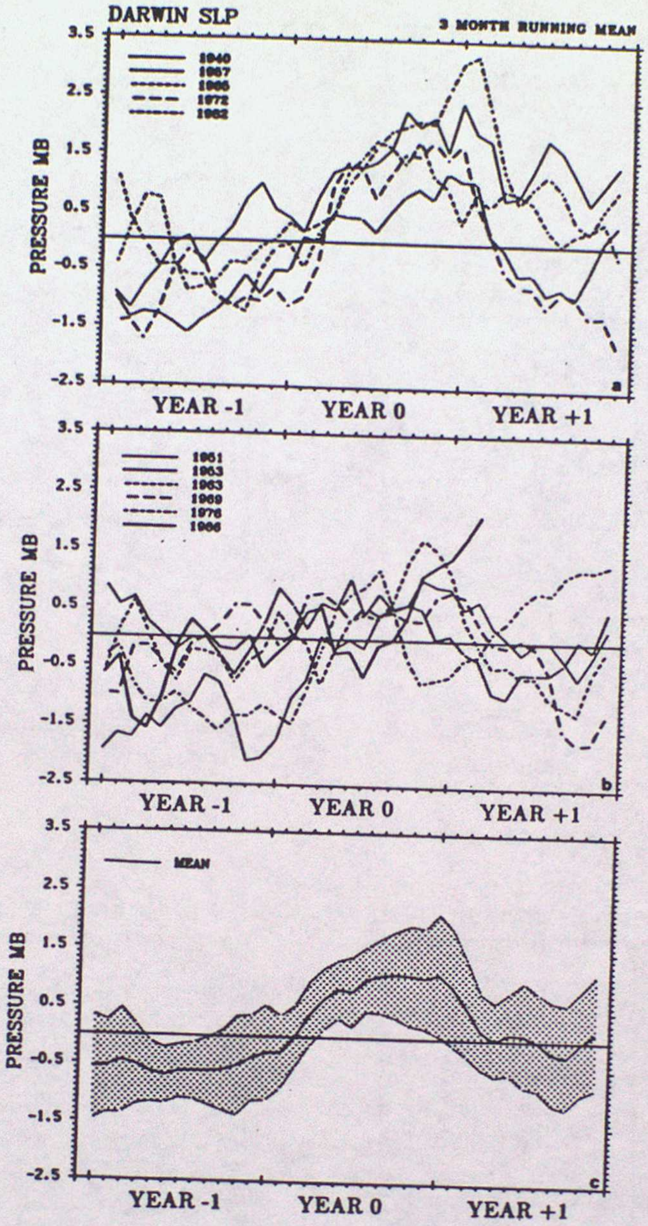

. Sequences of anomalies in sea level pressure at Darwin over all El Niño events since 1939 from the year before (year −1) to the year following (year +1) the event. Each event is labeled by the central year (year 0). The larger events are shown in (a), the smaller events in (b), and the composite mean (excluding 1986) plus and minus one standard deviation is given in (c).

Figure 6.13 From Trenberth and Shea (1987)

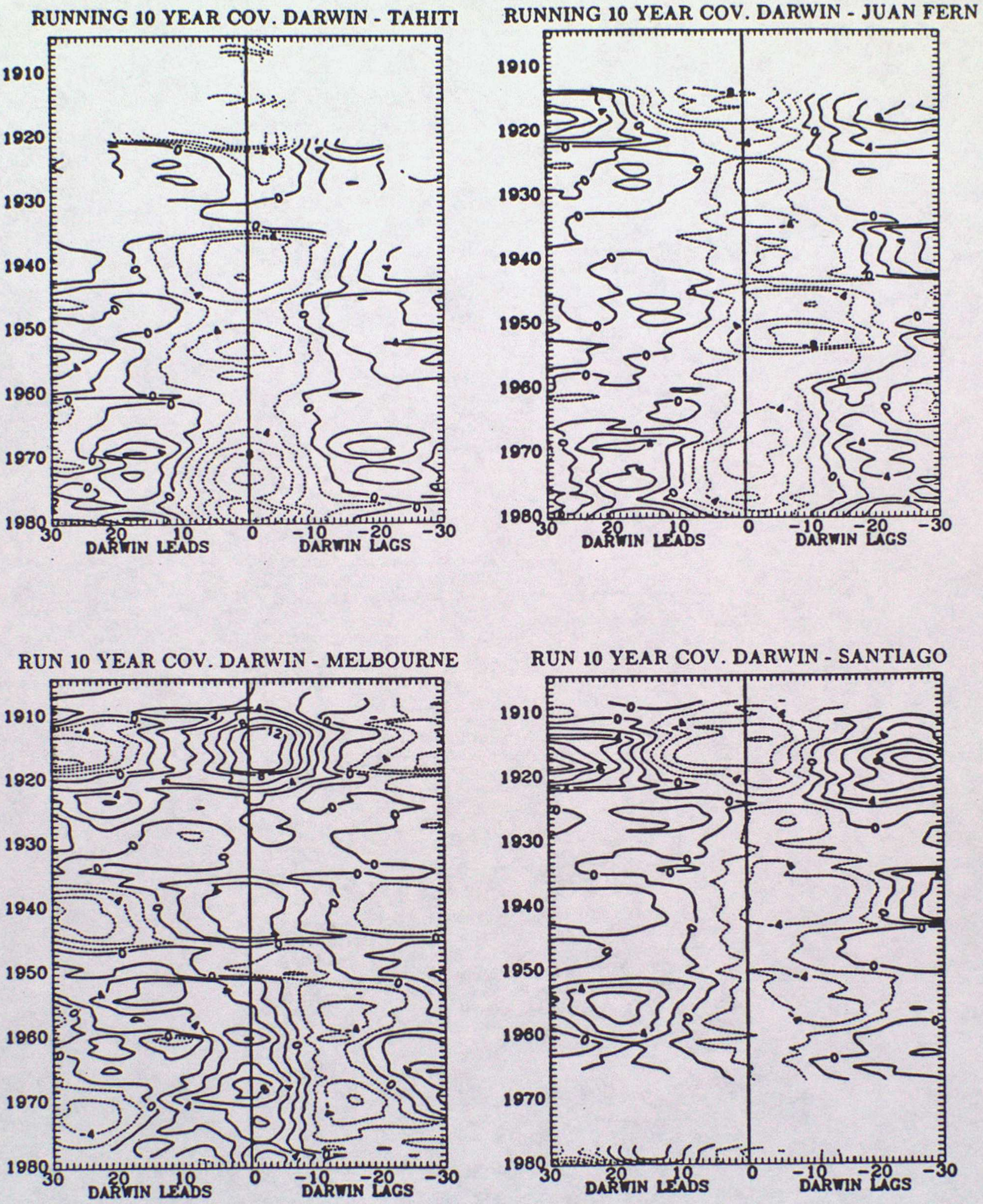

Ten-year running cross covariances (×10) normalized by the standard deviations for the whole series so that they approximate correlations, as a function of lag up to ±30 months, of Darwin with Tahiti, Juan Fernandez, Melbourne and Santiago for 1900–84. Missing data areas are left blank.

Figure 6.14 From Trenbeth and Shea (1987).

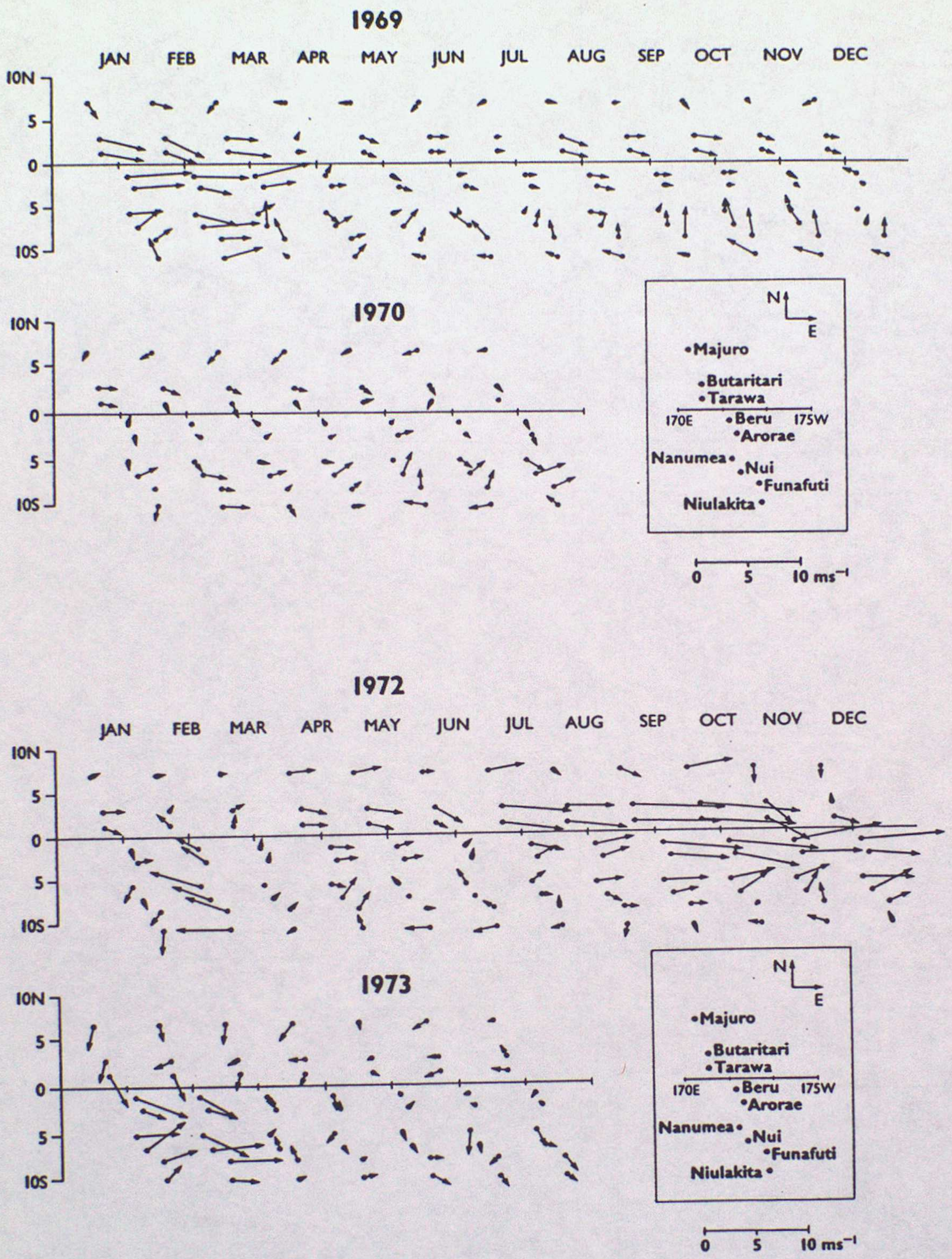

Figure 6.15 Monthly mean wind anomalies for the El Nino periods of 1969-70 and 1972-3.. From Harrison (1987).

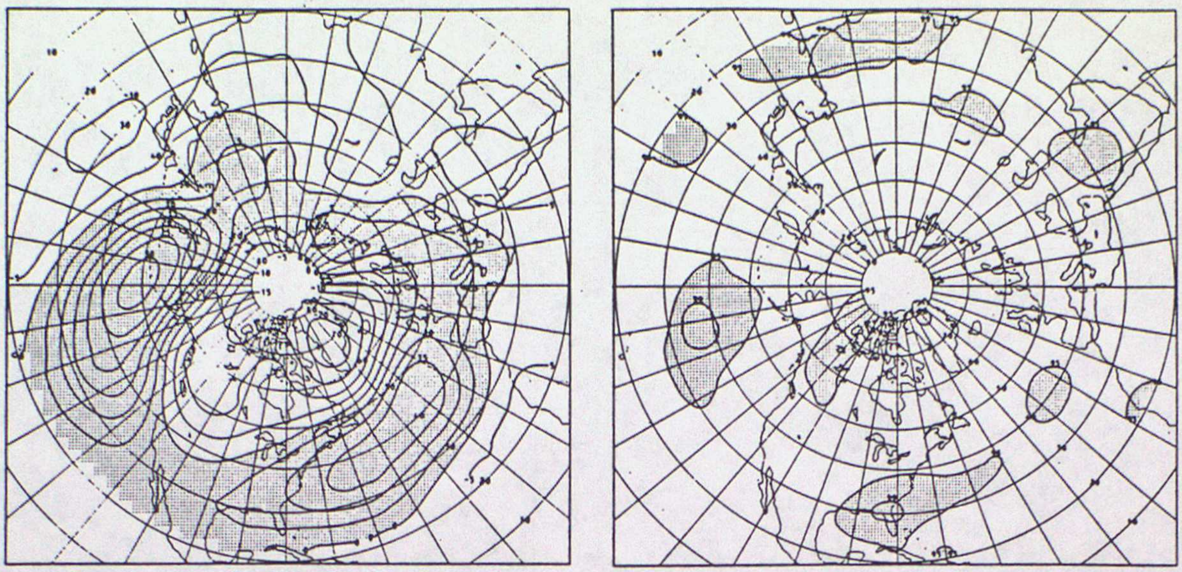

DJF 700 MB ANOMALIES FOR HGH SOI YEARS, LAG=0

CONF.LIMIT OF DJF COMPOSITE FOR HGH SOI YRS,LAG=0

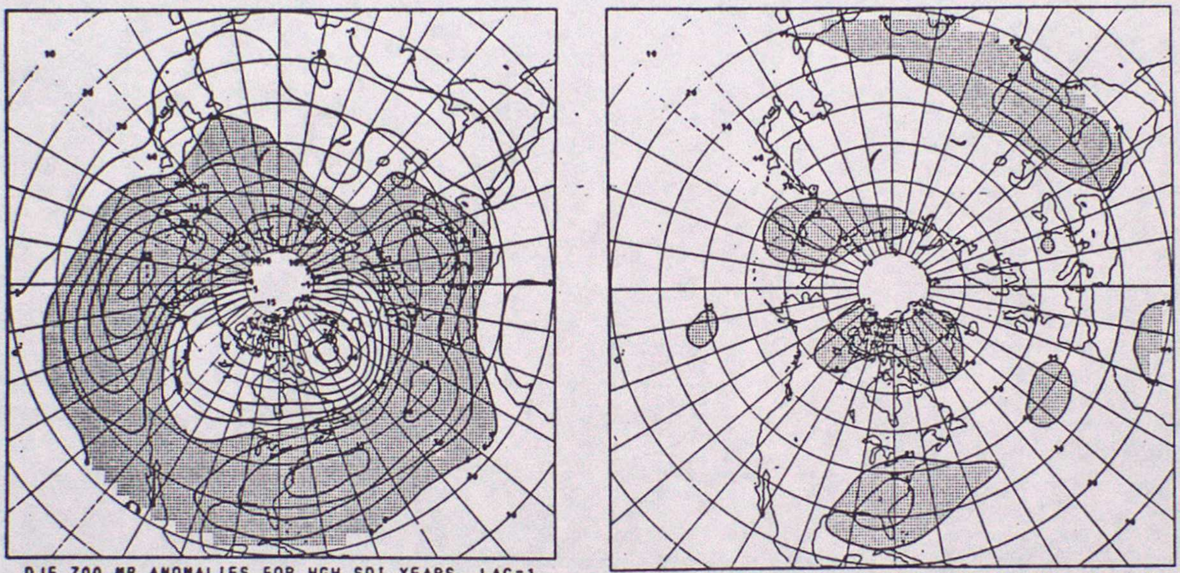

DJF 700 MB ANOMALIES FOR HGH SOI YEARS, LAG=1

CONF.LIMIT OF DJF COMPOSITE FOR HGH SOI YRS,LAG=1

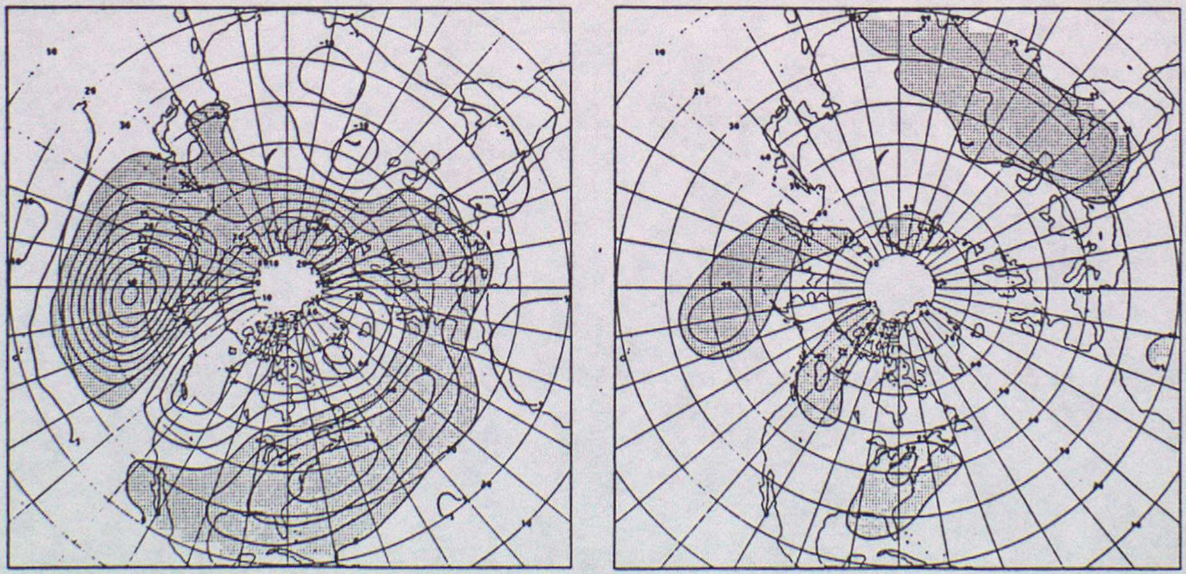

DJF 700 MB ANOMALIES FOR HGH SOI YEARS, LAG=2

CONF.LIMIT OF DJF COMPOSITE FOR HGH SOI YRS,LAG=2

Winter composites associated with high SOI values with the latter leading the height field by various seasons. The shaded areas are positive and the contour interval is 5 m. Confidence limits of the anomalies are presented on the right.

Figure 6.16A. From Chen (1982).

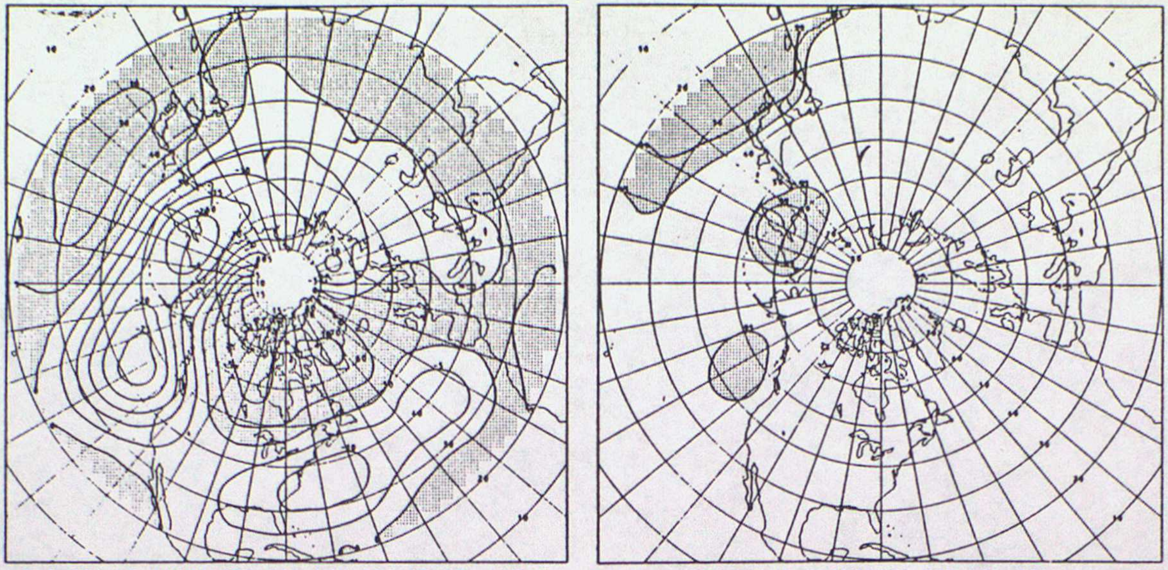

DJF 700 MB ANOMALIES FOR LOW SOI YEARS, LAG=0 CONF.LIMIT OF DJF COMPOSITE FOR LOW SOI YRS,LAG=0

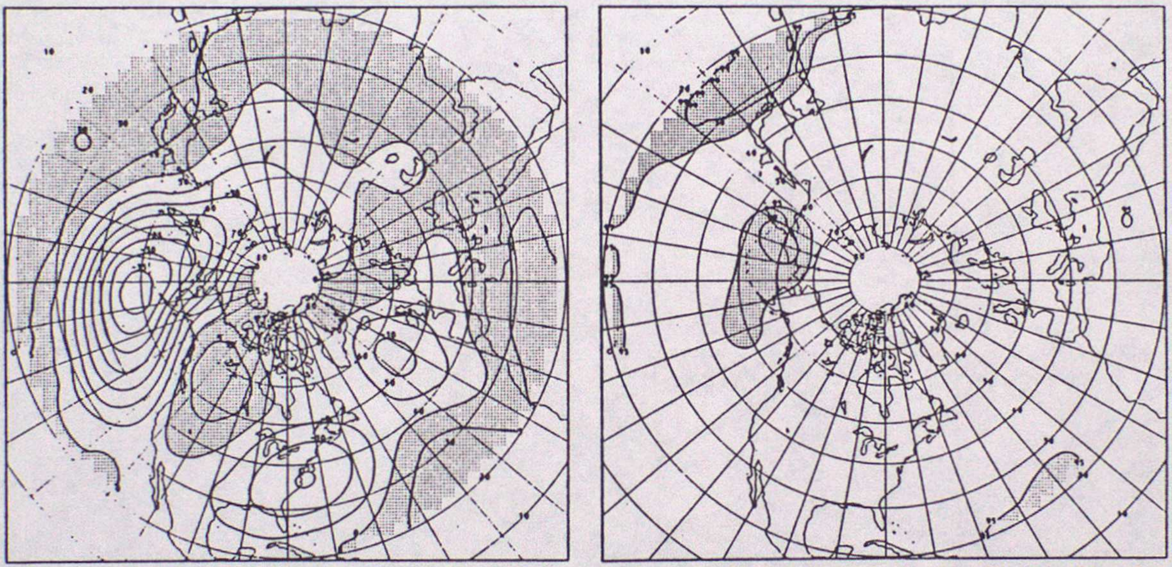

DJF 700 MB ANOMALIES FOR LOW SOI YEARS, LAG=1 CONF.LIMIT OF DJF COMPOSITE FOR LOW SOI YRS,LAG=1

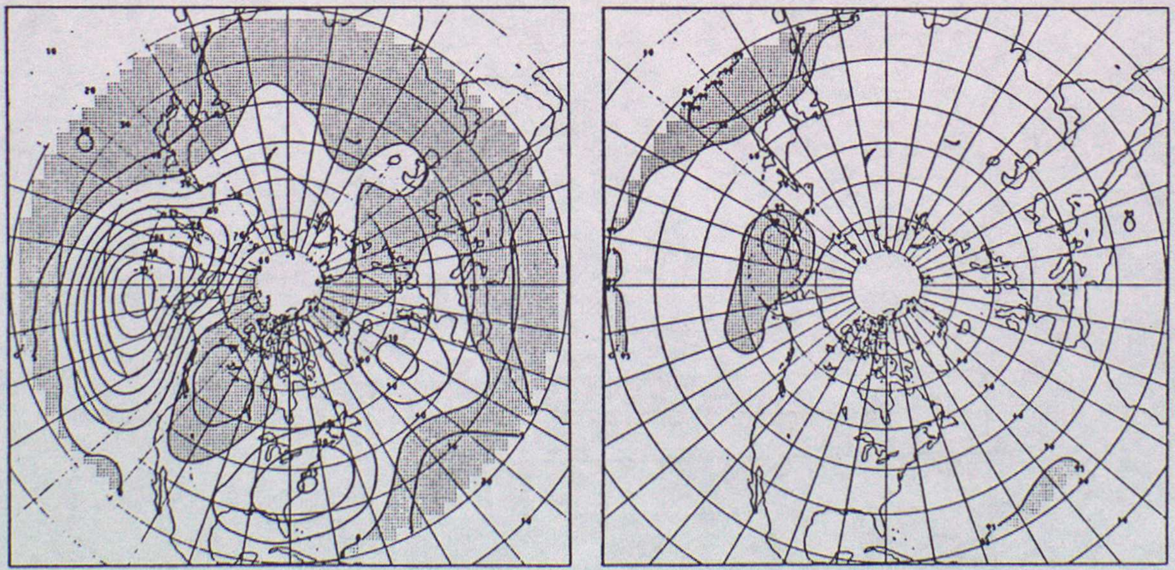

DJF 700 MB ANOMALIES FOR LOW SOI YEARS, LAG=2 CONF.LIMIT OF DJF COMPOSITE FOR LOW SOI YRS,LAG=2

Figure 6.16B. As Fig. 6.16A,but for low SOI values.
From Chen (1982).

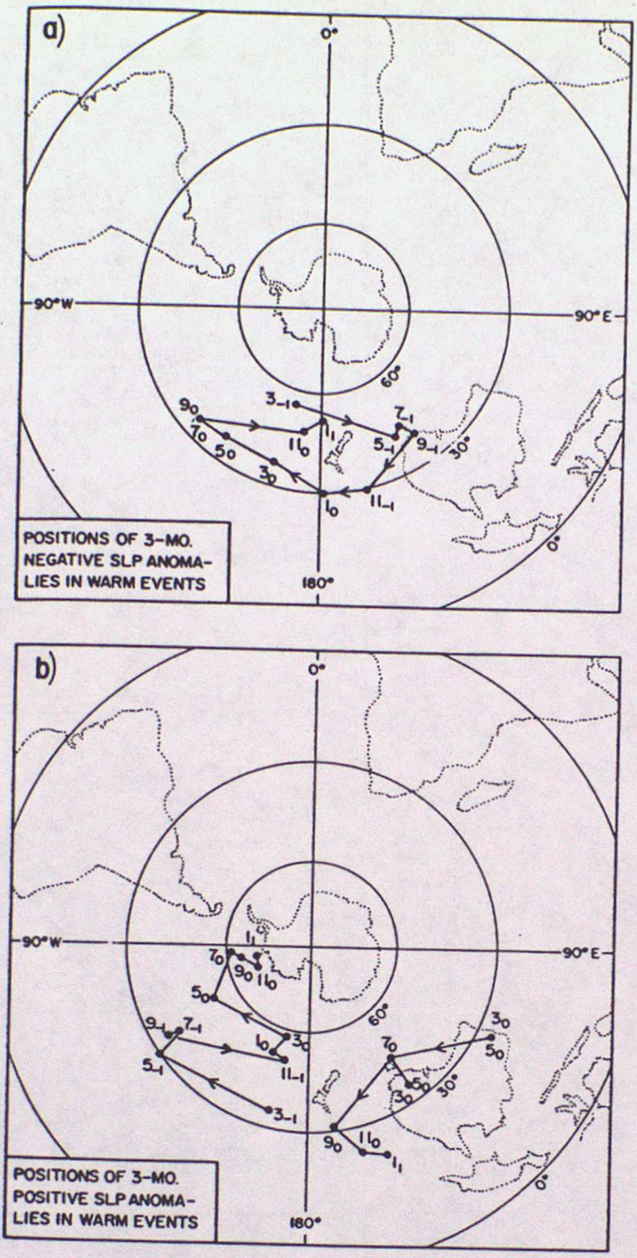
a)
0°
90°W
90°E
60°
30°
0°
180°
3_{-1}
9_0
7_0
5_0
3_0
1_0
11_0
1_1
7_{-1}
5_{-1}
9_{-1}
11_{-1}
POSITIONS OF 3-MO. NEGATIVE SLP ANOMALIES IN WARM EVENTS
b)
0°
90°W
90°E
60°
30°
0°
180°
1_1
7_0
9_0
11_0
5_0
9_{-1}
7_{-1}
5_{-1}
1_0
3_0
11_{-1}
3_{-1}
7_0
3_0
5_0
9_0
11_0
1_1
POSITIONS OF 3-MO. POSITIVE SLP ANOMALIES IN WARM EVENTS

The movement of the major three-month average anomalies of sea level pressure. The averages overlap by one month: 3_{-1} is Feb–Mar–Apr of Year$_{-1}$ and 5_{-1} is Apr–May–Jun of Year$_{-1}$. b) As in Fig. a, but for positive anomalies.

Figure 6.17 From van Loon and Shea (1987).

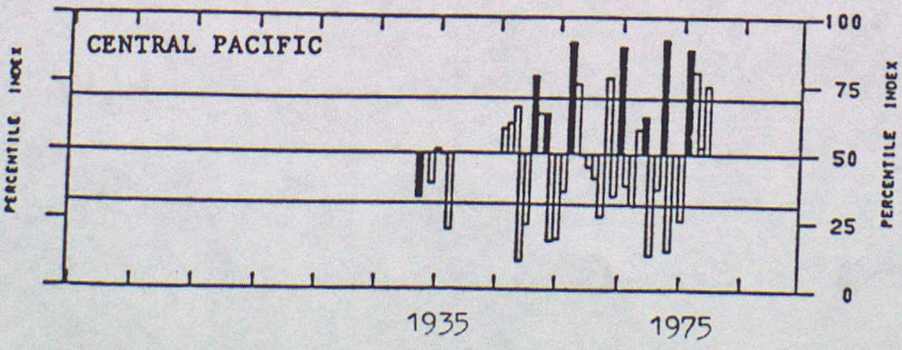

Figure 6.18 Central Pacific rainfall series from Ropelewski and Halpert (1987). El Nino years are shaded.

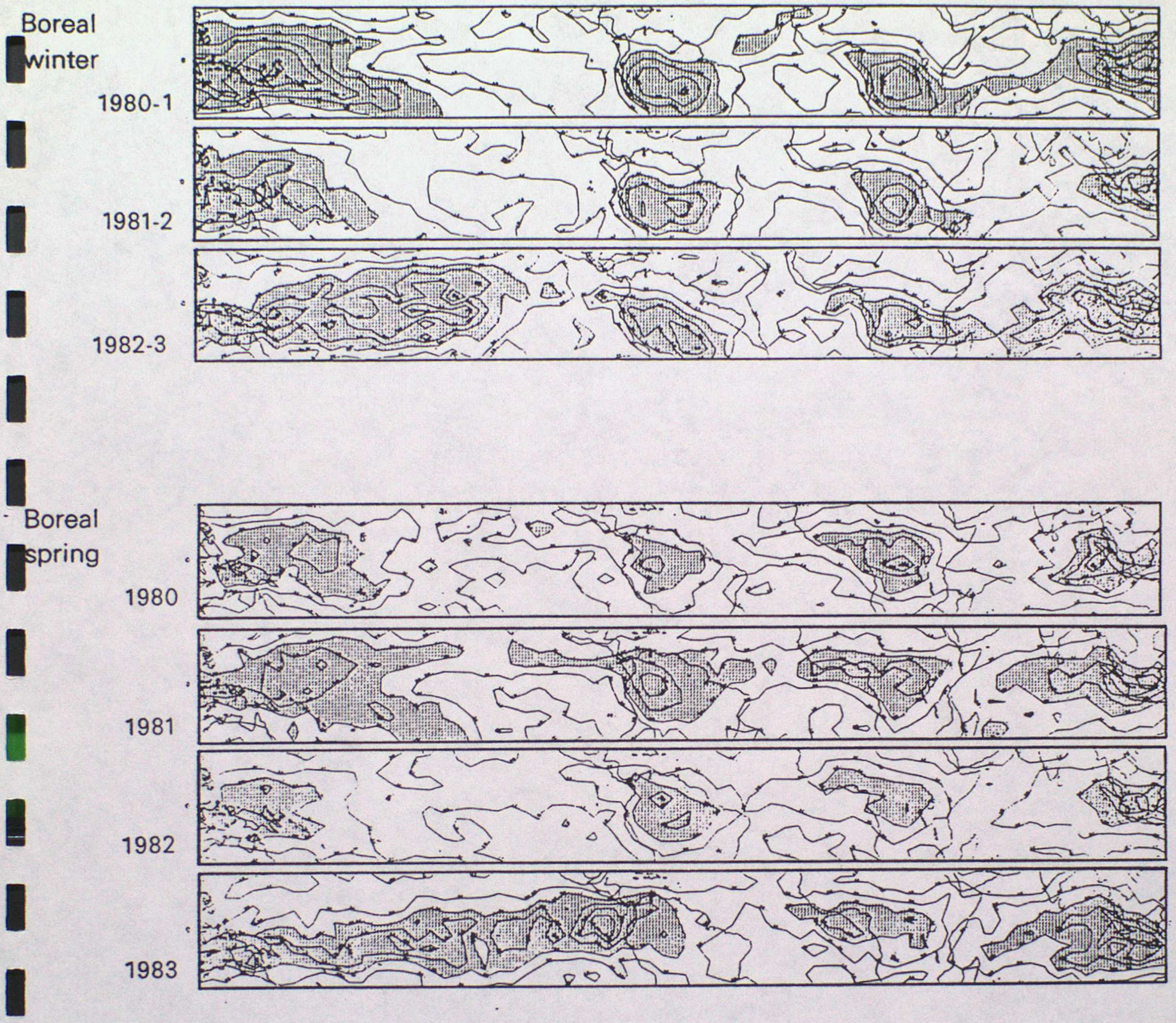
Boreal winter
1980-1
1981-2
1982-3
Boreal spring
1980
1981
1982
1983

Percentage cover of cloudtops with radiative temperatures less than 235° K. Contours drawn at 10% intervals. Areas of ⩾30% cloud cover are shaded.

Figure 6.19. From Newman (1984).

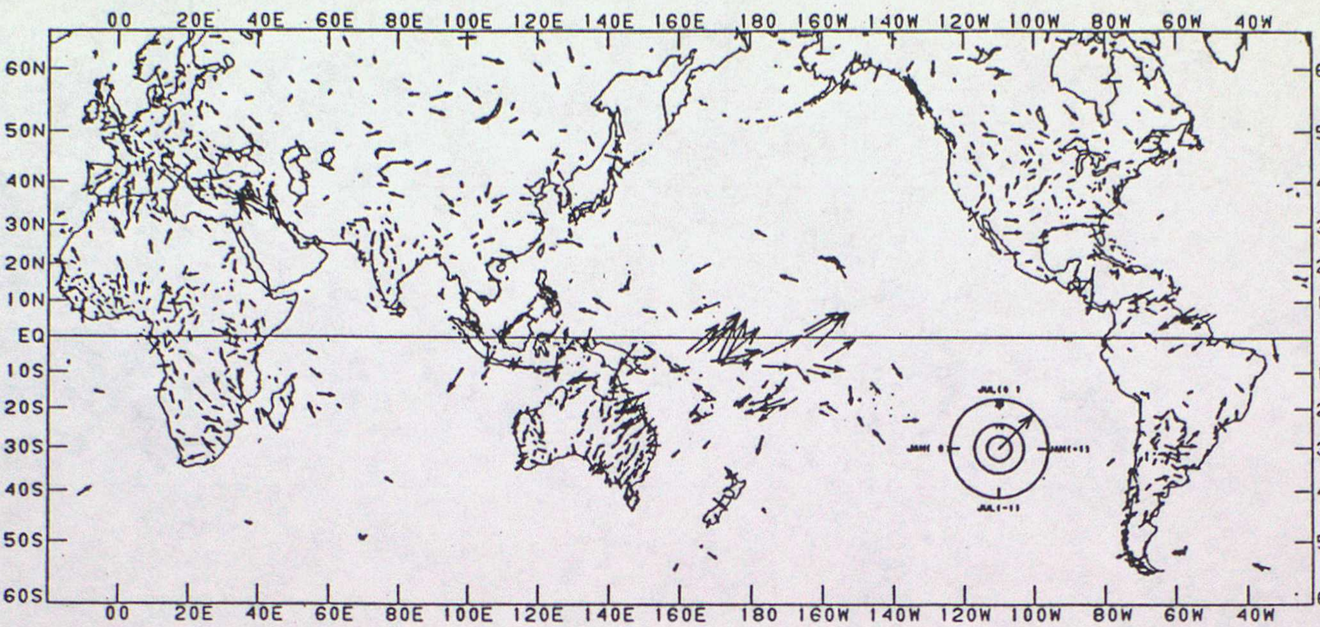
00
20E
40E
60E
80E
100E
120E
140E
160E
180
160W
140W
120W
100W
80W
60W
40W
60N
50N
40N
30N
20N
10N
EQ
10S
20S
30S
40S
50S
60S
JUL(0)
JAN(0)
JAN(+1)
JUL(-1)

The amplitudes and phases of ENSO composite ranked precipitation plotted as vectors. The vectors are based on a 24-month harmonic fitted to ranked precipitation composites for ENSO episodes. The phases and relative magnitudes of these vectors are indicated by the "vector clock" in the figure.

Figure 6.20 From Ropelewski and Halpert (1987).

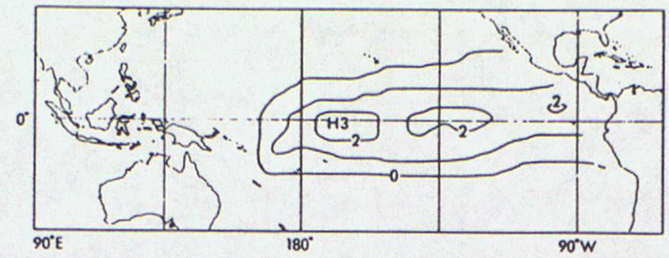
0°
H3
2
2
2
0
90°E
180°
90°W

Figure 6.21A. Composite El Nino SSTA (°C) used by Palmer and Mansfield (1986a).

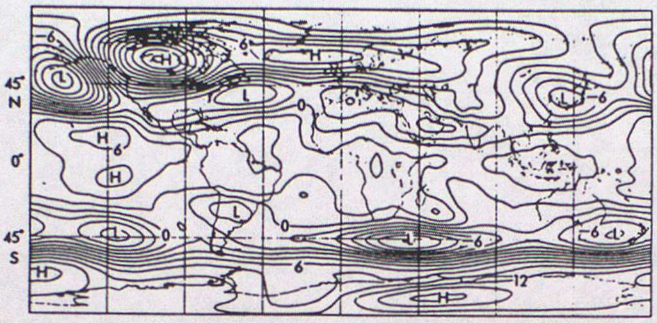
45°
N
0°
45°
S
H
L
6
0
12

Figure 6.21B. Anomalous 250mb height (dam) for above composite SSTA. From Palmer and Mansfield (1986a).

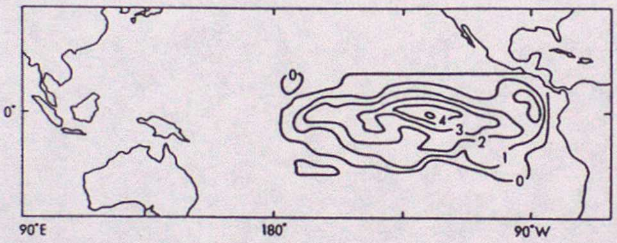
0°
4
3
2
1
0
90°E
180°
90°W

Figure 6.21C. El Nino SSTA (°C) for December 1982 used by Palmer and Mansfield (1986b).

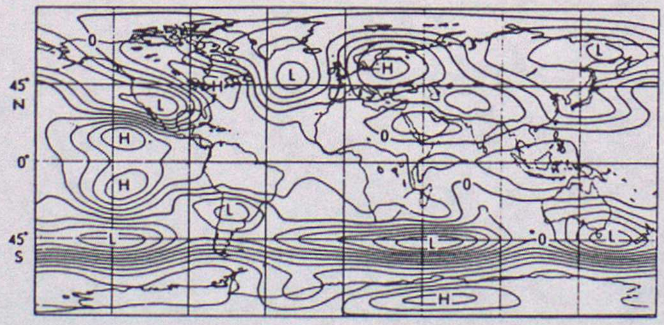
45°
N
0°
45°
S
H
L
0

Figure 6.21D. Anomalous 250mb height (contours every 2 dam) for SSTA in Figure 6.21C and envelope orography. From Palmer and Mansfield (1986b).

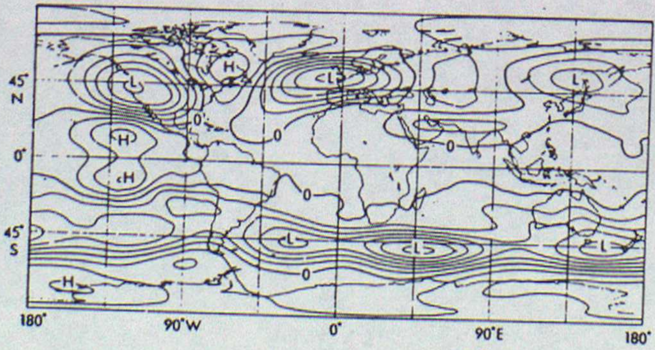
45°
N
0°
45°
S
H
L
0
180°
90°W
0°
90°E
180°

Figure 6.21E. As Fig. 6.21D but using standard orography.

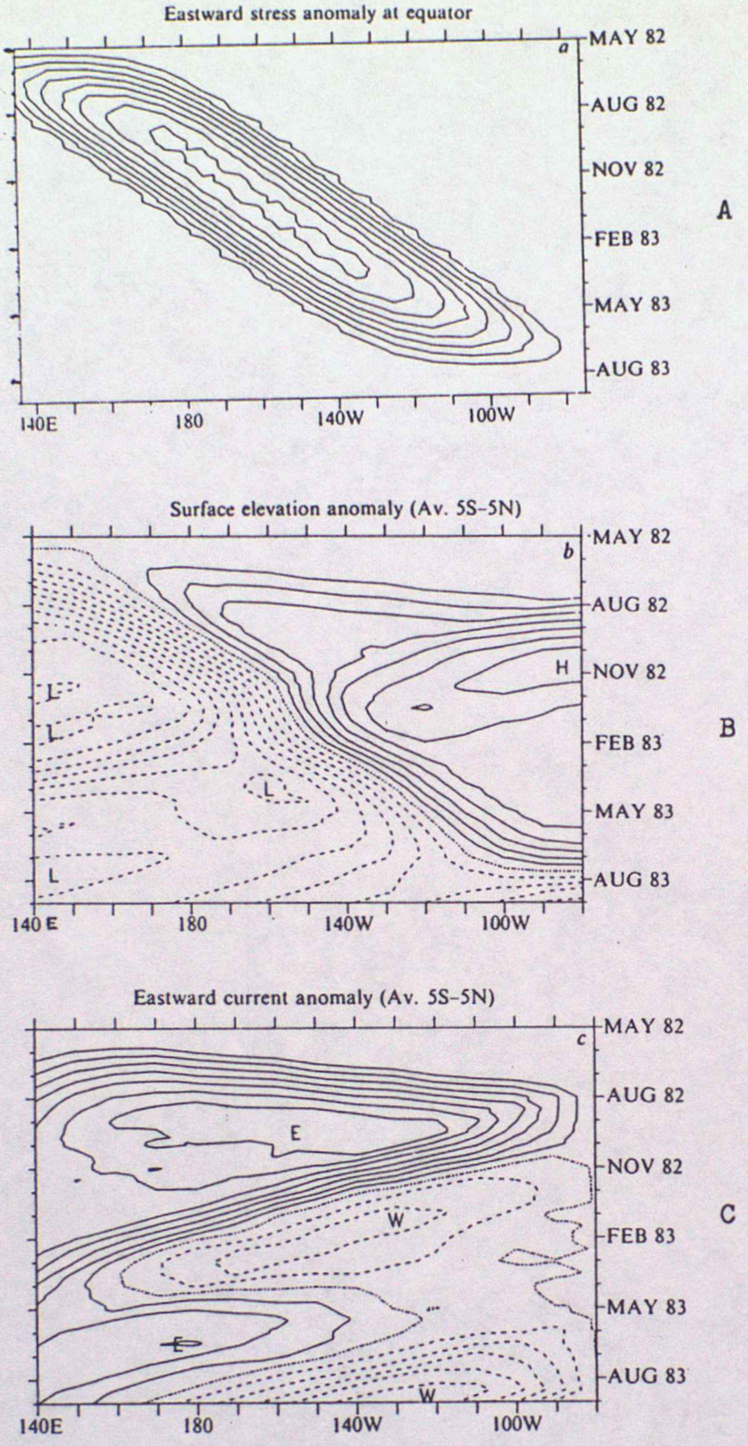

Longitude–time plots along the Equator of A, eastward stress anomaly, B, surface elevation and C, zonal surface current. Values are averages between 5° S and 5° N. B and C are the results of a model calculation in which A is the forcing function. Solid contours represent positive values and broken contours negative values.

Figure 6.22. From Gill and Rasmusson (1983).

SST anomalies (°C) averaged over the eastern equatorial Pacific NINO3 region (90° W to 150° W, 5° S to 5° N) for four periods centred on 1972, 1976, 1979 and 1982. Heavy curves, observed values as reported by CAC/NOAA (note repetition of vertical scale). Light curves, values from six forecasts initiated at 3-month intervals from the October two years ahead to the January of the nominal year. Dashed curve, average of the six forecasts (the consensus forecast).

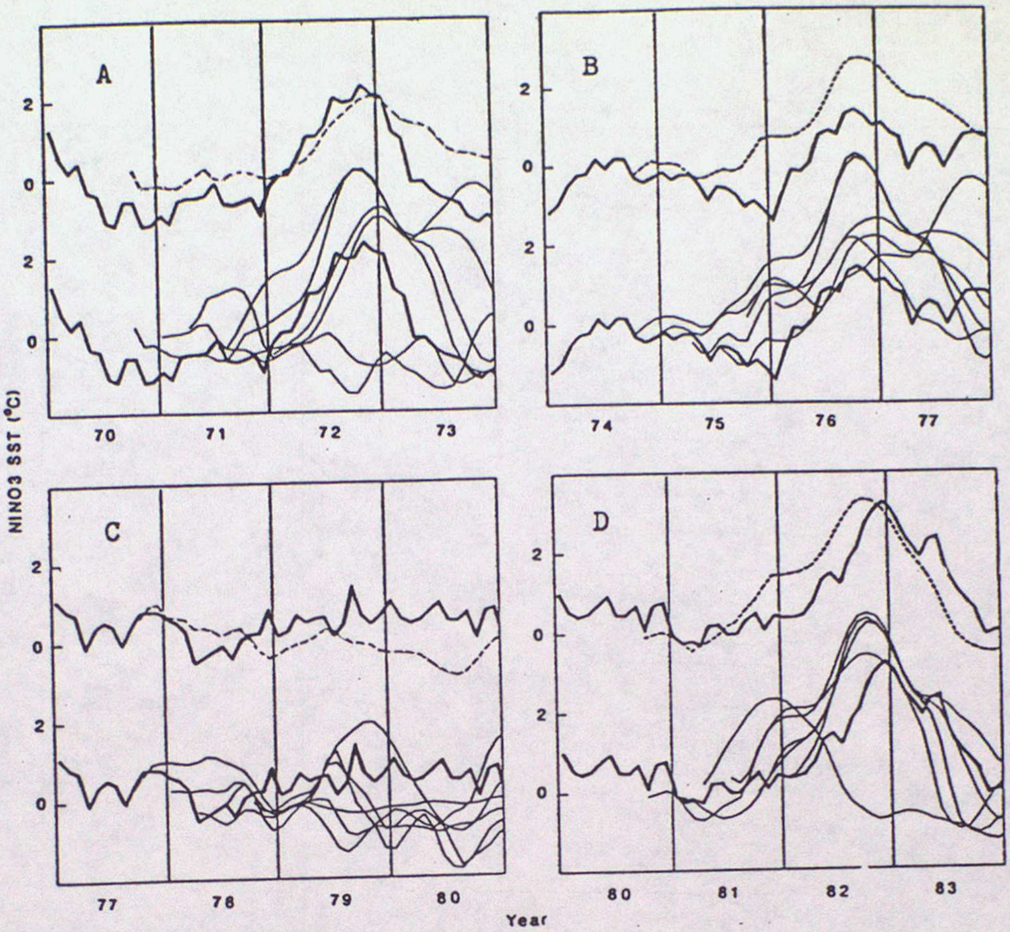

Figure 6.23 From Cane et al (1986).

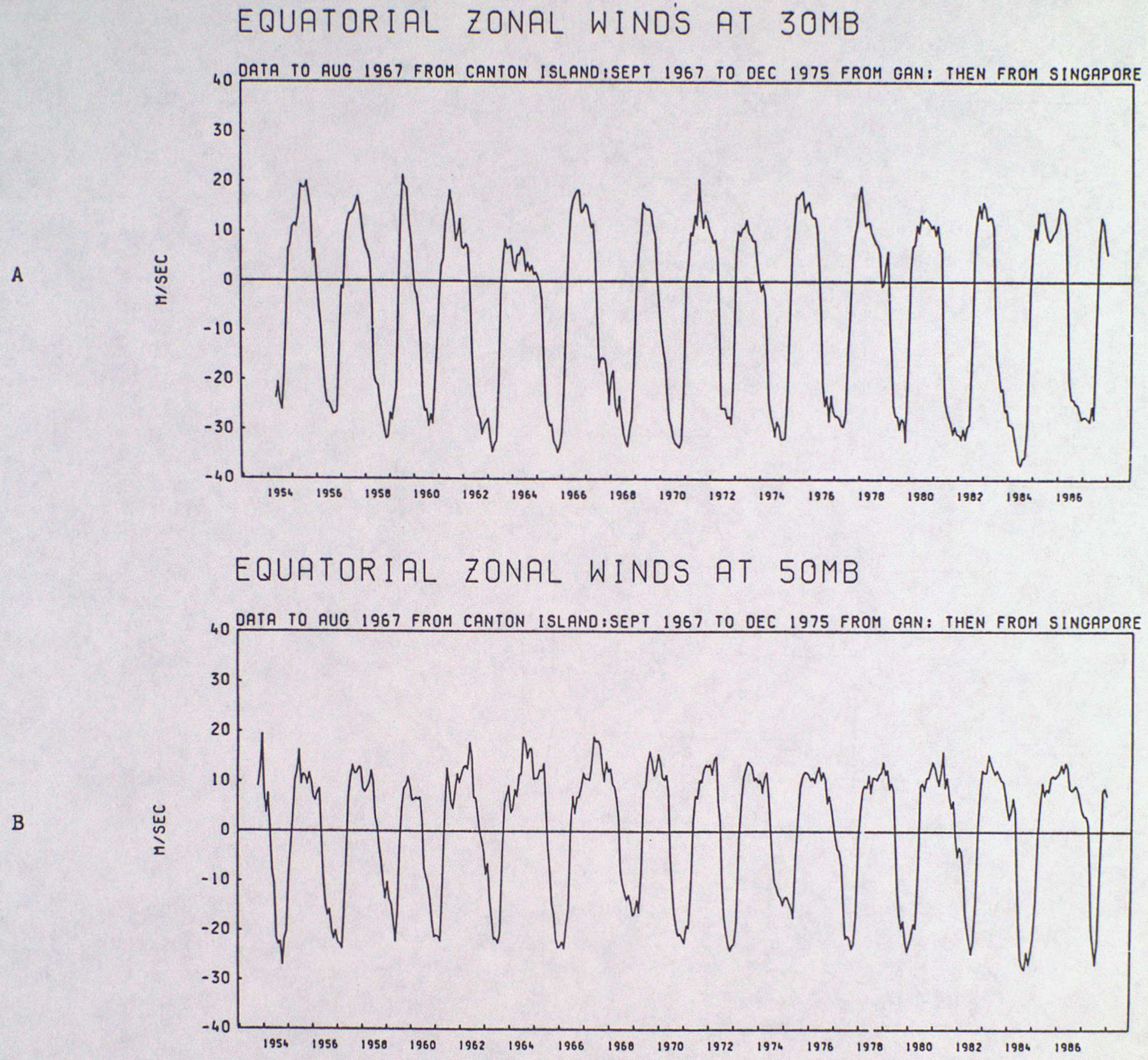
A
EQUATORIAL ZONAL WINDS AT 30MB
DATA TO AUG 1967 FROM CANTON ISLAND:SEPT 1967 TO DEC 1975 FROM GAN: THEN FROM SINGAPORE
M/SEC
40
30
20
10
0
-10
-20
-30
-40
1954
1956
1958
1960
1962
1964
1966
1968
1970
1972
1974
1976
1978
1980
1982
1984
1986
B
EQUATORIAL ZONAL WINDS AT 50MB
DATA TO AUG 1967 FROM CANTON ISLAND:SEPT 1967 TO DEC 1975 FROM GAN: THEN FROM SINGAPORE
M/SEC
40
30
20
10
0
-10
-20
-30
-40
1954
1956
1958
1960
1962
1964
1966
1968
1970
1972
1974
1976
1978
1980
1982
1984
1986

Figure 6.24.

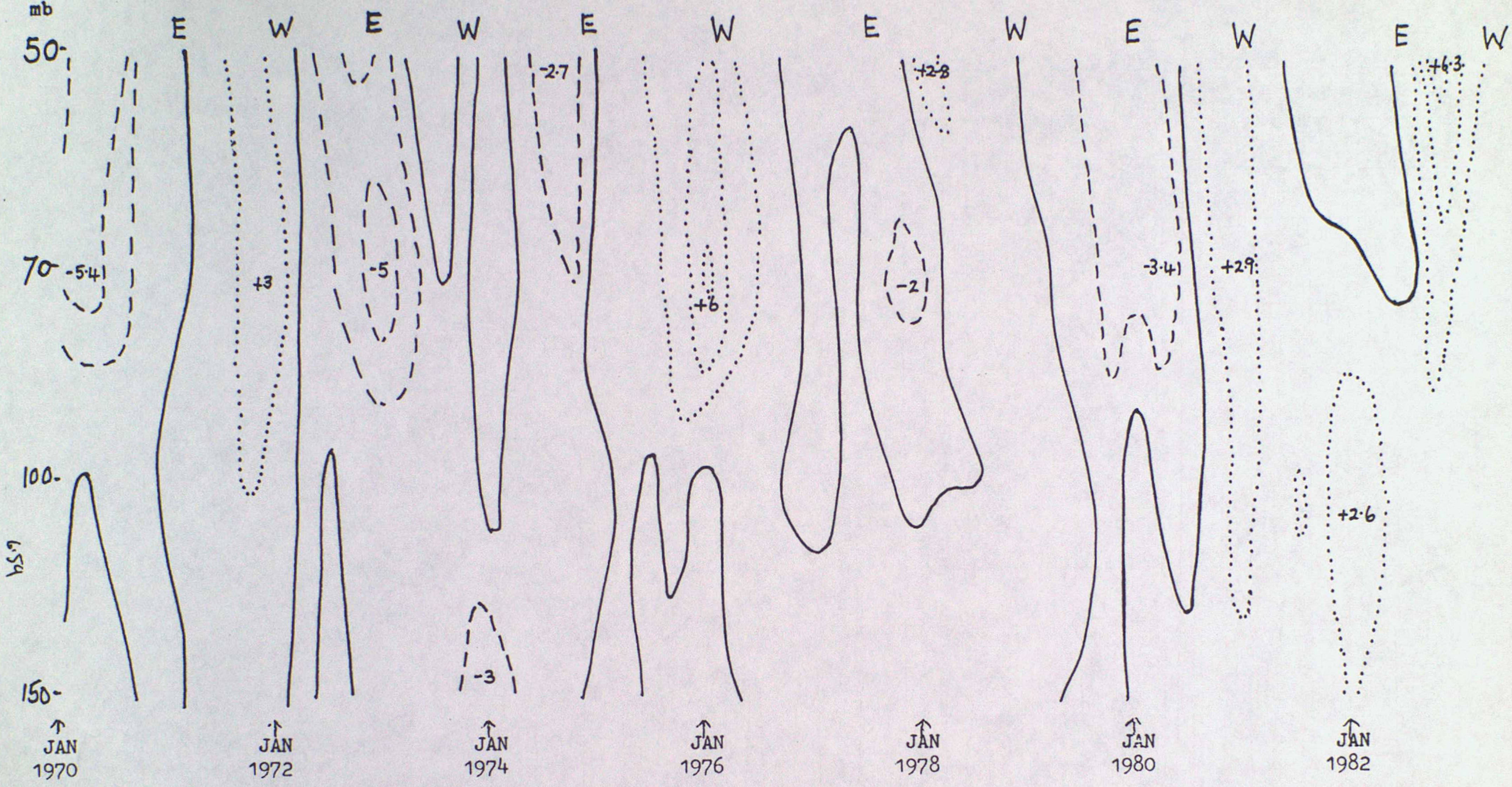

Figure 6.25. Temperature anomalies (w.r.t. 1971–80 average) over Singapore. Isotherms at 2°C intervals.

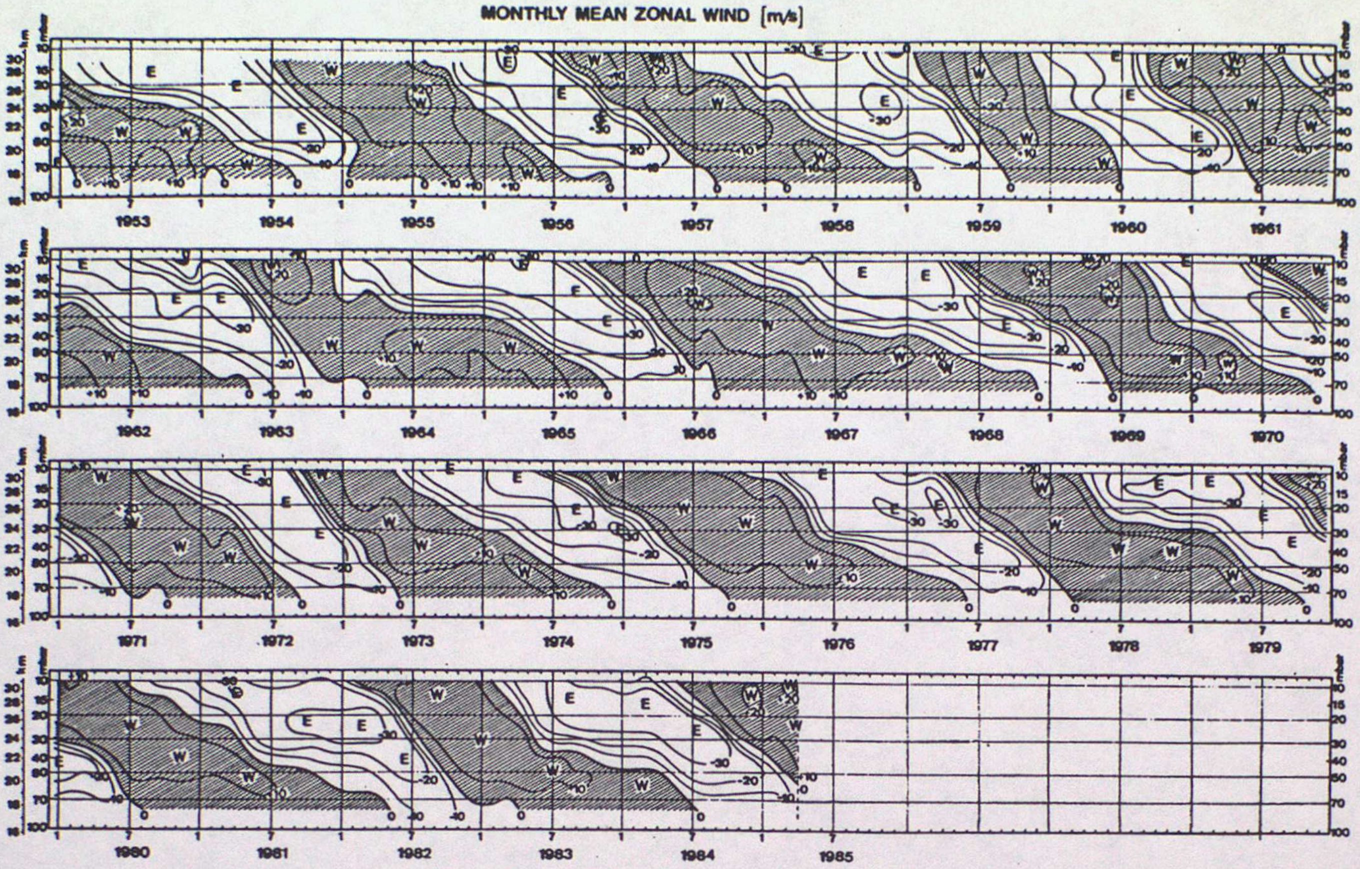

Time–height section of the monthly mean zonal wind components (m s^{-1}) at Canton Island (Jan 1953–Aug 1967), Gan/Maldive Islands (Sep 1967–Dec 1975), and Singapore (Jan 1976–Apr 1985).

Figure 6.26. From Naujokat (1986).

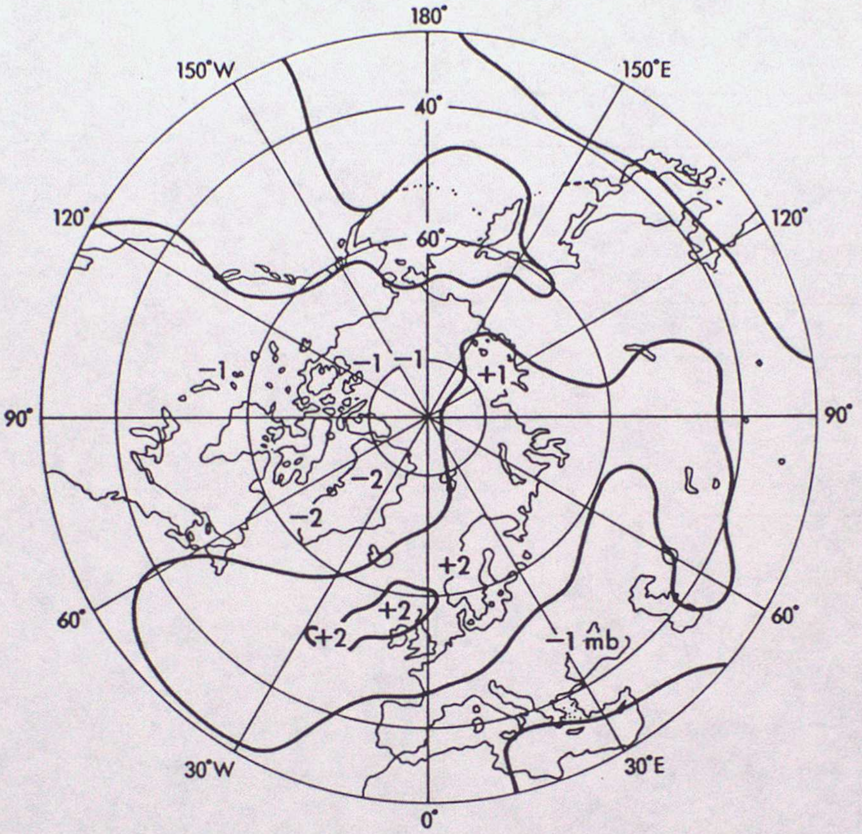
180°
150°W
150°E
40°
120°
120°
60°
−1
−1
−1
+1
90°
90°
−2
−2
+2
+2
+2
−1 mb
60°
60°
30°W
30°E
0°

Surface pressure anomaly from 1951—70 average, July.
After Ebdon (1975).
Mean of eight Julys with westerly phase of QBO at 30 mb.

Figure 6.27.

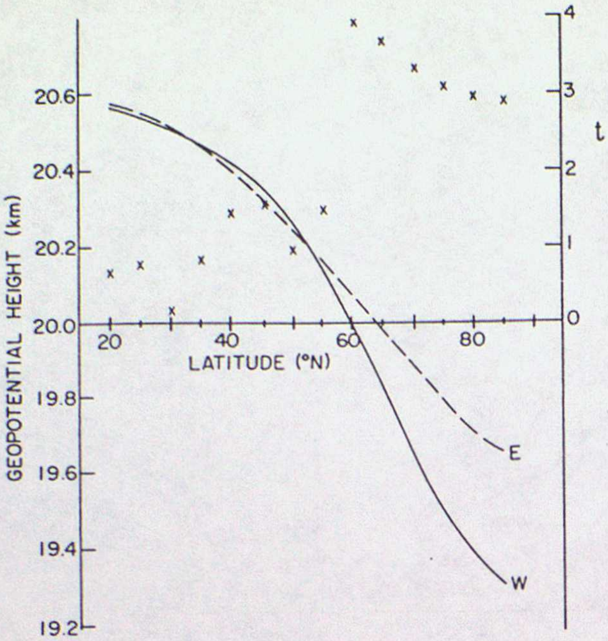

A. Composite meridional profiles of the zonal mean 50mb geopotential height for January to March. W and E denote westerly and easterly categories of equatorial 50mb QBO. Crosses denote Student's t values (right hand scale). t values of 2.16, 3.01, and 4.22 correspond t significance levels of 5%, 1% and 0.1% (13 degrees of freedom).

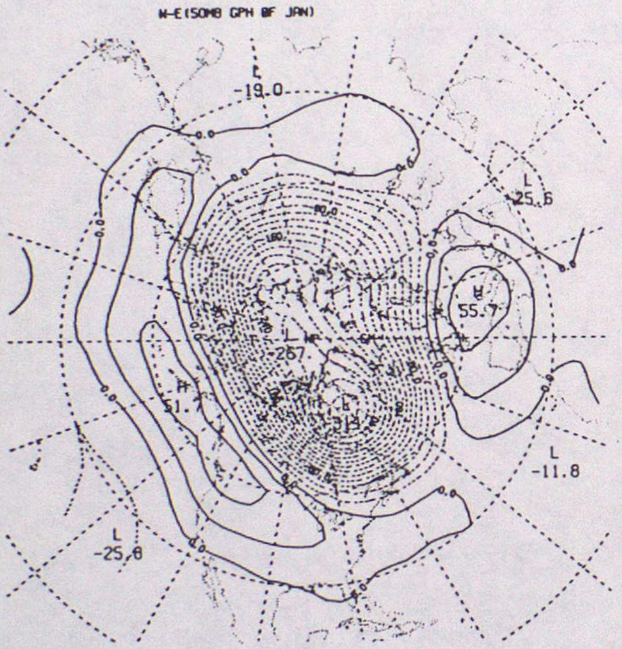
W-E(50MB GPH BF JAN)
L
-19.0
L
-25.6
H
55.7
L
-257
H
51.7
L
-11.8
L
-25.8
0.0

B. Monthly mean 50mb geopotential height difference (westerly minus easterly category of equatorial 50mb QBO) for January (gpm).

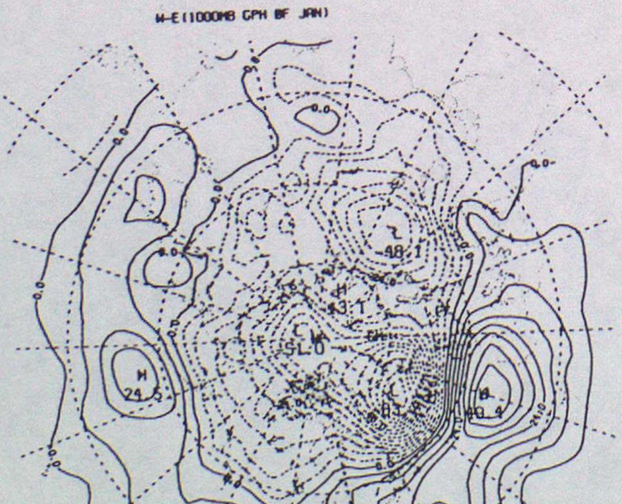
W-E(1000MB GPH BF JAN)
0.0
L
48.1
H
21.5
H
40.4
0.0

C. As B but for 1000mb geopotential height.

Figure 6.28. From Holton and Tan (1980).

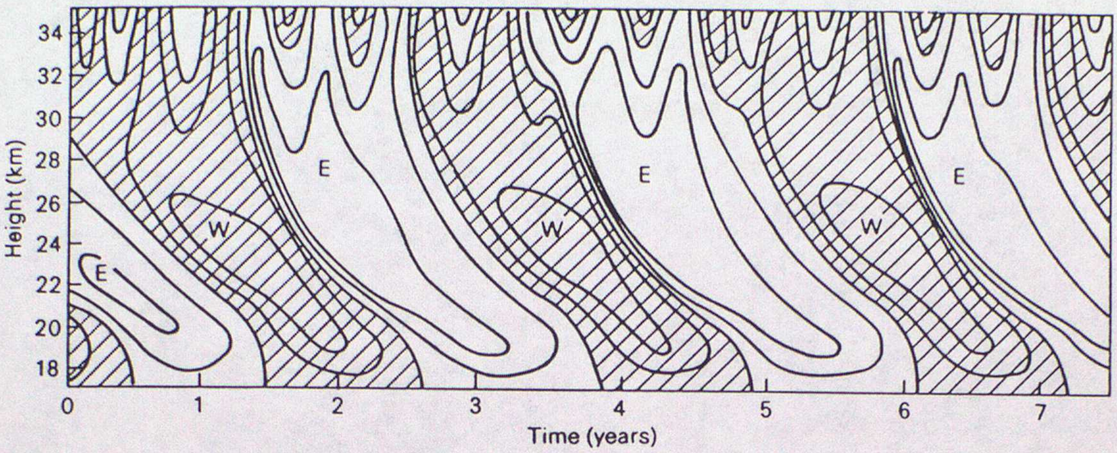

Time-height cross-section of mean zonal wind. After the model of Holton and Lindzen (1972).
Isopleths are drawn at 10 m s⁻¹ intervals.
Regions of westerly flow are shaded.

Figure 6.29.

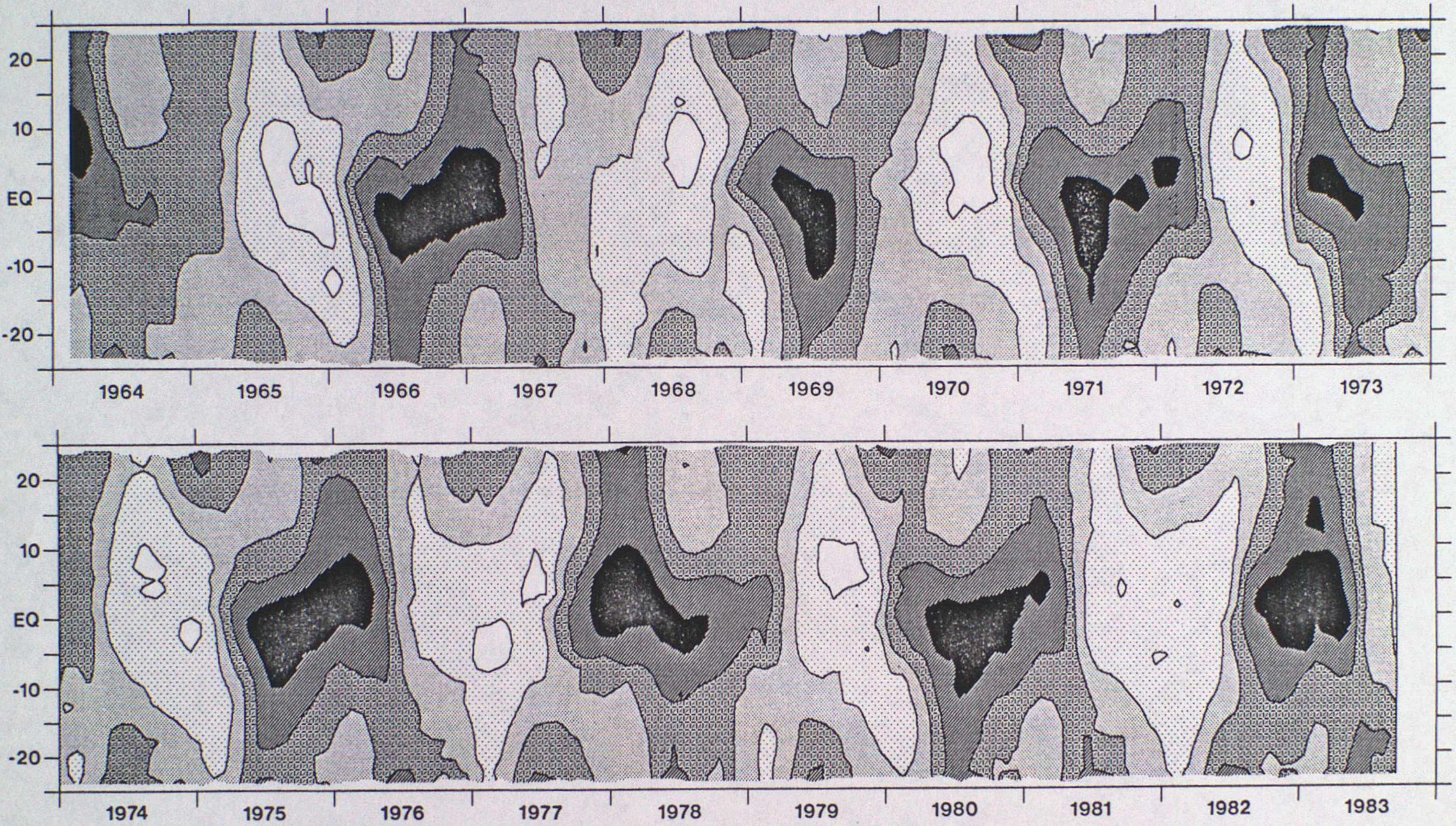

Latitude-time plot of monthly mean zonal wind at 30 mb. Shading interval is 10 m s^{-1}, proceeding from negative (light) values to positive (dark). White shading is for winds just below -30 m s^{-1}, and black indicates winds greater than 10 m s^{-1}. Computer plotting utilized a ¼–½–¼ smoothing in both latitude and time. (The zero wind line is the outer boundary of the diagonally striped region.)

Figure 6.30. From Dunkerton and Delisi (1985).

VELOCITY POTENTIAL (200MB) CONTOURS 30-50FILTER 06/09/79 12Z INT=.10E+07

VELOCITY POTENTIAL (200MB) CONTOURS 30-50FILTER 06/14/79 12Z INT=.10E+07

VELOCITY POTENTIAL (200MB) CONTOURS 30-50FILTER 06/19/79 12Z INT=.10E+07

VELOCITY POTENTIAL (200MB) CONTOURS 30-50FILTER 06/24/79 12Z INT=.10E+07

VELOCITY POTENTIAL (200MB) CONTOURS 30-50FILTER 06/29/79 12Z INT=.10E+07

VELOCITY POTENTIAL (200MB) CONTOURS 30-50FILTER 07/04/79 12Z INT=.10E+07

VELOCITY POTENTIAL (200MB) CONTOURS 30-50FILTER 07/09/79 12Z INT=.10E+07

VELOCITY POTENTIAL (200MB) CONTOURS 30-50FILTER 07/14/79 12Z INT=.10E+07

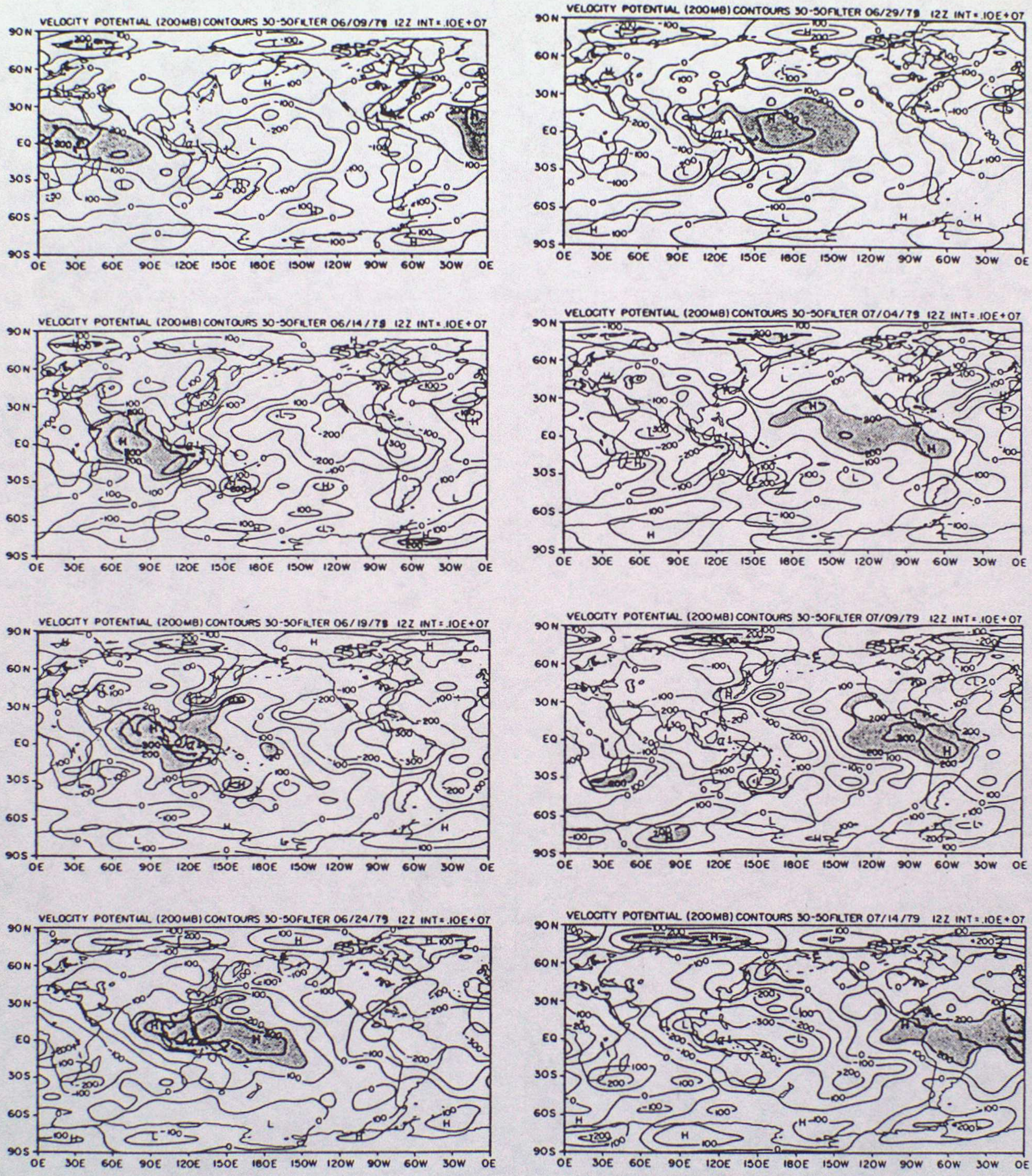

Velocity potential at 200 mb over the globe on the time scale of 30 to 50 days. The maps shown here cover the period 9 June through 14 July 1979 at intervals of 5 days. The isopleths are drawn at an interval of 100 × 10^4 m^2 s^{-1}. The shaded area shows values larger than 200 × 10^4 units. These are a subset of maps from the entire year of data.

Figure 6.31. From Krishnamurti et al (1985).

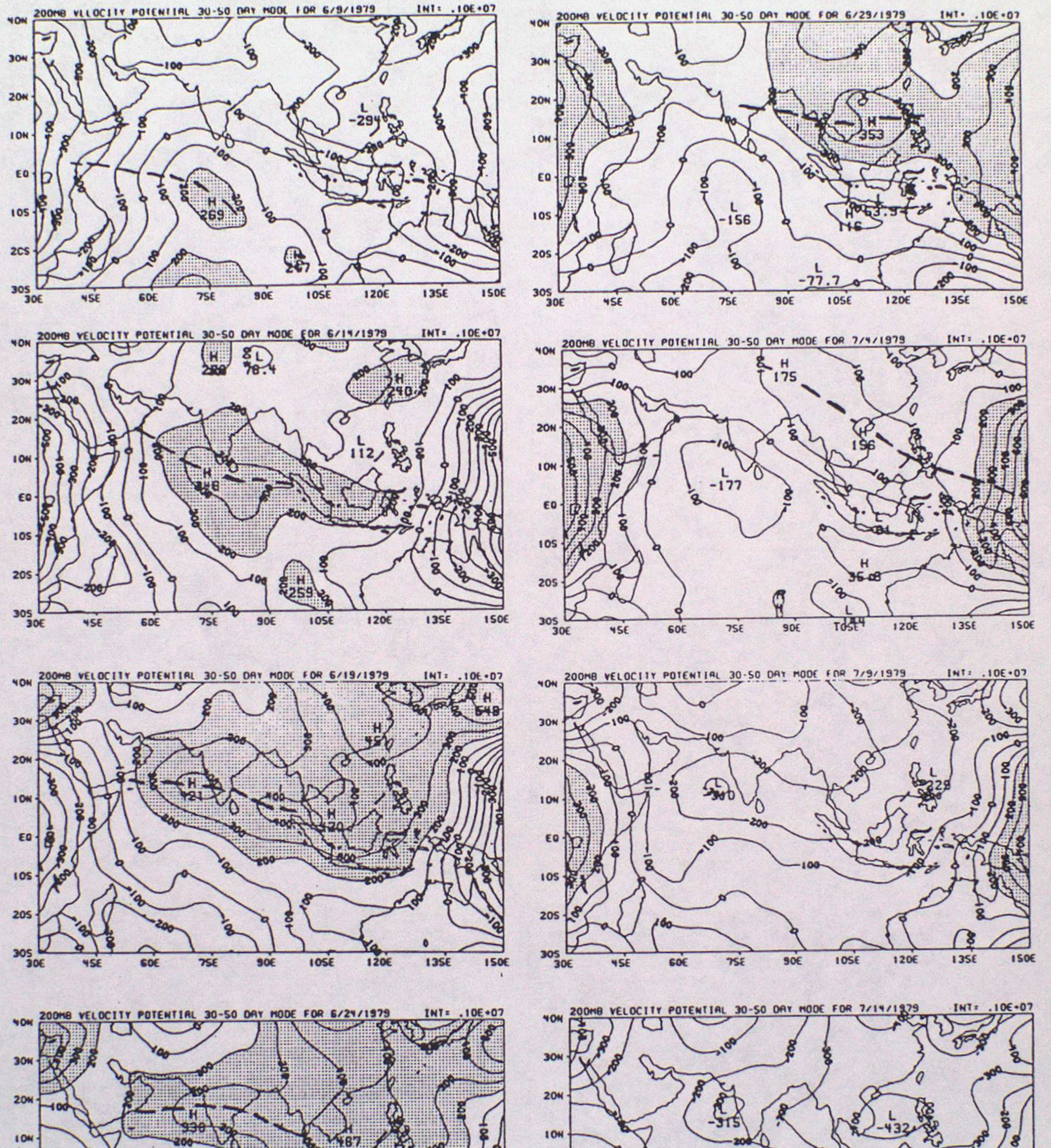
200MB VELOCITY POTENTIAL 30-50 DAY MODE FOR 6/9/1979 INT: .10E+07
200MB VELOCITY POTENTIAL 30-50 DAY MODE FOR 6/29/1979 INT: .10E+07
200MB VELOCITY POTENTIAL 30-50 DAY MODE FOR 6/14/1979 INT: .10E+07
200MB VELOCITY POTENTIAL 30-50 DAY MODE FOR 7/4/1979 INT: .10E+07
200MB VELOCITY POTENTIAL 30-50 DAY MODE FOR 6/19/1979 INT: .10E+07
200MB VELOCITY POTENTIAL 30-50 DAY MODE FOR 7/9/1979 INT: .10E+07
200MB VELOCITY POTENTIAL 30-50 DAY MODE FOR 6/24/1979 INT: .10E+07
200MB VELOCITY POTENTIAL 30-50 DAY MODE FOR 7/14/1979 INT: .10E+07

Velocity potential at 200 mb, for the MONEX region based on a high resolution data set, on the time scale of 30 to 50 days. The maps shown here cover the period 9 June through 14 July 1979 at intervals of 5 days. The isopleths are drawn at an interval of 100 × 10^4 m^2 s^{-1}. The shaded area shows values larger than 200 × 10^4. These are a subset of maps from the entire year of data.

Figure 6.32. From Krishnamurti et al (1985).

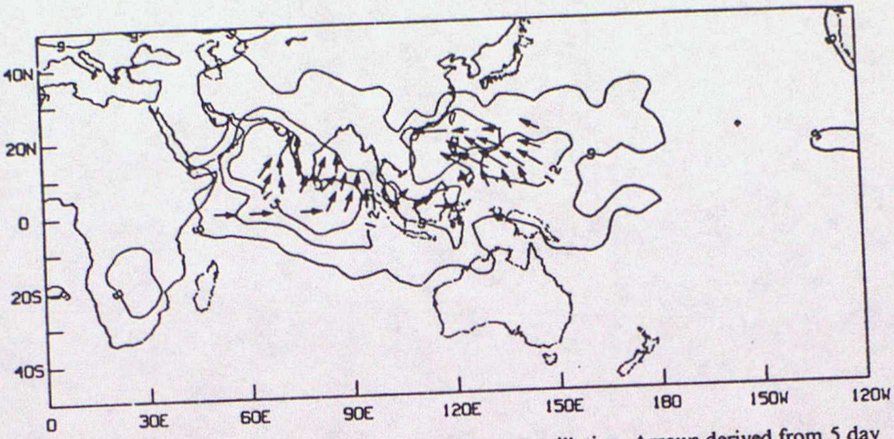
40N
20N
0
20S
40S
0
30E
60E
90E
120E
150E
180
150W
120W
9

Percentage variance distribution of 40–50 day oscillation. Arrows derived from 5 day lag correlations indicate tendencies of OLR anomaly propagation.

Figure 6.33. From Lau and Chan (1986).

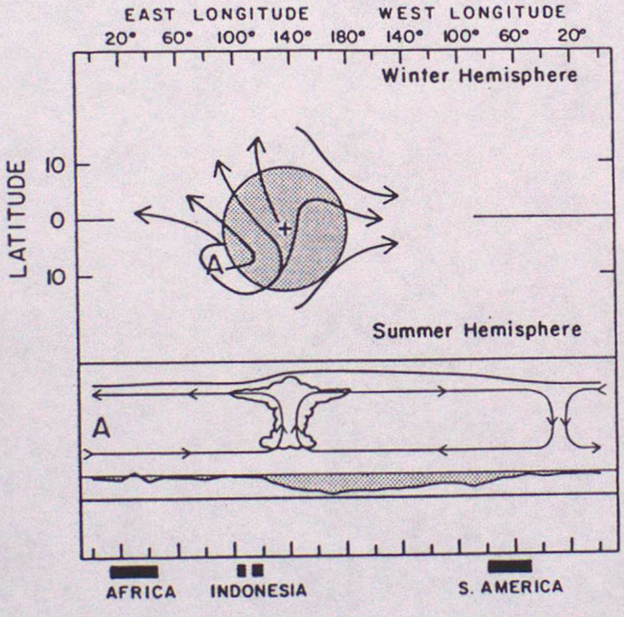
EAST LONGITUDE
WEST LONGITUDE
20°
60°
100°
140°
180°
140°
100°
60°
20°
Winter Hemisphere
LATITUDE
10
0
10
A
+
Summer Hemisphere
A
AFRICA
INDONESIA
S. AMERICA

Schematic depiction of the structure of the 40–50 day oscillation at a time of large amplitude. The lower panel represents the structure in the equatorial plane. Shading at the bottom represents the negative pressure anomalies. The line at the top of the lower panel represents the tropopause. The upper panel is a plan view of the disturbance in the upper troposphere. The shaded area there corresponds to a positive anomaly in convection that is centered in the summer hemisphere.

Figure 6.34. From Madden(1986).

A REVIEW OF PALAEOCLIMATE FROM THE EARLY EARTH TO THE PLEISTOCENE ICE AGES

C K FOLLAND AND D E PARKER

MET O 13

SUMMARY

This lecture concentrates on selected aspects of past climate, which have been chosen either because our knowledge is most secure, or to illustrate particular techniques used to establish and date past eras and events. The evidence for, and climatic implications of, continental drift are reviewed briefly. After an introductory discussion of climate in the Tertiary, a more detailed account of the Pleistocene ice ages is given, along with an explanation in terms of the Milankovitch hypothesis for the modulation of the ice ages by radiation changes associated with regular variations of the earth's orbit on time-scales of 10^4 to 10^6 years. The results of numerical model experiments designed to simulate the peak of the most recent glaciation are presented. Particular methods used in palaeoclimatology and reviewed here are magnetic dating and the oxygen isotope method for deducing past global ice volume, ocean temperature, and air temperature over ice sheets.

7.1 INTRODUCTION

Lectures 7-9 are concerned with the history of the Earth's climate. The subject is vast and we shall concentrate on selected aspects which are either particularly interesting or most securely known. The further one goes back into the past, the more fragmented the evidence for past climates becomes and it is difficult to establish whether the evidence for a particular climatic feature is really synchronous in time. The level of confidence concerning past climates can thus never be as high as for today's climate, and many of the deductions depend on combinations of disparate strands of evidence, bound together sometimes by a measure of circular argument. The recent use of AGCM's to study specific aspects of past climates has tended to support empirical reconstructions; so the joint use of observations and models points the way to improvements in our understanding of the remarkable changes of climate that have occurred during the long history of the earth.

7.2 THE FAINT SUN PARADOX

Fig 7.1, from Lamb (1977), shows the characteristic time-scales over which some influences on climate operate. The first difficulty one meets is that of solar variability. Astronomers are convinced from theory and from observation of other stars that solar luminosity has increased in the way shown in Fig 7.2. The age of the sun is placed near 4.7 billion years (b.y.) and the age of the earth at 4.5-4.65 b.y. An increase of solar constant, Q, of about 15% since the first recorded ice-age at about 2,250 m.y. million years ago (m.y) is embarassingly large. Fig A10.13, in Appendix I to this set of lectures (with Lecture 10), which is derived from an energy-balance model, suggests that, other things being equal, the early Earth should have been covered in ice and should not yet have escaped this fate. Compensating mechanisms that would have increased the past surface temperature include a different composition of the Earth's atmosphere, i.e. less oxygen and much more carbon dioxide. A much increased transport of heat from equator to pole or an increased flux of geothermal heat could presumably also have provided less favourable conditions in high latitudes for the onset of glaciation. The latter possibility is not now thought to be significant.

Endal and Schatten (1982) used a simple energy-balance climate model due to North (1975) (See also Appendix I to this set of lectures) to see if an ice-covered earth could be avoided with today's atmospheric composition if they increased a parameter D that is used in North's model to represent eddy diffusion of heat across latitude circles. Fig 7.3 shows some results which have some complex features; X_s is the sine of the latitude of the ice edge in both hemispheres. Concentrating on D = infinity, an ice-free earth is just possible for $Q/Q_0 = 0.81$ (Q_0 = today's solar constant). The slope of the line for D = infinity, and adjacent lines, is negative so once ice forms, the model solution jumps to a completely ice-covered earth. An extra atmospheric greenhouse effect would obviously have helped to increase temperature, but would have needed to have been very large 2,000 million years ago and to have declined since that time at a rather precise rate to have avoided a later "white" earth catastrophe.

7.3 EVIDENCE FOR CLIMATE OF THE EARTH 2500-200 M.Y

Fig 7.4, taken from Lamb (1977) lists the geological eras, their divisions into periods and their sub-divisions into epochs. Fig 7.4 also summarises some opinions about past climates. Fig 7.5 gives a simpler summary of the likely times of ice-age cycles.

7.3.1 Dating ancient rocks - how do we know when geological features were formed?

Dating past rock formations is complex and a main preoccupation of geology. For the ancient past, the relative ages of rocks can be estimated by stratigraphy, i.e. by studying the order in which the rocks were laid down. Absolute dating requires measurements of the proportions of various radio-active isotopes existing in the rocks, so that use of a specific method depends on whether a given chemical element exists in the rock. For example, the decay of the radioactive isotope of potassium ^{40}K to ^{40}A has a half-life of 1.3×10^9 years. So measurements of the amount of argon gas trapped in the rock expressed as a ratio of the amount of ^{40}K still remaining can be used to date some ancient rocks. The date estimated is the time of their solidification; while they were liquid the argon will, it is assumed, have escaped. Extremely old rocks can sometimes be dated using the decay of ^{87}Rb to ^{87}Sr (the rubidium-strontium method); the half-life of this decay is very long: 53×10^9 years. For details of other methods see Lamb (1977), pp 68-71.

7.3.2 Earliest evidence of past climate

The first half of the Earth's history has left rather little evidence in its rocks but the second half is increasingly rich in indications of past conditions. For most of the Earth's more recent history the climates have been warmer than now, but there is much evidence that from time to time the climate has cooled, at least in some parts of the world. The earliest record of glaciation is the Huronian of about 2250 million years ago (Harland and Herod (1975)) discovered in the USA in the region of Lake Huron. There is little evidence of glaciation in the next 1000 million years but the Precambrian period of 950-650 million years ago produces evidence of (perhaps) three widespread glaciations down to quite low latitudes.

Harland and Herod (1975) discuss the Precambrian glaciations but it is difficult to make reliable deductions as the relative proportions and extent of the continents at that time are not well known. However, Harland and Herod believe that the Precambrian ice-sheets have at least approached the equator so there is a possibility that a close approach (surely not reached!) to a "white" Earth occurred at that time.

7.3.3 Cambrian (500 m.y.) to Permian (200 m.y.) times

Understanding of this period of Earth's history has been revolutionised in the last few decades by the ideas of continental drift and plate tectonics. A lively account is given by Tarling and Tarling (1974). Some details remain controversial, but the crucial step that converted speculations about the meaning of the remarkable geometrical fits between various continents (especially if their shapes were measured near the edges of the continental shelves) into an almost universally accepted theory of continental drift involved the measurement of remanent palaeomagnetism in ancient rocks. When rocks containing iron cool, they retain a remanent magnetism that reflects the local magnetic field at that time, i.e. the angle of dip, magnetic north vector, etc. From time to time, geologically very sudden changes in the direction of the remanent magnetic field occur, usually by 180°. This indicates a recurring total reversal of the earth's magnetic field. These reversals can be followed in many continental rocks; the last reversal occurred about 730,000 years ago. Even more convincingly, these ancient magnetic fields are preserved with great clarity in the basaltic ocean floors as a series of magnetic stripes so that each stripe is reversed in polarity by 180° with respect to adjacent stripes. These observations indicate that the ocean floor is continually being formed by spreading out from the observed volcanically active (submerged) mid-ocean ridges. The convective cells in the Earth's mantle that cause the sea-floor spreading also provide the energy to move the continents or at least individual continental blocks known as "plates". It is possible to fix the latitudes of the plates in ancient times by measuring the remanent palaeomagnetic vectors using a magnetometer, and assuming that Earth's magnetic poles were always near the geographical poles. The reconstruction of palaeogeography is, of course, only completed when the rocks are dated.

Fig 7.6(A) (B) and (C) give reconstructions of the continents 480 m.y., 360 m.y., 240 m.y. 120 m.y. and 60 m.y from Smith et al (1981). The values denoted by "alpha-95" in the headings are likely error estimates in the form of 95% confidence limits on the positions of the poles relative to the continents in great-circle degrees. N denotes the number of independent palaeomagnetic studies used in the reconstructions. The changing positions of the continents are likely to affect climate:-

(a) Locally, because the latitude of a given location changes. Fig 7.6 shows that England both "existed" and was probably near 10°S at 360 m.y., 10°N at 240 m.y. and 40°N at 60 m.y.

(b) Because the global proportion of land in higher and lower latitudes progressively changes.

(c) Because, the meridional heat flux (equivalent to D in Fig 7.3) should change with the changing ocean currents and atmospheric circulation resulting from (b).

Fig 7.7, taken from Sellers and Meadows (1975), shows how the broad pattern of ice ages shown in Fig 7.5 is reflected in variations in the fraction of latitudes higher than 60°N or 60°S estimated to have been occupied by land. So glaciation may require a large land surface in high latitudes whose albedo can be increased by snow and eventually by ice, but some mechanism for delivering large quantities of precipitation to these surfaces over long periods is also needed. Crowley et al (1987) used a two-dimensional (horizontal plane) seasonal energy balance model to show that glaciation may require a near-coastal, as opposed to inner-continental, pole, because only the former would result in sufficiently low summer time temperatures.

Figs 7.8 and 7.9 show two reconstructions of past glaciations:-

(a) Ordovician times (about 450 m.y.)

(b) In Permo-Carboniferous times (about 250 m.y.)

The Ordovician ice age affected the Sahara (Fig 7.8) and parts of S America. Before the widespread acceptance of continental drift, this glaciation posed a severe problem to climatologists who had to invent a climate with an equatorial ice cap and no high latitude ice caps. Brooks (1949) proposed an elaborate theory of a world containing an ice cap in equatorial regions only. The evidence for the Ordovician ice age is strong, with eroded but recognisable geological features which are widespread in parts of the dry Sahara eg in the Tibesti Mountains; the remnants include U-shaped valleys, glacial moraines etc. Note the near coastal south pole at 480 m.y in Figure 7.6A. The subsequent Permo-Carboniferous ice age affected Antarctica, Australia and southern India as well as S America and southern Africa. In fact, Antarctica has probably remained quite close to the S Pole since that time (Fig 7.6), and, given the difficulty of obtaining evidence from Antarctica, it is not absolutely clear whether deglaciation has ever been complete since

Permo-Carboniferous times. Finally both glacial periods show signs of interglacials, as in the recent ice age, but the geological evidence is only capable of showing gross fluctuations.

7.3.4 Cosmic theories of ice ages

The apparently rhythmic nature of the 3 or 4 Ice Age epochs since the Precambrian has prompted theories about their possible cosmic origins. Cosmic factors would now be regarded as additional to those involving continental drift.

One theory due to Urey (see Opik (1965)) suggests that the sun varies in its radiation output as it goes round the galactic centre. This would produce variations on time scales of 250 million years. Another theory (due to McCrae),which would produce variations on the same time-scale, suggests that, as the solar system orbits around the centre of our galaxy, it passes through galactic dust clouds which reduce the solar radiation reaching the earth (Opik (1965)). These dust clouds are not now evident so this theory would indicate that the most recent ice age epoch has finished.

7.4 THE MESOZOIC ERA AND THE CENOZOIC ERA, BEFORE THE PLEISTOCENE EPOCH (200-3 M.Y)

7.4.1 Mesozoic era

This era was the heyday of the dinosaurs. Fig 7.6B indicates that both Poles were open or virtually open to the global ocean circulation: considerable evidence of warm climates has been found, though there is also evidence of transport of erratic deposits by ice-rafting at high palaeolatitudes in both hemispheres in the Jurassic and the Cretaceous (Frakes and Francis (1988)). This was a period when limestone rocks were laid down, many of which show a banded structure with depth; evidence has started to accumulate that these structures are associated with Milankovitch radiation variations. The latter part of this period is mysterious; quite suddenly the dinosaurs and many other animals died out in what appeared to be mass extinctions. There is accumulating geological evidence of a volcanic or meteoric "glassy" layer in the rocks in several parts of the world dated at about 65 m.y. So it is possible that massive volcanism or an impact with a giant meteorite may have occured, perhaps causing mass extinctions via the "nuclear winter" effect. If so, the climate did not change for long enough for the evidence to have survived, and no ice-age resulted. In fact Rampino and Volk (1988) have linked a climatic warming with these major extinctions, by invoking a reduction of cloud albedo as a result of a decrease in biogenic sulphurous condensation nuclei in the atmosphere.

7.4.2 Cenozoic Era - Tertiary period

The Tertiary provides the first quantitative evidence for the values of oceanic temperatures. The main tool is the measurement of the quantity of the isotope of oxygen ^{18}O in marine foraminifera, which are types of plankton whose ancient shells are found on the ocean bed. Annex I to this lecture describes the oxygen isotope method of measuring palaeotemperatures. The shells are made of calcium carbonate and Fig 7.10 shows an example: the species globorotalia menardii. We shall discuss these types of measurement in the next section, but remark here that the ^{18}O method requires measurement of the ratio of $^{18}O/^{16}O$ in the calcarious shells of the foraminifera. Unfortunately, this ratio depends not only on oceanic temperature but also on whether the oxygen isotope ratio in the oceans also changes. Such changes would occur if glaciers formed on land: the concentration of ^{18}O would rise in the oceans as the glaciers developed. The exact interpretation of specific cases of changes of foraminiferal ^{18}O is often a matter of debate (e.g. Labeyrie et al (1987); Mix and Pisias (1988)).

Over the last 30 years or so the USA Deep-sea Drilling Project has provided many deep-sea sedimentary cores containing these shells. Because the length of the cores that can be extracted from the ocean bed is currently limited to about 20 m, areas of the deep ocean which have a very low sedimentation rate are required for measuring temperature profiles through the long time interval encompassed by the Tertiary. Dating of these cores can sometimes be done using the magnetic reversals mentioned above. In addition, the relative proportions of different planktonic species in the sediments and whether certain species are present or not can be used as a guide to past sea temperatures, assuming that present-day relationships are valid. However this becomes more difficult for the Tertiary because some species have changed since that time. The sea temperatures which the planktonic shells represent depend, of course, on the depth at which the plankton lived. Some lived near the surface but other forms lived at great depths and these must be correctly identified. Errors can arise if changes occurred in the depth at which particular species lived. Fig 7.11 is a generalised picture of the variation of Tertiary worldwide tropical ocean temperatures deduced by several workers from such cores. This interpretation has been challenged (Matthews and Poore (1980)) and alternative explanations of these measurements include a period of low tropical SST with no ice or a period of high tropical SST with a considerable amount of land ice. Fig 7.12 shows other estimates of climatic variations through the Tertiary including suggestions of a gradual reduction in temperatures towards the present. About 30 m.y., Antarctica and S America drifted far enough apart so that the Drake Passage between them opened up sufficiently for a free flow of ocean water. This is thought to have changed the ocean circulation and helped to give rise to a gradual reduction in ocean bottom water temperatures. There is considerable evidence of glaciation in Antarctica from about 17 m.y. (Frakes (1978)) and it is now thought that Antarctica has remained partially or wholly glaciated since that time, though there is faunal and floral evidence for a major deglaciation in the Pliocene (late Tertiary): see the discussion in the review by Weller et al (1987).

7.5 THE QUATERNARY (PLEISTOCENE) ICE AGES (FROM ABOUT 3 M.Y.-15000 BP)

Imbrie and Imbrie (1979) contains an easy-to-read account of the history of the evidence of, and ideas about the Ice Ages. In the last decade or so there have been two major developments in ideas:-

(a) Evidence is now strong that the Glacial/Interglacial oscillations have been almost regular on a 100,000 year time scale for the last 800 k.y. and possibly for considerably longer. This regularity has been shown to be empirically related to the Milankovitch radiation variations discussed in Lecture 3. So theories that require random internal variations of the climate system to be the prime initiators of ice ages do not seem to be correct, even if "random changes" play a subsidiary role.

(b) Recent calculations using GCM's suggest that Milankovitch radiation variations are of sufficient size to affect the integrations strongly. However it has not yet been possible to work out the causes of the formation and destruction of the ice age continental ice sheets in any detail, though a number of "simple" models of ice sheets have been constructed, giving a variety of results.

So although many influences have undoubtedly been at work, the Milankovitch radiation variations can probably be regarded as the "pace-makers" of the ice ages. The evidence for this contention will be reviewed briefly. Cnanges in oceanic circulation and in atmospheric carbon dioxide concentration will also be discussed. Finally some GCM integrations carried out for Ice Age radiation conditions will be discussed to sum up the problems and prospects.

7.5.1 Empirical evidence for Milankovitch effects

7.5.1.1 The Wrong Evidence

Until fairly recently, a major problem was that crucial observational evidence concerning the timing of past ice ages was wrongly interpreted (Imbrie and Imbrie (1979)). Fig 7.13 is a diagram of the "four Pleistocene ice ages" which you may have heard about at school - the Gunz, Mindel, Riss, and Wurm ice ages which were worked out by Penck and Bruckner early this century (Imbrie (1982)). It has been shown that, except for the Wurm ice age, these ice ages simply did not exist. The timing of the Wurm ice age was roughly coincident with what is now known to have been the timing of the last glacial maximum but this is regarded as Imbrie as an accident! The four glaciations were derived from a study of glacial deposits in the Alps; not only have the dates ascribed to the earlier glacial deposits been shown to be incorrect, but the stratification of these glacial deposits has been shown, apparently, to result from tectonic movements and has had nothing to do with climatic change at all!.

7.5.1.2 A breakthrough

The initial breakthrough probably came in 1973 when Shackleton and Opdyke (1973), following pioneering work by Emiliani (1966), produced convincing estimates of the fluctuating volume of ice on the global continents over much of the last million years (Fig 7.14). The evidence was deduced from a study of plankton shells in a deep sea core in the equatorial Pacific using the oxygen isotope method (Annex I). Absolute dating of deep sea cores is difficult unless palaeo-magnetic field reversals can be detected, so Shackleton and Opdyke chose a core which could provide detail on much less than a 10,000 year time-scale but which nevertheless extended beyond the most recent known magnetic field reversal horizon, known as the Brunhes-Matuyama magnetic reversal. This reversal is now dated at about 730,000 k.y., and its detection in the core allowed the age of different sections of the core to be fixed reasonably well. It is known that deep-ocean sedimentation rates vary in time and that cores can be compressed at depth; so this core by itself did not provide an absolute age for all the temperature variations deduced from the oxygen isotope method. However, it turned out that the ages could be deduced quite well given the one measurement of absolute age described above, because sedimentation rates did not vary greatly. In Fig 7.14 the ups and downs in $\delta\,^{18}O$ should be mainly a record of the changes of worldwide ice volume (Annex I); less negative values of $\delta\,^{18}O$ correspond to more ice (or, to some extent, lower sea temperature). Seven quasi-regular major peaks and troughs can be seen with superimposed higher-frequency fluctuations. This suggests that seven ice ages occurred at roughly equal intervals back to 730,000 k.y. It was found possible to match this long core to many previously analysed, shorter, cores obtained elsewhere in the ocean, and it began to seem that major ice ages tended to recur at almost fixed intervals of 100,000 years.

Spectral analysis of the series in Figure 7.14 suggested strongly that periods of roughly 41,000 and 22,000 years were present in addition to a 100,000 year peak; the shorter time scales correspond to those of the "Milankovitch" variations in northern and southern hemisphere seasonal radiation as described in Lecture 3 (Figure 3.8), shown now in spectral form for several latitudes and months in Fig 7.15. Fig 7.16 shows data from a later deep sea core, analysed using similar methods, that seemed to support Shackleton and Opdyke's results, together with its spectrum. A puzzle however was that no spectral peak of 100,000 years exists in the Milankovitch radiation variations, even though this time scale is dominant in the cores. Nevertheless the amplitudes of the higher-frequency seasonal radiation peaks are modulated on the 100,000 year time scale by variations in the eccentricity of earth's orbit, though by a very variable amount.

7.5.1.3 Strong Confirmation of the Ice-Age Milankovitch radiation variation link

In 1982, Imbrie et al presented a key paper at a special conference held in USA to debate the Milankovitch radiation variations and their effect on climate. This paper brings together the five most reliably analysed deep-sea ocean cores and their $\delta\ ^{18}O$ records, three of which are long enough to reach the Brunhes-Mutuyama magnetic reversal (Imbrie et al (1984)). The locations of these cores are shown in Fig 7.17, while Fig 7.18 shows the $\delta\ ^{18}O$ data filtered on the obliquity (41,000 year) (curve A) and precession (19000 -23000 year) time scales separately, together with similar curves for the amplitude and phase of the astronomical variations of obliquity and precession. Both pairs of curves are normalised to the same vertical scale and small, constant, offsets between the astronomical and $\delta\ ^{18}O$ curves have been removed. The match in amplitude and phase between the $\delta\ ^{18}O$ and astronomical curves is striking as this type of test is quite a sensitive one. However it must be pointed out that this excellent match does reflect several artificial adjustments to the data:

Imbrie et al compensated for uncertainties in dating by optimising the phase match. It is still difficult to explain the dominant 10^6 year cycle in the deep sea cores in terms of the Milankovitch radiation variations, as the 10^6 year amplitude modulation of the shorter time scale radiation fluctuations is far from consistent in magnitude. Many tentative explanations of this cycle have been given, relating to the dynamics of ice-sheets and the time it takes for the sheets to form and to melt. (eg Le Treut and Ghil (1983); Lindzen (1986); Bryson and Goodman (1986)). An improtant factor is that, when ice sheets form, the rocks beneath and around sink isostatically, possibly helping to amplify externally-forced disintegrations of the ice sheets by steepening the retreating front and thereby increasing ice-flow into a warmer zone where thawing is rapid (Hyde and Peltier (1987)). This may explain the rapid deglaciations evident in Figures 7.14 and 7.16. When the ice sheets have melted, it can take a long time for the rocks to rebound. So, if for example, an extensive area of land above a certain altitude in a critical geographical situation were required for glaciation to start during a summer radiation minimum, it could take many thousands of years after the ending of a previous glacial period before this altitude was again reached. A newly-formed ice sheet, minimally affected by isostatic sinking of the rocks, would be less sensitive to external forcings which might otherwise have triggered its disintegration. Hyde and Peltier (1987) applied Milankovitch radiation variations to an ice sheet model incorporating isostatic movements and dynamical ice flows, and obtained a simulated ice-volume series with 10^6 year fluctuations similar to those deduced from the $\delta\ ^{18}O$ record. The isostatic movements and ice-sheet dynamics act effectively as a transfer function on the Milankovitch radiation variations, generating a spectrum with a maximum of power at about 10^6 years.

7.5.2 Changes in oceanic circulations during the late Pleistocene

Variations with time of the abundance of the carbon isotope ^{13}C in oceanic CO_2 can also be deduced from deep sea cores, and the results interpreted in terms of integrated biological production at lesser depths since the deep water was isolated from the atmosphere (Duplessy and Shackleton (1985)). Thereby, given reliable estimates of biological productivity rates based on foraminiferal abundances deduced from the cores, it is possible to infer oceanic circulation rates, in particular the rates of formation of deep water. Duplessy and Shackleton (1985) found that during the transition from glacial conditions to the Eemian interglacial (127 k.y) the formation of North Atlantic Deep Water by downward convection of cold high-latitude water from the surface virtually ceased. This suppression of convection probably resulted from the release of a large amount of low-salinity (and therefore low-density) melt-water onto the surface of the northern part of the ocean. Conversely, the formation of North Atlantic Deep Water was enhanced during the subsequent phase of ice growth (about 107 k.y), probably because the surface layers lost more water by evaporation than was gained by runoff, and were thus more saline and denser. The Southern Hemisphere source of bottom water was, however, much more constant in the period (135 to 107 k.y) studied by Duplessy and Shackleton. Keigwin (1987) found no evidence of the formation of North Pacific deep water during the most recent glaciation (10 to 18 k.y). In the modern North Pacific there is no deep water formation because the surface waters are too fresh.

Ghil et al (1987) have linked deep water formation and Quaternary glaciations in a conceptual model (Fig 7.19), and their results indicate that coupling between ice-sheet melting and reformation, sea-ice extent, and the thermohaline circulation of the Atlantic Ocean, can result in regular oscillations in global temperature and ice extent and in the Atlantic Ocean abyssal circulation, the latter being slowed down during glaciations. Their model includes albedo-temperature feedback but not the Milankovitch radiation variations.

7.5.3 Changes in atmospheric carbon dioxide concentration during the late Pleistocene

In a trio of papers Jouzel et al (1987), Barnola et al (1987) and Genthon et al (1987) have analysed an ice core over 2000 m long from Vostok in Antarctica, representing the last 160 k.y. First, they obtained a deuterium profile from the core: this profile was considered to be a better measure of temperature changes than the ^{18}O profile, because the isotopic fractionation of hydrogen-deuterium is less sensitive to relative humidity than is that of oxygen (Jouzel et al (1987)), and climatic changes of relative humidity could not be ruled out. The temperature time-series showed spectral peaks near 25, 41 and 107 k.y, the first two roughly corresponding to those of the Milankovitch radiation variations at latitude 65°N. Next, they analysed the CO_2 concentration in the air trapped in the core (Barnola et al (1987)) thus obtaining the time-series of concentration shown with the temperature time-series in Figure 7.20, which shows dramatic increases of CO_2 concentration near the times of the last and penultimate deglaciations. A 21 k.y peak (corresponding to the precessional cycle) was evident in Barnola et al's spectral analysis, with little if any phase difference between CO_2 and temperature on this time-scale. The results in Figure 7.20 were found to agree with those from a marine core and from other ice cores in Antarctica and Greenland, in indicating large CO_2 increases associated with the two deglaciations and highest CO_2 values during the integlacial periods. However, there were substantial differences in detail, eg the sudden decrease in CO_2 between about 71 k.y and 62 k.y in Figure 7.20 did not appear in the marine core, which also indicated CO_2 concentrations approaching Holocene levels several times during the last glaciation. The lag of the CO_2 change behind reglaciation at the end of the Eemian interglacial (ca 120 k.y) was ascribed tentatively to changes in the circulation of the deep ocean. Finally, Genthon et al (1987) used a statistical model to relate the temperature changes to the CO_2 changes and the insolation changes. They suggested that the CO_2 changes greatly amplified the effects of the orbitally-induced changes of insolation, and also served to force the temperatures and glaciations of the two hemispheres to be in phase, which the Milankovitch changes alone could not do. However, their conclusions were tentative: the CO_2 changes could be interpreted as a response to the glacial changes, and the hemispheres may in that case have been held in phase by changes in the circulation of the deep ocean.

Neftel et al (1988) obtained a CO_2 record from an ice core from Byrd, Antarctica, for 50-5 k.y. Their results were consistent with those of Barnola et al (1987). The sudden CO_2 increase at the time of deglaciation lagged the Byrd $\delta\, ^{18}O$ (ie temperature) change by 200 to 1200 years, suggesting that CO_2 responded to, rather than triggered, the deglaciation. CO_2 could, of course, have helped to maintain the warmer post-glacial climate.

According to Raynaud et al (1988) an increase of atmospheric methane at the end of the penultimate interglacial may have made a minor contribution to the global climatic warming, about 25% of the contribution from increasing CO_2.

7.6 CONDITIONS AT THE GLACIAL MAXIMUM

An interdisciplinary project called CLIMAP (Climate Long-Range Investigation Mapping and Predictions) has attempted to reconstruct the geography of the Ice Age ice sheets and the values of surface ocean temperatures for each month of the year for about 18,000 years before present (BP) (CLIMAP (1981)). Evidence was derived from land geology measurements of $\delta\ ^{18}O$, and most importantly, the distribution of species of surface-dwelling plankton found in deep-sea cores which were used as palaeo-thermometers. If we know the current distribution of different kinds of plankton and can relate these to variations of sea temperature, then for a period as recent as 18,000 BP for which evolution of species is not a problem, we can reconstruct past distributions of SST. A complex, multivariate analysis scheme was used to estimate worldwide calendar monthly ocean temperatures. Fig 7.21 shows the reconstructed global SST, together with the extent of the land and ocean ice sheets for August 18,000 BP. Fig 7.22 shows, for the North Atlantic, an estimate of the difference of SST from modern values; this ocean cooled most. See Imbrie and Imbrie (1979) for further details. According to Rind and Peteet (1985), however, the CLIMAP SSTs may be too warm. They used the CLIMAP SSTs to force an atmospheric general circulation model, and found that the predicted tropical air temperatures were higher than those inferred from evidence of snow-line depressions and from pollen distributions. Reducing atmospheric CO_2 to glacial levels had little impact (Rind (1987)). The model's tropics were also wetter than inferred from fossil sand-dunes and lake levels and from faunal and floral evidence. An integration with SSTs 2°C below the CLIMAP values gave results more consistent with the observations.

7.7 NUMERICAL MODEL EXPERIMENTS

7.7.1 Manabe and Broccoli (1985) (MB); Broccoli and Manabe (1987) (BM)

MB used a coupled mixed-layer ocean spectral AGCM. They set out to determine what the physical effects of the land ice sheets existing at 18,000 BP on SST might be. The model was integrated for 20 model years and the last 5 years of the integrations were averaged. So all months of the year were modelled.

(a) Control experiment

Modern continental ice, today's radiation conditions.

(b) Anomaly experiment

CLIMAP continental ice extent, today's radiation conditions. At 18000 BP the radiation conditions happened to be similar to today's, as the ice age summer radiation minimum and winter radiation maximum in the Northern Hemisphere occurred several thousand years previous to this time.

Fig 7.23 shows, for February and for August, the difference between anomaly and control experiments and also the difference between the SST values reconstructed by CLIMAP for 18,000 BP and today's values. In the Northern Hemisphere, SST's in the anomaly experiment are much lower in both months in the N Atlantic and N Pacific, and these changes agree quite well with the CLIMAP reconstructions. In the Southern Hemisphere the differences in SST between anomaly and control experiments are mostly positive so that Southern Hemisphere SST was mostly warmer in the anomaly experiment, ie at 18000 BP. The CLIMAP reconstruction shows that some areas of the Southern Hemisphere were warmer but many areas were substantially colder than now. The model results suggest, therefore, that the presence of the Northern Hemisphere ice sheet may have had little effect on SST in the Southern Hemisphere. The reason (in the model) appears to be that although the Northern Hemisphere reflected more incoming solar radiation at 18,000 BP, this was almost exactly compensated by a lower emission rate of long wave radiation. So only an insignificant change in net hemispheric heat exchange was required to maintain equilibrium. Thus some other mechanism may be needed to provide the observed cooling of the Southern Hemisphere. The subsequent experiments of BM suggest that recent measurements (see section 7.5.3 and Lecture 10) that show a lower concentration of carbon dioxide in the atmosphere at that time might provide the missing physical link. BM carried out a set of AGCM experiments, with a model similar to that used by MB, in order to isolate the effects of continental ice, atmospheric CO_2, and land (not snow) albedo on the climate of the last glacial maximum. They found that the effects of land albedo (as specified by CLIMAP) were small, but that CO_2, though much less influential in the Northern Hemisphere than continental ice, was the largest single influence in much of the Southern Hemisphere (Figure 7.24 A, B). The influence of changes in deep ocean circulation could not, however, be assessed by BM as the oceanic component of their model was only a 50 m mixed-layer. BM did find an amplified atmospheric flow pattern in their model with ice sheets, with a stronger Rockies ridge and enhanced mid-tropospheric westerlies from USA to southern Europe. Other experiments (eg Rind (1987) have also produced these features to some extent. In Rind's experiments an interesting result was that the stationary-wave change in the Northern Hemsiphere was accompanied by a similar change in the Southern Hemisphere, where ice-sheets were little changed, thus suggesting a dynamical connection between the hemispheres.

7.7.2 Royer et al (1984)

Royer et al used a numerical model to study the annual cycle of climate at 125,000 BP when Northern Hemisphere radiation was at a maximum and at 115,000 BP when Northern Hemisphere radiation was at a minimum. The earlier date coincided with the last (Eemian) interglacial. The orbit of the earth was highly eccentric at both times ($e = 0.05$) so an especially large change in Northern Hemisphere summer radiation occurred between these two dates. The experiment was rather short, the model being integrated only through one annual cycle. In both cases the modern distribution of land ice and modern values of SST were assumed. We shall highlight only one aspect of the results - does the model provide evidence that ice might preferentially form in eastern Canada in 115,000 BP where the largest of the continental ice sheets in fact developed in recent Ice Ages (Fig 7.21)? Fig 7.25 shows the difference in simulated annual mean surface temperature 115,000 BP -125,000 BP. The largest cooling in the Northern Hemisphere at 115,000 BP is indeed in Eastern Canada. Furthermore, model "soil water content", which in their model included the effect of snow accumulation, also increased in this region. Fig 7.26 shows the differences in MSL pressure. It was found that the model maintained colder conditions in most of the year in Eastern Canada, partly because of higher pressure to the northwest in winter at 115,000 BP giving northerly flow and clear skies with resulting loss of radiation, but also because of cloudier summers which of course were accompanied by less insolation. So the results of these experiments, although tentative, are encouraging.

7.7.3 Prell and Kutzbach (1987)

Prell and Kutzbach used AGCM simulations, incorporating a large range of solar radiation and surface boundary conditions, to estimate sensitivity coefficients for the effects of solar radiation and glaciation-associated surface boundary conditions on model-simulated precipitation in the northern summer monsoons in southern Asia and in northern Africa. Under interglacial conditions, an increase in Northern hemisphere summer solar radiation in the model produced stronger monsoons ie larger pressure differences between ocean and land, stronger winds, and more precipitation. Under glacial conditions (including ice sheets, appropriate CO_2, appropriate SST etc) with radiation similar to that at present the model produced a weaker monsoon in southern Asia but precipitation was increased over the equatorial west Indian Ocean and in equatorial North Africa. The effects of radiation and of surface boundary conditions were approximately additive. The sensitivity coefficients were used, with the known histories of solar radiation and of surface boundary conditions to reconstruct histories of monsoon variability for the past 125 k.y. The results compared very favourably with indices of southern Asian monsoon strength based on pollen (Figure 7.27 A,B) and indices of equatorial North African aridity based on aeolian deposits (Figure 7.2 C, D). Prell and Kutzbach note, however, that though the equatorial north African aridity index shows continuing moist conditions during the late glacial (10-20 k.y) evidence from lake levels in tropical Africa suggests an arid phase at that time.

ANNEX I TO LECTURE 7

OXYGEN ISOTOPE METHOD FOR DEDUCING GLOBAL ICE VOLUME, OCEAN TEMPERATURE AND AN INDEX OF AIR TEMPERATURE OVER LARGE LAND GLACIERS

7A(1) δ in polar ice

Consider the evaporation of water from the ocean surface (Fig 7AI). There are three oxygen isotopes ^{16}O, ^{17}O, ^{18}O, of which ^{17}O can be neglected. The average ratio of ^{16}O:^{18}O in today's oceans is 998:2. The saturation vapour pressure of (A) $H_2\,^{18}O$ is less than that of (B) $H_2\,^{16}O$; the ratio $^{A}/_{B}$ = 0.99 at 0°C and 0.992 at 25°C and the difference continues to reduce at higher temperatures. So there is always a lower fraction of ^{18}O in atmospheric water vapour than in the ocean. Now, $H_2\,^{18}O$ vapour preferentially condenses into the liquid or solid form as its saturation vapour pressure is lower than that of $H_2\,^{16}O$. The varying values of the ratio A/B above suggests that condensation will produce relatively more ^{18}O in rain and snow at lower temperatures than at high temperatures. This effect is offset at higher latitudes by (a) the fact that the water in precipitation will have been derived from cooler seas (mainly sub-tropical or mid-latitude) so less ^{18}O is evaporated than in the tropics and (b) most importantly, condensation and precipitation at higher latitudes and altitudes will be from water vapour already further depleted in ^{18}O by preferential condensation and precipitation of $H_2\,^{18}O$ vapour at lower latitudes and lower altitudes. Any condensed precipitation will nearly always contain at least a little less ^{18}O than the parent ocean water. The process becomes impossibly complex to unravel if precipitation falls on land and is re-evaporated and reprecipitated, so measurements of ^{18}O in frozen precipitation on ice sheets only have a meaning in terms of temperature if the precipitated vapour is mostly derived directly from the oceans. The amount of ^{18}O is measured by δ:-

$$\delta = 1000\ \frac{(^{18}O/^{16}O\ (\text{sample}) - {}^{18}O/^{16}O\ \text{smow})}{^{18}O/^{16}O\ \text{smow}}$$

where smow = standard mean ocean water. In one set of measurements (Dansgaard (1964)), quoted by Lamb (1977), the following was found ($\delta_p = \delta$ in precipitation:)

At Valentia $\delta_p = -6$ annual mean surface air temp $T_a = 11°C$
At Upenowsk (Greenland) $\delta_p = -18$ " " " " " " $= -7°C$
At South Pole $\delta_p = -49$ " " " " " " $= -49°C$

Note that all values are negative because virtually all precipitation will contain at least a little less ^{18}O than is contained in smow, as stated above.

Dansgaard gives a formula relating T_a to δ_p.

$$0.7\ T_a = \delta_p + 13.6$$

The δ values are preserved in glacier ice and show substantial seasonal variations which are easily detected in some ice samples as δ can be measured with a standard error of about ± 0.2 which is considerably less than the seasonal variations.

7A(2) δ in the shells of plankton and global ice volume

Shells made of calcium carbonate contain in principle more ^{18}O than sea water. The equilibrium amount depends on water temperature; the ratio $^{18}O_{SHELL}/^{18}O$ SEA ($^{18}O_s/^{18}O_w$) varies from 1.025 at 0°C to 1.021 at 25°C. So δ_s becomes more positive as sea temperature falls. In practice the δ_s values have a further "constant" offset from calculated equilibrium values by an amount which depends on the specific plankton species (of foraminifera usually). This can cause the δ_s value to be negative but the temperature response will remain the same. An equation often used is

$$T = 16.9 - 4.38\ (\delta_s - \delta_w) - 0.10\ (\delta_s - \delta_w)^2$$

where δ_w is the δ of ambient sea water (relative to smow), when the plankton was alive.

It used to be thought that δ_s-δ_w in deep sea cores mostly varied with temperature, ie δ_w did not change much through time eg through the ice ages at a specific location. This is now known not to be true. δ_w rises if large quantities of land ice form as land ice contains less ^{18}O than the ocean, as shown in Section 7A(1). So the presence of continental ice sheets increases the concentration of ^{18}O in the ocean. The amount of the increase depends mainly on the change in the volume of land ice relative to that of the oceans and, appreciably, on the sea and air temperatures prevailing when the land ice was formed. Observations of δ in ice sheets and in deep sea cores show that δ_w varies considerably more than δ_s-δ_w, under most conditions. It is then easy to show that δ_s represents the changes through time of δ_w, rather than those of T, ie the changes mainly represent the changes in global ice volume. Note, however, that near ice sheets the $\delta^{18}O$ signal in surface waters may from time to time be overshelmed by ^{16}O rich local meltwater (Ruddiman (1985)).

So, from δ measurements in ice sheets, δ_s from suitable locations can be calibrated to measure the approximate changes in the volume of worldwide land ice, in km^3. The rate is roughly $1^0/oo$ change of δ per 30×10^6 km^3 of ice. However the effect of sea temperature on δ_s is not always negligible, and global ice volume changes can only be monitored semi-quantitatively unless additional geological evidence is at hand. If we assume an ice free world, as some authors do for the Tertiary epoch, quite large changes in sea temperature can be deduced from δ_s measurements, which would be exaggerated if land ice volume, in reality, changed appreciably.

REFERENCES TO ADVANCED LECTURE 7

BARNOLA, J M, RAYNAUD, D, KOROTKEVICH, Y S AND LORIUS, C (1987) Vostok ice core provides 160,000-year record of atmospheric CO_2 Nature, 329, 408-414.

BERGER, A and PESTIAUX, P (1984) Accuracy and Stability of the Quaternary Terrestrial Insolation. Milankovitch and Climate, Pt I. Ed: A Berger et al, NATO ASI 126, pp 83-111.

BROCCOLI, A J and MANABE, S (1987) The influence of continental ice, atmospheric CO_2, and land albedo on the climate of the last glacial maximum. Climate Dynamics, 1, 87-99

BROOKS, C E P (1949) Climate through the ages. Benn, London, Revised Ed.

BRYSON, R A and GOODMAN, B M (1986) Milankovitch and global ice volume simulation. Theor. Appl. Clim., 37, 22-28

CLIMAP Project Members (1981). Seasonal reconstruction of the Earth's surface at the last glacial maximum. Geological Society of America Map and Chart Series MC-36.

CROWLEY, T J, MENGEL, J G and SHORT, D A (1987) Gondwanaland's seasonal cycle. Nature, 329, 803-807.

DANSGAARD, W (1964) Stable isotopes in precipitation. Tellus, 16, 436-468.

DUPLESSEY, J C and SHACKLETON, N J (1985) Response of global deep water circulation to Earth's climatic change 135,000-107,000 years ago. Nature, 316, 500-507.

EMILIANI, C (1966) Paleotemperature analysis of Caribbean cores P6304-8 and P6304-9 and a generalized temperature curve for the past 425,000 years. J. Geol. 74, 109-126

ENDAL, A S AND SCHATTEN, K W (1982). The faint young sun-climate paradox: continental influences. J Geophys Res, 87, C9, 7295-7302.

FRAKES, L A (1978) The long-term climatic record: Cenozoic climates: Antarctica and the Southern Ocean. In Climatic Change and Variability - a Southern perspective. Ed: A B Pittock et al. Cambridge Univ Press, pp 53-69.

FRAKES, L A (1979) Climates throughout geologic time. Elsevier.

FRAKES, L A and FRANCIS J E (1988) A guide to phanerozoic cold polar climates from high-latitude ice rafting in the Cretaceous. Nature, 333, 547-549.

GENTHON, C, BARNOLA, J M, RAYNAUD, D, LORIUS, C, JOUZEL, J, BARKOV, N I, KOROTKEVICH, Y S and KOTLYAKOV, V M (1987) Vostok ice core: climatic response to CO_2 and orbital forcing changes over the last climatic cycle. Nature, 329, 414-418.

GHIL, M, MULLHAUPT, A and PESTIAUX, P (1987) Deep water formation and Quaternary glaciations. Climate Dynamics, 2, 1-10.

HARLAND, W B AND HEROD, K N (1975). Glaciations through time. In "Ice Ages Ancient and Modern", pp 189-216. Seel House Press, Liverpool.

HOLMES, A (1965) Principles of Physical Geology (2nd edition). Nelson.

HYDE, W T and PELTIER, W R (1987) Sensitivity experiments with a model of the ice age cycle: the response to Milankovitch forcing. J. Atm. Sci., 44, 1351-1374.

IMBRIE, J (1982) Astronomical theory of the Pleistocene Ice Ages: A brief historical review. Icarus, 50, 408-422.

IMBRIE, J, HAYS, J D, MARTINSON, D G, McINTYRE, A, MIX, A C, MORLEY, J J, PISIAS, N G, PRELL, W L and SHACKLETON, N J (1984) The orbital theory of Pleistocene Climate: Support from a revised chronology of the marine $\delta^{18}O$ record. Milankovitch and Climate, Pt I. Ed: A.Berger et al, NATO ASI 126, pp 269-305.

IMBRIE, J and IMBRIE, K P (1979) Ice Ages - solving the Mystery. MacMillan, London. 224 pp.

JOUZEL, J, LORIUS, C, PETIT, J R, GENTHON, C BARKOV, N I, KOTLYAKOV, V M and PETROV, V M (1987) Vostok ice core: a continuous isotope temperature record over the last climatic cycle (160,000 years). Nature, 329, 403-408

KEIGWIN, L D (1987) North Pacific deep water formation during the latest glaciation. Nature, 330, 362-364.

LABEYRIE, L D, DUPLESSY, J C and BLANC, P L (1987) Variations in mode of formation and temperature of oceanic deep waters over the last 125,000 years. Nature, 327, 477-482.

LAMB, H H (1977). Climate: present, past and future Vol 2. Methuen, 835 pp.

LeTREUT, H and GHIL, M, (1983) Orbital forcing, climatic interactions, and glaciation cycles. J Geophys. Res, 88, C9, 5167-5190.

LINDZEN, R S (1986) A simple model for 100 k-year oscillations in glaciation. J. Atm. Sci, 43, 986-996.

MANABE, S and BROCCOLI, A J (1985) The influence of continental ice sheets on the climate of an ice age. J. Geophys. Res. 90, D1, 2167-2190.

MATTHEWS, R K AND POORE, R Z (1980). Tertiary $\delta^{18}O$ record and glacio-eustatic sea-level fluctuations. Geology, 8, 501-504.

MIX, A C and PISIAS, N G (1988) Oxygen isotope analyses and deep-sea temperature changes: implications for rates of oceanic mixing. Nature, 331, 249-251.

NEFTEL, A, OESCHGER, H, STAFFELBACH, T and STAUFFER, B (1988) CO_2 record in the Byrd ice core 50,000-5,000 years BP. Nature, 331, 609-611.

NORTH, G R (1975) Analytical solution to a simple climate model with diffusive heat transport J Atm. Sci, 32, 1301-1307.

OPIK, E J (1965) Climatic change in cosmic perspective. Icarus N-Y, 4, 289-307.

PRELL, W L and KUTZBACH, J E (1987) Monsoon variability over the past 150,000 years. J Geophys. Res., 92, D7, 8411-8425.

RAMPINO, M R and VOLK, T (1988) Mass extinctions, atmospheric sulphur and climatic warming at the K/T boundary. Nature, 332, 63-65.

RAYNAUD, D, CHAPPELLAZ, J, BARNOLA, J M, KOROTKEV, Y S and LORIUS C (1988) Climatic and CH_4 cycle implications of glacial-interglacial CH_4 change in the Vostok ice core. Nature, 333, 655-657.

RIND, D (1987) Components of the ice age circulation. J. Geophys. Res., 92, D4, 4241-4281.

RIND, D and PETEET, D (1985) Terrestrial conditions at the last glacial maximum and CLIMAP sea surface temperature estimates: are they consistent? Quaternary Research, 24, 1-22.

ROYER, J F, DEQUE, M and PESTIAUX, P (1984). A sensitivity experiment to astronomical forcing with a spectral GCM: simulation of the annual cycle at 125000 BP and 115000 BP. Milankovitch and Climate, Pt II. Ed: A Berger et al. NATO ASI 126. pp 733-763.

RUDDIMAN, W F (1985) Climate studies in ocean cores. In "Paleoclimate analysis and modeling", Ed. A D HECHT, Wiley, pp 197-257.

SELLERS, A and MEADOWS, A (1975) Long term variations in the albedo and surface temperature of the earth. Nature, 254, p 44.

SHACKLETON, N J and OPDYKE, N D (1973) Oxygen isotopic and paleomagnetic stratigraphy of equatorial Pacific core V28-238: oxygen isotope temperatures and ice volume on a 10^5 year and 10^6 year scale. Quaternary Research, 3, 39-55.

SMITH, A G, HURLEY, A M and BRIDEN, J C, (1981) Phanerozoic Paleocontinental World Maps. Cambridge University Press, 102 pp.

TARLING, D H and TARLING, M P (1974) Continental Drift. Penguin Books.

WELLER, G, BENTLEY, C R, ELLIOT, D H, LANZEROTTI, L J AND WEBBER, P J (1987) Laboratory Antarctica: Research contributions to global problems. Science, 238, 1361-1368.

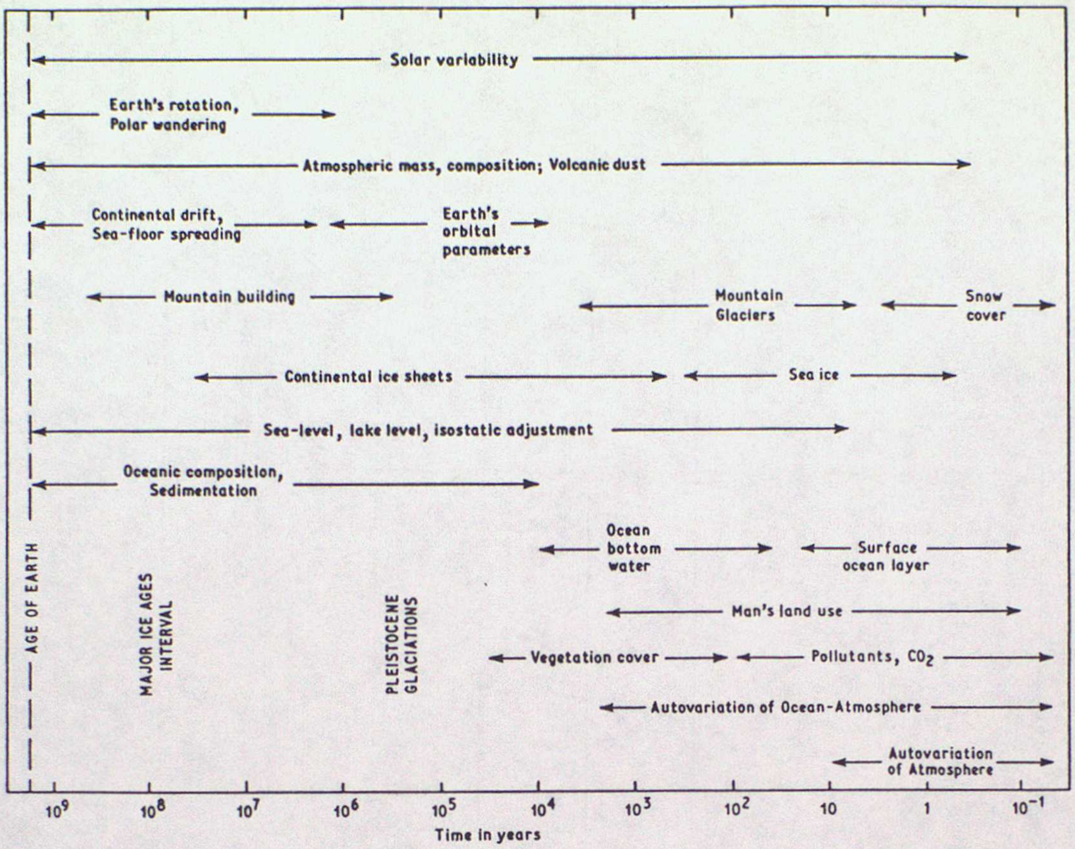
Solar variability
Earth's rotation, Polar wandering
Atmospheric mass, composition; Volcanic dust
Continental drift, Sea-floor spreading
Earth's orbital parameters
Mountain building
Mountain Glaciers
Snow cover
Continental ice sheets
Sea ice
Sea-level, lake level, isostatic adjustment
Oceanic composition, Sedimentation
Ocean bottom water
Surface ocean layer
Man's land use
Vegetation cover
Pollutants, CO_2
Autovariation of Ocean-Atmosphere
Autovariation of Atmosphere
AGE OF EARTH
MAJOR ICE AGES INTERVAL
PLEISTOCENE GLACIATIONS
10^9
10^8
10^7
10^6
10^5
10^4
10^3
10^2
10
1
10^{-1}
Time in years

Summary diagram to show the characteristic time-scales over which changes in various influences upon the global climate operate.
(*Adapted from a diagram by* W. L. GATES.)

Figure 7.1. From Lamb (1977).

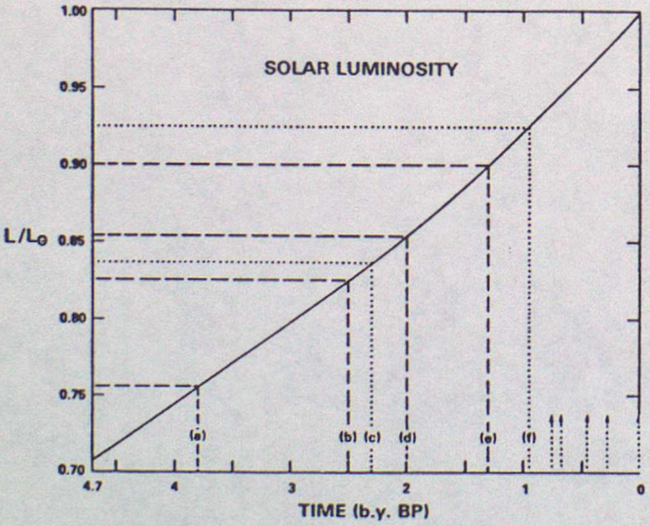

Figure 7.2. Modelled history of solar luminosity.

From Endal and Schatten (1982).

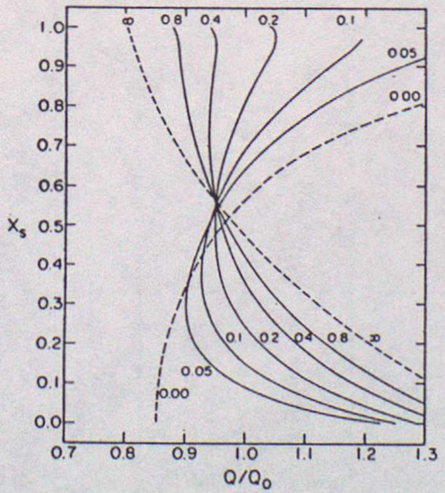

Figure 7.3. Ice-edge latitude versus solar radiation input for models with various values of atmospheric eddy diffusion parameter D.

From Endal and Schatten (1982).

Geological eras and their subdivisions, with time scale

Era	*System or Period*	*Series or Epoch*	*Notes on climate, fauna and flora*	*Radiometric age*
CENOZOIC (Kainozoic)	Quaternary	Holocene or Recent (post-glacial)		c. 10 000 years ago
		Pleistocene	Glaciations and Interglacial ages alternating. *Homo sapiens* emerged about mid last glacial (40 000 years ago). Earliest forms of Man in early Pleistocene.	1–3 million years ago
	Tertiary	Pliocene	Becoming colder. Large carnivorous animals.	c. 10 million years ago
		Miocene	Warm to moderate. Whales, apes and grazing animals.	c. 25 million years ago
		Oligocene	Warm. First monkeys and man-like apes.	c. 40 million years ago
		Eocene	Moderate becoming warm.	c. 60 million years ago
		Palaeocene	Becoming warmer. Early horses, elephants, etc. Most modern genera of flora present, but world distribution different.	c. 70 million years ago
MESOZOIC	Cretaceous		Some evidence of a cold, but not glacial phase towards end. Ichthyosaurus became extinct; many other extinctions about end of Cretaceous to early Tertiary including among phytoplankton, marine turtles, dinosaurs.	c. 130 million years ago
	Jurassic		First birds and small mammals. Dinosaurs' heyday. First crocodiles and flying reptiles.	c. 180 million years ago
	Triassic		First dionosaurs, ichthyosaurus, etc.	c. 230 million years ago
PALAEOZOIC	Permian		Glacial at first, later moderate. Conifers abundant.	c. 270 million years ago
	Carboniferous		Warm at first, becoming glacial in some regions. First winged insects. First spiders. Climax of seed ferns and clubmoss trees; great coal forests. First coniferous trees.	c. 350 million years ago
	Devonian		Moderate, becoming warm. First insects. First trees. Fish abundant.	c. 400 million years ago
	Silurian		Warm. First known land plants and animals.	c. 440 million years ago
	Ordovician		Moderate to warm. First corals. First fishes.	c. 500 million years ago
	Cambrian		Climates becoming warm. First foraminifera, starfish, snails (mollusks), bivalve shells.	c. 600 million years ago
PRECAMBRIAN	Proterozoic (first period with life forms)		First algae, radiolaria and worms. Evidence of some ice ages, perhaps severe enough to cover the whole Earth.	
	Azoic or Archaean		Before the dawn of life.	> 3000 million years ago

Figure 7.4. From Lamb (1977).

The Geological Time Scale

(millions of years).

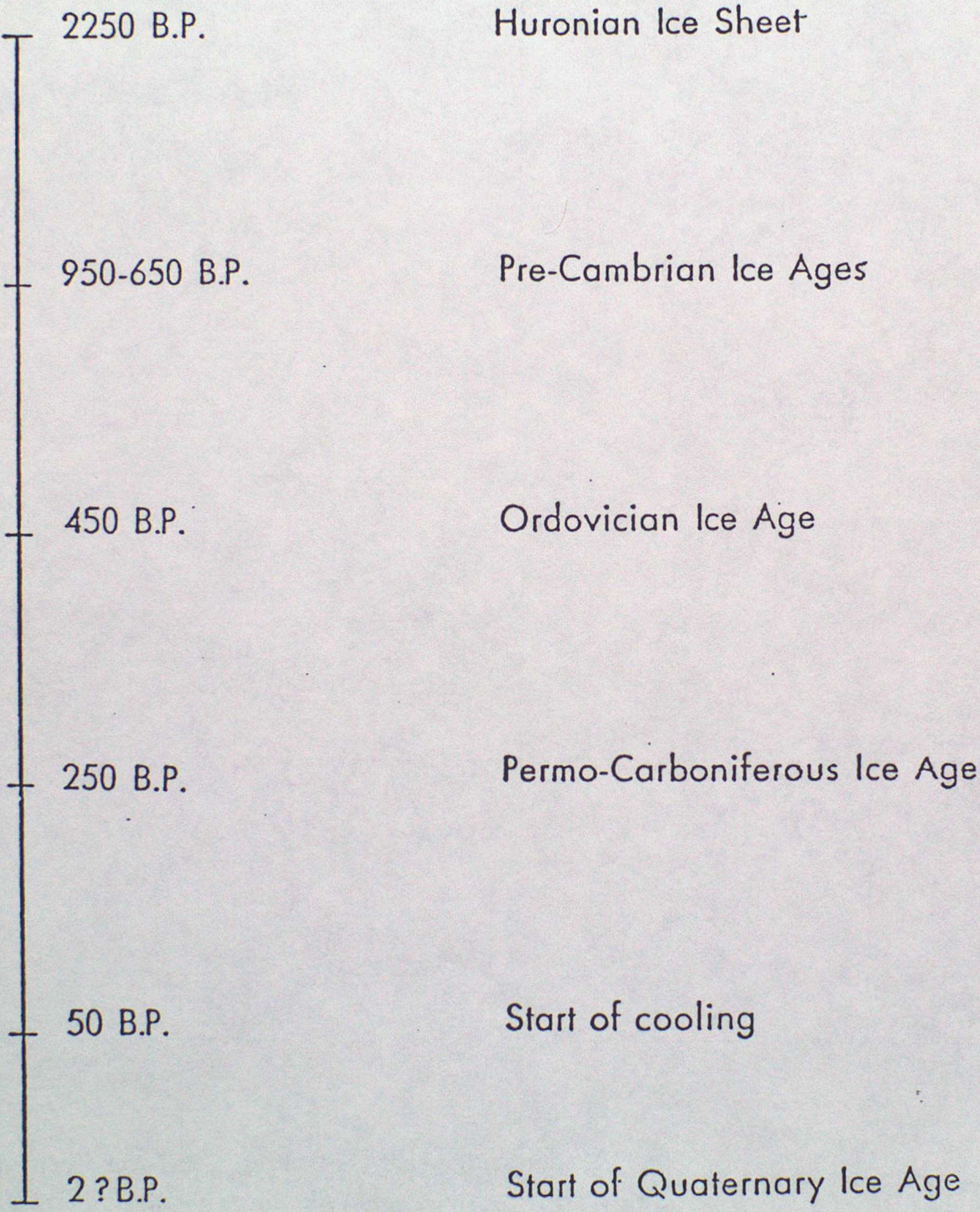
2250 B.P.
Huronian Ice Sheet
950-650 B.P.
Pre-Cambrian Ice Ages
450 B.P.
Ordovician Ice Age
250 B.P.
Permo-Carboniferous Ice Age
50 B.P.
Start of cooling
2 ? B.P.
Start of Quaternary Ice Age

Figure 7.5.

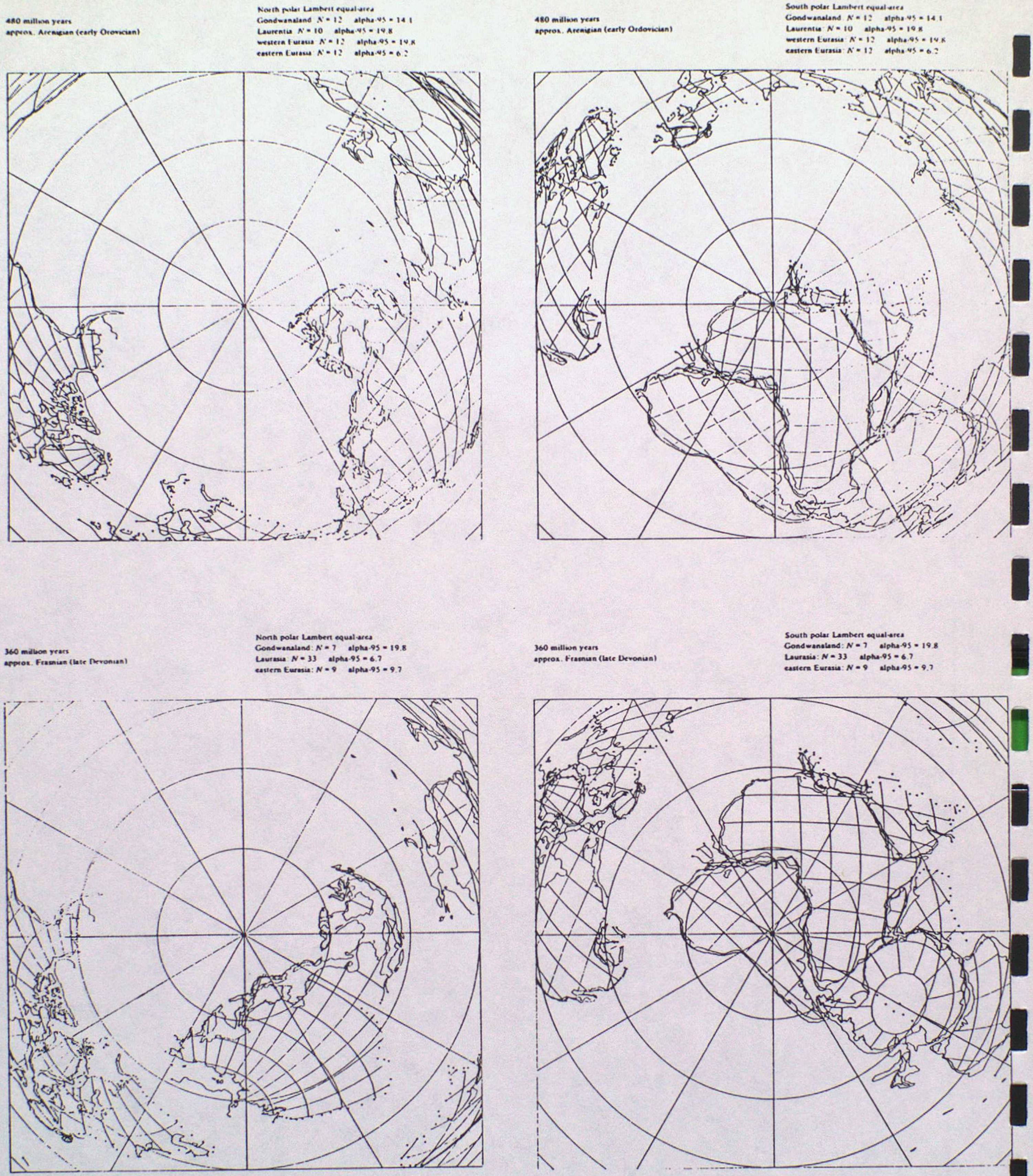
480 million years
approx. Arenigian (early Orovician)
North polar Lambert equal-area
Gondwanaland N = 12 alpha-95 = 14.1
Laurentia N = 10 alpha-95 = 19.8
western Eurasia N = 12 alpha-95 = 19.8
eastern Eurasia N = 12 alpha-95 = 6.2
480 million years
approx. Arenigian (early Ordovician)
South polar Lambert equal-area
Gondwanaland: N = 12 alpha-95 = 14.1
Laurentia: N = 10 alpha-95 = 19.8
western Eurasia: N = 12 alpha-95 = 19.8
eastern Eurasia: N = 12 alpha-95 = 6.2
360 million years
approx. Frasnian (late Devonian)
North polar Lambert equal-area
Gondwanaland: N = 7 alpha-95 = 19.8
Laurasia: N = 33 alpha-95 = 6.7
eastern Eurasia: N = 9 alpha-95 = 9.7
360 million years
approx. Frasnian (late Devonian)
South polar Lambert equal-area
Gondwanaland: N = 7 alpha-95 = 19.8
Laurasia: N = 33 alpha-95 = 6.7
eastern Eurasia: N = 9 alpha-95 = 9.7

Figure 7.6A Palaeogeographies.

© Cambridge University Press 1981, taken from Smith, Hurley and Briden *Phanerozoic paleocontinental world maps.*

240 million years
approx. Tatarian (late Permian)

North polar Lambert equal-area
Gondwanaland: $N = 29$ alpha-95 = 5.1
Laurasia: $N = 80$ alpha-95 = 3.5

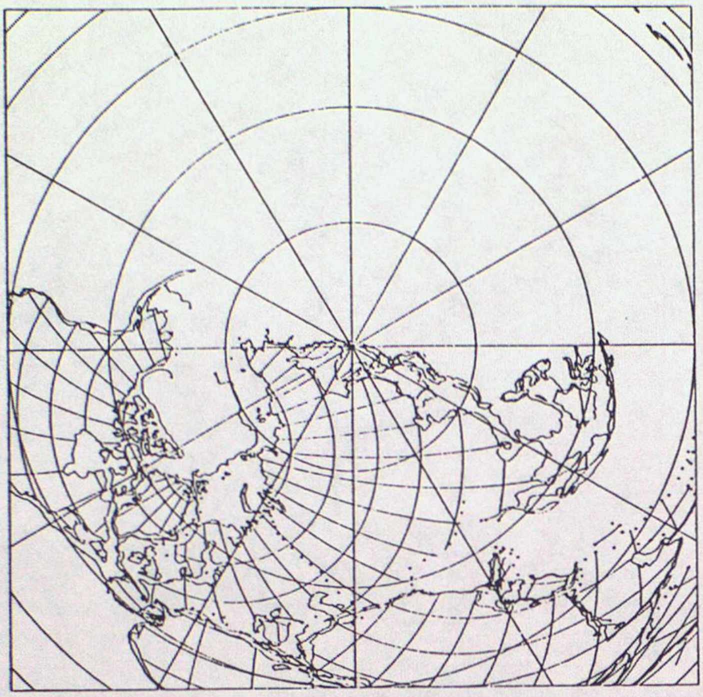

240 million years
approx. Tatarian (late Permian)

South polar Lambert equal-area
Gondwanaland: $N = 29$ alpha-95 = 5.1
Laurasia: $N = 80$ alpha-95 = 3.5

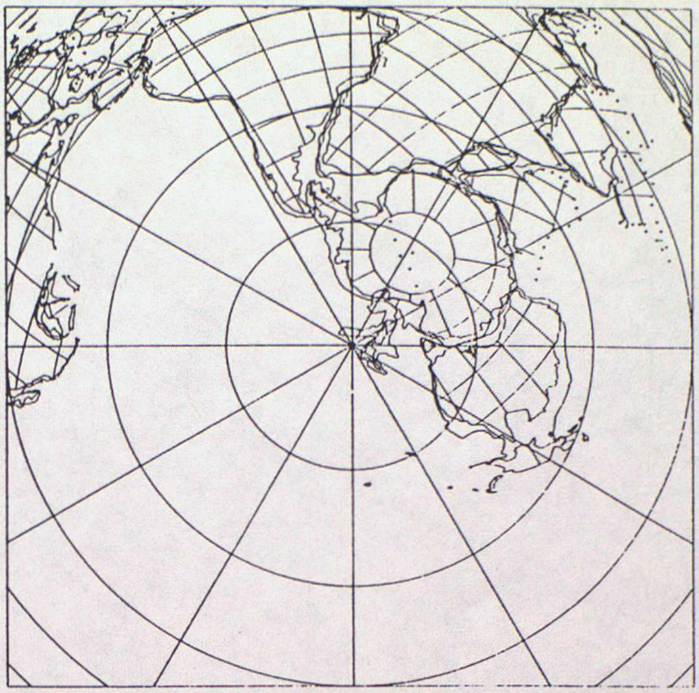

120 million years
Hauterivian (early Cretaceous)

North polar Lambert equal-area
$N = 44$ alpha-95 = 5.7

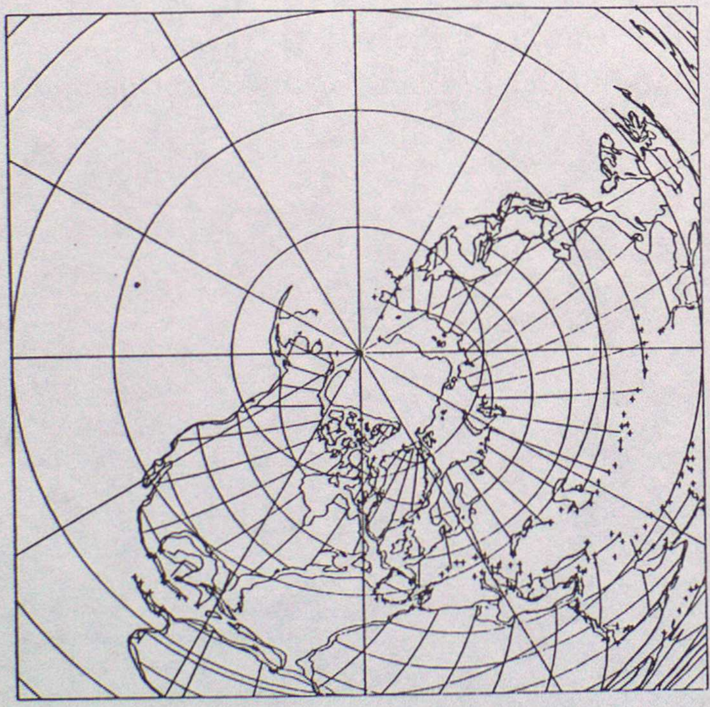

120 million years
Hauterivian (early Cretaceous)

South polar Lambert equal-area
$N = 44$ alpha-95 = 5.7

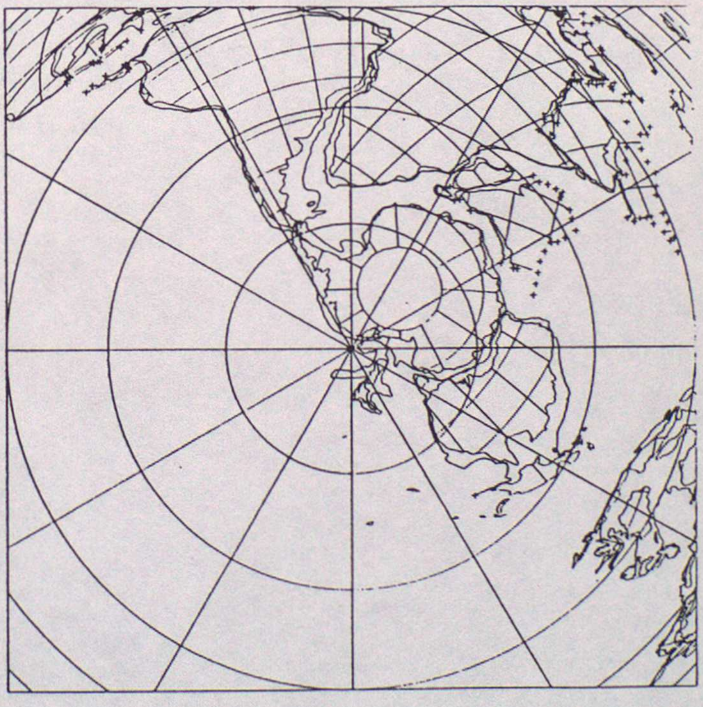

Figure 7.6B Palaeogeographies. © Cambridge University Press 1981, taken from Smith, Hurley and Briden *Phanerozoic paleocontinental world maps.*

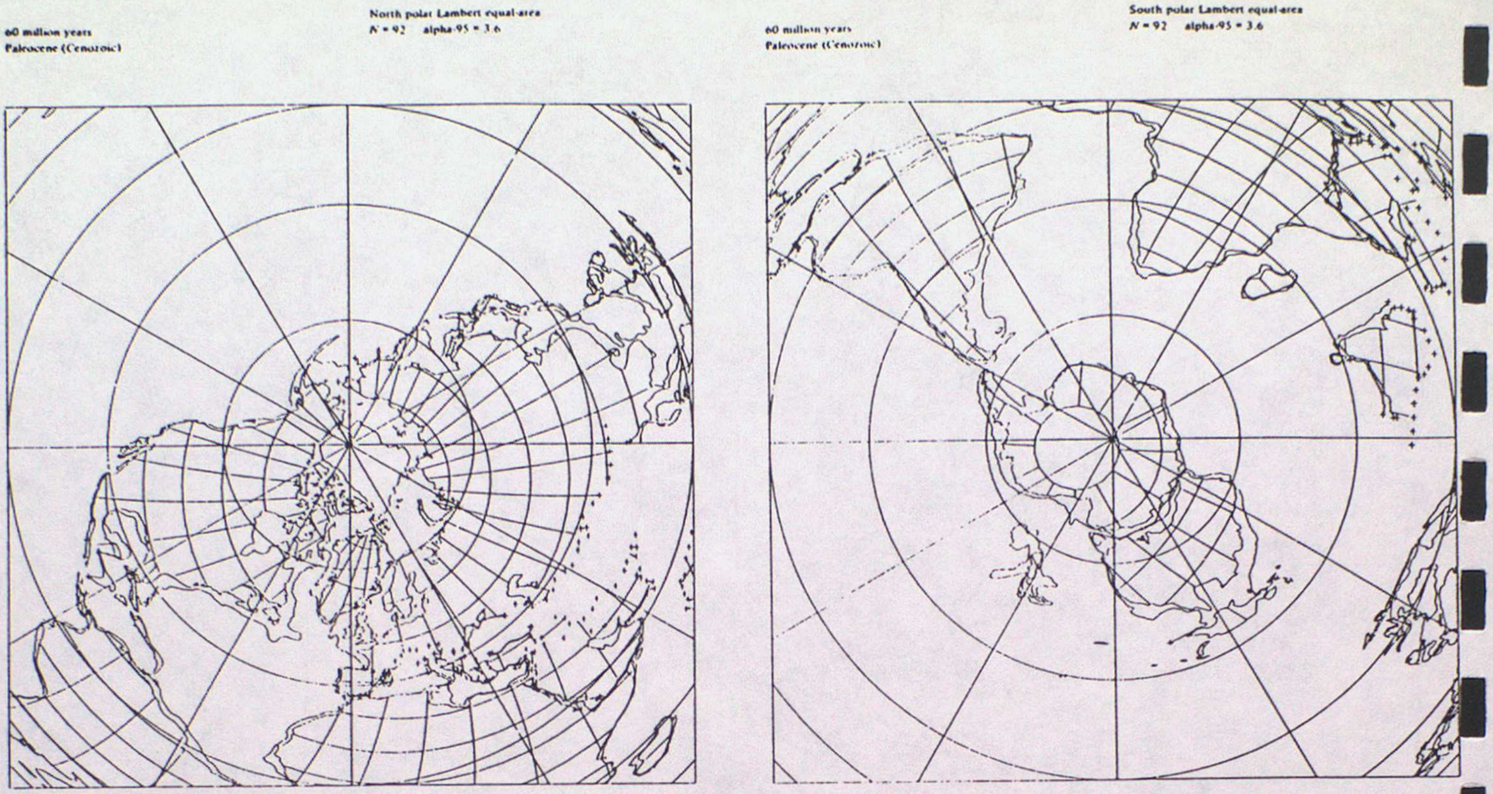
60 million years
Paleocene (Cenozoic)
North polar Lambert equal-area
$N = 92$ alpha-95 = 3.6
60 million years
Paleocene (Cenozoic)
South polar Lambert equal-area
$N = 92$ alpha-95 = 3.6

Figure 7.6C Palaeogeographies.

© Cambridge University Press 1981, taken from Smith, Hurley and Briden *Phanerozoic paleocontinental world maps.*

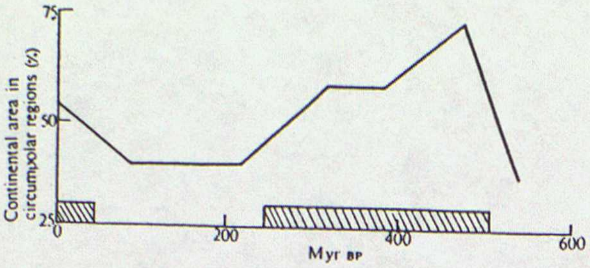

Variation of continental area within 30° of poles as a function of time. The shaded parts of the time axis include all extensive glaciations .

Figure 7.7.

From Sellers and Meadows (1975).

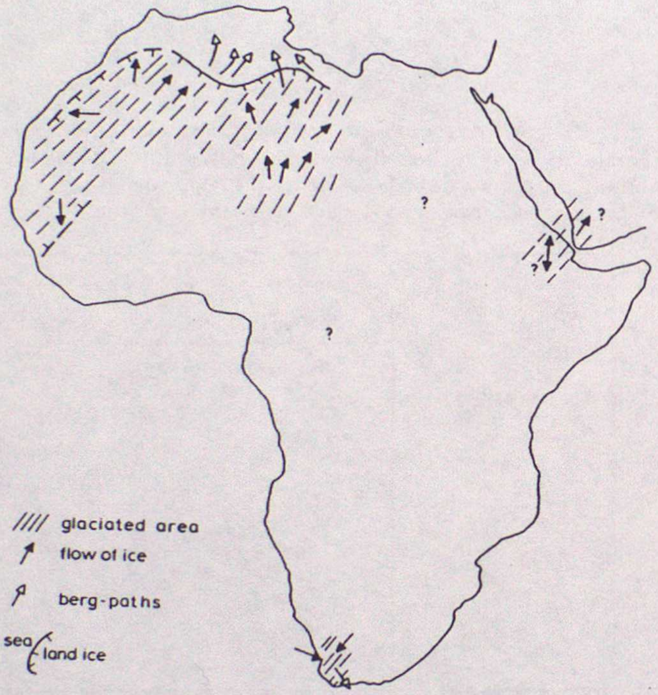

Glacial paleogeography of Africa in latest Ordovician—earliest Silurian time. Note that glacial marine conditions occupy the northwestern and western parts of the continent, and possibly southernmost Africa.

Figure 7.8.

From Frakes (1979).

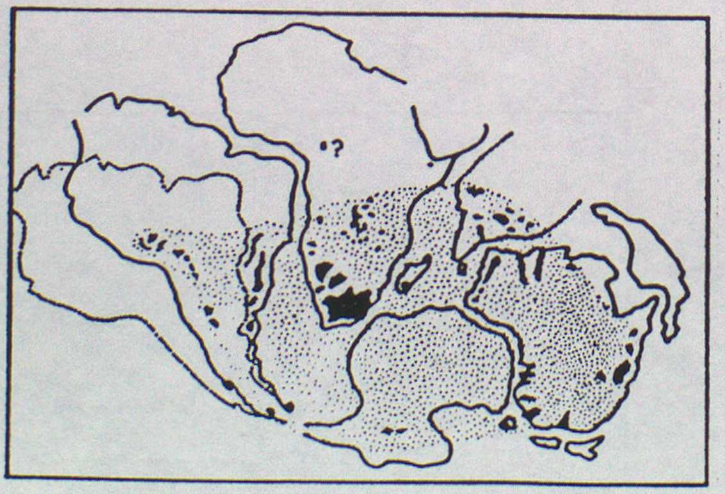

Figure 7.9.
Permo-Carboniferous glaciations.

After Holmes (1965).

Figure 7.10.

From Imbrie and Imbrie (1979).

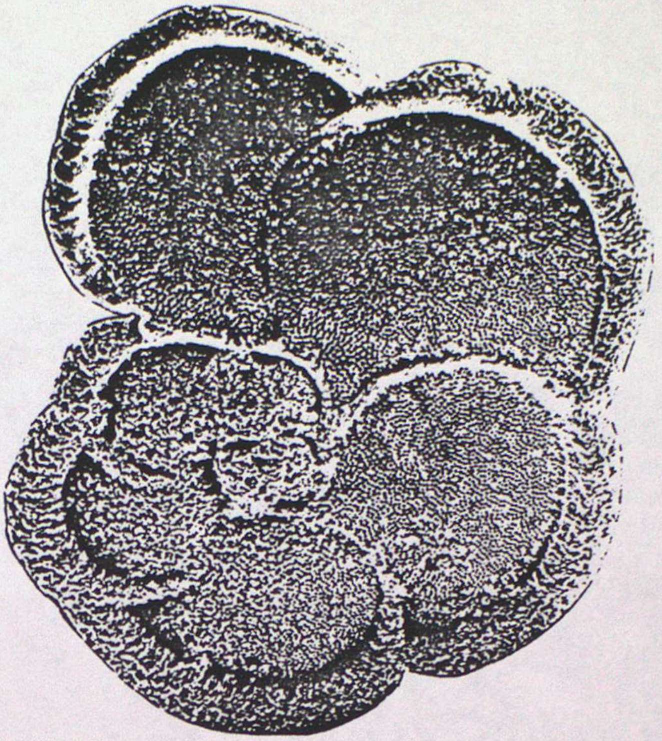

A fossil from the deep-sea floor. Upon death, the mineral remains of many surface-dwelling animals and plants fall to the sea floor and build up thick deposits of sediment. The shell shown here is that o *Globorotalia menardii*, a species of planktonic foram .

Figure 7.11.

Generalised oxygen-18 isotope record and its interpretation.

From Matthews and Poore (1980).

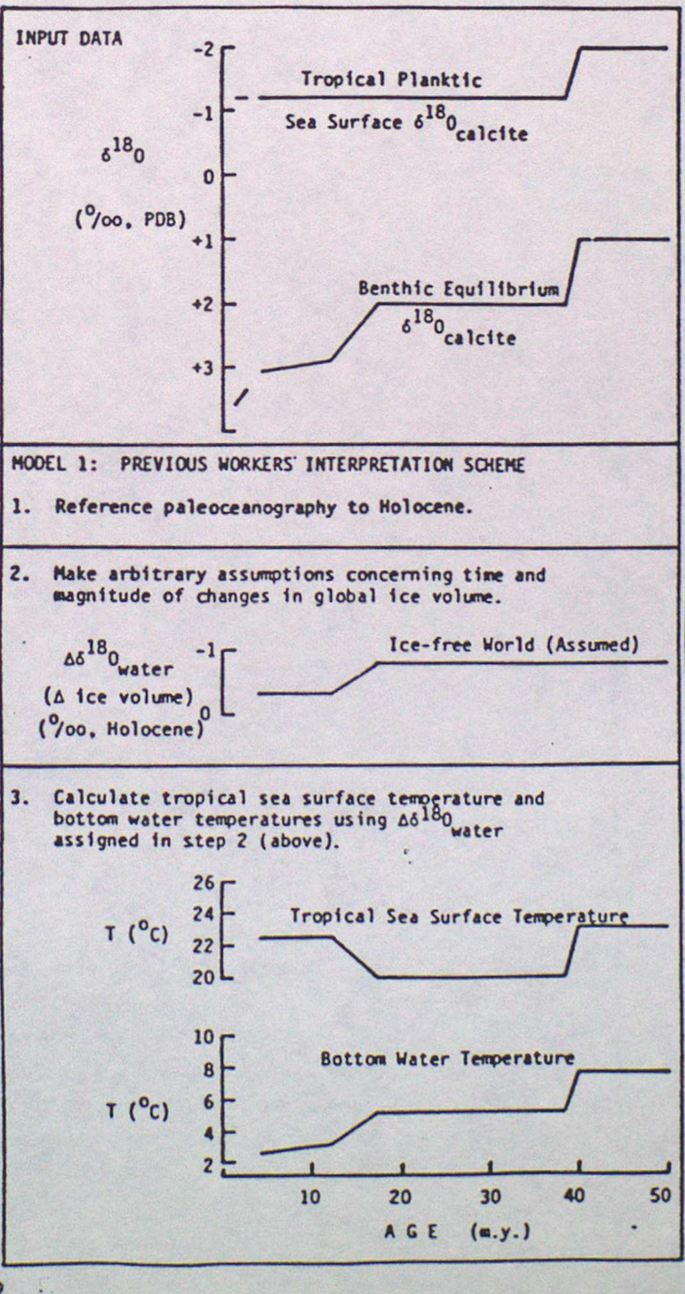

MODEL 1: PREVIOUS WORKERS' INTERPRETATION SCHEME

1. Reference paleoceanography to Holocene.

2. Make arbitrary assumptions concerning time and magnitude of changes in global ice volume.

3. Calculate tropical sea surface temperature and bottom water temperatures using $\Delta\delta^{18}O_{water}$ assigned in step 2 (above).

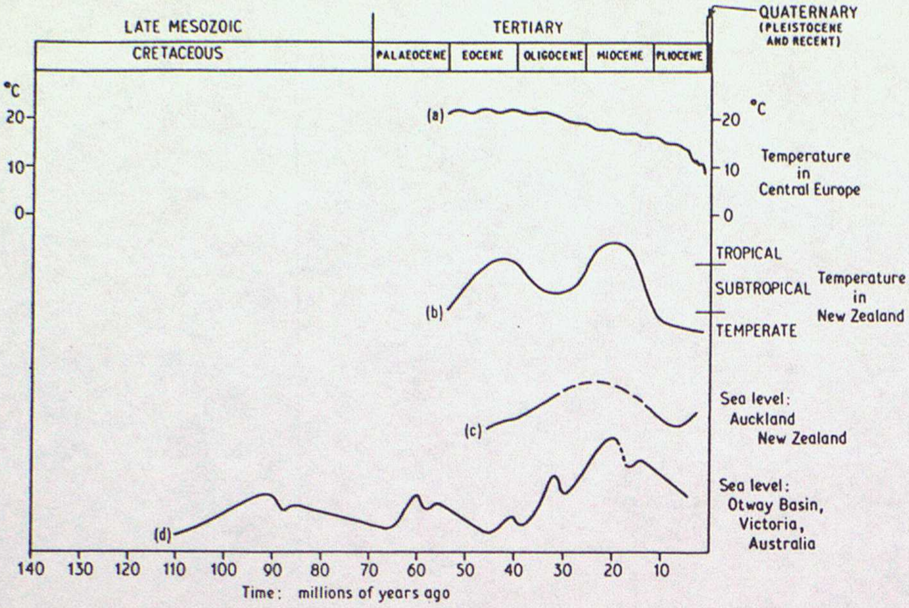

Figure 7.12.

Temperature and sea level in the Tertiary.

From Lamb (1977).

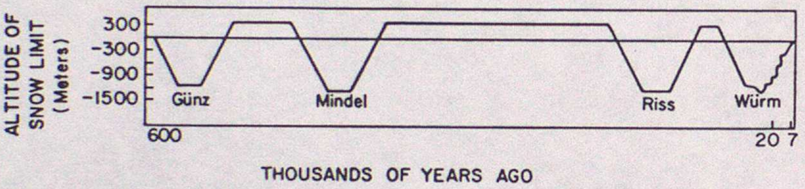

Figure 7.13.
Traditional scheme of Pleistocene ice ages.

From Imbrie and Imbrie (1979).

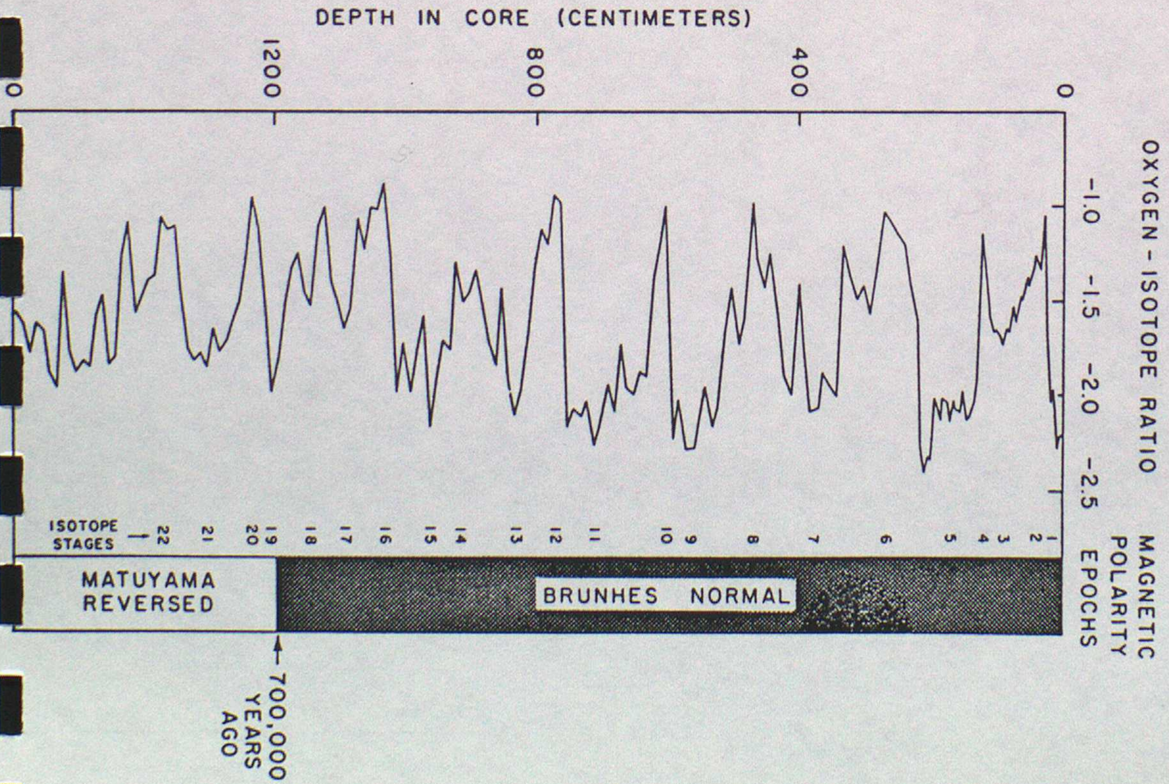

Figure 7.14.
Comparison of isotopic and magnetic measurements for the Pleistocene.

From Imbrie and Imbrie (1979).

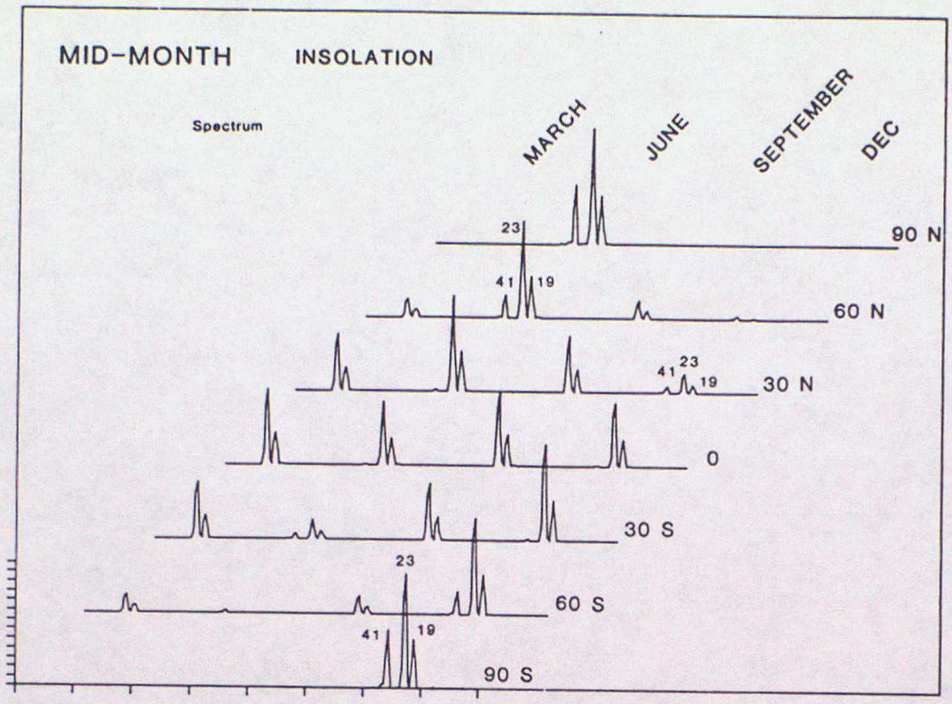

Figure 7.15. Spectral analysis of mid-month insolation. From Berger and Pestiaux (1984).

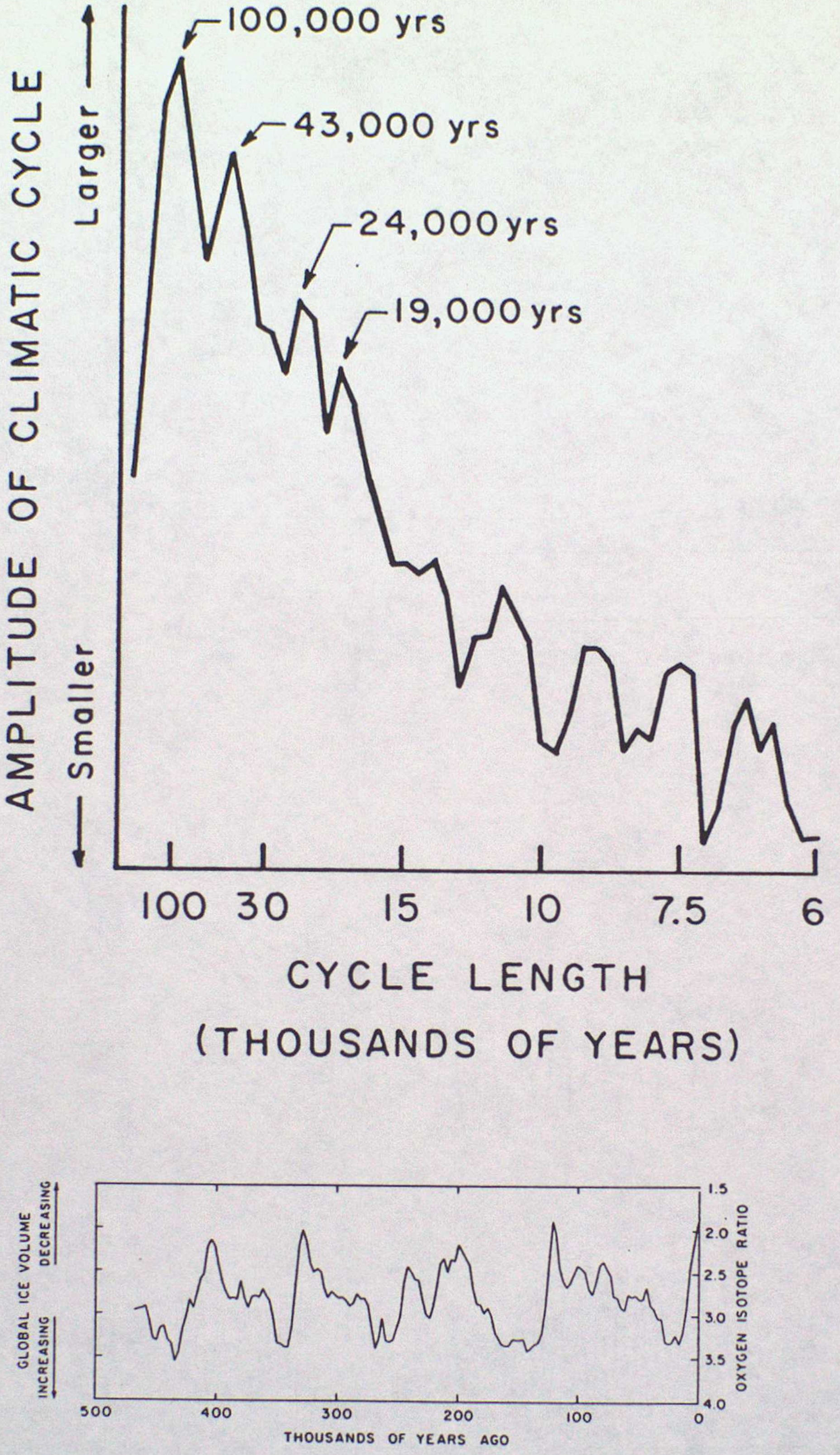

Figure 7.16. Isotopic measurements made on two Indian Ocean cores (below) and the resulting power-spectrum (above).

From Imbrie and Imbrie (1979).

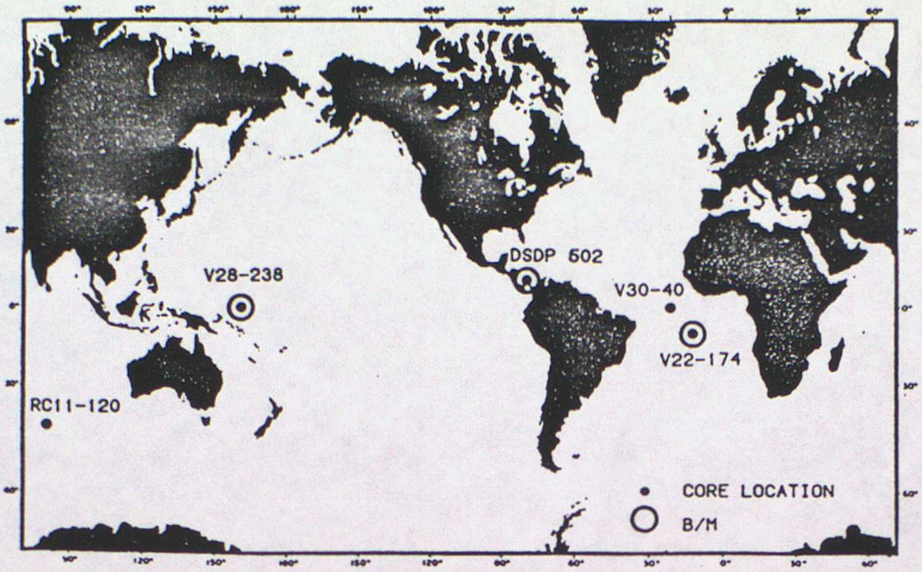
V28-238
DSDP 502
V30-40
V22-174
RC11-120
CORE LOCATION
B/M

Figure 7.17. Locations of cores used by Imbrie et al (1984). The symbol B/M indicates a core that penetrates the Brunhes-Matuyama magnetic reversal.

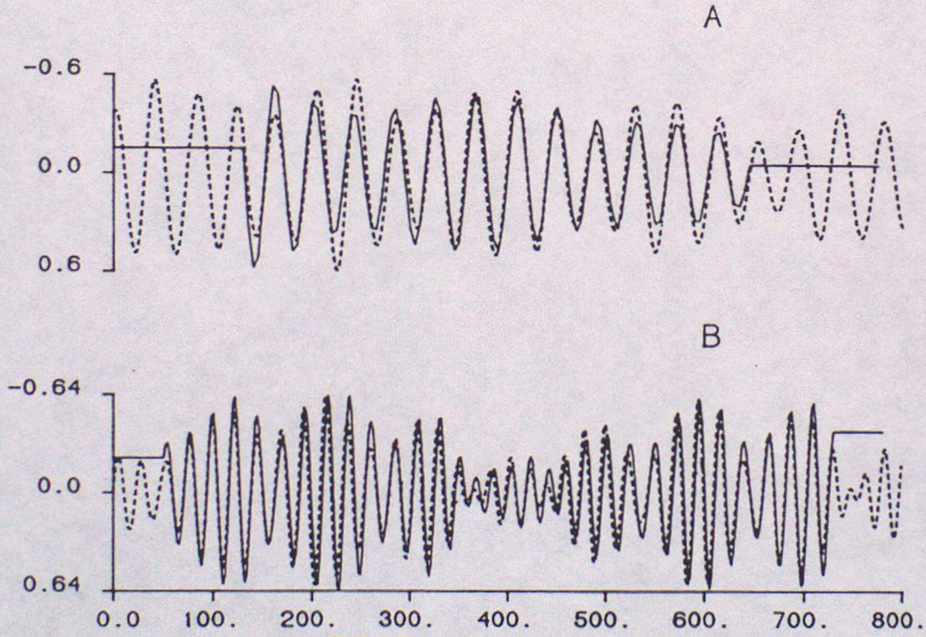

Figure 7.18. Match between oxygen isotope and obliquity (A) and precession (B) curves. Oxygen isotope curves are solid lines and were obtained by filtering the original data.

From Imbrie et al (1984).

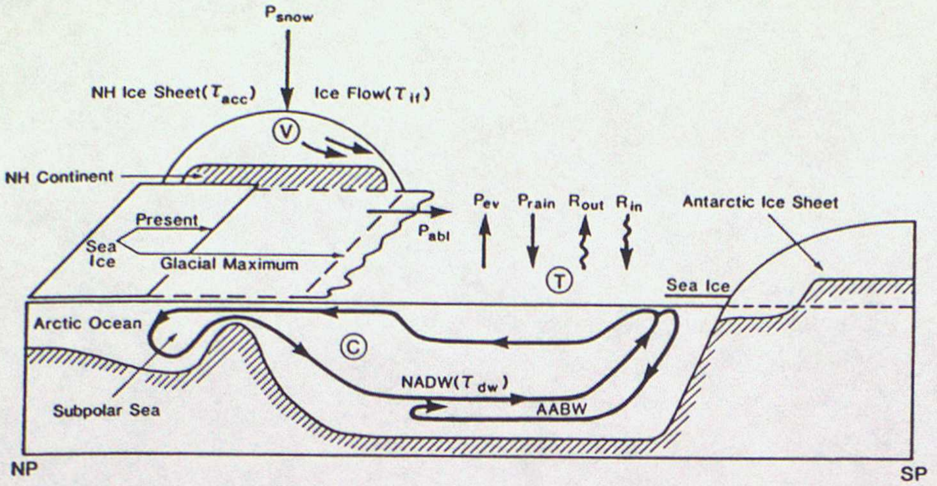
P_{snow}
NH Ice Sheet(τ_{acc})
Ice Flow(τ_{if})
V
NH Continent
Present
Sea Ice
Glacial Maximum
P_{abl}
P_{ev}
P_{rain}
R_{out}
R_{in}
T
Antarctic Ice Sheet
Sea Ice
Arctic Ocean
C
NADW(τ_{dw})
AABW
Subpolar Sea
NP
SP

Schematic diagram of an Atlantic meridional cross section from North Pole (NP) to South Pole (SP), showing the mechanisms included in our formal conceptual model of glaciation cycles. Changes in the radiation balance $R_{in}-R_{out}$ are due to changes in the volume V (t) and meridional extent of Northern Hemisphere (NH) ice sheets, and they affect the global temperature T (t). The ice sheets change their extent with a characteristic time τ_{if} due to viscoplastic flow, and change their volume with a characteristic time τ_{acc} due to changes in precipitation balance $P_{snow}-P_{abl}$. The volume and extent of Southern Hemisphere ice are assumed constant. The change in hydrologic cycle is due to changes in ocean temperature. Deep-water formation in the North Atlantic Subpolar Sea is affected by changes in ice volume and extent, and regulates the intensity C (t) of the thermohaline circulation after a delay time τ_{dw}. C (t) in turn affects the system's temperature, and is also affected by it.

Figure 7.19 From Ghil et al (1987)

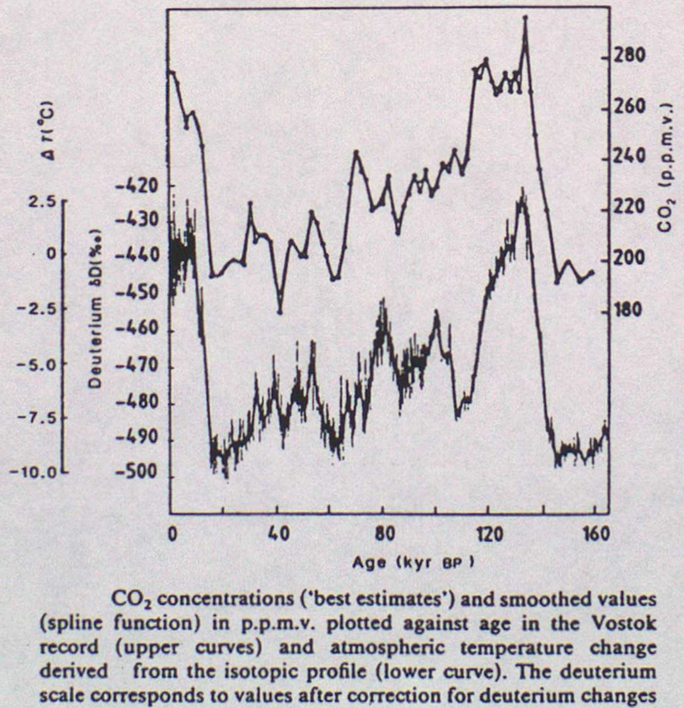

CO_2 concentrations ('best estimates') and smoothed values (spline function) in p.p.m.v. plotted against age in the Vostok record (upper curves) and atmospheric temperature change derived from the isotopic profile (lower curve). The deuterium scale corresponds to values after correction for deuterium changes of oceanic water .

Figure 7.20 From Barnola et al (1987)

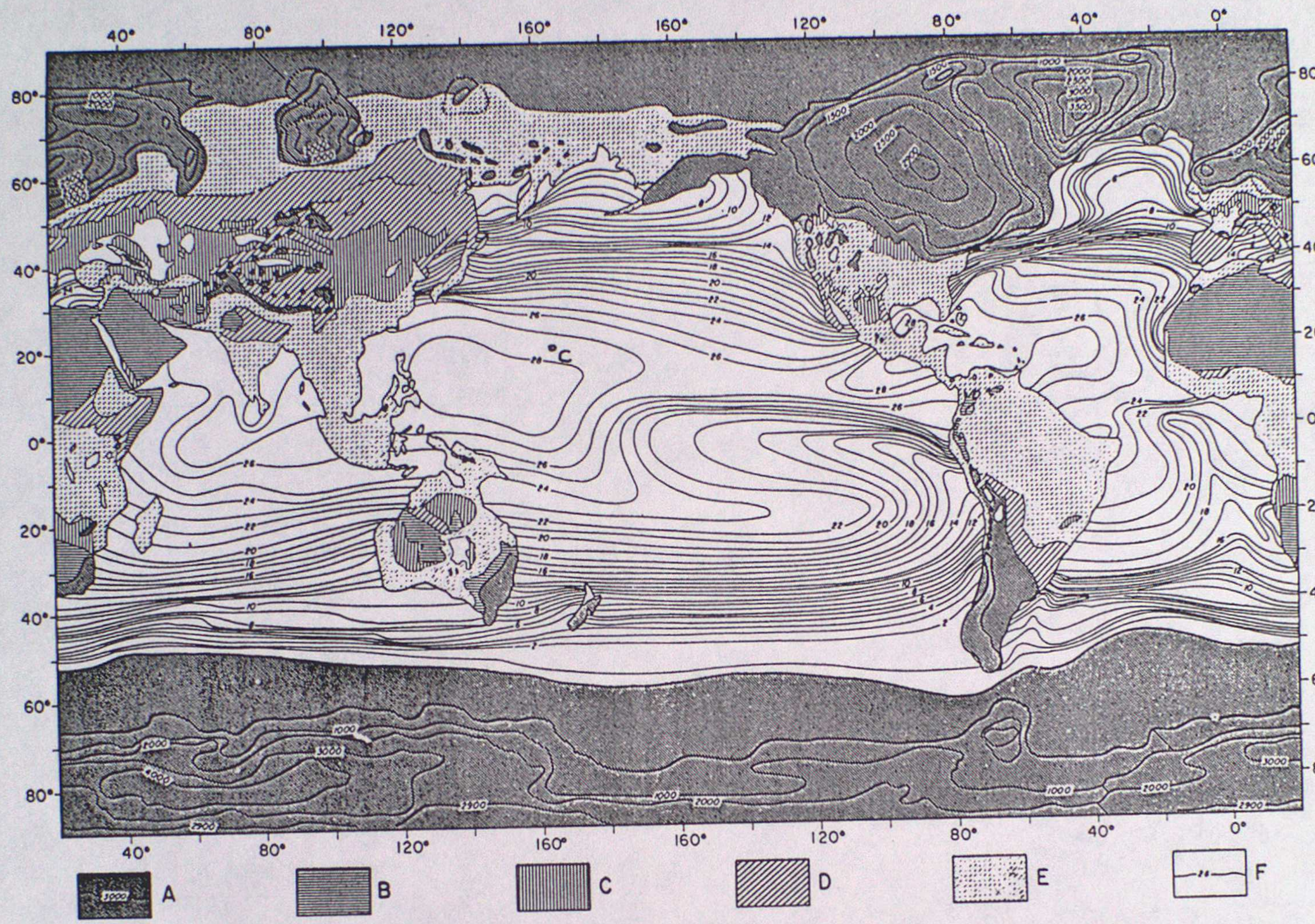
40°
80°
120°
160°
160°
120°
80°
40°
0°
80°
60°
40°
20°
0°
20°
40°
60°
80°
°C
A
B
C
D
E
F

Sea-surface temperatures, ice extent, ice elevation (m) and continental albedo, α (%), for southern winter 18,000 years ago with sea level at −85 m. From CLIMAP.
A, $\alpha > 40$; B, $30 \leqslant \alpha \leqslant 39$; C, $25 \leqslant \alpha \leqslant 29$; D, $20 \leqslant \alpha \leqslant 24$; E, $11 \leqslant \alpha \leqslant 19$;

F, $\alpha \leqslant 10$.

Figure 7.21.

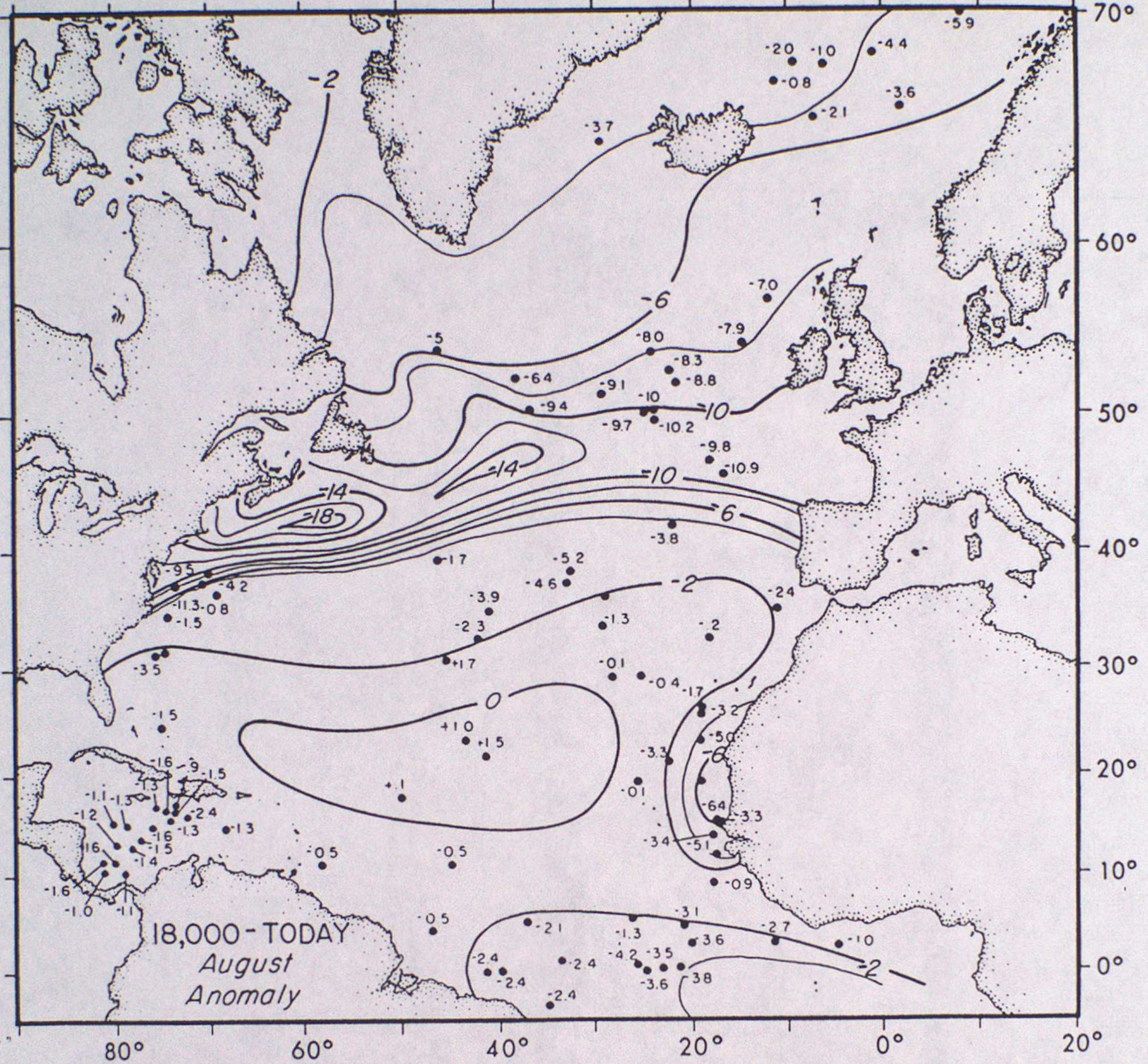
18,000 - TODAY
August
Anomaly
70°
60°
50°
40°
30°
20°
10°
0°
80°
60°
40°
20°
0°
20°
-2
-6
-10
-14
-18
-10
-6
-2
0
-6
-2
-5.9
-2.0
-1.0
-4.4
-0.8
-3.6
-2.1
-3.7
-7.0
-5
-8.0
-7.9
-6.4
-8.3
-8.8
-9.1
-10
-9.4
-9.7
-10.2
-9.8
-10.9
-3.8
-1.7
-5.2
-4.6
-9.5
-4.2
-11.3
-0.8
-1.5
-3.9
-2.3
-1.3
-2.4
-2
-3.5
+1.7
-0.1
-0.4
-1.7
-3.2
-1.5
+1.0
+1.5
-5.0
-3.3
-1.6
-9
-1.5
+.1
-0.1
-6.4
-3.3
-1.1
-1.3
-2.4
-1.2
-1.3
-1.3
-1.6
-1.5
-3.4
-5.1
-1.6
-1.4
-0.5
-0.5
-0.9
-1.6
-1.0
-1.1
-0.5
-2.1
-3.1
-1.3
-3.6
-2.7
-1.0
-4.2
-3.5
-2.4
-2.4
-3.6
3.8
-2.4
-2.4

Temperature-anomaly map for August in degrees Celsius. Values were derived by subtracting average modern surface-water temperatures from 18,000 B.P. values. Contour interval is 2°C.

Figure 7.22. From CLIMAP.

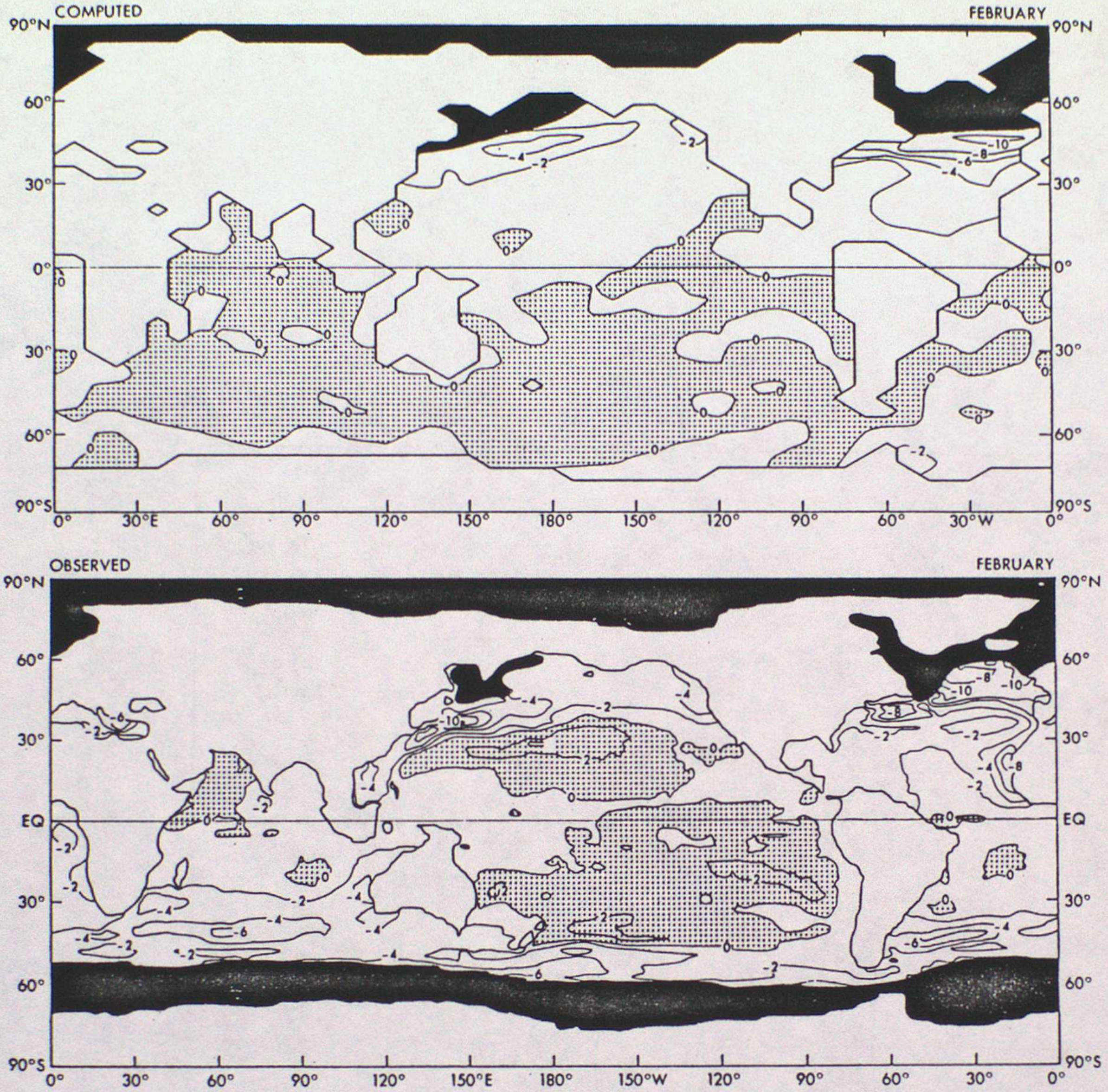
COMPUTED
FEBRUARY
90°N
60°
30°
0°
30°
60°
90°S
0°
30°E
60°
90°
120°
150°
180°
150°
120°
90°
60°
30°W
0°
OBSERVED
FEBRUARY
90°N
60°
30°
EQ
30°
60°
90°S
0°
30°
60°
90°
120°
150°E
180°
150°W
120°
90°
60°
30°
0°

February monthly mean SST difference (degrees Kelvin, stippling indicates positive difference): (top) difference between ice sheet and standard experiments; (bottom) difference between 18K B.P. and present (as reconstructed by CLIMAP). Areas covered by sea ice in the ice sheet experiment and at 18K B.P. are indicated by black shading.

Figure 7.23A. From Manabe and Broccoli (1985).

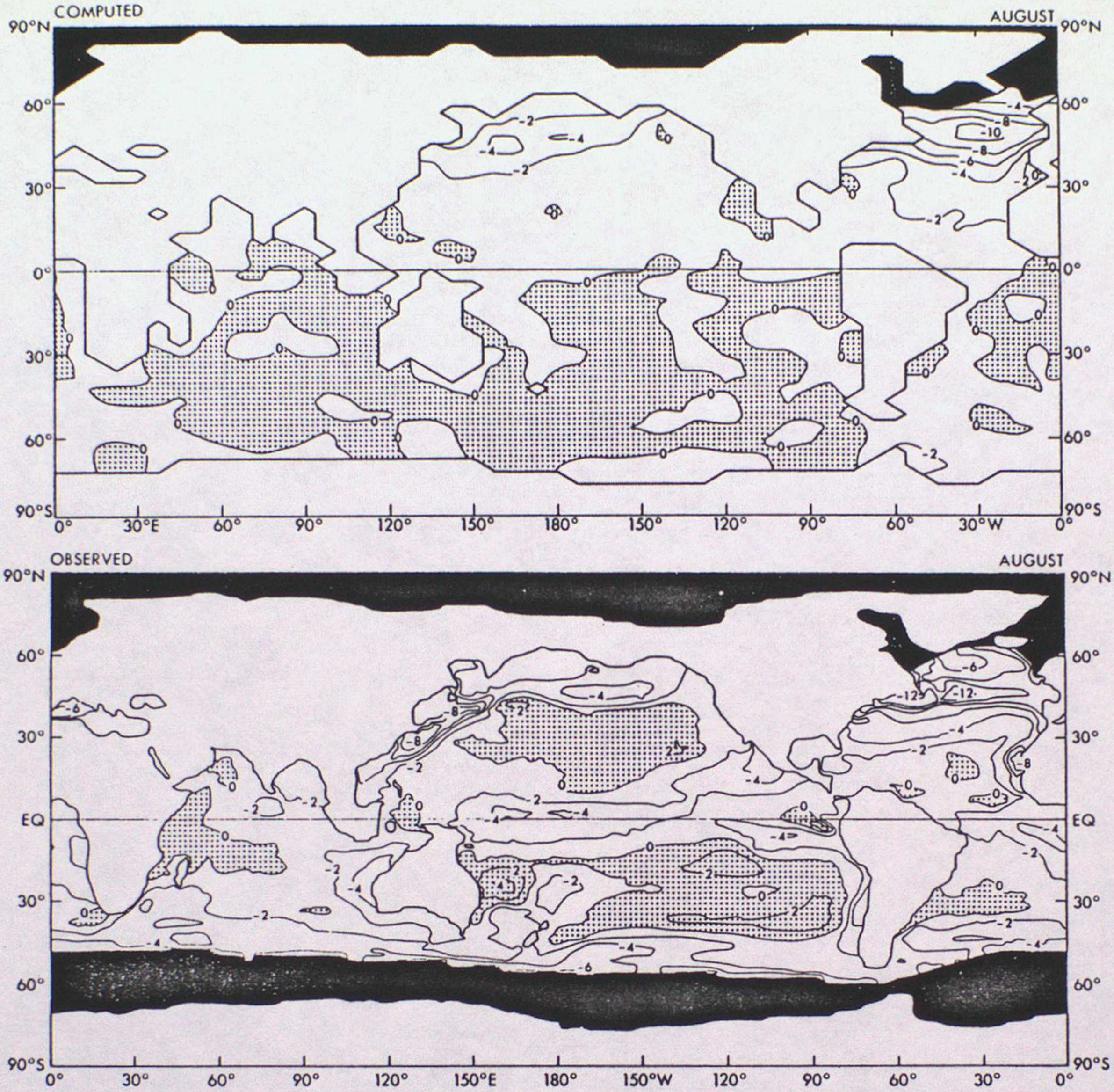
COMPUTED
AUGUST
90°N
60°
30°
0°
30°
60°
90°S
0°
30°E
60°
90°
120°
150°
180°
150°
120°
90°
60°
30°W
0°
OBSERVED
AUGUST
90°N
60°
30°
EQ
30°
60°
90°S
0°
30°
60°
90°
120°
150°E
180°
150°W
120°
90°
60°
30°
0°

Figure 7.23B. As Fig. 7.23A but for August.
From Manabe and Broccoli (1985).

A

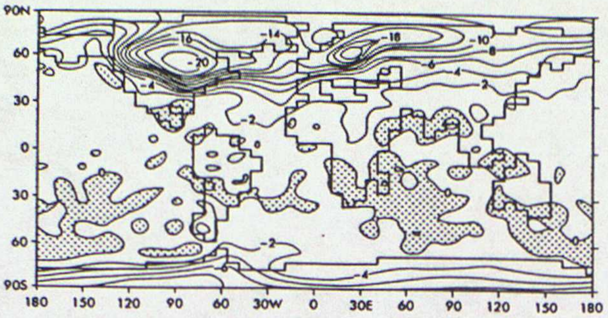

90N
60
30
0
30
60
90S
180
150
120
90
60
30W
0
30E
60
90
120
150
180
-16
-14
-18
-10
-20
-8
-6
-4
-2

Difference in annual mean surface air temperature (°C) between experiments E2 and E1, indicative of the response to changes in the ice sheet distribution. Regions of temperature increase are *stippled*

B

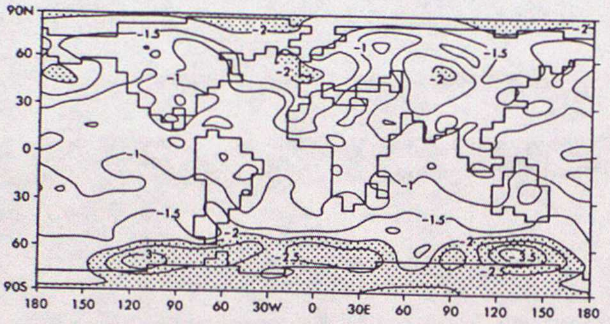

90N
60
30
0
30
60
90S
180
150
120
90
60
30W
0
30E
60
90
120
150
180
-1.5
-2
-1
-2.5
-3
-3.5

Difference in annual mean surface air temperature (° C) between experiments E4 and E3, indicative of the response to reduced CO_2. *Stippling* indicates regions in which the temperature decrease is greater than 2 °C

Figure 7.24 From Broccoli and Manabe (1987)

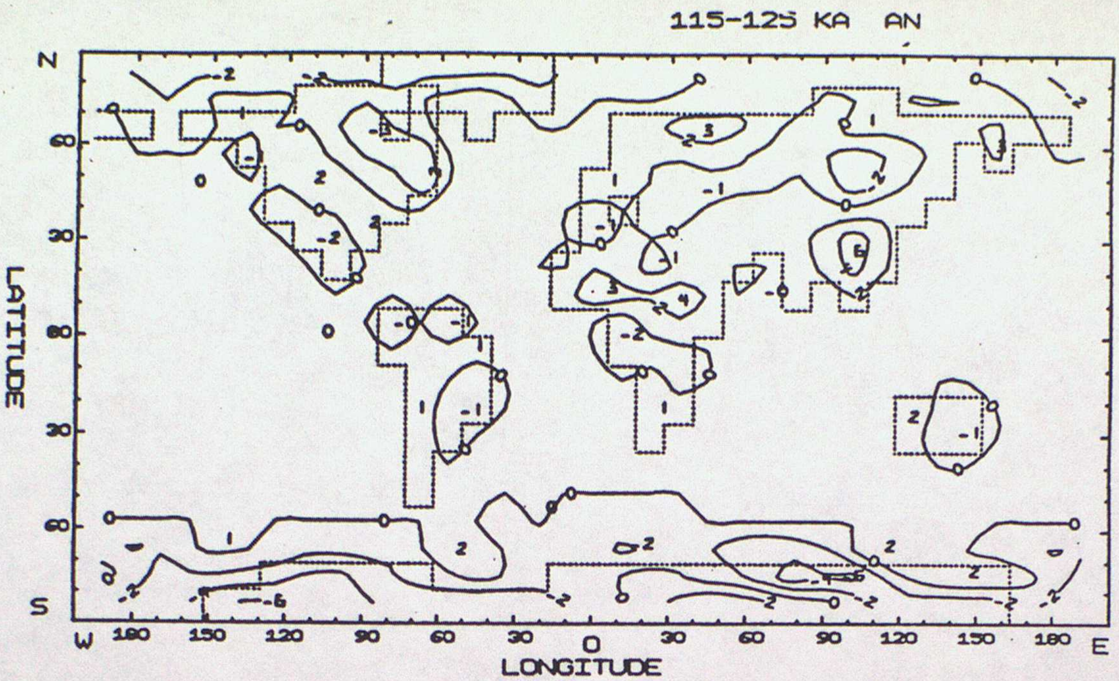
115-125 KA AN
N
S
LATITUDE
60
30
0
30
60
W
E
180
150
120
90
60
30
0
30
60
90
120
150
180
LONGITUDE

Figure 7.25. Difference in annual mean surface temperature, between 115 kyr and 125 kyr simulations. Contours every 2°C. From Royer et al (1984).

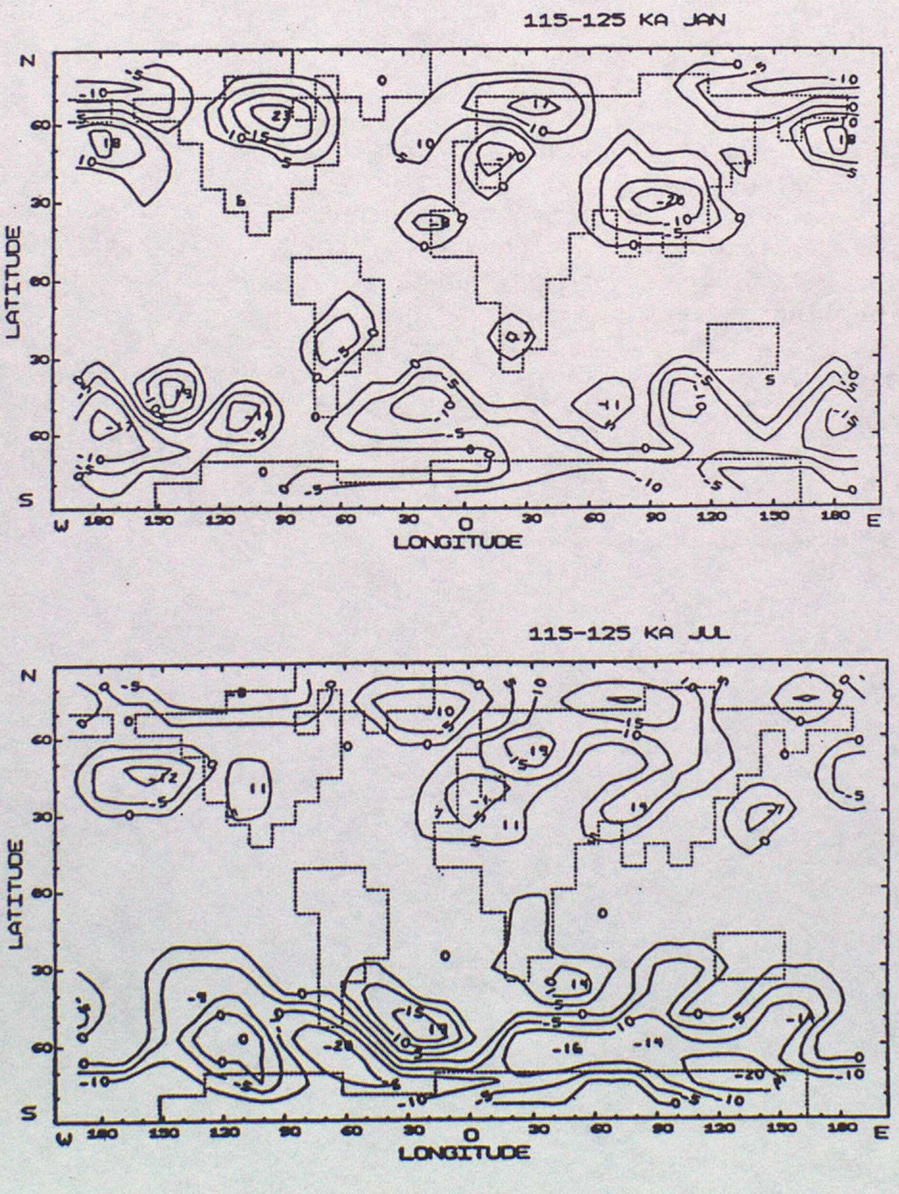
115-125 KA JAN
115-125 KA JUL
N
S
LATITUDE
W
E
LONGITUDE

Figure 7.26. As Figure 7.25 but for MSL pressure for January (above) and July (below). Contours every 5mb. From Royer et al (1984).

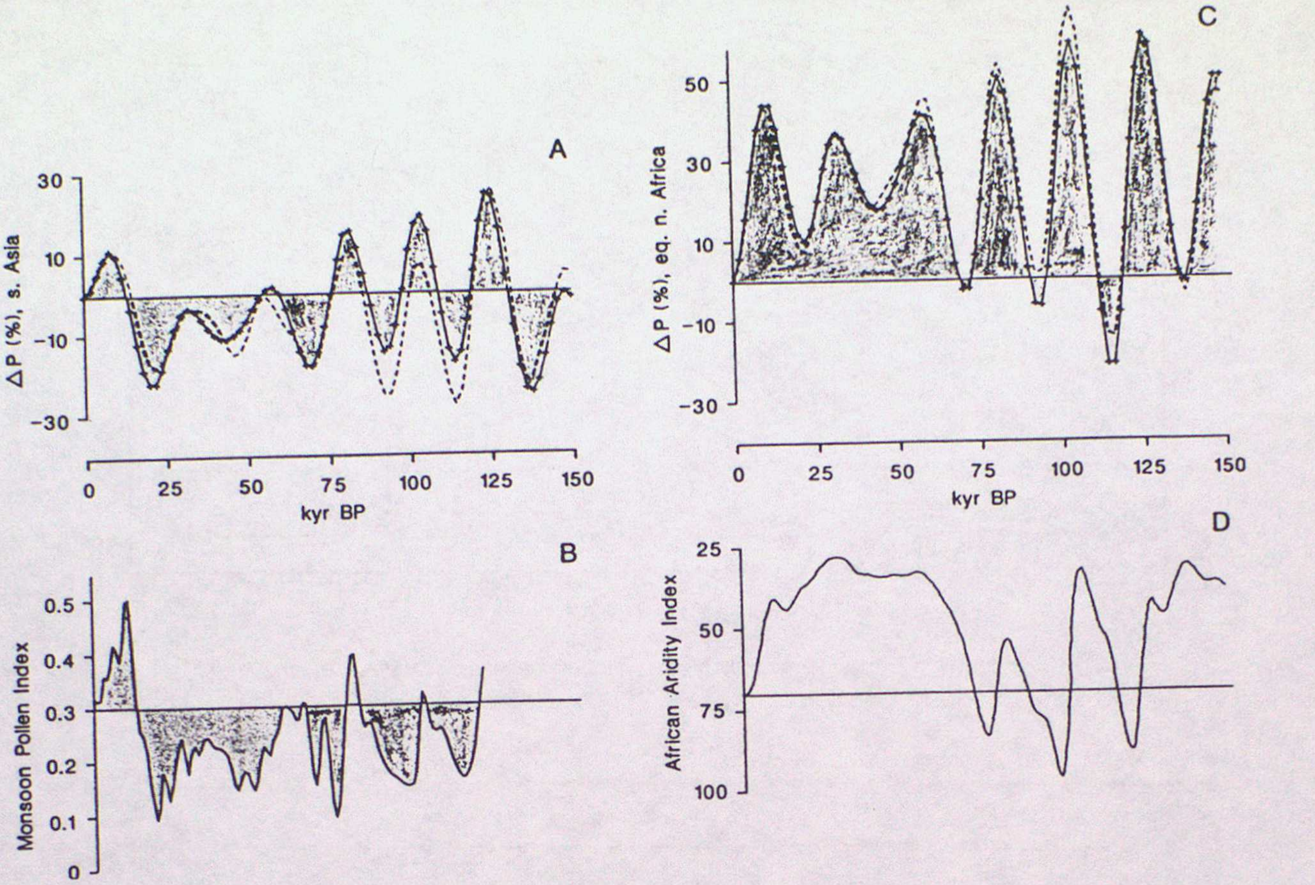

Figure 7.27 Comparison of (A) simulated precipitation difference ΔP(%) for southern Asia with (B) a monsoon pollen record (% of total pollen) from the Gulf of Aden (in which pollen is postulated to increase with wind strength); and comparison of (C) simulated ΔP for equatorial North Africa with (D) the record of equatorial North African wet and dry intervals (arbitrary aridity scale) from Atlantic Ocean aeolian sediments.
In the ΔP plots, the solid line indicates estimates made with global surface boundary conditions (i.e. degree of glaciation and proportionate accompanying changes including SST) based on the $\delta^{18}O$ record: the dashed line indicates estimates made with global surface boundary conditions based on an independent estimate of western Indian Ocean SST.

After Prell and Kutzbach (1987).

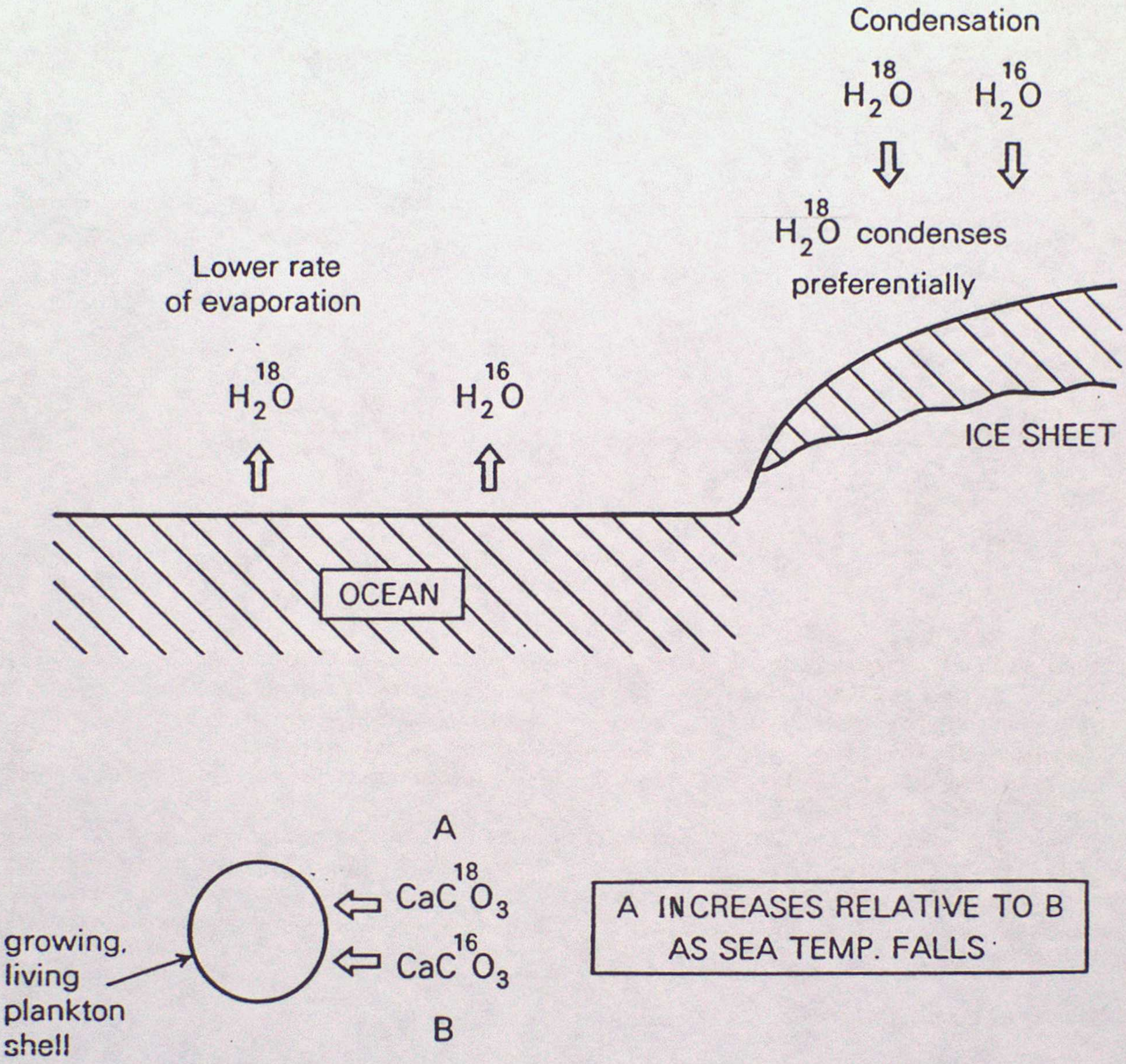
Condensation
$H_2{}^{18}O$
$H_2{}^{16}O$
$H_2{}^{18}O$ condenses preferentially
Lower rate of evaporation
$H_2{}^{18}O$
$H_2{}^{16}O$
ICE SHEET
OCEAN
A
$CaC{}^{18}O_3$
$CaC{}^{16}O_3$
B
growing, living plankton shell
A INCREASES RELATIVE TO B AS SEA TEMP. FALLS

Oxygen isotope method

DO 3723

Figure 7A.1.

CLIMATE FROM THE LATE GLACIAL TO THE LITTLE ICE AGE

C K FOLLAND AND D E PARKER

MET O 13

SUMMARY

After a brief discussion of the physical processes likely to influence climatic change on time-scales of hundreds to thousands of years, we review "proxy" techniques used to reconstruct Holocene climate prior to the historical period. Sea-level variations are discussed in particular. Climatic change in the Holocene is presented with emphasis on the "Younger Dryas" readvance about 10,000 to 11,000 years ago, and on the period about 9,000 years ago when the last maximum of Northern Hemisphere summer radiation occurred. Numerical model simulations of these periods are discussed. Finally, we concentrate on evidence for a cooling of the climate between about 1300 and 1650-1850 AD, the "Little Ice Age".

8.1 PHYSICAL PROCESSES IN CLIMATIC CHANGE

Fig 8.1 from Lamb (1977), provides a useful summary of physical processes affecting climatic change and their time scales. We have already studied some of these in Lecture 7. On time scales of 10^3 - 10^4 years many processes compete. The dynamics and time constants of ice sheet development and decay, and the longest time-scale oceanic processes that may involve the interchange of oceanic bottom waters with the surface oceanic circulation, are very important. Over the last few thousand years man's influence on the land surface has been considerable - in clearing forests, draining marshes and inadvertently extending deserts. Fluctuations in carbon dioxide are also increasingly seen to have occurred on millennial as well as century time-scales (Delmas et al (1980)). As we approach century and lesser time-scales, many of the oceanic circulation processes are likely to occupy a leading position in influencing climatic variability. The role of truly external forcing (e.g. solar variability, volcanic dust) is unclear. Finally, on the shortest time scales relevant to climate and possibly on longer ones as suggested in Fig 8.1 and Lecture 5, internally-caused variations in the atmosphere - surface boundary (ocean and land) system may become important. Interactions involving soil moisture are considered in Lecture 4: Lecture 5 includes some discussion of the interannual time-scale ocean-atmosphere interactions involved in the El Nino-Southern Oscillation (ENSO) but the main treatment of ENSO is in Lecture 6.

8.1.1 Transitivity, intransitivity and almost-intransitivity

A particular problem, raised by Lorenz (1968), is whether the climate is internally stable. Non-linear systems far simpler than the atmosphere - cryosphere - ocean system display a tendency to fluctuate in an irregular manner between two or more internal states (Fig 8.2). In a transitive system, a climatic state B will approach a new state A after the climatic system has been forced from time t=0 by new boundary conditions appropriate to state A. So given boundary conditions correspond to a given climate. In an intransitive system B stays unchanged despite the new forcing, e.g. the "white earth" stays white (Lecture 7) even when the solar constant increases by reasonable amounts. A third type of behaviour is one where the system stays in state B despite the new forcing but after some time it starts to shift toward A where it might remain - or perhaps spontaneously shift back to B. This "flip-flop" behaviour is called "almost intransitive". Until recently, at least, many climatologists considered that ice-age-interglacial fluctuations were quite likely to have been the result of an almost intransitive process of this kind.

8.2 METHODS OF STUDYING POST-GLACIAL CLIMATES

Lamb (1977) gives an extensive description of methods while Critchfield (1983) and Crane (1981) provide a useful summary. The subject is vast. We shall list and describe a few of the main techniques, but see Lecture 7 for some other methods. Fig 8.3 is a diagrammatic summary of some of the techniques.

8.2.1 Radiometric methods for dating

These involve the decay of radioactive isotopes contained in the material being studied; the ratio of the concentration of a radioactive to a non-radioactive isotope of a given element is a measure of the age of a sample. The most usual method for dating Holocene organic material uses the decay of ^{14}C to ^{12}C and assumes a knowledge of the ^{14}C content of the atmospheric carbon dioxide absorbed by the sample when living. ^{14}C is continually created in the atmospheric carbon dioxide by cosmic rays, though not at quite a constant rate because of the variable effects of solar-caused interplanetary magnetic fields. Fig. 8.4 gives an idea of the accuracy of this technique. The technique is not very useful for young samples (less than 150 years old) partly because of the long half-life of ^{14}C (5700 years) and partly because man has changed the proportion of ^{14}C in the atmosphere, and thus in organic samples, through burning of fossil fuel; the resulting carbon dioxide contains a higher proportion of ^{12}C than does the naturally occurring carbon dioxide in the atmosphere.

Other methods include (1) the protoactinium-ionium method (the decay of ^{231}P to ^{230}Th, an isotope of thorium known as ionium), whose standard error of dating is about $\pm$ 1000y for ages 7000 BP - 30000 BP: this decay process has been used occasionally to date deep-sea cores. (2) The uranium -thorium method: this includes several radioactive decay techniques one of which involves the decay ^{234}U to ^{230}Th (ionium) with a half life of 75000 years; the method has been used to date fossil coral reefs which provide important evidence of past sea-level fluctuations.

8.2.2 Varve chronology - dating and climatic evidence

Varves are annual layers of silt and clay deposited on the bottom of certain lakes and ponds which are subject to freezing in winter and thawing in summer. In winter, ice prevents other than fine sediments from settling to the bottom of the lake; in summer a flux of fresh water brings in coarse sediments. Successive years will exhibit different thicknesses of coarse sediment when a core is taken through the sediments. If the varves are of climatic origin, parallel dating of lake beds in a region is possible through matching of varve thickness (Fig 8.5). When the lakes are buried under glaciers, no varves are formed so a comparison of varves in different lake beds can indicate when and where glaciers retreated in a region if parallel dating of the varves can be successfully done. Radiometric dating is often applied, and palaeomagnetic measurements can confirm correlations between sequences. The latter are useful on time-scales of 100 to 10,000 years because of changes of declination and inclination within major magnetic epochs (Street-Perrott and Harrison (1985)). Nearly absolute dating is occasionally possible, depending on the effects of more recent climate variations on the varves previously laid down and on a lack of disturbance to the varves by burrowing creatures, floods etc. Fossil lake varves provide powerful evidence for the geography and timing of the retreat of the Scandinavian ice-sheet in the early Holocene period, for example.

8.2.3 Growth of lichens - Lichenometry

Lichens reaching newly exposed rock-faces after glacier retreat often exhibit (after an initial growth flush) remarkably constant growth rates. Measurements of the sizes of the largest lichens present can therefore provide evidence of the timing of glacier retreat, but only for the last few hundred years. Uncertainties in this method may result from the delay between deglaciation and colonisation by lichen, and from variations in growth rate between lichen types and between sites with differing microclimates and types of rock.

8.2.4 Pollen analysis, soil changes and evidence for past climates

Pollen analysis is a technique for use on land whose approach parallels the study of changes in the species of foraminifera in Lecture 7. By studying the present relationships (ranges and limits) of trees, flowers and shrubs to climate in terms of the density of (very durable) fossil pollen grains left in the soil beneath, it is possible to estimate previous climates by extracting, in widespread locations, cores of soil and identifying and quantifying and dating the fossil pollen grains. The method is not easy to use as trees may take a long while to migrate after a climatic change, disease may strike widely, and trees and plants may compete in complex ways, even in a constant climate. Nevertheless, with the aid of ^{14}C dating and the study of associated past changes in soil type, such as drying out of peat bogs or their re-establishment, it has been possible to construct detailed pictures of Holocene climatic variation in many parts of the world using this technique. Webb (1985) illustrates the use of pollen data for the North American Midwest to reconstruct fields of temperature and precipitation at 9000, 6000 and 3000 BP using multiple linear regressions based on carefully screened modern data. Webb also describes the development of a global palynological data base for the Holocene, as part of the Co-operative Holocene Mapping Project (COHMAP).

8.2.5 Levels of old lakes

Geological evidence of past lake shorelines can indicate changes in the balance between local precipitation and evaporation, given that there have been no past tectonic changes, and that the geography of supply and outlet channels has not altered. Dating of the old shorelines can be done using ^{14}C and other radiometric techniques or by studying fosil varves. Geochemical studies (of past salinity etc deduced from sediments) and palaeoecological techniques can provide further information on past lake depths (Street-Perrott and Harrison (1985)).

8.2.6 Dendrochronology - "Tree Rings"

This technique is based on the observed annual increment of tree growth, the tree ring, and has mainly been used in middle and high latitudes (Fig 8.5). A close relationship between annual rainfall or temperature and the widths of growth rings of trees under climatic stress was demonstrated by A E Douglass, an American, early this century. This relationship includes the longest living of all trees, the bristlecone pine of SW USA (oldest specimens 6-8000 years old). Recently the technique has been extended to forest trees like oak living in W. Europe, where tree rings reflect (mainly) May-September climatic conditions, though in a complex way. Dendrochronology is controversial as complex statistical procedures are needed to allow for many non-climatic factors like ageing of the tree, disease, competition, "weather" factors like isolated late frosts, and the fact that the remaining climatic response itself is often complex, involving, for example, interannual time-lags and persistence in growth characteristics. The sites for analysis need to be chosen to maximise climatic stress factors and to minimise the influence of human interference, fire, disease and competition. Because of occasional missing or double rings, dating has to be confirmed by comparison with sequences from suitable nearby sites. Frequently, empirical orthogonal functions are formed from fields of dendrochronological data and related to empirical orthogonal functions representing climatic patterns. It is necessary to form these relationships using meteorological observations for a recent period and to verify them using data for an independent period. If the relationships are stable, reconstructions of climatic patterns for pre-instrumental periods can be made. The reconstructions made have included not only fields of precipitation and temperature, but also fields of atmospheric pressure, and time-series of river-flows. Examples are given by Stockton et al (1985). The chief reference work is Fritts (1976). Dendrochronology has now been extended to other aspects of tree growth, such as wood density, measured using x-rays. The amount of ^{18}O in a tree ring can possibly be used, with care, as a palaeothermometer, but the uncertainties inherent in isotopic analyses of trees are stressed by Stuiver and Burk in an appendix to Stockton et al (1985).

8.2.7 Beetles

It is believed by some workers that insects react quickly to climatic change. They are useful palaeoclimatic indicators because their ancient remains in soils can be very numerous and can be ^{14}C dated. Beetles have apparently shown almost no tendency to evolution over about the last 250000 years, so by studying the relationships between today's distributions of beetles and temperature, past summer and winter temperatures can be inferred from the past distribution of the remains of different beetle species. Figure 8.6 shows temperatures for Britain (south of 55°N) since 22,000 B.P. deduced in this way by Atkinson et al (1987). The results agree with other palaeoclimatic indicators.

8.2.8 Raised beaches and coral reefs

It is sometimes possible to date raised beaches and, especially, old coral reefs. Corals only grow at or down to about 20-30 m below sea-level. If slow tectonic movements steadily raise reefs, a past, constant sea level is indicated as an extended almost horizontal growth of the exposed fossil reef; rapid falls in sea level will produce rapid downward growth from this level. If the rate of tectonic movement is just correct, a series of stepped surfaces will be created above the changing shore-line. Fig 8.7 shows the most famous example, in New Guinea, which has been used to support the timing of the ice-age-interglacial cycles inferred from deep-sea cores and the Milankovitch radiation cycles.

8.3 SEA-LEVEL VARIATIONS

Fig 8.8 (A) shows a reconstruction (Lamb (1977), p114) of sea-level variations from the mid Tertiary (20 m.y) to the present. Some of the glacial-interglacial cycles are indicated. A long-term fall in sea level seems to be superimposed on the glacial-interglacial cycles; Lamb suggests that this fall may be due to crustal sinking under the ocean floor. The rise at the end of the curve of about 100 m is consistent with the total volume of ice that is believed to have melted since 18000 BP. Fig 8.8 (B) shows a more detailed reconstruction of sea-level over the last 200,000 years while Fig 8.8 (C) gives details of changes in Holocene sea-level, from diverse indicators, due to Fairbridge (1978).

Holocene sea-level reached a global maximum (corrected for tectonic movements) about 4000 BP and has declined by about 4 m since then. There are suggestions of mid-Holocene fluctuations to levels at or below the present level. Fairbridge claims that the sea-level fluctuation about 4900 BP (during the reigns of the early Pharoahs of Egypt) was abrupt, with a 5 m increase in perhaps 250 years. If true, this corresponds to a melting of more ice than currently exists on all mountain glaciers together excluding the Greenland and Antarctic ice caps.

Fairbridge (1987) discusses the non-climatic influences on sea-level. In the Holocene time-frame these include changes in ocean basin shape resulting from changes in the loading of water; filling of basins by sediments; regional glacio-isostatic changes in response to loading and unloading of the Earth's crust by ice; local and regional sedimental loading and compaction; and seismic displacement. Furthermore, local change in the geometric form of embayments, as mean-sea-level changes, can affect tidal ranges, and secular meteorological changes affecting local storminess can result in beach ridges. Nevertheless he concludes that the major global changes in mean sea level in the Holocene are well established.

8.4 POST-GLACIAL CLIMATIC FLUCTUATIONS AND THE MELTING OF THE LAURENTIDE (N AMERICAN) AND SCANDINAVIAN ICE SHEETS

8.4.1 General scheme of temperature fluctuations

Temperature changes in central and southern Britain inferred from beetle remains (Fig 8.6) show a major fluctuation around 12,000 to 9,000 BP. The warm stage at about 12,000 to 11,000 BP is known as the Allerod and the cold period afterwards, from about 10,800 to 10,200 BP, is called the Younger Dryas. The fossil beetle evidence suggests that during the Allerod, summers in central and southern Britain were 1°C or 2°C warmer than at present. The timing of the changes in Fig 8.6 is consistent with estimates based on the evidence from pollen (Lamb (1977), p 232) but the botanical data indicate that the changes had a smaller magnitude.

Rind et al (1986) have compiled palynological (= pollen) and other evidence for, or against, the occurrence of a worldwide temperature fluctuation corresponding to the Allerod-Younger Dryas oscillation. Their results are summarised in Fig 8.9. Evidence for such a fluctuation is strong in northwestern and central Europe and around Newfoundland and Nova Scotia. There is support for the temperature oscillation in two Greenland Ice cores (Dansgaard et al (1982)), at Dye 3 and Camp Century; (see Fig 8.10 (A), especially the area of the Figure between "3" and "2"). A fluctuation from wet (Allerod) to dry (Younger Dryas) conditions in the Colombian Cordillera (5°N, 2850 m) is reported in Flohn (1978); a hint of a decrease of temperature and a strong indication of a decrease of CO_2 (by about 100 ppm) is reported for the same period from the Antarctic "Dome C" ice core (Delmas et al (1980)) (Fig 8.10 (B)). This core also shows a rise in CO_2 from 15000 BP -13000 BP (dates uncertain by $\pm$1000) of about 100 ppm (from 190 ppm to 300 ppm), suggesting that the waxing and waning of world-wide temperature was accompanied by quite large changes in CO_2 on more than one time scale. The results of Barnola et al (1987) for Vostok, Antarctica, also include a suggestion of a temporary reversion to lower temperatures and CO_2 concentrations around the time of the Younger Dryas (Fig 7.20 in Lecture 7). On the other hand, there does not appear to have been a temperature fluctuation in the United States or Australia at the time of the Allerod-Younger Dryas. There is only ambivalent evidence of a temperature oscillation from the New Guinea mountains. Warming occurred up to about 14,000 BP, but then a small glacial advance occurred on Mt Carstensz (5000 m), West Irian, Indonesia (Fig 8.11), where glacier snouts currently reach down to 4300 m. The date of the Younger Dryas deduced from pollen data at Sirunki (Fig 8.11) is later than that implied by the glacial advance, and is more consistent with that estimated for Britain in Fig 8.6. Fig 8.11 is also striking in that it indicates a large warming from 18000 BP - 5000 BP when the CLIMAP SST reconstruction (Lecture 7, Fig 7.23) suggests that SST in the tropical W Pacific region at 18000 BP was, on an annual average, only about 1.5-2.0°C below today's values. Large, roughly contemporary, high mountain warmings have also been inferred by several workers in the equatorial Andes. However an increase of 2°C in SST could give rise to nearly double that increase at 4000 m near the equator. Because of changes in latent heat release in convection, equivalent potential temperature, rather than air temperature, should have changed nearly uniformly with height i.e. the lapse rate probably changed. A modern example of this is given in Lecture 6, viz the fluctuations of tropical tropospheric temperatures and lapse rate associated with El Nino-Southern Oscillation described by Pan and Oort (1983) (Fig 6.10). Alternatively, the CLIMAP SSTs may be too high, since the model of Rind and Peteet (1985) which includes moist convection, yielded tropical air temperatures lower than what pollen and glaciological data indicate, when forced with CLIMAP SSTs (see also Lecture 7).

Fig 8.12 shows a reconstruction of mid-latitude tree lines from 13,000 BP to the present. Fig 8.13 summarises the broad changes in mid-latitude Northern Hemisphere temperatures on several time-scales over the last million years (Lamb (1977), p334) including the Holocene (10000 year) time scale. Research since Lamb published this summary has not greatly altered our estimates of these climatic variations.

8.4.2 The recession of N. Hemisphere ice sheets in the early Holocene

This description is mostly taken from Lamb (1977). Figs 8.14 (A) -(C) show reconstructed positions of the ice sheets for (a) 18000 BP, (b) the Allerod warm phase and (c) the Younger Dryas. Ice had nearly disappeared from Scotland by the end of the Allerod but then strongly readvanced in the Scottish Highlands for a few hundred years in the Younger Dryas. This "Loch Lomond Readvance" left many traces in old moraines and occurred near the Northern Hemisphere Milankovitch radiation maximum. Fig 8.15 shows a reconstruction of the stages in the contraction of the Scandinavian Ice Sheet; the associated emergence of the Baltic is shown in Fig 8.16 (A) - (D). Much of the evidence comes from old shore lines. At first the Baltic was probably a fresh water lake (Fig 8.16 (A)), then as sea-level rose it became the salty "Yaldia Sea", connected now with the Atlantic. The land continued to rise ("isostatic uplift") as the burden of ice disappeared and the Baltic became fresh again (8000 BP). As sea-level rose further, due to melting of the Laurentide ice sheet in N America, the Baltic became salty again. At present the land is rising by up to 1 cm a year in the northern Gulf of Bothnia (near 65°N) so widespread re-emergence of land may occur there in the next 1-2 thousand years unless global sea-level rises. Fig 8.17 shows an old, but apparently acceptable reconstruction of the geography of Britain and NW Europe 1000-2000 years before sea-level rose high enough to turn Britain into an island. Fig 8.18 shows isochrones of the withdrawal of the Laurentide ice sheet. Slowing of the retreat in the Younger Dryas period is suggested. Extensive remnants still exist on Baffin Island (eg Barnes Ice Cap), Devon Island and Ellesmere Island.

8.4.3 Oceanic events during the Younger Dryas

Rind et al (1986) summarised evidence from faunal abundances that there was a large cooling of the sea surface in the extratropical North Atlantic during the Younger Dryas. This cooling was associated with a southward readvance of the oceanic polar front (Fig 8.9 and Ruddiman and McIntyre (1981)), and may have been caused by a major influx of glacial meltwater, which will have been less dense than the saline ocean, and therefore liable to remain at the surface. Boyle and Keigwin (1987) found, from an analysis of ^{13}C and nutrients in a core from the ocean bed (see also Section 7.5.2 in Lecture 7), that the formation of North Atlantic Deep Water was reduced during the Younger Dryas, as it had been during the preceding main glacial epoch. They suggested that this change was accompanied by an increased flux of surface water to intermediate depths, and that the underlying cause was reduced evaporation from a colder sea surface: as a result, salinity and therefore, density would have been reduced, increasing the stability and reducing the depth to which convection in high latitudes penetrated.

Rind et al (1986) carried out atmospheric general circulation model simulations to assess the effects of the cold surface of the extratropical North Atlantic during the Younger Dryas. In the absence of a detailed knowledge of SST for that episode, they forced that model with a) modern boundary conditions and b) CLIMAP (1981) SSTs appropriate to 18,000 BP for the extratropical North Atlantic but present-day SSTs elsewhere, along with present-day land and sea ice, solar radiation, and sea level everywhere. They then repeated the experiments with land ice, solar radiation, and sea-level appropriate to 11,000 BP and with c) present-day SSTs everywhere and d) 18,000 BP SSTs for the extratropical North Atlantic but present-day SSTs elsewhere. Comparison of b) with a) and of d) with c) was taken to indicate the influence of the lower SST on climate in the present-day and in Younger Dryas times respectively. The comparisons (eg Figs 8.19 A, B) both indicated cooling of the air over Europe as well as over the extratropical North Atlantic. In winter the cooling penetrated further east into Asia as a result of advection by the stronger atmospheric circulation. Changes were small in other parts of the world. Mean sea level pressure was increased over the extratropical North Atlantic and the 200 mb jet-stream over the North Atlantic was displaced southward. Comparison of c) with a) was taken to show the influence of land ice, solar radiation, and sea-level: the main difference was that c) was much colder than a) over the ice-caps: in winter the remaining areas of the midlatitude Northern Hemisphere continents were colder in c) than in a) but the reverse held true in summer, when the solar radiation was greater than at present. Finally, comparison of d) with a) was used as a measure of the combined influence of Younger Dryas boundary conditions. The temperature changes (Figs 8.19 C, D) were considered to be broadly consistent with the palynological and other evidence. The warmth southeast of the Scandinavian ice-cap in summer (Fig 8.19 D) was probably a result of atmospheric subsidence caused by the glacial topography.

Mix et al (1986) used faunal abundances deduced from ocean-bed cores to map annual-mean tropical Atlantic SSTs at 2,000 year intervals from 20,000 BP to the present. The main mode of variation occurred symmetrically north and south of the equator and dominated the eastern boundary currents and tropical upwelling areas, which were coldest in glacial times. It may have been driven by a glacial modification of surface winds. The second mode was a weak inter-hemispheric contrast, with the northern (southern) tropical Atlantic relatively cold (warm) during deglaciation, ie, around the time of the Younger Dryas. These features can be seen by comparing their results for 10,000 BP (Younger Dryas) with those for 12,000 BP in Figure 8.20, which also includes a present-day field for comparison.

8.5 THE HOLOCENE MILANKOVITCH RADIATION MAXIMUM - THE SAHARA AND THE SAHEL

There is considerable evidence of increased rainfall in the southern Sahara and the Sahel about 4000-9000 years ago. Cave and rock paintings of many species of savannah animals being hunted or farmed are found from the latter part of this time. An excellent example is shown in Lockwood (1979), p.121. Widespread evidence of expanded lakes occurs in the region (Nicholson and Flohn (1980)), including an enormously extended Lake Chad (Lake Megachad), and other equatorial African and Sahel lakes were larger too (Street-Perrott and Harrison (1985), and Fig 8.21 from Lamb (1977)). The geological, botanical, faunal and anthropological evidence for the moist epoch continues to accumulate. The multidisciplinary study of Petit-Maire (1986) carried out in Mali, and the investigation of an extinct tributary of the Nile by Pachur and Kropelin (1987), are good recent examples. Kutzbach and Guetter (KG) (1984) have carried out two experiments for radiation conditions for 9000 BP to determine if a high resolution AGCM (the NCAR Community Climate model) indicates that a more vigorous African and Asian Summer monsoon was likely during the Holocene radiation maximum. KG carried out two types of "anomaly versus control" experiments:-

(a) Perpetual January and July experiments, with 9000 BP radiation and an extensive Laurentide ice sheet in the anomaly experiments and present day radiation and ice in the control experiment.

(b) Similar, but no Laurentide ice sheet at 9000 BP.

Climatological-mean SST is believed to have been similar, averaged over the year, but with a slightly larger annual range (perhaps 1°C); the model was, however, given modern climatological mean SST in all experiments. Each experiment was run for 120 days and the final 90 days averaged. Global maps of the differences between anomaly and control experiments are shown in Fig 8.22 (A) - (C) for surface temperature and 8.23 (A) -(C) for MSL pressure.

In winter, Northern Hemisphere land at higher latitudes is simulated to be colder at 9000 BP than now as a result of the reduced winter radiation but in summer the land is much warmer than now because radiation is larger. Thus the seasonal range increases, by 3°C over Northern Hemisphere land as a whole. In summer, the Laurentide ice sheet only lowers temperatures in its immediate vicinity: just upstream, (Fig 8.22 (B)) the surface temperature is considerably higher than now in summer. In winter, the Laurentide ice sheet reduces MSL pressure considerably over the N. Atlantic/W. European region by inducing a large lee trough (Fig 8.23C). In summer, the 9000 BP monsoon circulation over N. Africa and S. Asia is considerably enhanced (Fig 8.23 (B)). Precipitation increases in the area from 30°E to the east Asian coast and south of 40°N by 20% according to KG. Fig 8.24 summarises the zonally-averaged precipitation changes. In July, increased precipitation associated with the ITCZ at 9000 BP is shown; the vertical bars represent 1 standard deviation of the control integrations (1050 model days were available for modern (control) conditions). So given the archaeological evidence as well it is very likely that summer rainfall was larger in the Sahel/Sahara at 9000 BP than now and probably for some thousands of years afterwards.

In a further development of this work, Kutzbach and Gallimore (1988) obtained a similar sensitivity to orbital forcing at 9000 BP using a coupled atmosphere - mixed layer ocean model. As a result of changed ocean-atmosphere heat fluxes, the ocean generally warmed relative to their control in northern autumn, but cooled in other seasons, especially northern spring, though all the changes were small. However, they did not include the Laurentide ice sheet in this study, and they acknowledged the need to incorporate ocean dynamics and more realistic treatments of sea ice and cloudiness. Mitchell et al (1988) have performed similar experiments and also obtained strengthened monsoon circulations, though over western North Africa precipitation was reduced because of reduced soil moisture resulting from a lack of early-season precipitation. They also obtained warmer oceans at all seasons in the extratropical Northern Hemisphere, partly because of a reduction of cloudiness in summer allowing increased insolation.

8.6 HOLOCENE MAXIMUM (HYPSITHERMAL)

Figs 8.12 and 8.13 suggested that rather modest changes of worldwide climate have occurred since 5000 BP (3000 BC), at least up to 1000 AD. Details are difficult to unravel but about 3000-3500 BC there is evidence of a near-global short period cooling, the "Piora Oscillation" (Fig 8.25). The details of Holocene climate are currently being pieced together for the whole globe by COHMAP (Cooperative Holocene Mapping Project) in USA (Webb (1985)). Many proxy techniques are being used including pollen analysis and deep-sea core analysis. It is hoped to reconstruct a mean picture of climate about every 3000 years since 18,000 BP. Fig 8.26 is an example of vegetation mapping in N. America for 10000 BP, 6000 BP and 1500 AD (Kerr (1984)). Note the close approach of forest to the margin of the Laurentide Ice Sheet at 10,000 BP.

About 4000 BP (2000 BC), the advanced Harrapan culture of the now Thar Desert in Rajastan (N India) declined and disappeared. Fig 8.27, from Lamb (1982), suggests this was due to a strong reduction of summer monsoon rainfall towards current conditions. The climatic evidence has mostly been obtained from pollen cores drilled beneath the beds of former lakes that now occupy positions between sand dunes.

Subsequently there is evidence that soon after 1000 BC a sharp cooling occurred. During this "sub-Atlantic pessimum" temperature may have been widely lower by about 2°C, and the mountain glaciers advanced (Fig 8.25). In classical Roman times the climate was probably rather like nowadays but in early Rome the climate was probably cooler according to the testimony of several Latin authors. By around 500 AD the glaciers advanced again (Fig 8.25) but about 800 AD, possibly later, there is evidence of a climatic warming in the middle and high N. Hemisphere latitudes. This was the time (870-950) of the settlement by the Norse of, first, Iceland and then, Greenland. In the High Middle Ages vineyards were common in England and good quality wines were produced where wine growing is hazardous nowadays. This was the so-called Little Optimum (at least in W. Europe) and shows well on the graph of temperatures of the last 1000 years (Fig 8.13). The Little Optimum appears to represent a change in climate in many parts of the Northern Hemisphere but it may have been absent in the Southern Hemisphere (Fig 8.25). Growth of some of the Bristlecone pines in south-west USA when near the tree line is believed to be controlled by summer temperature. Fig 8.28A (from two locations in California) shows slight evidence of the Piora temperature oscillation, the 1000 BC - 500 BC cool period and the cooling since the Medieval Optimum; the latter does not show as a peak but rather as a halt in a steady decline of temperature. The Alpine tree-line curve (Fig 8.28 B) is broadly similar in shape except it shows a more definite medieval climatic optimum, and it does not extend back to the Piora oscillation.

8.7 "LITTLE ICE AGE": WAS IT WORLDWIDE?

There is geographically widespread evidence for a cooler climate worldwide from after 1400 AD until about 1850 (Grove (1988)). Not every location shows this, however, possibly because of changes in atmospheric circulation patterns. For example, Fig 8.29 from Lamb (1977) shows the results of a survey of historical documents and weather records in Europe and Japan that attempts to summarise the changing frequency of cold winters in these two areas 120° of longitude apart. The diagram suggests that Japanese winter temperatures have fluctuated largely out of phase with those of European winters. A further caveat is that changes in the phase of the midlatitude long waves can give an impression of global warmth or coldness if sampling is longitudinally restricted. Also, as shown in Lectures 5 and 9, it is not necessarily true that, if one hemisphere cools or warms, the other behaves similarly. However, the following evidence does suggest a widespread cooler climate in the "Little Ice Age".

Fig 8.30, from Lamb (1977), shows indirect evidence of century time-scale temperature variations in New Zealand. The 17th century appears to have been the coldest.

It is possible to use ^{18}O measurements in the wood of oaks to determine past changes of temperature, at least in a relative sense. Dating is done by counting tree rings, and the ^{18}O concentration is measured in the individual rings. Fig 8.31, from Lamb (1977), shows such a reconstruction for some trees in Germany. The period 1600 to 1900 AD was, apparently, generally the coldest, except for short-lived warmth around 1720-60.

Lamb (1987) discusses the documentary and tree ring evidence for the breakdown of the mediaeval warm climate in Europe in the 14th and 15th Centuries, and presents schematic average MSL pressure fields for summer and winter for some decades and for some individual years. There appears to have been more variability than in the preceding centuries. Severe winters and cold, wet summers were both more frequent. Freezing of rivers and canals was more frequent in Europe around 1600-1800.

Most impressive are the results of widespread investigations of the moraines left by mountain glaciers (Fig 8.25). In many parts of the world there is increasingly strong evidence that the glaciers on many mountains were the most advanced around 1600-1800 AD since the time of the Younger Dryas. Grove (1988) gives a comprehensive presentation of the evidence in all parts of the world. LeRoy Ladurie (1971) gives an excellent description for the Alps, and Hastenrath (1981) for the Ecuadorian Andes and other tropical areas. Hastenrath's study, in fact, reaches back to the Pleistocene.

There is no doubt that conditions in the Iceland-Greenland area became much colder after 1200 AD and especially after 1550 AD. In Lecture 3 we showed a diagram (Fig 3.15) of the reconstructed variation of sea-ice around Iceland in weeks per year; the period around 1800 seems to have been the worst for sea-ice. The Norse colony in S. Greenland established around 900 AD probably died out in the fifteenth century as climatic conditions became worse, sea ice prevented access (from Iceland and Europe) and crops failed (LeRoy Ladurie (1971), Grove (1988)).

Fig 8.32 shows the variation of ^{18}O in a Greenland ice core (Dansgaard et al (1975)); absolute dates are probably not accurate but a tendency to coolness after about 1100-1200 AD is clearly shown as is the rise in temperature at the beginning of the twentieth century. Temperature increases to the right on this diagram. Similar trends are suggested by the results of Morgan (1985) for an Antarctic ice core.

Lamb also describes documentary evidence of observations of extensive sea ice flows around the Faeroe Islands in a few winters in the seventeenth century and once or twice, ice floes reached the Shetland Isles. Eighteenth century travellers frequently mention permanent snowbeds in the Cairngorms. In recent years lichenometry has been used to indicate that certain hollows in the Scottish mountains might well have been permanently filled with snow for lengthy periods up to the middle of the last century.

Grove (1988) discusses possible causes of the Little Ice Age. These include:

a) Ocean-atmosphere interactions entailing southward displacement of the Gulf Stream and North Atlantic Drift;

b) Changes of deep-ocean circulation, possibly also involving changes in atmospheric CO_2 content;

c) Reduction of salinity in the North Atlantic as a result of changed transports of water vapour in the atmosphere. This would facilitate the formation of sea-ice. The thermohalne circulation would also be inhibited, resulting in a positive feedback, via reduced poleward advection of both heat and salt.

d) Positive ice-albedo feedback.

e) Variations in solar radiation, possibly associated with variations of numbers of sunspots (see Lecture 3 (Section 3.1.2 and Fig 3.6)).

f) The effects of volcanic eruptions. Fig 8.33 shows a strong negative correlation between indices of Northern Hemisphere temperature and (volcano-induced) acidity in a core in the Greenland ice.

The latter part of the Little Ice Age overlaps with the instrumental period so we can analyse it further in Lecture 9.

REFERENCES TO ADVANCED LECTURE 8

ATKINSON, T C, BRIFFA, K R and COOPE, G R (1987) Seasonal temperatures in Britain during the past 22,000 years, reconstructed using beetle remains. Nature, 325, 587-592.

BARNOLA, J M, RAYNAUD, D, KOROTKEVICH, Y S and LORIUS, C (1987) Vostok ice core provides 160,000 - year record of atmospheric CO_2. Nature, 329, 408-414.

BOWLER, J M, HOPE, G S, JENNINGS, J N, SINGH, G, and WALKER, D (1976) Late Quaternary Climates of Australia and New Guinea. Quaternary Research, 6, 359-394.

BOYLE, E A and KEIGWIN, L (1987) North Atlantic thermohaline circulation during the past 20,000 years linked to high-latitude surface temperature. Nature, 330, 35-40.

BRYSON, R A, WENDLAND, W A, IVES, J D, and ANDREWS, J T (1969) Radiocarbon isochrones on the disintegration of the Laurentide ice sheet. Arctic and Alpine Research, 1, 1-14. Boulder, Colorado.

BURROWS, C J (1973) Studies on some glacial moraines in New Zealand. II. The ages of moraines of the Mueller, Hooker and Tasman glaciers. New Zealand J. Geol. Geophys, 16, 831-856.

BURROWS, C J (1975) Late Pleistocene and Holocene moraines of the Cameron valley, Arrowsmith Range, Canterbury, New Zealand. Arctic and Alpine Research, 7, 125-140.

BUTZER, K W, ISAAC, G L, RICHARDSON, J L and WASHBOURN-KAMAU, C (1972) Radiocarbon dating of East African lake levels. Science, 175, 1069-1076.

CLIMAP Project Members (1981). Seasonal reconstruction of the Earth's surface at the last glacial maximum. Geological Society of America Map and Chart Series MC-36.

CRANE, A J (1981) Techniques for reconstructing Past Climates. In "Climatic Variations and Variability: Facts and Theories". Ed:- A Berger. Reidel.

CRITCHFIELD, H J (1983) General Climatology. 4th Edition. Prentice-Hall.

DANSGAARD, W, CLAUSEN, H B, GUNDESTRUP, N, HAMMER, C U, JOHNSEN, S F, KRISTINSDOTTIR, P M and REEH, N (1982) A new Greenland Deep Ice Core. Science, 218, 1273-1277.

DANSGAARD, W, JOHNSEN, S J, CLAUSEN, H B and LANGWAY, C C Jr. (1971) Climatic record revealed by the Camp Century ice core. In "The Late Cenozoic Glacial Ages", ed. K.K. Turekian. Yale Univ. Press, New Haven, pp 37-56.

DANSGAARD, W, JOHNSEN, S J, REEH, N, GUNDESTRUP, N, CLAUSEN, H B, AND HAMMER C U (1975) Climatic changes, Norsemen, and modern man. Nature, 255, 24-28.

DE GEER, E H (1954) Skandinaviens geokronologi. Geol. Foren. Forhandl., (GFF), 76, 299-329. Stockholm.

DELMAS, R J, ASCENCIO J M and LEGRAND M (1980) Polar ice evidence that atmospheric CO_2 20000 yr BP was 59% of present. Nature, 284, 155-157.

DENTON, G H and KARLEN, W (1973) Holocene climatic changes, their pattern and possible cause. Quaternary Research, 3, 155-205.

FAIRBRIDGE, R W (1961) Eustatic changes in sea level. In "Physics and Chemistry of the Earth", Vol. 4, Pergamon Press, London, pp. 99-185.

FAIRBRIDGE, R W (1962) World sea level and climatic changes. Quaternaria, 6, 111-134.

FAIRBRIDGE, R W (1976) Shellfish-eating preceramic Indians in Coastal Brazil. Science, 191, 353-359.

FAIRBRIDGE, R W (1978) Models of Climatic Change: Global Cycles and Climate. In "Climatic Change and Variability - a Southern Perspective". Eds: A B Pittock et al. Cambridge Univ. Press, pp. 200-211.

FAIRBRIDGE, R W (1987) The spectra of sea level in a Holocene time frame. In "Climate. History, Periodicity, and Predictability", Eds M R Rampino, J E Sanders, W S Newman and L K Konigsson. Van Nostrand Reinhold Co. New York. pp 127-143.

FLOHN H (1978) The long-term climatic record: Abrupt events in climatic history. In: "Climatic Change and Variability - a Southern Perspective". Ed: A B Pittock et al, Cambridge University Press, pp. 124-134.

FRITTS, H C (1976) Tree rings and climate. Academic Press.

GEYH, M A and JAKEL, D. (1974) Late Glacial and Holocene climatic history of the Sahara Desert derived from a statistical assay of carbon-14 dates. Palaeogeography, Palaeoclimatology and Palaeoecology, 15, 205-208.

GODWIN, H (1956) The History of the British Flora. Cambridge Univ. Press. 384 pp.

GROVE, J M (1988) The Little Ice Age. Methuen, 498 pp.

HAMMER, C U, CLAUSEN, H B and DANSGAARD, D W (1981) Past volcanism and climate revealed by Greenland ice cores. J Volcanology and Geothermal Research, 11, 3-10.

HASTENRATH, S (1981) The Glaciation of the Ecuadorian Andes. A A Balkema, Rotterdam, 159 pp.

HULTEN, E (1971) Atlas over vaxternas utbredning I norden. Stockholm (Generalstabens Litografiska Anstalt). 531 pp.

IMBRIE, J and IMBRIE, K P (1979) Ice Ages - solving the Mystery. MacMillan, London. 224 pp.

KERR, R A (1984) "Climate since the ice began to melt", Science, 226, 326-327.

KUTZBACH, J E and GALLIMORE, R G (1988) Sensitivity of a coupled atmosphere/mixed layer ocean model to changes in orbital forcing at 9000 years BP. J Geophys. Res., 93, D1, 803-821.

KUTZBACH, J E AND GUETTER, P J (1984) The sensitivity of monsoon climates to orbital parameter changes for 9000 years BP: Experiments with the NCAR general circulation model. Milankovitch and Climate, Vol 2, pp 801-820.

LAMARCHE, V C (1974) Palaeoclimatic inferences from long tree-ring records. Science, 183, 1043-1048.

LAMB, H H (1969) Climatic fluctuations. Pp. 173-249 in "World Survey of Climatology" (general Ed. H.E. Landsberg), Vol. 2: General Climatology (Ed. H. Flohn). Elsevier, Amsterdam.

LAMB, H H (1977) Climate: Present, Past and Future Vol 2. Methuen. 835 pp.

LAMB, H H (1982) Climate, history and the modern world. Methuen.

LAMB, H H (1987) What can historical records tell us about the breakdown of the medieval warm climate in Europe in the Fourteenth and Fifteenth Centuries - an experiment. Beitr. Phys. Atmos, 60, 131-143.

LE ROY LADURIE, E (1971) Times of Feast, Times of Famine: A History of Climate since the year 1000. Trans. B Bray; Doubleday.

LEVITUS, S (1982) Climatological Atlas of the World Ocean. NOAA Prof. Pap. 13. NOAA, Washington, DC, 188 pp + 17 fiche.

LOCKWOOD, J G (1979) Causes of Climate. Edward Arnold, London, 260 pp.

LORENZ, E N (1968) Climatic Determinism. In "Causes of Climatic Change" Ed: J M Mitchell, Met Monograph 8, pp 1-3. Boston: Amer. Met. Soc.

MARKGRAF, V (1974) Palaeoclimatic evidence derived from timberline fluctuations. Pp. 67-83 in "Les Methodes quantitatives d'etude des variations du climat au cours du Pleistocene" (Ed. J. Labeyrie). Colloques internat. du. C.N.R.S. No. 219, Paris (C.N.R.S). 317 pp.

MITCHELL, J F B, GRAHAME, N S and NEEDHAM, K J (1988) Climate simulations for 9000 years before present: seasonal variations and effect of the Laurentide ice sheet. Submitted to J Geophys. Res.

MITCHELL, J M (1963) On the world-wide pattern of secular temperature change. Pp 161-181 in "Changes of Climate": Proc. UNESCO/WMO Rome 1961 Symp. (UNESCO Arid Zone Research Series, XX). Paris.

MIX, A C, RUDDIMAN, W F and McINTYRE, A (1986). Late Quaternary paleoceanography of the tropical Atlantic, 1: Spatial variability of annual mean sea-surface temperatures, 0-20,000 years BP. Paleoceanography, 1, 43-66.

MORGAN, V I (1985) An oxygen isotope - climate record from the Law Dome, Antarctica. Climatic Change, 7, 415-426.

MORNER, N A (1969) The late Quaternary history of the Kattegatt Sea and the Swedish west coast. Sveriges Geologiska Undersokning, Ser. C, No. 640, 487 pp.

NATIONAL ACADEMY OF SCIENCES (1975). Understanding Climatic Change - A Program for Action. Washington, D.C.

NICHOLSON, S E AND FLOHN, H (1980) African environmental and climatic changes and the general atmospheric circulation in Late Pleistocene and Holocene. Climatic Change, 2, 313-348.

PACHUR, H-J and KROPELIN, S (1987) Wadi Howar: Paleoclimatic evidence from an extinct river system in the Southeastern Sahara. Science, 237, 298-300.

PAN, Y H and OORT, A.H. (1983) Global climate variations connected with sea surface temperature anomalies in the eastern equatorial Pacific for the 1958-73 period. Mon. Weath. Rev., 111, 1244-1258.

PETIT-MAIRE, N (1986) Palaeoclimates in the Sahara of Mali. A multidisciplinary study. Episodes, 9, 7-16. International Union of Geological Sciences.

RIND, D and PETEET, D (1985) Terrestrial conditions at the last glacial maximum and CLIMAP sea-surface temperature extimates: are they consistent? Quaternary Research, 24, 1-22.

RIND, D, PETEET, D, BROECKER, W, McINTYRE, A and RUDDIMAN, W F, (1986) The impact of cold North Atlantic sea surface temperatures on climate: implications for the Younger Dryas cooling (11-10K). Climate Dynamics, 1, 3-33.

RUDDIMAN, W F and McINTYRE, A (1981) The North Atlantic Ocean during the last glaciation. Palaeogeography, Palaeoclimatology and Palaeoecology, 35, 145-214.

STOCKTON, C W, BOGGESS, W R and MEKO, D M (1985) Climate and tree rings. In "Paleoclimate analysis and modeling", Ed. A D HECHT, Wiley, pp 71-161.

STREET-PERROTT, F A and HARRISON, S P (1985) Lake levels and climate reconstruction. In "Paleoclimate analysis and modelling", Ed A D HECHT, Wiley, pp 291-340.

TEN BRINK, N W and WEIDICK, A (1974) Greenland ice sheet history since the last glaciation. Quaternary Research, 4, 429-440.

VEEH, H H and CHAPPELL, J (1970) Astronomical theory of climatic change: support from New Guinea. Science, 167, 862-865.

WEBB, T (1985) Holocene Palynology and Climate. In "Paleoclimate analysis and modelling", Ed. A D HECHT, Wiley, pp 163-195.

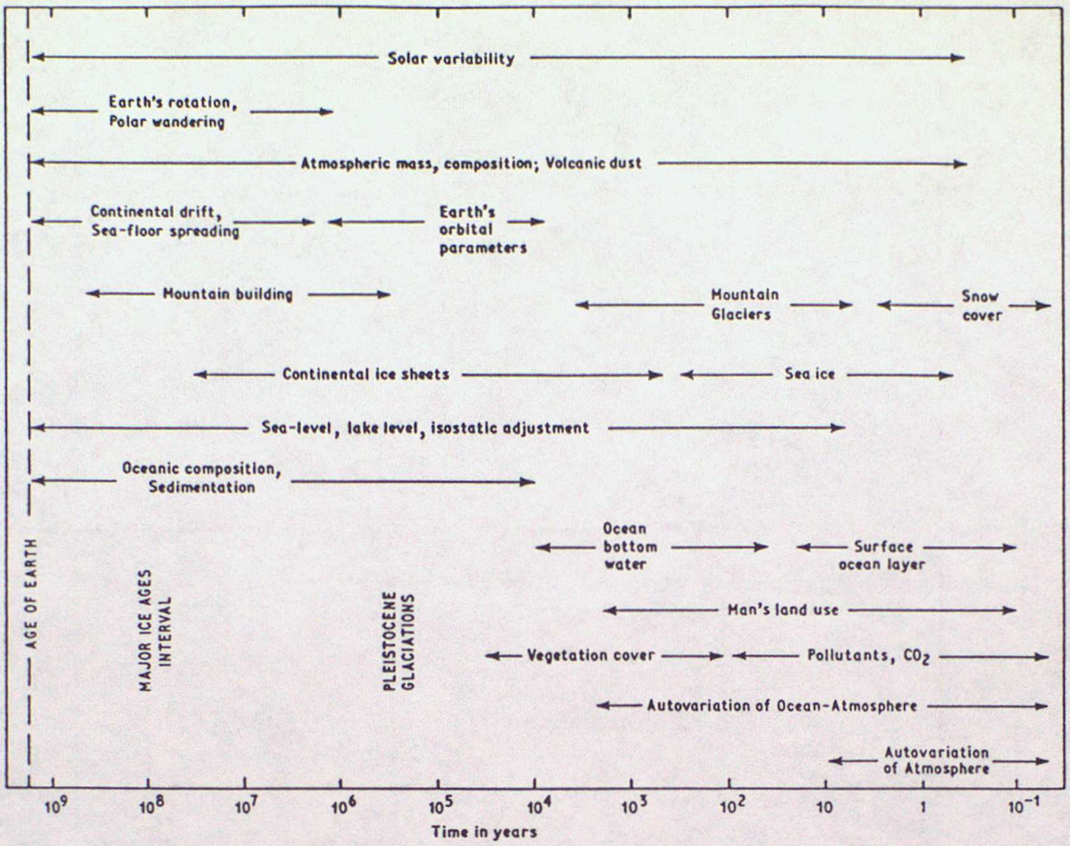

Summary diagram to show the characteristic time-scales over which changes in various influences upon the global climate operate.

(*Adapted from a diagram by* W. L. GATES.)

Figure 8.1. From Lamb (1977).

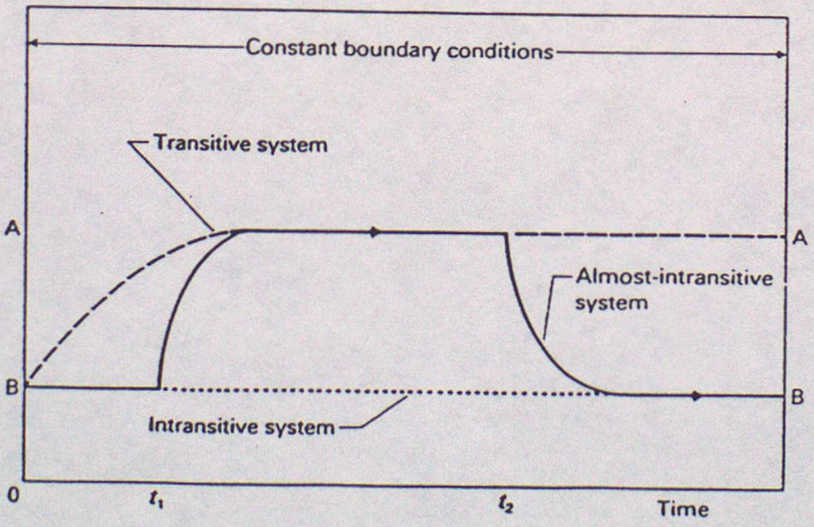
Constant boundary conditions
Transitive system
A
A
Almost-intransitive system
B
B
Intransitive system
0
t_1
t_2
Time

Illustration of the behaviour of transitive, intransitive and almost-intransitive climatic systems with respect to an initial climatic state B. The climatic state A is an alternative bistable state under the same boundary conditions (*after US National Academy of Sciences, 1975*).

Figure 8.2.

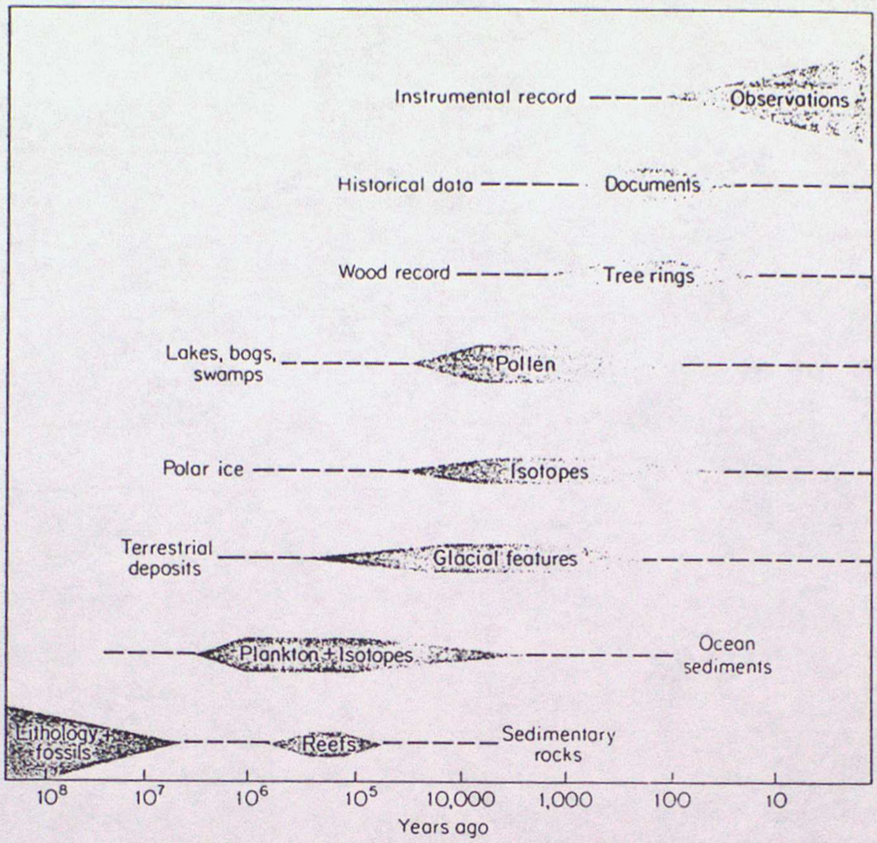
Instrumental record
Observations
Historical data
Documents
Wood record
Tree rings
Lakes, bogs, swamps
Pollen
Polar ice
Isotopes
Terrestrial deposits
Glacial features
Plankton + Isotopes
Ocean sediments
Lithology + fossils
Reefs
Sedimentary rocks
10^8
10^7
10^6
10^5
10,000
1,000
100
10
Years ago

Types of evidence for climatic change and their approximate time scales.
(After Bernabo, *EDIS*.)

Figure 8.3. From Critchfield (1983).

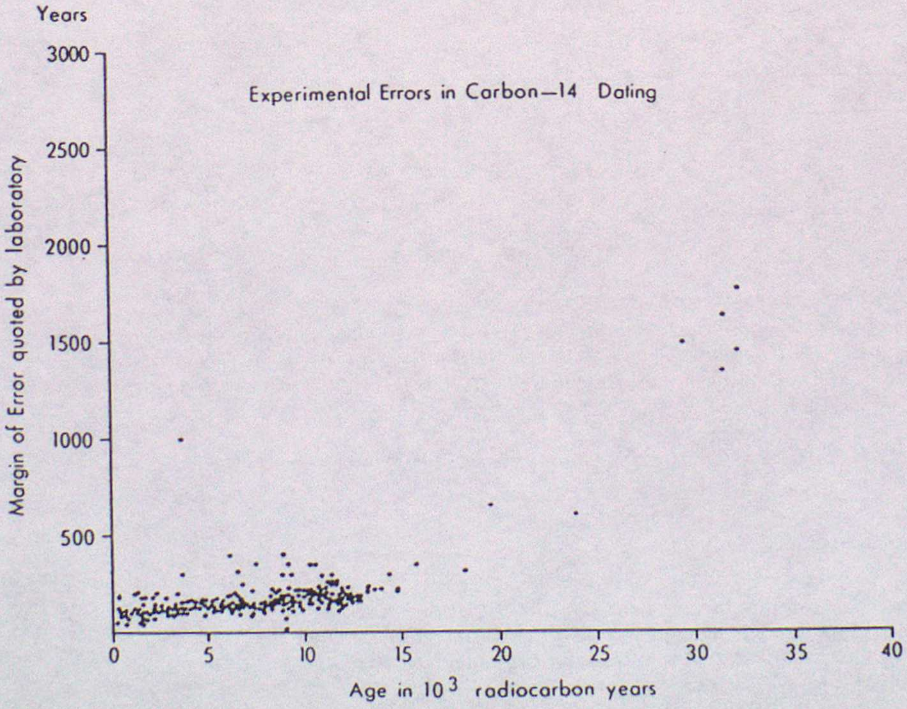

Experimental errors (i.e. random error) in radiocarbon dating.
The plotted points are estimates of one sigma error published with the age results of measurements made in the Cambridge, Copenhagen and Washington University radiocarbon laboratories between 1959 and 1968.
(*From Radiocarbon, vols. 1–10.*)

Figure 8.4. From Lamb (1977).

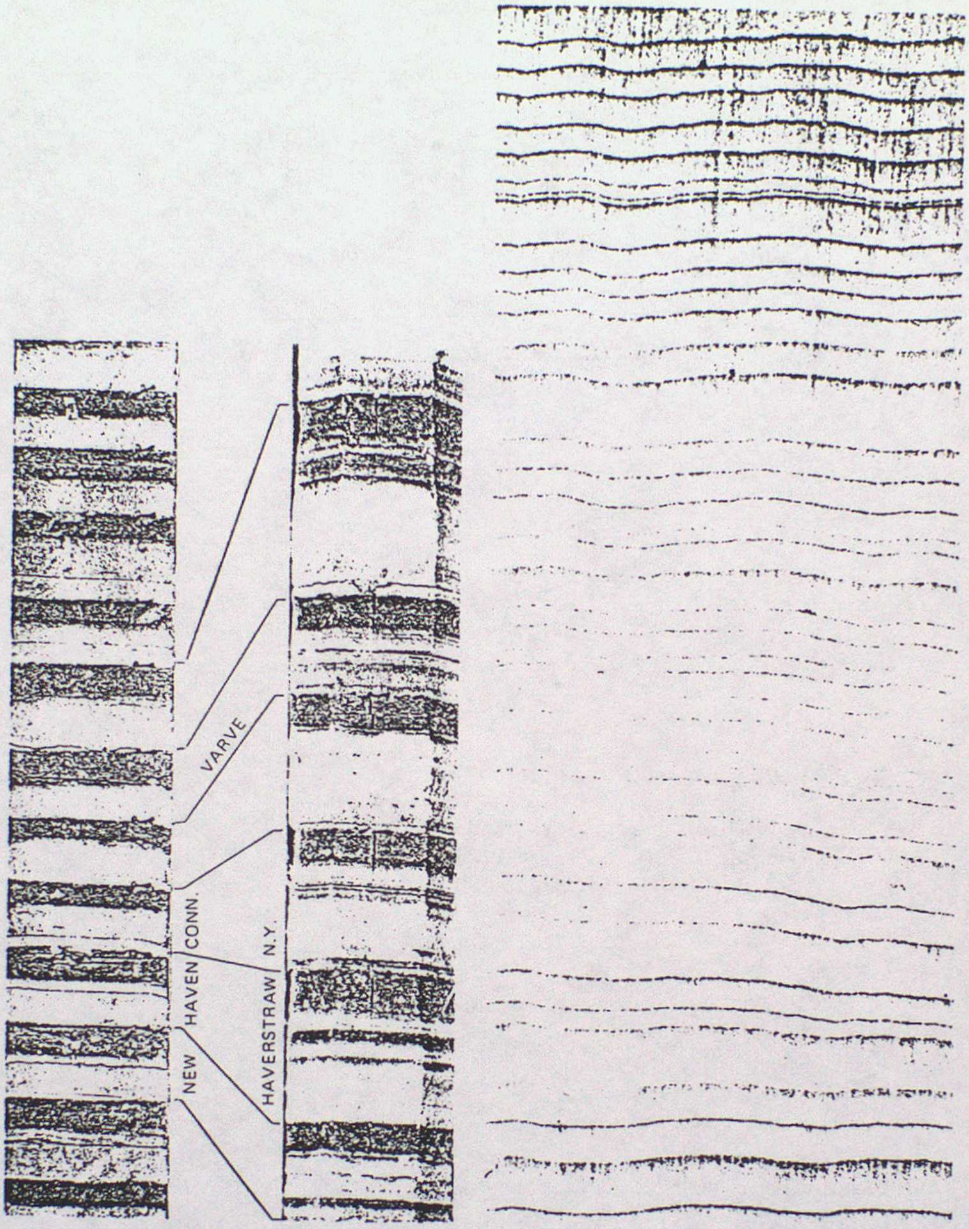

Examples of proxy evidence for geochronology. Varve correlations on the left are from sites near New Haven, Connecticut, and Haverstraw, New York. The tree-ring cross section on the right indicates variations in annual growth of a New Zealand conifer. (Varve photograph courtesy The American Museum of Natural History; tree-ring photograph courtesy Peter Dunwiddie, Quaternary Research Center, University of Washington.)

Figure 8.5. From Critchfield (1983).

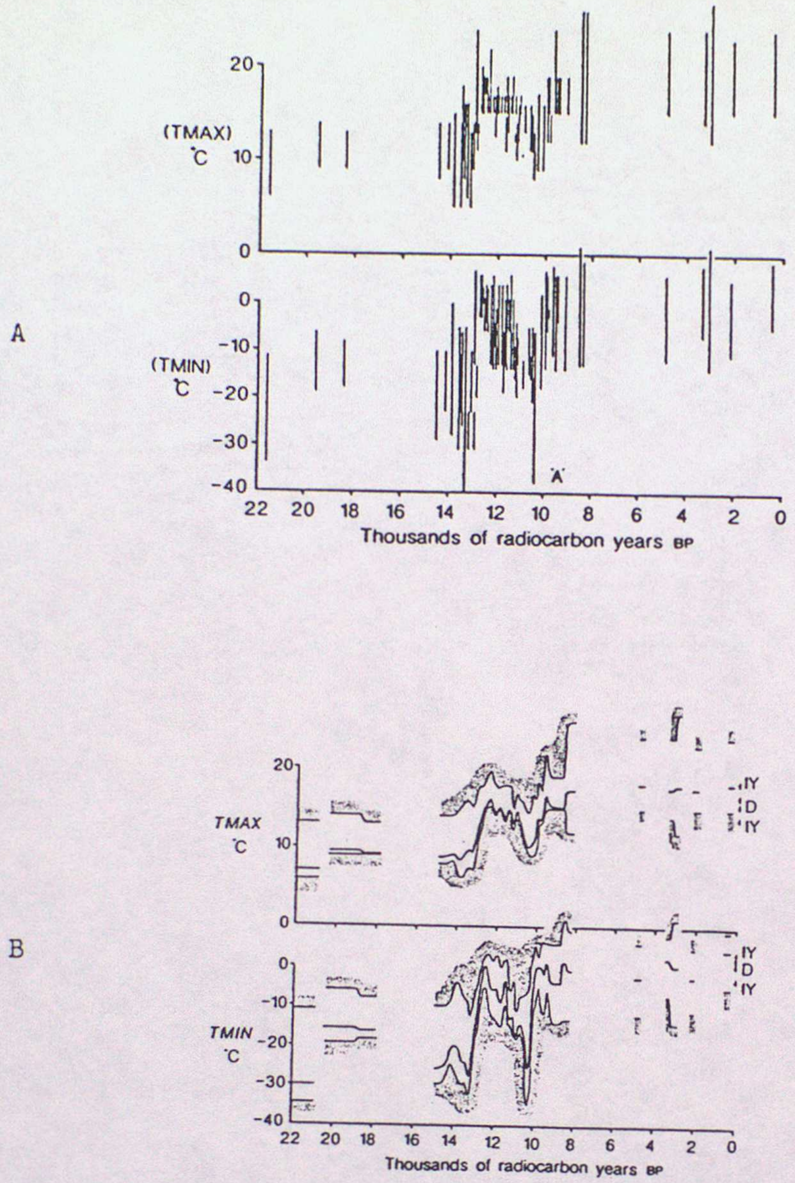

Figure 8.6 Temperatures for Britain (south of 55°N) for the warmest (TMAX) and coldest (TMIN) months of the year since 22,000 B.P, deduced from beetle remains.
A. Unsmoothed. B. Smoothed. Arrows at right in B show the ranges of TMAX and TMIN in Central England between 1659 and 1980; inner arrows (D), decadal means; outer arrows (IY), individual years. The rest of B shows most probable values and limits.

Adapted from Atkinson et al (1987).

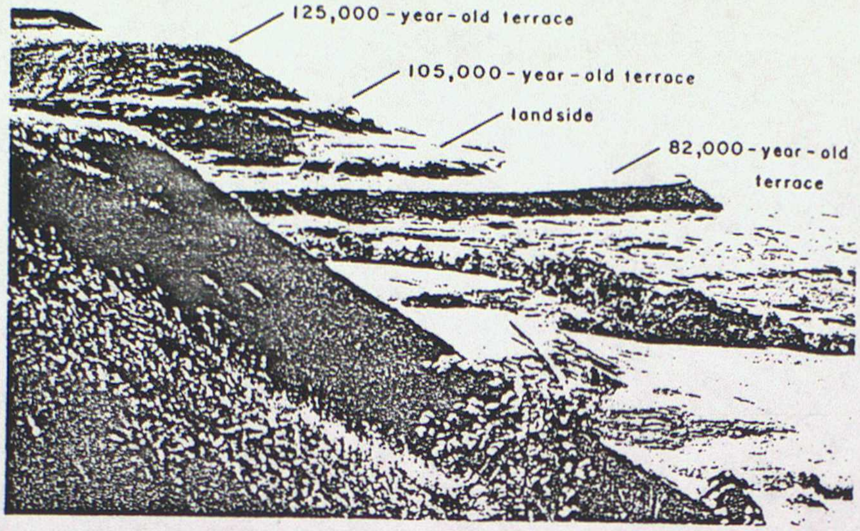
125,000-year-old terrace
105,000-year-old terrace
landside
82,000-year-old terrace

Reef terraces on New Guinea. A view along the north coast of the Huon Peninsula, showing uplifted terraces formed by Pleistocene coral reefs. Terraces similar to these were first dated on the Caribbean island of Barbados. (Courtesy of A. Bloom.)

Figure 8.7. From Imbrie and Imbrie (1979).

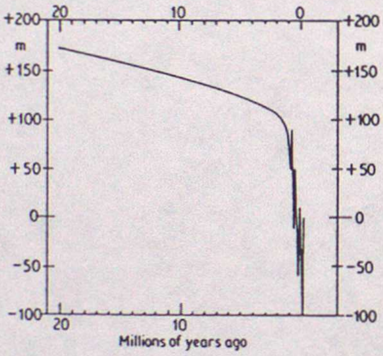

World sea level changes since the late Tertiary (Miocene).

(Ice-age-interglacial variations only schematically indicated – in reduced numbers).

Figure 8.8A. From Lamb (1977).

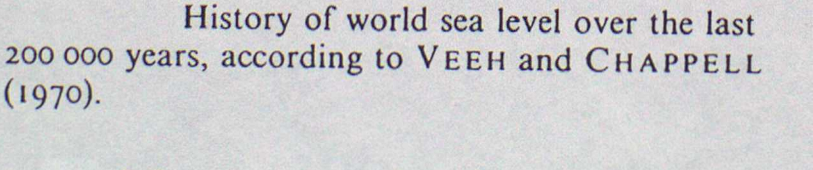

History of world sea level over the last 200 000 years, according to VEEH and CHAPPELL (1970).

Figure 8.8B. From Lamb (1977).

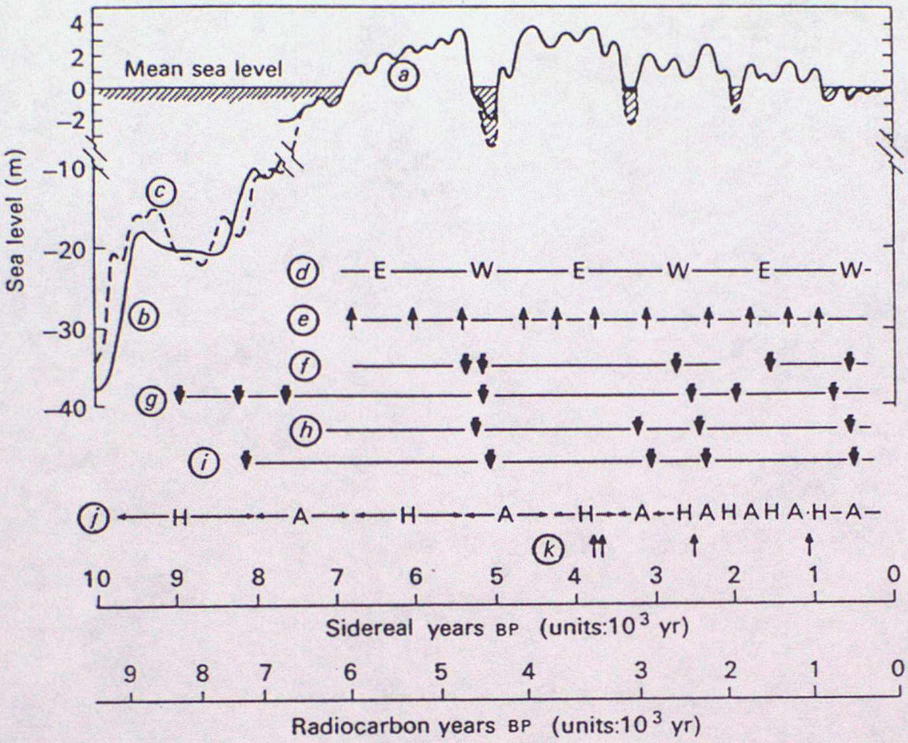

Trace of eustatic sea level over the last 10,000 years, as indicated (*a*) by an example from Brazil (Fairbridge, 1976), based on radiocarbon-dated beach deposits, coral reefs and Indian middens, for the last 7,000 years, and for the previous 3,000 years by data (*b*) from Scandinavia (Mörner, 1969), and (*c*) elsewhere (Fairbridge, 1961). Note that time is given in both sidereal and radiocarbon years. Comparisons are presented (from top to bottom) with (*d*) the magnetic declination cycle (approximately 2,850 years) with its E–W inflections; (*e*) the $^{18}O/^{16}O$ isotope ratio peaks from Greenland (Dansgaard *et al.*, 1971) indicative of maximum warming; the glacial readvances (*f*) from New Zealand (Burrows, 1973, 1975), (*g*) from Greenland (Ten Brink & Weidick, 1974), (*h*) from Alaska and (*i*) from Lapland (Denton & Karlén, 1973); (*j*) the Sahara climates (Geyh & Jäkel, 1974) where H denotes humid, and A denotes arid; and (*k*) maximum flood levels of the Nile (Fairbridge, 1962, and pharonic inscriptions). Note that imperfections in the datings exist that might present false impressions of one region 'leading' another.

Figure 8.8C.

From Fairbridge (1978).

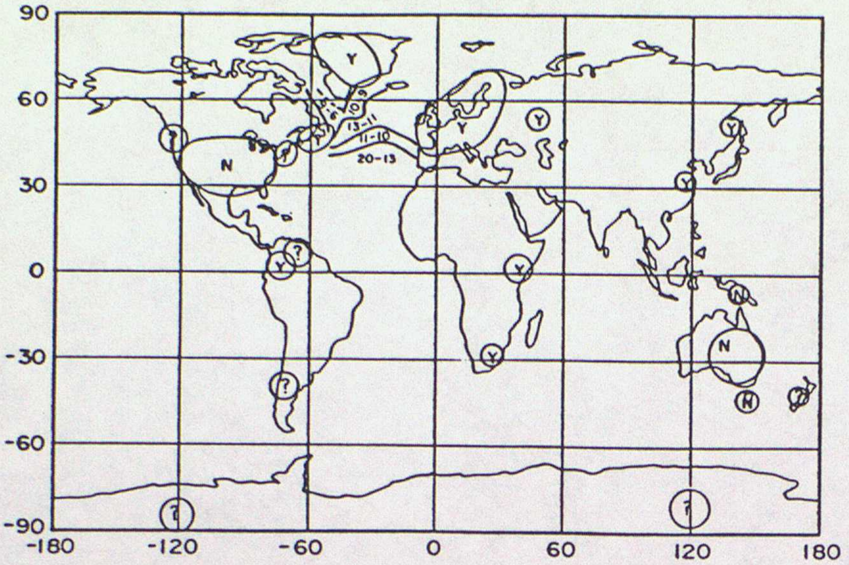

Worldwide assessment of the published results indicating the presence (Y), absence (N), or possible (?) paleoclimatic indication of a late-glacial climatic oscillation which may or may not be correlative with the Alleröd-Younger Dryas. Blank areas indicate regions where an assessment has not been reported. Also included is the location of the North Atlantic polar front for different time periods (Ruddiman and McIntyre 1981). Deglacial retreat was interrupted by the readvance from 11–10 k

Figure 8.9 From Rind et al (1986)

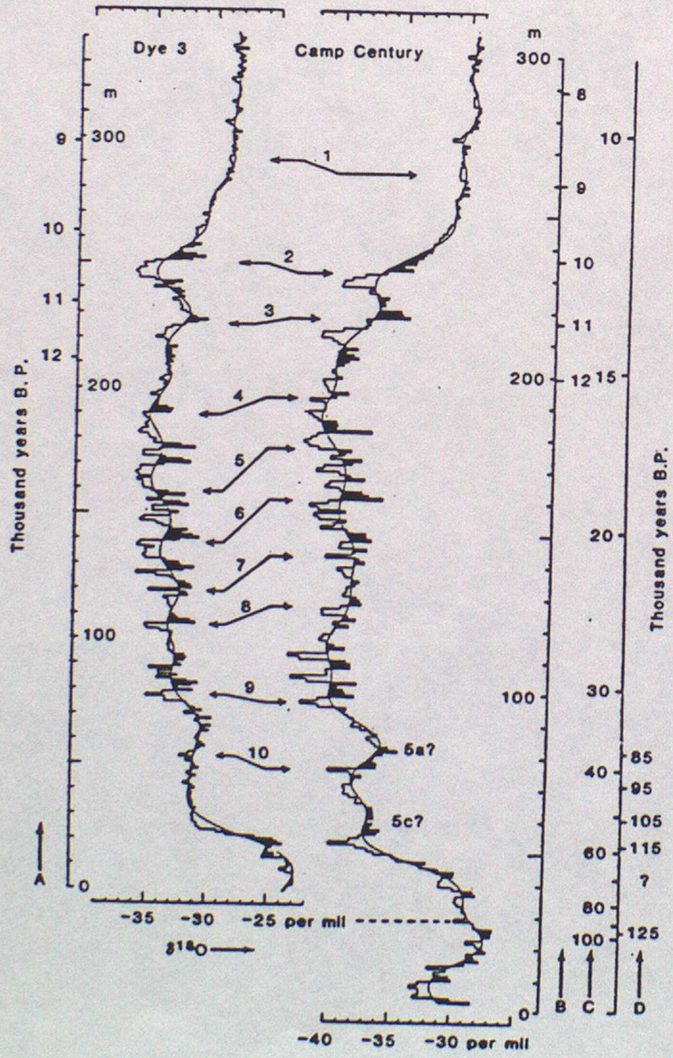

Figure 8.10A. Greenland $\delta^{18}O$ profiles.

Timescales A,B are based on simple ice-flow modelling; C is based on spectral analyses of Camp Century record; D is based on comparison with a deep-sea record. From Dansgaard et al (1982).

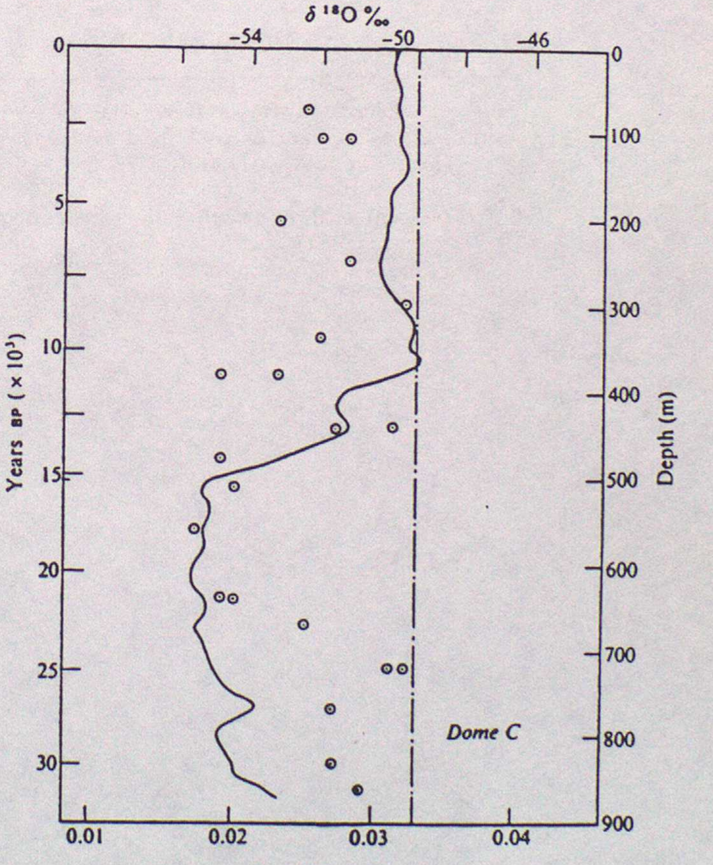

Figure 8.10B. Evidence from an Antarctic ice core that the atmospheric CO_2 concentration (dots) was half the present value (dashed line) at the peak of the last glaciation 18000 B.P. The change of ocean volume as the ice melted is shown by the change in ^{18}O:^{16}O ratio (continuous curve). From Delmas et al (1980).

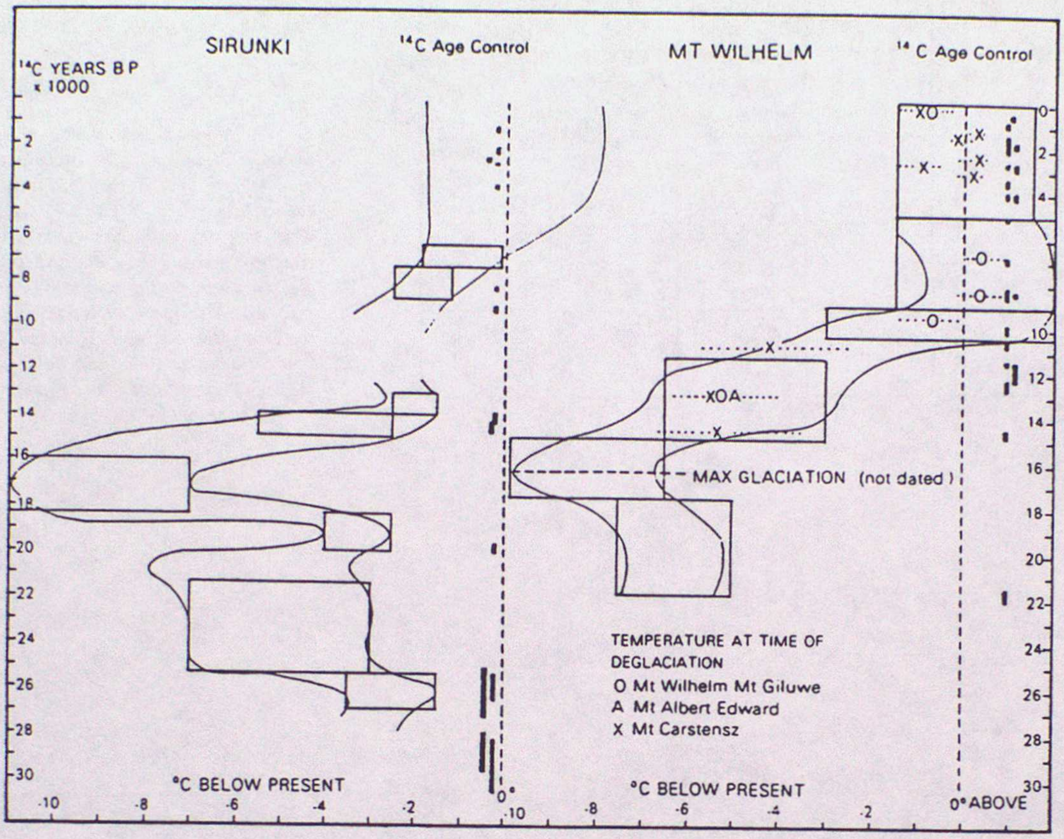

Limits of temperature variation through the past 28,000 years at two sites in the highlands of New Guinea derived from pollen analysis, with estimates of temperature indicated by glacial stages on four mountains.

Black rectangles show periods when ^{14}C dates were available.

Figure 8.11. After Bowler et al (1976).

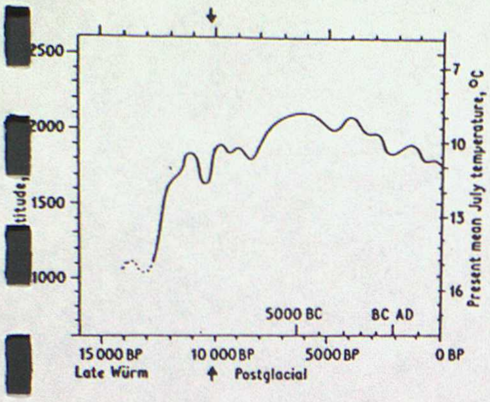

Generalized graph of height changes of the upper tree line in the Alps and other temperate mountain regions over the last 15 000 years.

(From MARKGRAF *(1974), p. 71; reproduced by kind permission.)*

Figure 8.12.

From Lamb (1977).

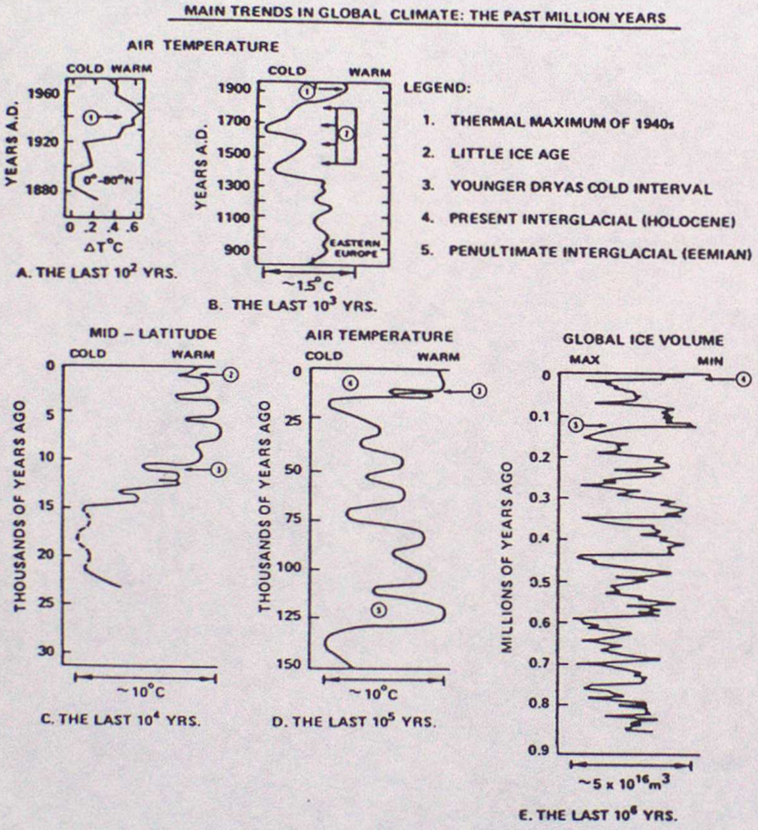

Indicators of global temperature change: different time spans compared.

(*a*) Successive 5-year mean observed surface air temperatures, last 100 years (MITCHELL *1963*).
(*b*) Winter severity index for Europe near 50°N 35°E, last 1000 years (LAMB *1969*).
(*c*) Generalized temperature changes in middle latitudes of the northern hemisphere, from tree line studies, last 10 000 years (LAMARCHE *1974*).
(*d*) Middle latitudes northern hemisphere air temperature variations, from diagnosis of sea temperatures and from pollen records on land, last 100 000 years (compiled by W. L. GATES)

(*e*) Global ice volume changes from isotope measurements on plankton in a Pacific Ocean sediment core, last million years.

(Diagram kindly supplied by Drs W. L. GATES *and* J. S. PERRY *with the permission of the U.S. National Academy of Sciences.)*

Figure 8.13.

From Lamb (1977).

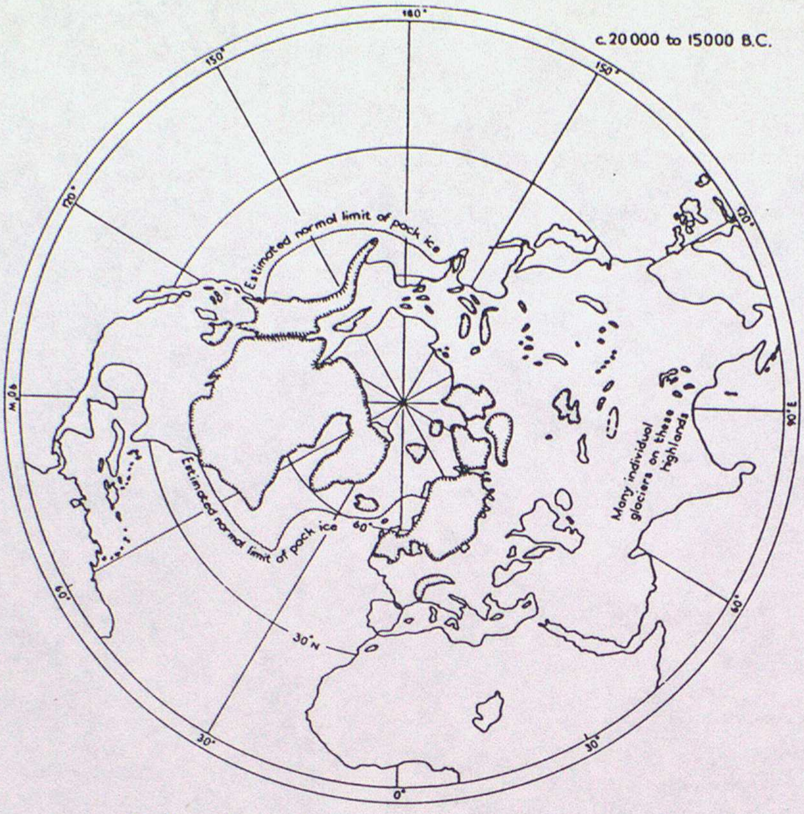
c.20000 to 15000 B.C.
180°
150°
150°
120°
120°
90°W
90°E
60°
60°
30°
30°
0°
30°N
60°
Estimated normal limit of pack ice
Estimated normal limit of pack ice
Many individual glaciers on these highlands

Northern hemisphere geography at the time of the last climax of glaciation about 18 000 years ago.

Figure 8.14A.
From Lamb (1977).

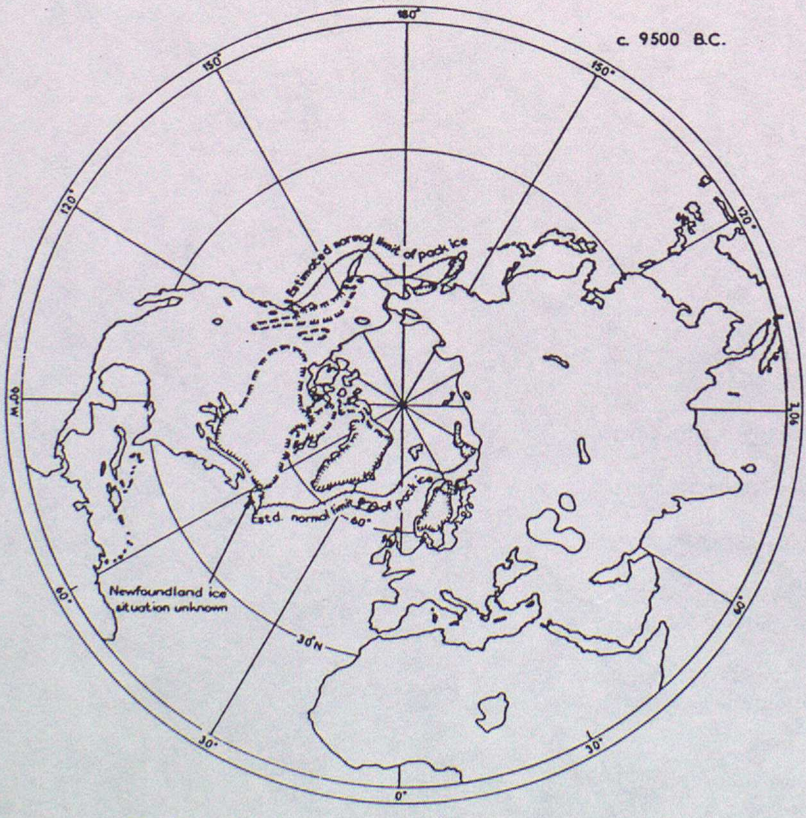
c. 9500 B.C.
180°
150°
150°
120°
120°
90°W
90°E
60°
60°
30°
30°
0°
30°N
60°
Estimated normal limit of pack ice
Estd. normal limit of pack ice
Newfoundland ice situation unknown

Northern hemisphere geography at the time of the Allerød (warm) interstadial 11 000–12 000 years ago.

Figure 8.14B.
From Lamb (1977).

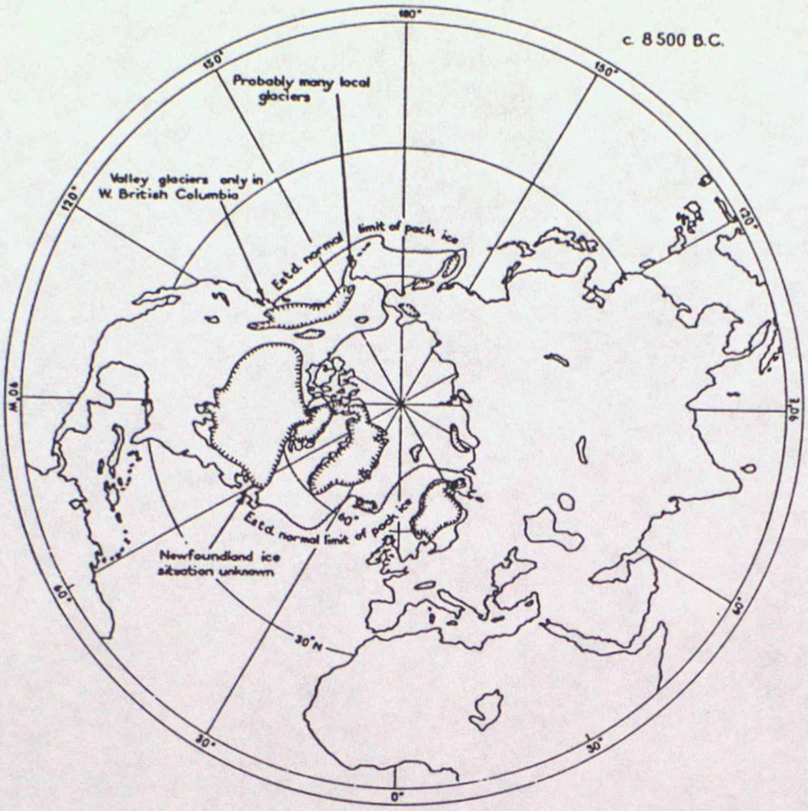
180°
c. 8 500 B.C.
150°
150°
Probably many local glaciers
Valley glaciers only in W. British Columbia
120°
120°
Estd. normal limit of pack ice
90°W
90°E
Estd. normal limit of pack ice
60°
Newfoundland ice situation unknown
60°
60°
30°N
30°
30°
0°

Figure 8.14C.
From Lamb (1977).

Northern hemisphere geography during the post-Allerød cold time between about 10 200 and 10 800 years ago.

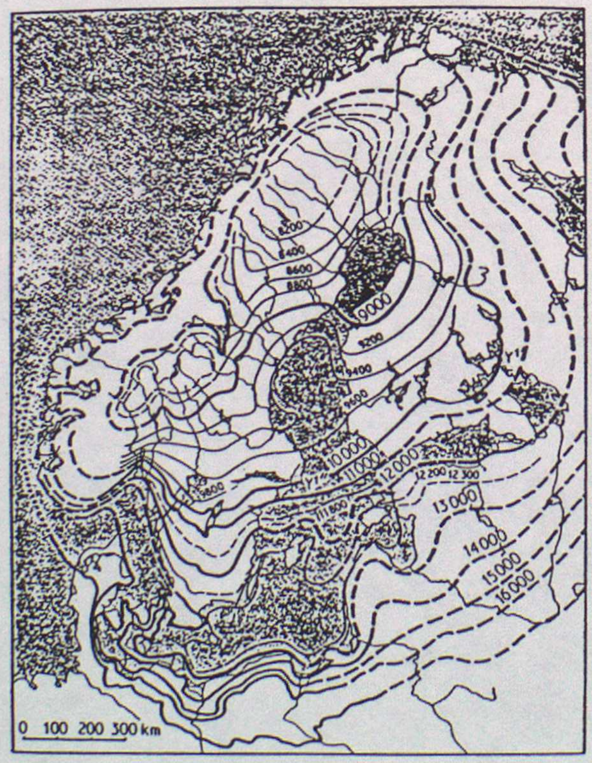
8200
8400
8600
8800
9000
9200
9400
9600
10000
11000
11800
12000
12200
12300
13000
14000
15000
16000
0 100 200 300 km

Positions of the retreating edge of the main north European ice sheet from about 17 000 to 8200 years ago. Dates based on Swedish varve chronology.
(*After* DE GEER *1954*.)

Figure 8.15.
From Lamb (1977).

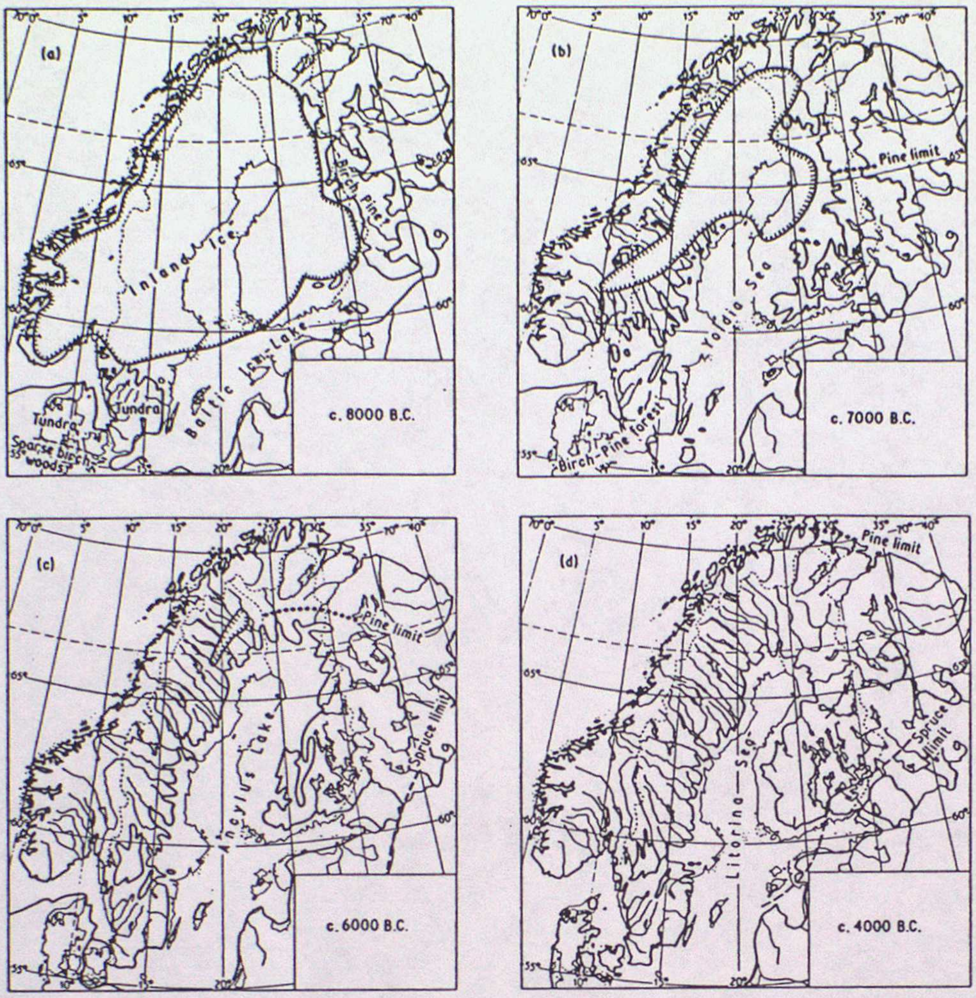
A
B
C
D
(a)
Inland Ice
Baltic Ice-Lake
Tundra
Sparse birch woods
Birch
Pine
c. 8000 B.C.
(b)
Pine limit
Yoldia Sea
Birch-Pine forest
c. 7000 B.C.
(c)
Pine limit
Ancylus Lake
Spruce limit
c. 6000 B.C.
(d)
Pine limit
Litorina Sea
Spruce limit
c. 4000 B.C.

The postglacial development of the Baltic. (*a*) 8000 B.C. (*b*) 7000 B.C. (*c*) 6000 B.C. (*d*) 4000 B.C.
(*After* HULTÉN *1971*.)

Figure 8.16.
From Lamb (1977).

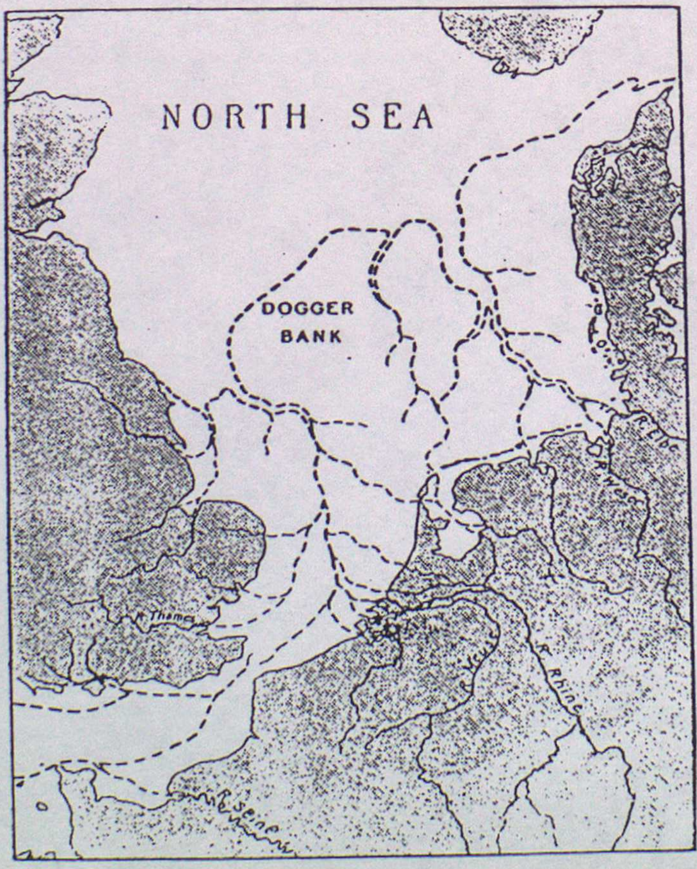
NORTH SEA
DOGGER BANK
R. Thames
R. Rhine
R. Seine

The geography of Northsealand about 7000 B.C.
(*First published by* CLEMENT REID *in 1902; also in* GODWIN *1956*.)

Figure 8.17.
From Lamb (1977).

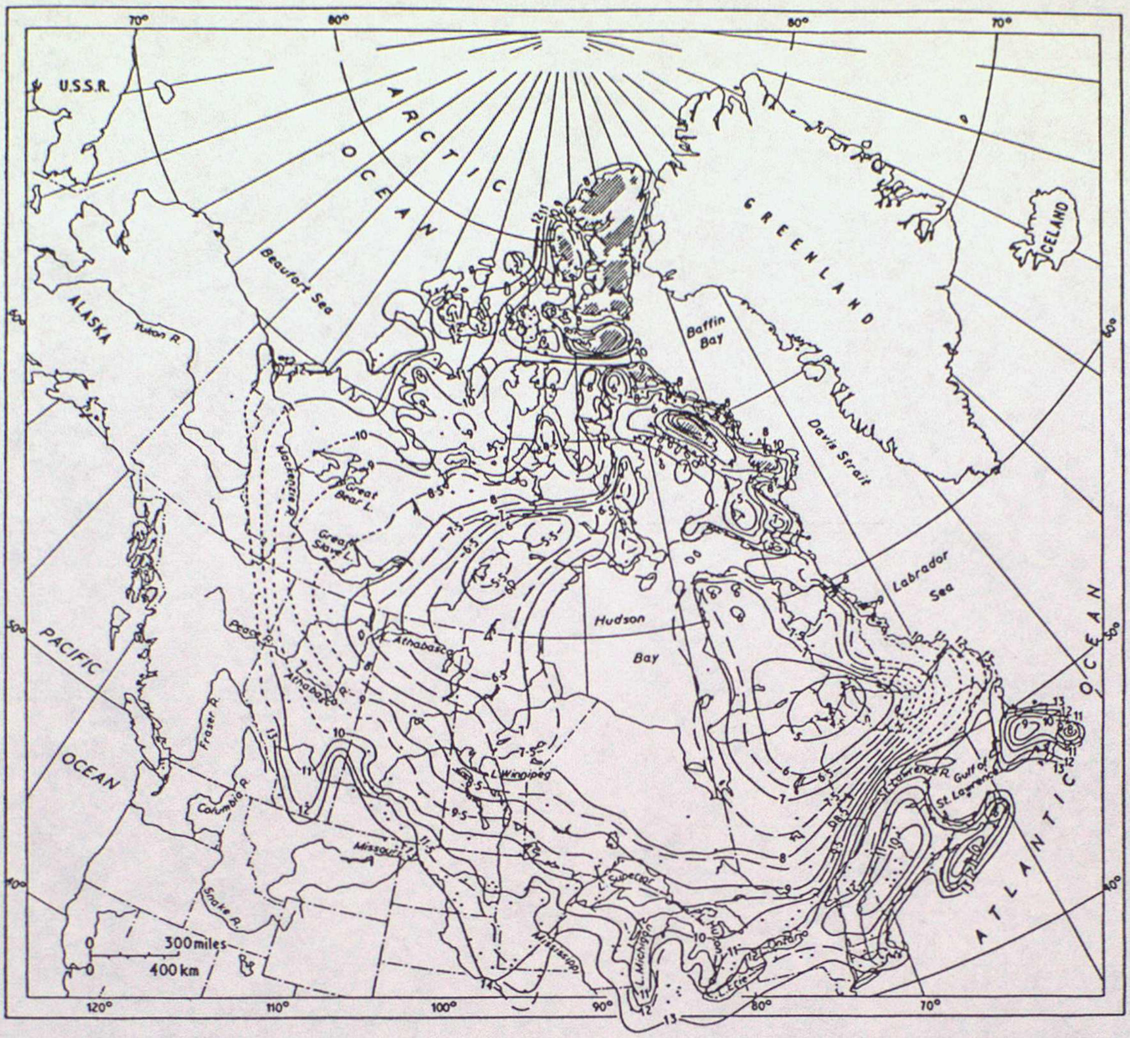
U.S.S.R.
ARCTIC OCEAN
Beaufort Sea
GREENLAND
ICELAND
ALASKA
Yukon R.
Baffin Bay
Davis Strait
Labrador Sea
ATLANTIC OCEAN
PACIFIC OCEAN
Hudson Bay
Great Bear L.
Great Slave L.
Mackenzie R.
Peace R.
Athabasca R.
L. Athabasca
L. Winnipeg
Fraser R.
Columbia R.
Missouri
Snake R.
Mississippi
L. Superior
L. Michigan
L. Huron
L. Erie
L. Ontario
St. Lawrence R.
Gulf of St. Lawrence
300 miles
400 km
70°
80°
120°
110°
100°
90°
60°
50°
40°

Isochromes of the withdrawal of the North American (Laurentide) ice sheet.
All dates B.P. (before present).
Dots show where radiocarbon dates have been established.
Moraines, coastlines and all other available field evidence used.
(*Reproduced from* BRYSON *et al.* (*1969*)*; by kind permission.*)

Figure 8.18. From Lamb (1977).

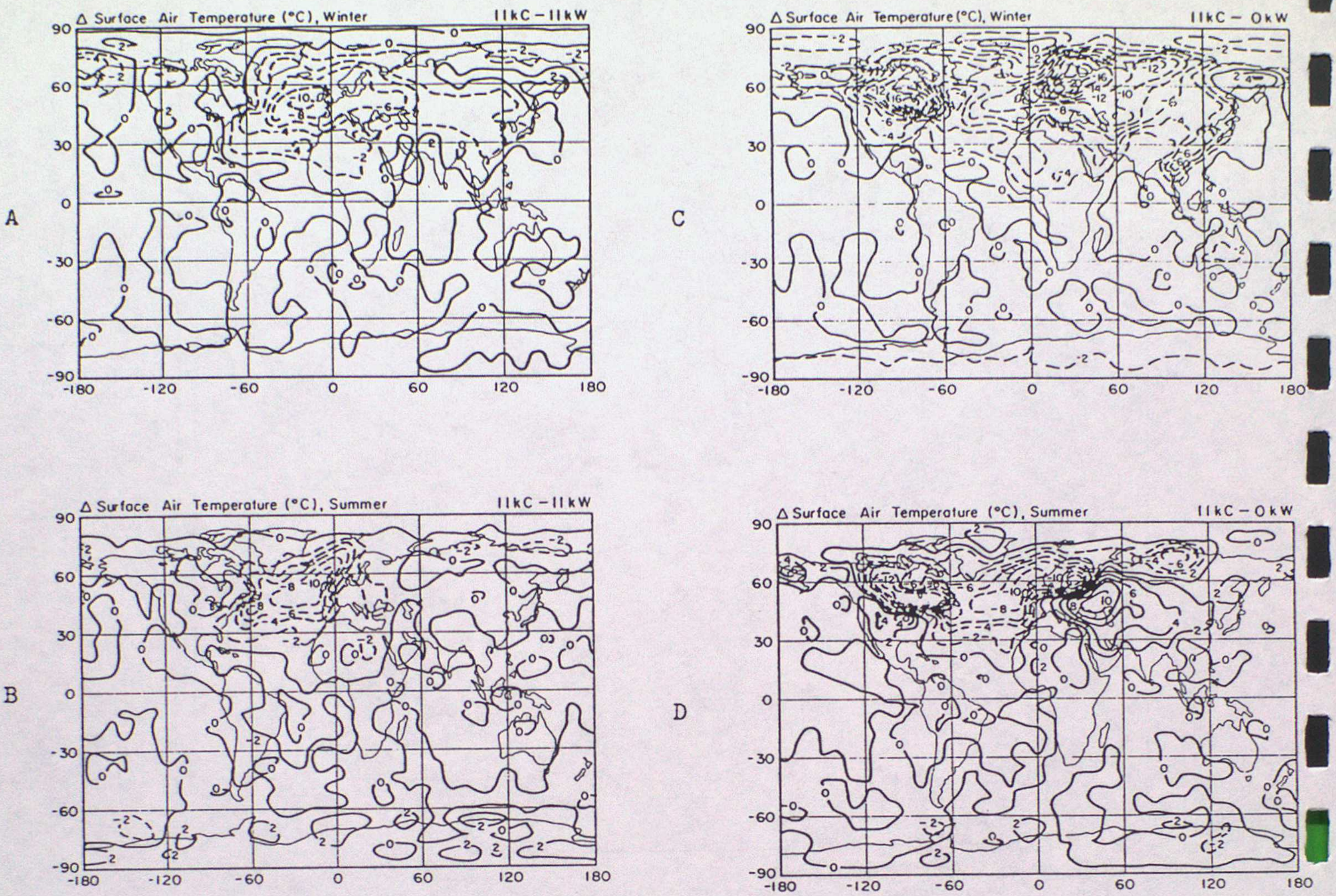
A
Δ Surface Air Temperature (°C), Winter
11kC – 11kW
B
Δ Surface Air Temperature (°C), Summer
11kC – 11kW
C
Δ Surface Air Temperature (°C), Winter
11kC – 0kW
D
Δ Surface Air Temperature (°C), Summer
11kC – 0kW
90
60
30
0
-30
-60
-90
-180
-120
-60
0
60
120
180

Figure 8.19 Surface air temperature changes from the modelling experiments of Rind et al (1986).

A. The effects of changing from modern to CLIMAP extratropical North Atlantic SSTs, given Younger Dryas land ice, solar radiation and sea-level, northern winter.

B. As A but northern summer.

C. The effects of changing from full modern conditions to CLIMAP extratropical North Atlantic SSTs combined with Younger Dryas land ice, solar radiation and sea-level, northern winter.

D. As C but northern summer.

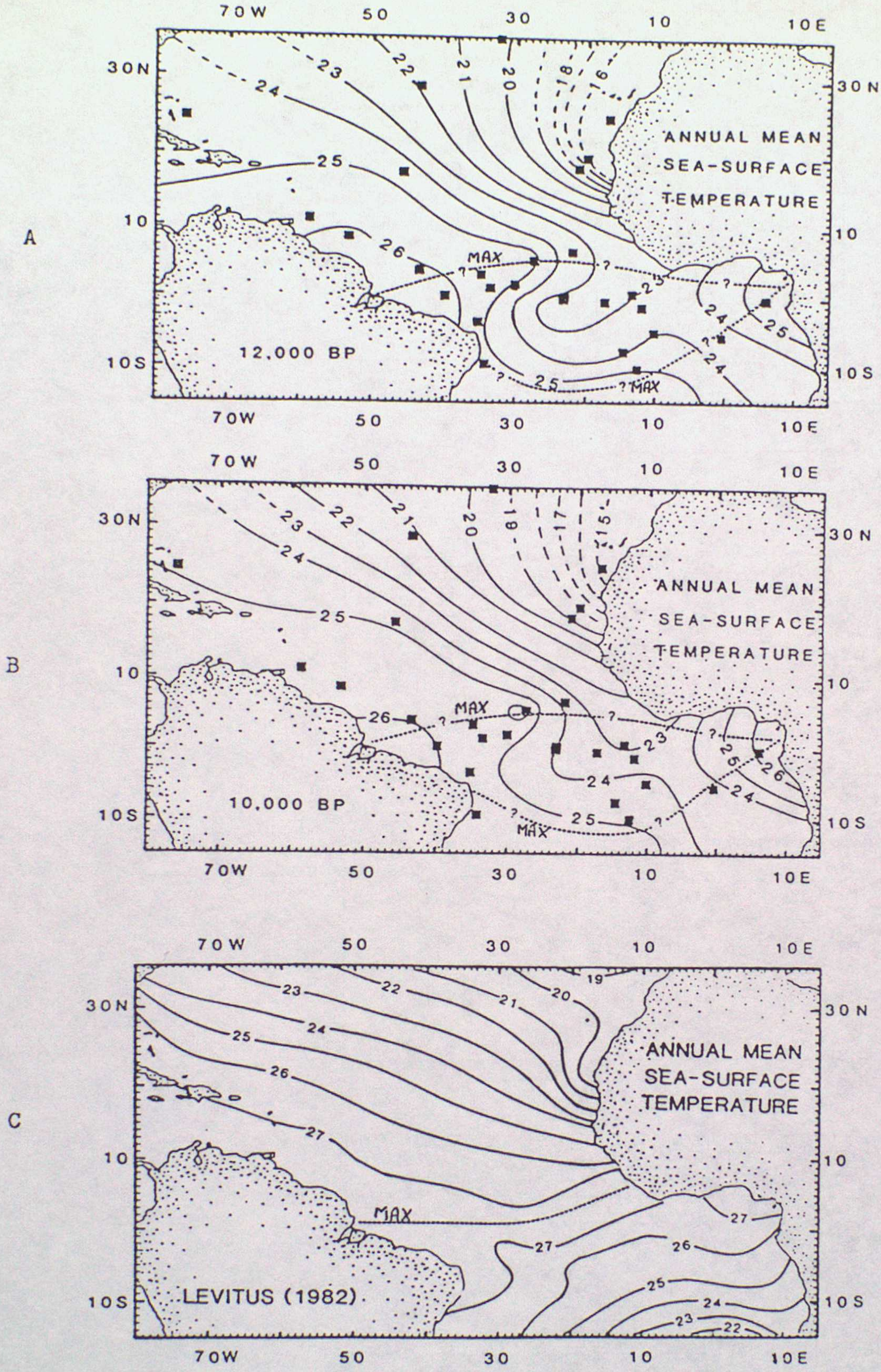
A
ANNUAL MEAN SEA-SURFACE TEMPERATURE
12,000 BP
MAX
70W
50
30
10
10E
30N
10
10S
B
ANNUAL MEAN SEA-SURFACE TEMPERATURE
10,000 BP
MAX
C
ANNUAL MEAN SEA-SURFACE TEMPERATURE
LEVITUS (1982)
MAX

Figure 8.20 Annual mean sea-surface temperatures for the tropical Atlantic.

A. 12,000 B.P. from Mix et al (1986)

■ denotes location of core used.

B. 10,000 B.P. from Mix et al (1986)

C. At the present time from Levitus (1982)

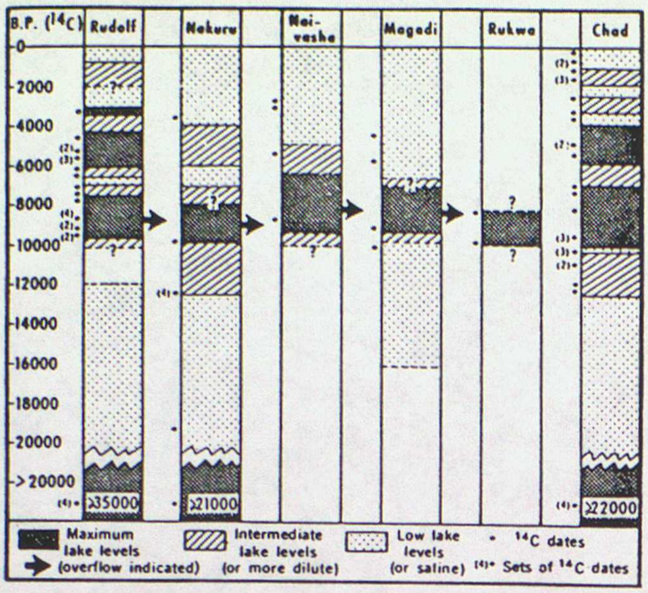

Lake levels in equatorial and tropical Africa. Radiocarbon dated high stands and low stands.

Lake Rudolf (4°30′–2°20′N 35°50′–36°40′E)
Lake Nakuru (0°20′S–36°05′E)
Lake Naivasha (0°50′S 36°20′E)
Lake Magadi (1°55′S 36°15′E)
Lake Rukwa (8°S 32°20′E)
Lake Chad (approx. 13°N 13°E)

(From BUTZER *et al. 1972; reproduced by kind permission of the authors and of* Science.)

Figure 8.21.

From Lamb (1977).

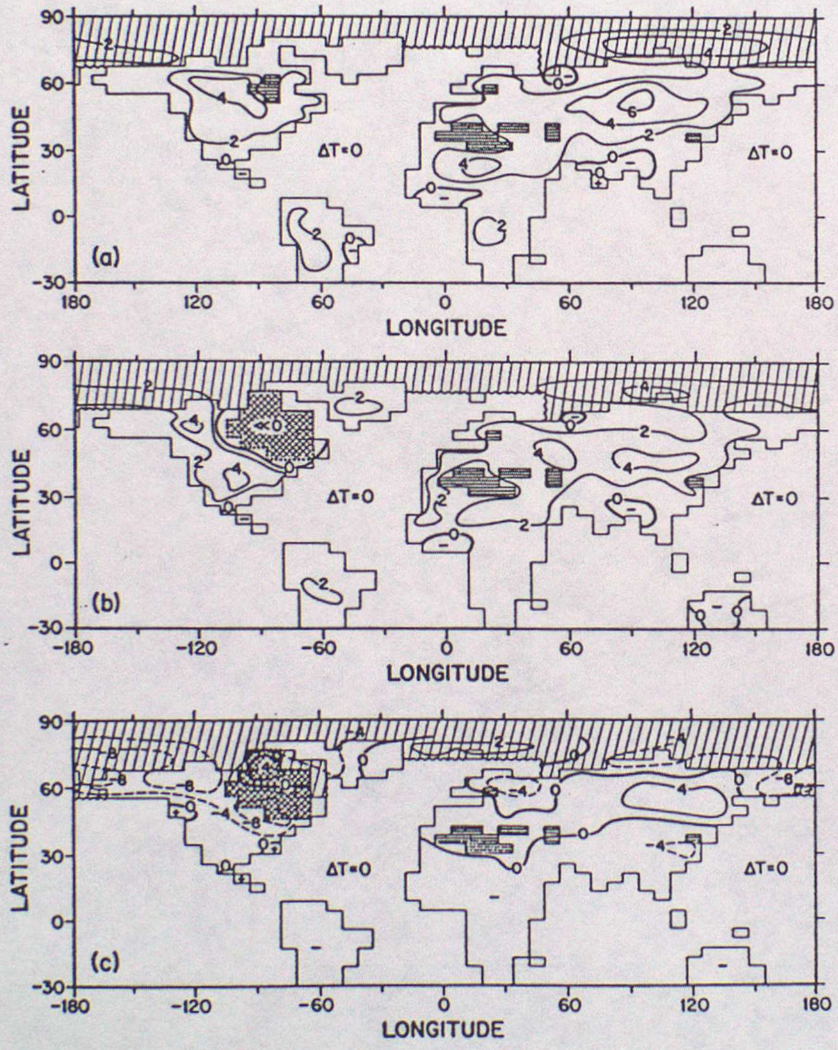

Figure 8.22.

From Kutzbach and Guetter (1984).

Simulated land surface temperature (K) differences (9 kyr BP minus present) for a) an experiment with solar radiation for July 9 kyr BP, present July ocean surface temperature, and no North American ice sheet ; b) same as (a) except with North American ice-sheet ; c) same as (b) except for January. Temperature difference is prescribed to be zero at ocean gridpoints and at interior sea gridpoints (wavey lines) but not over sea ice (hatched). The area covered by the North American ice sheet is indicated with cross-hatching. Results of the simulation for the region south of 30° s are not shown because the number of land gridpoints is small.

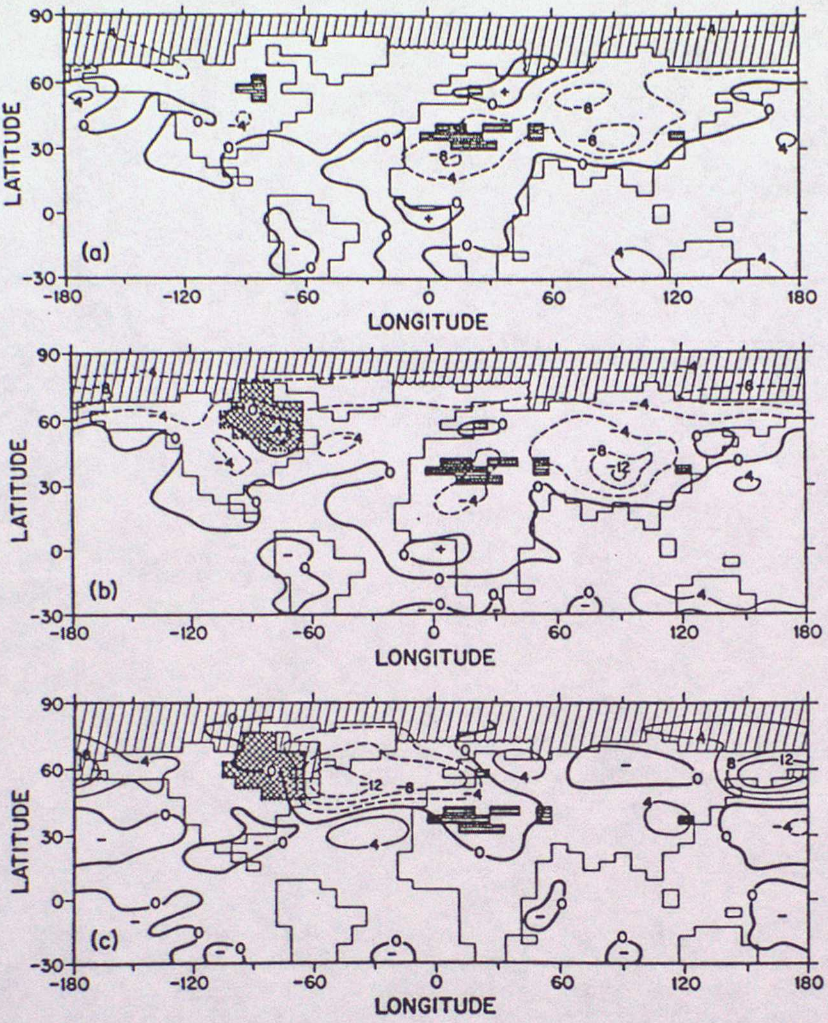
90
60
30
0
-30
LATITUDE
-180
-120
-60
0
60
120
180
LONGITUDE
(a)
(b)
(c)

Simulated sea-level pressure (mb) differences (9 kyr BP minus Present) for : a) an experiment with solar radiation for July 9 kyr BP, present July ocean surface temperature, and no North American ice-sheet ; b) same as (a), except with North American ice-sheet ; c) same as (b), except for January.

Figure 8.23. From Kutzbach and Guetter (1984).

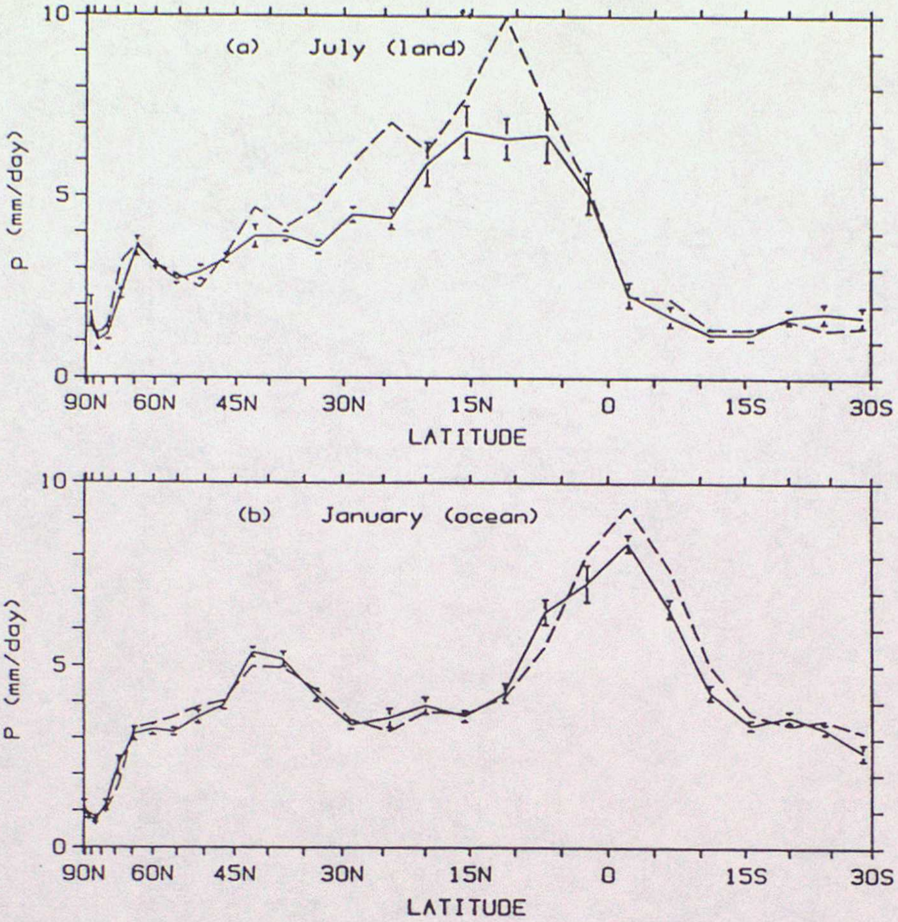

Latitudinal average of simulated precipitation (mm/day) as a function of sine of latitude : a) July—land precipitation; the control simulation (solid line) and the experiment with 9 kyr BP solar radiation and with the North American ice sheet (dashed line) ; b) January—ocean precipitation ; the control simulation (solid line) and the experiment with 9 kyr BP solar radiation and with the North American ice-sheet (dashed line). Vertical bars indicate one standard deviation about the modern control simulation.

Figure 8.24. From Kutzbach and Guetter (1984).

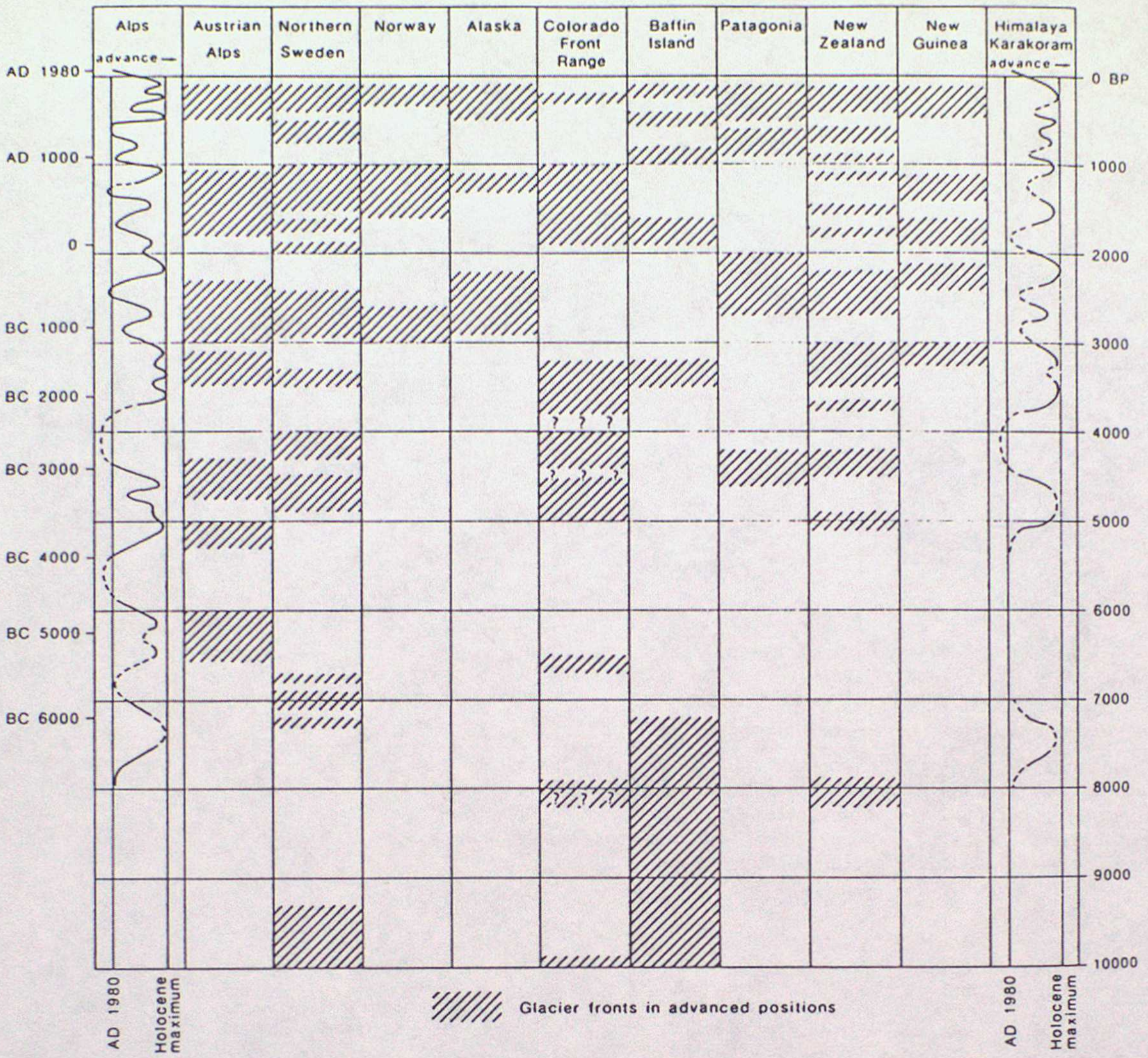

Regional summaries of glacier expansion phases. Some advance phases shown as having been lengthy may in fact have been imprecisely dated and consist in fact of one or more shorter phases. The diagram suggests a lack of synchroneity, except in the Little Ice Age and possibly around 2500 BP and also 3200 BP, but this impression cannot be taken as conclusive because of the varying quality and quantity of the data.

Figure 8.25. From Grove(1988).

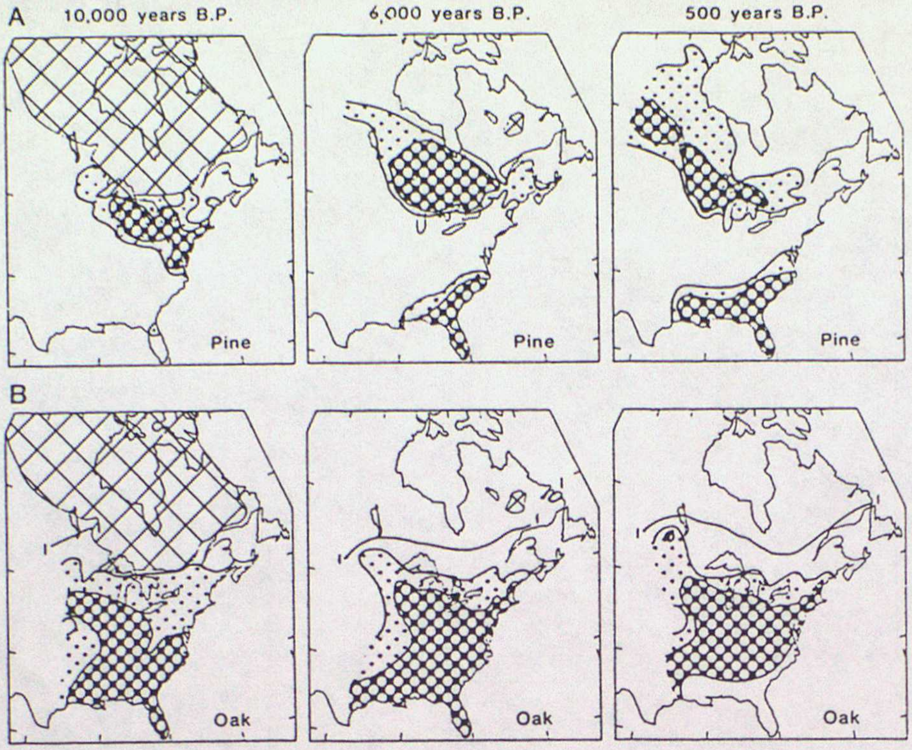

Figure 8.26.
From Kerr (1984)

Pollen clues to shifting Holocene climate

These maps illustrate the continuing adjustment of plants to changing climate. A decrease in summer solar radiation and the withdrawal of the cold ice sheet (crosshatch) combined to withdraw the oak and northern pine forests to the north and then to develop the southern pine forest. Light stippling is 5 to 20 percent oak or 20 to 40 percent pine; heavy stippling is greater than 20 percent oak or greater than 40 percent pine.

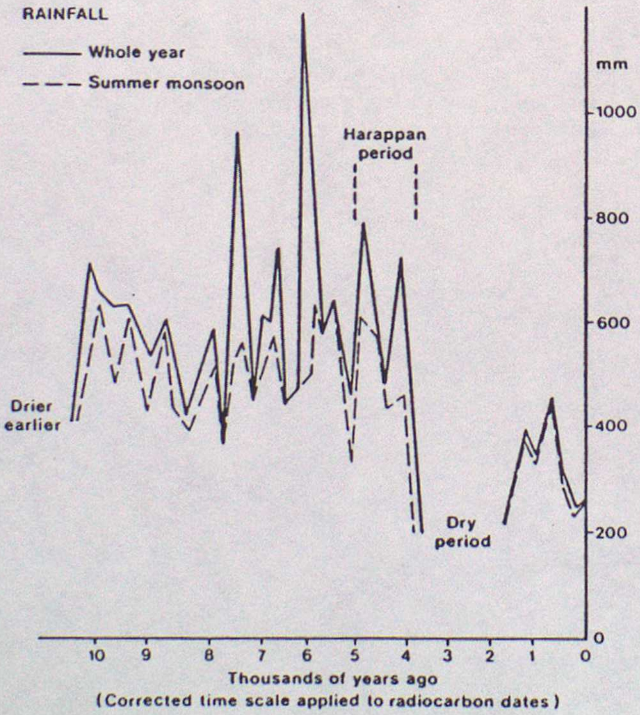

Figure 8.27.
From Lamb (1982).

Estimated variations of the rainfall in Rajasthan, northwest India over the last 10,000 years, from lake levels and botanical (pollen analysis) evidence. (Adapted from a diagram by R. A. Bryson, based on the work of G. Singh)

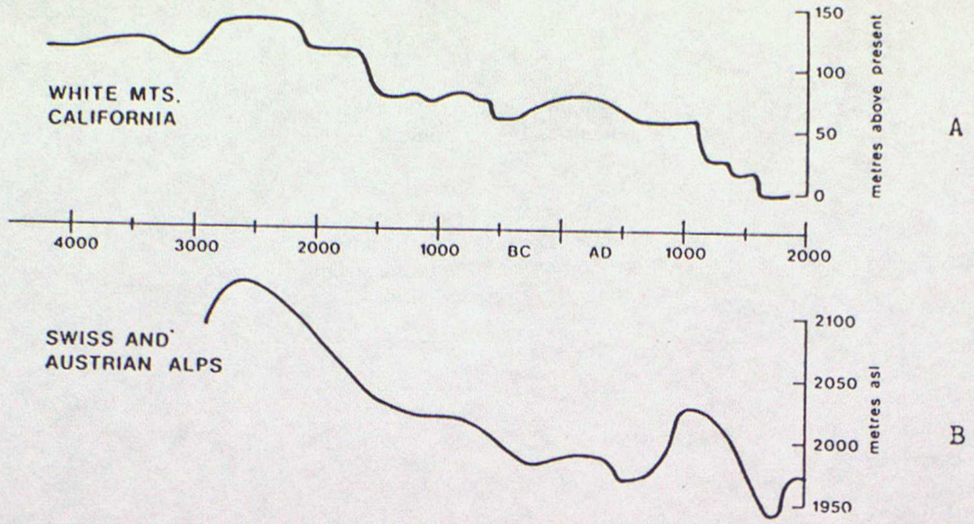

Changes in the height of the upper tree line in two areas in the White Mountains, California and in the Alps in Switzerland and Austria. (From work by V. C. La Marche and V. Markgraf)

Figure 8.28.
From Lamb (1982).

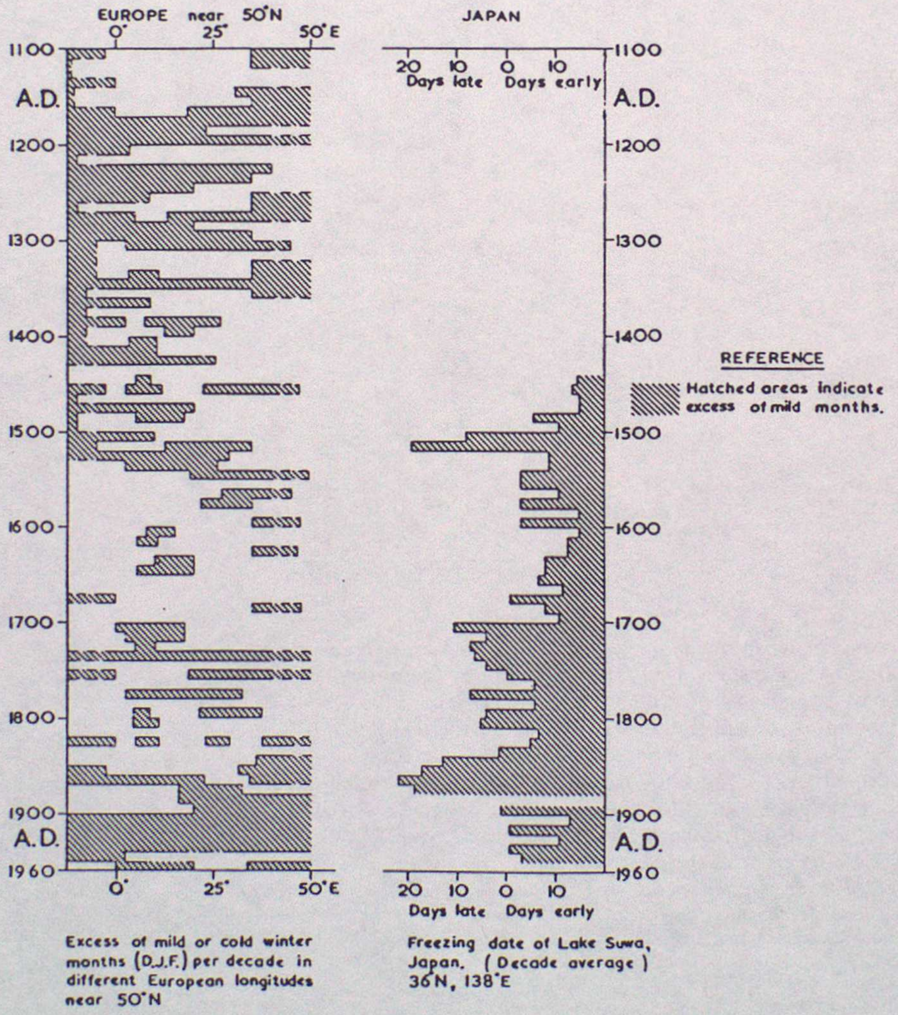

Survey of historical weather records by decades in Europe and Japan.

Left-hand side: Predominance of winter mildness (shaded) or severity (clear) in different European longitudes near 50°N.

Right-hand side: Variations of average freezing date of a small lake in central Japan, decade by decade, from the overall mean date.
Europe: decades from A.D. 1100.
Japan: decades from A.D. 1440.

Figure 8.29.
From Lamb (1977).

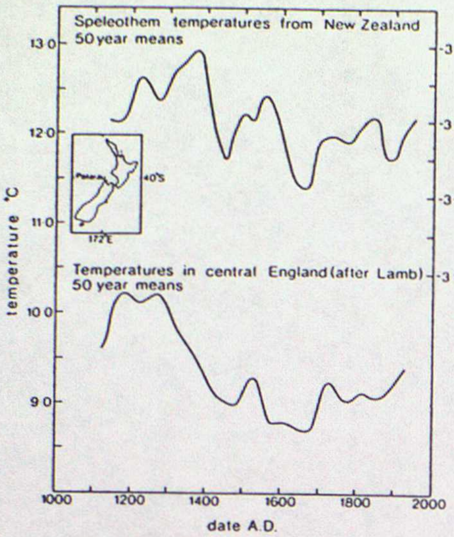

Course of the 50-year mean temperatures in the Nelson area, South Island, New Zealand, since A.D. 1100, derived from oxygen isotope measurements on a stalagmite in a cave at Patarau.

Temperatures derived by LAMB for Central England, as shown in Volume 1, p. 236, are repeated here for comparison.

(*Adapted from the original diagram kindly supplied by Professor* A. T. WILSON.)

Figure 8.30. From Lamb (1977).

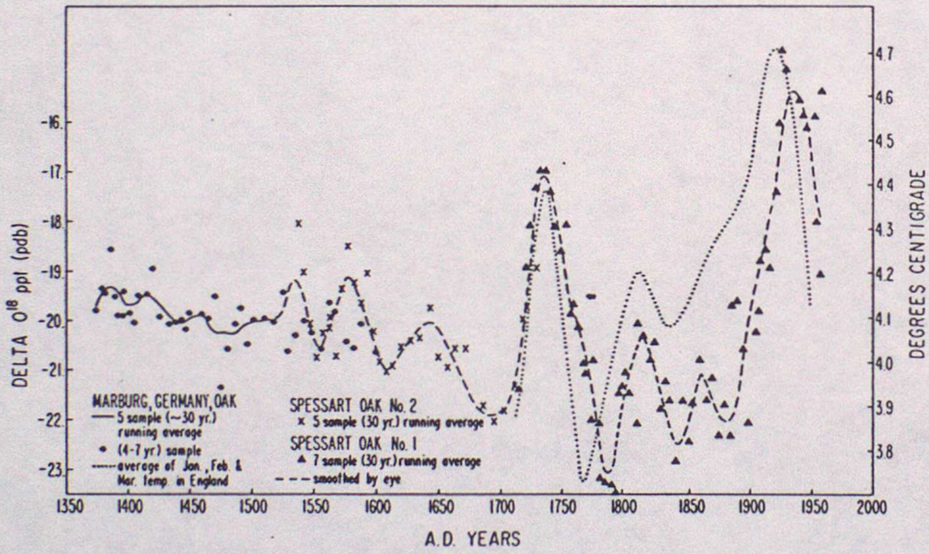

Composite record made up of the oxygen isotope ratio anomaly measured in the (tree-ring-dated) wood of oak trees in two areas of Germany (Marburg: 50°49′N 8°45′E) and Spessart (around 50°N 9°30′E).

Internal consistency/continuity of the record is suggested by the overlap.

Calibration against the last 270 years of winter temperatures (average for January, February and March) observed in England is suggested by the dotted curve.

Note: The very low dot plotted about 1480 would fit much better with other data for the 1430s, and it seems that the overlap with Spessart would fit equally well if there were about a 50-year dating error in the Marburg tree.

(*Diagram kindly provided while measurements were still incomplete by Dr* LEONA M. LIBBY *and reproduced with her permission.*)

Figure 8.31. From Lamb (1977).

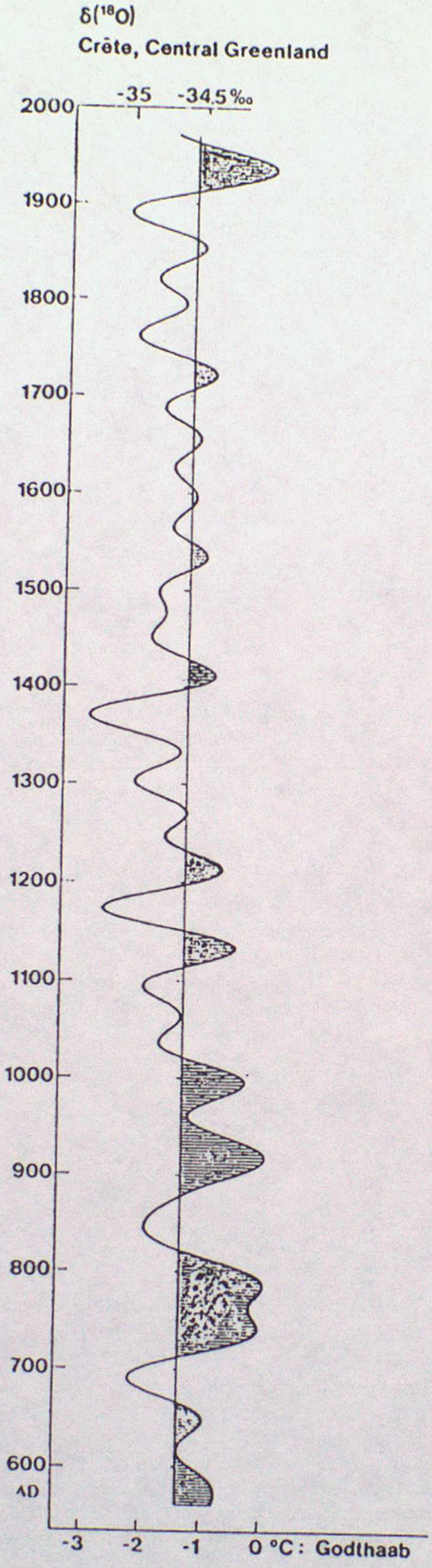

Figure 8.32 After Dansgaard et al (1975)

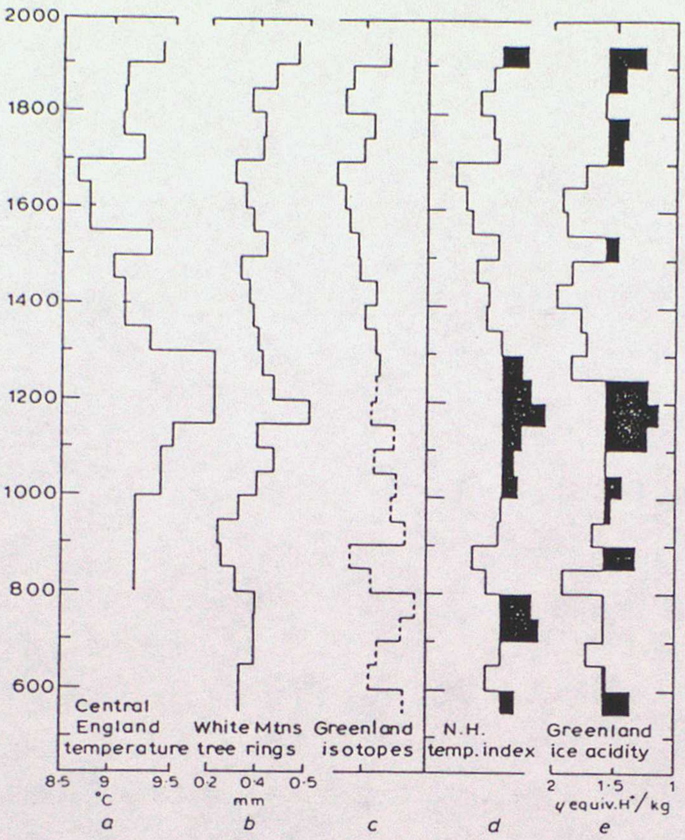

The correlation between temperature variations in the northern hemisphere and volcanic activity: (a) central England temperature estimates; (b) tree-ring width in the White Mountains of California; (c) long-term isotopic variations in Greenland; (d) a northern hemisphere temperature index (no scale), formed by combination of (a)–(c); (e) Greenland acidity from the Crete core profile, with 50-year average values. Warm periods are shown in black. (From Hammer *et al.* 1981)

Figure 8.33.

CLIMATIC CHANGE IN THE INSTRUMENTAL PERIOD

D E PARKER AND C K FOLLAND

MET O 13

SUMMARY

The reality and nature of fluctuations in climate in the last 300 years are discussed in the light of the quality and quantity of instrumental data. Emphasis is placed on comparisons between the "Little Ice Age" and the modern era and on evidence for climatic variation over the most recent century. The regional as well as global nature of many observed climatic variations is stressed. Agreements and apparent contradictions between the various instrumental indications of climatic variations are discussed.

9.1 INTRODUCTION

This lecture covers climatic fluctuations on time scales from a decade to a few centuries and bridges the gap between studies of interannual variability and palaeoclimatology. The approach to climatic fluctuations in the instrumental period has traditionally differed from the approach to interannual variability, with necessary emphasis on a few long well-documented local or global time-series of data, mainly those of air and sea surface temperature and mean-sea-level pressure. There has been less stress on the physical links between climatic changes in different parts of the globe. We are, however, now able to begin to depart from this approach by considering the regional, as opposed to global, nature of some of the observed climatic fluctuations. We are also better able to assess the reliability of some of the long-term data series, by investigating relationships with different types of data, as well as by traditional checks on self-consistency and cross-checks with series of the same type of data for nearby locations. As a result of these advances, we are increasingly confident that the measured climatic changes have been real.

We begin with presentations of climatic fluctuations observed in local, regional and hemispheric series of land air temperatures. The results are discussed in terms of instrumental inhomogeneities, urbanisation and other likely sources of bias. A corresponding treatment of marine temperatures is followed by comparisons between observed land and marine temperature trends. For the first time, long hemispheric as well as local series of rainfall are becoming available and these are discussed in Section 9.5 in relation to instrumental and procedural changes. Next, long-term fluctuations of the atmospheric circulation are described and related to local and regional changes of temperature and rainfall, including the recent dessication in the Sahel. In the more recent decades, upper-air data have been available: trends in temperature aloft are presented in Section 9.7 and compared with trends at the surface. A brief review of data on sea-level is given in Section 9.8. Finally, some possible causes of interdecadal and century-scale climatic changes are discussed. These causes include the effects of increasing greenhouse gases in the atmosphere, which are more fully covered in Lecture 10.

9.2 CHANGES IN SURFACE AIR TEMPERATURE OVER LAND

The beginning of the instrumental period around the early eighteenth century coincides with the latter part of the "Little Ice Age", and part of the problem that must be tackled is whether temperature, and atmospheric circulation, have really varied appreciably since that time. According to Fig 8.31, Lecture 8, $\delta^{18}O$ measurements from tree rings in W Europe suggest a rise of winter/early spring temperature exceeding 0.5°C between the late seventeenth century and 1940. Of equal interest is a marked increase in temperature in 1720-1740 followed by a rapid reversal. Fig 8.31 used temperatures for January to March in Central England for the period after 1700 to support these findings. Central England Temperature (CET) is the longest available instrumental temperature series and we shall therefore first look at CET in detail.

9.2.1 Central England Temperature and the problems of homogenising ancient thermometer readings

A fundamental problem in constructing a local time-series is to ensure that the data are as temporally homogeneous as possible: in other words, that a given meteorological reality has always resulted in the same value in the series. Only to the extent that this is true can the series be used to make reliable deductions about local climatic fluctuations. A reliable time series of temperature in a restricted locality may also reflect fluctuations of climate on a larger scale, because local temperature is sensitive to larger-scale changes in atmospheric circulation.

Manley (1974) constructed a monthly temperature series for Central England and a smoothed updated series (see Jones (1987)) is shown in Figure 9.1. Manley chose to represent an area, rather than to reduce his series to a single point, because of the scattered locations of most of the early observations, and because the only concentrated observations were in London and thus were eventually affected by heating resulting from urban expansion. He adjusted the monthly data to compensate for the following variables:

a) Different times of observation: the traditional mean temperature computed as $^1/_2$ (max + min) differs from eg the mean of 8 am and noon, by amounts which vary with season but can be estimated from modern data. The problem of different observation times can be quite acute when studying very long time-scale temperature changes.

b) The change of calendar in September 1752 when 11 days were omitted in that month. Daily data facilitated this adjustment.

c) Housing of thermometers: in the 18th Century this was often an unheated north-facing room attached to a house; in later years, use was often made of either north-wall observations, or of Glaisher screens, which preceded Stevenson screens. The problem of changing thermometer screens is a potentially serious problem which requires further investigation.

d) Types of thermometer: pressure corrections were needed for early thermometers which consisted of a U-tube with one open end. Also different scales had to be converted to modern units. Unreliable instruments were excluded from Manley's compilation.

e) Geographical region and site: Manley found from modern data that so long as frost-hollows and other unrepresentative sites are excluded, the monthly deviations from a long-term average, or the successive differences between months of the same name, are almost uniform for English inland stations. Thus he could work with temperature differences rather than absolute temperature values, and produce a single series from overlapping records at sites scattered through much of England. This technique also aided cross calibration of early temperature scales and detection and elimination of the effects of changing observing time and instrumentation.

Manley checked his compilation against a series for Utrecht (Holland) and found good agreement. Also, in periods of sparse data he noted observations of wind direction and snowfall.

9.2.2 Local and regional climatic fluctuations as revealed by Central England Temperature

It can be seen from Figure 9.1 that, except in summer, it has been warmer in Central England in much of the 20th Century than in the previous 250 years: the peak warmth was generally in the mid-20th Century but the mildest winters were in the early 20th Century. The late 17th Century was particularly cold, corresponding to the peak of the supposed "Little Ice Age". There was notable warmth in the 1720's and 1730's however. These features are also found in instrumental temperatures series for Utrecht and for other locations in Northwest Europe. Other major features are the warming in October between 1890 and 1975 and the sharp cooling in April in the past 25 years.

Figure 9.2(A) shows a power spectrum analysis of the unsmoothed annual mean CET data from 1659-1975. The most significant peak is labelled 76 years and mainly reflects the temperature fluctuations between about 1890-1975 and 1700-1770 (final diagram of Figure 9.1). Fig 9.2(B) shows a power spectrum reported by Lamb (1972a), due to Siren, of tree-ring widths in N. Finland which probably mainly reflect summer temperature. The shapes of Figures 9.2(A) and 9.2(B) are surprisingly similar with more power in Figure 9.2(B) at the 70-200 year time scale presumably because of the longer (497 year) data series. The 23 year peak, like the 76 year peak, is statistically significant (using an "F" test) and has sometimes been linked with the "double sunspot" cycle of magnetic activity on the sun. The double sunspot cycle is constructed from the sunspot series shown in Figure 3.6 (Lecture 3) by reversing the sign of the values in the sunspot series between alternate sunspot cycles, which have opposite magnetic polarity. Figure 8.2C (Folland (1983)) shows, however, that a band-pass filtered time series of annual CET whose filter function is centred on the 23 year time scale bears no consistent long-term phase relationship with the double sunspot cycle. Indeed the 23 year peak disappeared after 1880 whereas the double sunspot cycle increased slightly in amplitude. The inconstancy of the spectra of long temperature series (see also Figure 1.7 in Lecture 1) is not unexpected in view of the multiple causative factors. One physical forcing directly affecting air temperatures over islands is the sea surface temperature (SST), and the influence of North Atlantic SST on CET is considered in Section 9.4. Fluctuations of the atmospheric circulation are also a major influence on surface air temperature and are discussed in Section 9.6.

Figure 9.3 shows an attempt (Lamb (1972a)) to estimate Central England temperatures back to the beginning of the Medieval "climatic optimum" including assessments of their uncertainties. Prior to 1680, the temperatures have been derived from a mixture of botanical and documentary evidence. A clear minimum in mean annual and winter CET is suggested around 1600-1700 with winter temperatures in the period 1900-1950 similar to those during the "Medieval optimum".

The effects of urban heating were avoided as far as possible by Manley in his construction of the instrumentally-based CET series. However, other long temperature records have not always been as carefully quality-controlled, and we therefore devote the next section to a discussion of the effects of urbanisation.

9.2.3 Effects of urban heating on temperature records

The effects of urban heating on long time series of temperature are illustrated for Paris in Figure 9.4A (after Dettwiller (1978)). Central Paris has warmed by over 1°C since 1900 relative to the surrounding countryside; much of the warming has been in the minimum temperatures as is typical (Oke (1982)) of urban heating. Studies like that of Dettwiller can, however, only be used to correct urban data if long series of homogeneous rural data exist. The problem of the effects of urbanisation is serious as many of the longest temperature series have been kept in what are now large cities; and even in major parks as may, for example, surround old observatories, the urban heating effect, though reduced, is not eliminated (Oke (1982)). Figure 9.4B compares a 200-year series of annual mean temperature for Vienna with that for an observatory on a low mountain in S Germany (Hohenpeissenberg) 600 km to the west (Angell and Gruza (1984)). A relative warming of Vienna appears to have occurred since 1920. The higher frequency fluctuations tend too be in phase, however, and a very long period temperature fluctuation with a flat minimum around 1880-1890 is common to both series; the period around 1800 is relatively warm, in contrast to Central England (Figure 9.1).

Urban heating will, through its effects on individual local time series, affect estimates of regional and global temperature trends. Hansen and Lebedeff (1987) estimated the impact of urban heating on hemispheric and global land surface air temperatures by eliminating from their data set all stations associated with population centres which had more than 100,000 people in 1970. The number of stations was reduced by about one third and overall warming trends over the past century were reduced by about 0.1°C (Figure 9.5). Hansen and Lebedeff subjectively estimated that complete elimination of urban heating, by compensating for data from the smaller towns, would not reduce the trends by more than a further 0.1°C. The magnitude of urban heating may, however, even be significant in small towns in relation to century-time scale climatic trends: Figure 9.6, from Oke, (1982), shows that on individual occasions the heat-island in midlatitude towns of population 10,000 may reach 4°C. Tropical cities also undergo urban heating because the major underlying mechanisms in both cases are increased storage of sensible heat from the sun in buildings and roads, and decreased long-wave radiation loss as a result of reduced sky-view. Only in high-latitude settlements in winter is addition of heat from burning of fuels a major contributor (Oke (1982)).

9.2.4 The effects of variations of coverage on estimates of the course of hemisphere land air temperatures

The geographical coverage of land-based observing stations was far from complete before the early part of the 20th Century. For example, the coverage in the Northern Hemisphere was largely limited to Europe and eastern North America until the late 19th Century (Hansen and Lebedeff (1987); Jones et al (1986)). Because interdecadal changes of temperature over particular regions often differ from the hemispherically-averaged changes (Jones and Kelly (1983)), limited sampling is likely to produce biases in estimates of trends ascribed to the hemispheres or to the globe even when the computations include the essential initial step of converting data to anomalies from local climatologies. Jones et al (1986) assessed the effects of incomplete coverage for the Northern Hemisphere by means of "frozen grid" experiments in which the course of "hemispheric" temperature was computed firstly using all available acceptable data, and then using only locations having acceptable data for at least 80% of the time in the 1850's, 1860's etc. Figure 9.7A shows the differences between the resulting sequences. Even the restriction of coverage to that available in the 1850's appears to allow an adequate simulation of the subsequent course of the average temperature anomaly of the entire expanding network on time-scales longer than about two decades, though there are marked biases in individual years or groups of years, eg the early 1940's when Europe had a succession of severe winters, thus giving a very low "hemispheric" average anomaly on the basis of the networks of the 1850's, 1860's and 1870's. Figure 9.7B shows that subsequent interdecadal changes over the Southern Hemisphere land-based observing network (excluding the Antarctic) are well simulated by the networks for the 1860's onwards. These results strongly suggest that the coverage of land air temperature data in the late 19th Century was sufficient to yield a good representation of true hemispheric decadal average land air temperature anomalies. In the absence of full knowledge of any persistent changes of atmospheric circulation, however, they do not constitute absolute proof.

9.2.5 Summary of large-scale trends of land surface air temperature

Figures 9.8A and B show the hemispheric trends of land surface air temperature from 1852 to 1984, subject to the unavoidable limitations of coverage described in the previous section. In the Northern Hemisphere, the major feature was a warming of about 0.5°C in all seasons between the 1890's and the 1940's. This warming was greatest over the Arctic (Figure 9.9 and Hansen and Lebedeff (1987)). Much of the warming period was accompanied by stronger westerlies in the midlatitude N Atlantic especially in winter (Section 9.6). A subsequent cooling of about 0.2°C in spring, summer and autumn has recently been reversed, while winter temperatures have fluctuated interdecadally, at least partly reflecting temperature changes in central and northern Europe (Figure 9.8C) which are likely to have resulted from changes in atmospheric circulation (Section 9.6). In the mid and late 19th Century the Northern Hemisphere was generally cold over land, by about 0.5°C relative to 1951-80, with the notable exception of the summers which were warmer than the 1951-80 average before the 1880's, a feature again also particularly evident over central and northern Europe (Figure 9.8C) and to a lesser extent over other areas of the hemisphere. The coverage in the early part of the northern hemispheric record is somewhat dominated by Europe (Section 9.2.4). In the Southern Hemisphere (Figure 9.8B) there appears to have been a monotonic long-term warming trend over land with superimposed fluctuations on a 10 to 20 year time scale. The indication of warmth at the start of the record is based on very few data, and the improving coverage through the series probably caused the increasing agreement between the seasons.

The interannual fluctuations superimposed on the longer-term trends of land surface air temperature can be seen for part of the Northern Hemisphere record in Figure 9.9A. They are, as expected, much smaller than the local interannual variations (compare Figure 9.4B), whereas the longer-term trends in local and hemispheric series are of comparable magnitude. Because the original data are largely the same, different authors' assessments of the course of hemispheric land temperatures are very highly correlated. Most of the published series are for the Northern Hemisphere and correlate at over 0.95, with both interannual and longer-term changes agreeing very well (Ellsaesser et al (1986b)).

Groveman and Landsberg (1979) have constructed a continuous Northern Hemisphere land surface air temperature series extending back to 1579 (Figure 9.10). To do this, they used regression formulae relating a near-hemispheric series of Northern Hemisphere land surface air temperature for 1881-1975, which had been previously constructed by Borzerkova et al (1976), to temperature values constructed for a few very long-period stations. Their series had to be based on a mixture of botanical and documentary data in the pre-instrumental era. Confidence limits for the series are shown and are comparable with the magnitude of the climatic changes suggested by the series. The series must be regarded as very uncertain, in the light of the spatial variation of long-term trends (Figure 9.9 and Hansen and Lebedeff (1987)). A cold period around 1600-1700 is suggested in common with European series, with a hint of warmth in the 1730's. The large temperature fluctuation in the first half of the nineteenth century is less expected but the early twentieth century warming (based on instrumental data) is clearly visible in their series and is comparable in magnitude with that of Jones et al (1986).

9.3 CHANGES IN MARINE TEMPERATURES

Ships' observations have been systematically recorded since the mid-19th Century when Maury (1852) put into action his plan to "belt the earth with stations". Since that time, almost 100 million observations have been made, but only in the past decade or so, with the growth in computing technology, has it become possible to realise the potential of these data. Even now, about 20 million valuable early observations await digitization.

A major compilation of marine data, known as the Comprehensive Ocean-Atmosphere Data Set (COADS) is described by Woodruff et al (1987). This data set includes monthly summaries of air and sea surface temperatures, wind, pressure, humidity and cloudiness on 2° latitude x 2° longitude resolution. Quality controls made by the compilers included the elimination of duplicate observations; consistency checks which resulted in the removal of, for example, reports from locations which are land; and "trimming" to remove extreme values.

A further compilation of marine temperature data has been made using observations archived in the Meteorological Office Main Marine Data Bank (Bottomley et al (1988)). This data set has two advantages over the COADS compilation:

a) The quality controls were carried out on the observations after conversion to deviations or "anomalies" from a climatological background field on 1° latitude x 1° longitude and pentad (5-day) resolution. Monthly anomalies for 5° latitude x 5° longitude areas were then assembled from the quality-controlled high-resolution anomalies. The results will have been more precise than COADS in regions of strong climatological temperature gradients (eg the Gulf Stream) and at times of year of rapid climatological warming or cooling. In such cases low-resolution processing of sparse data could result in substantial errors in the computed anomalies.

b) Only night-time air temperature data were used, in order to avoid most of the effects of on-deck solar heating (Glahn (1933); Hayashi (1974); Folland, Parker and Kates (1984)).

The quality-controls applied to the COADS and the initial quality-controls carried out by Bottomley et al (1988) were designed to compensate for random errors in the data. Some of these errors are truly random, for example errors in computer-keying, or parallax errors in reading a thermometer: others, such as faulty instrumental calibration, may be systematic for a given ship for at least one passage, but can be taken to be random when considering the whole data set which is based on data from many ships.

In addition to random errors, however, spurious systematic changes, of instrumental or procedural origin, occur in the marine data. For sea surface temperature (SST), these have resulted from the change in usage from mainly uninsulated buckets to largely engine intakes or insulated buckets for the readings.

For air temperature, false systematic trends appear to have arisen from the gradual increase in the elevation of the observations above sea level as ships have become larger. In studies of climatic change, systematic errors are usually a greater hindrance than random errors: the following subsection is therefore devoted to a discussion of the instrumental corrections which need to be applied to SST and marine air temperature data. Another potential source of bias in estimating global and hemispheric trends from marine temperature data is the systematic change of geographical coverage during the long period of record. A further subsection therefore assesses the effects of this problem. Similar considerations, of course, apply to land-based data and were discussed in Section 9.2. Biases resulting from changes of marine observation times appear, however, to have been small (Bottomley et al (1988)).

9.3.1 Instrumental Corrections

9.3.1.1 Sea Surface Temperature

Engine-intake readings of SST largely replaced uninsulated bucket observations around the beginning of 1942 (Folland, Parker and Kates (1984)). The main evidence for the sudden change comes from the SST data themselves. Around 1942, SST worldwide became suddenly higher by several tenths °C relative to marine air temperature (Folland, Parker and Kates (1984)). Also, relative to the climatology for 1951 to 1980, spurious annual cycles of SST are visible in many extratropical data until about 1942. Wright (1986) has documented this effect for the North Pacific. The power spectra of hemispheric SST anomalies computed by Folland, Parker and Newman (1985) show a peak at the annual frequency (Figure 9.11) which is not evident in the corresponding marine air temperature (MAT) anomalies. Figure 9.12 demonstrates the spurious annual cycles for an area of the Gulf Stream where air-sea temperature contrasts are especially large in winter leading to excessive winter cooling of uninsulated buckets but a much smaller cooling in summer. Figure 9.12 also includes corrected data. The corrections were derived by Bottomley et al (1988) using versions of a physically-based model of an uninsulated bucket. The model assumes that the water in the bucket is kept well-mixed, and it takes account of the heat fluxes arising from the following causes, given climatlolgical temperatures, humidities, insolation and probability distributions of wind speed.

a) The difference between the external air temperature and the temperature of the water in the bucket;

b) The difference between the atmospheric vapour pressure and the saturation vapour pressure at the temperature of the water in the bucket;

c) The strength of the wind around the bucket, with allowance for typical ships' motion and for the estimated sheltering effects of ships' structures;

d) The influence of the mass of the thermometer, assumed to be initially at the air temperature, when plunged into the bucket;

e) The short and long-wave radiation incident on the bucket.

The combination of a), b) and c) and to some extent (d) makes midlatitude winter uninsulated bucket SST too cold; but (e) and to a small extent (d) can make midlatitude summer uninsulated bucket SST less cold or even a little too warm: hence the spurious annual cycles of pre-war SST anomalies relative to a 1951 to 1980 climatology.

A crucial unknown quantity relevant to the computation of the corrections is the typical length of time which elapsed between the extraction of the bucket from the sea and the reading of the thermometer. Instructions to mariners suggest a variety of times ranging from "two or three minutes (five)" (Maury (1958)) to "30 seconds" (Marine Observers' Handbook (Her Majesty's Stationery Office (1950))). This problem was circumvented by varying the period allowed in the model for heat transfer until the implied corrections, when applied to observed SST, minimised the spurious annual cycles. Figure 9.13A shows series of 15-year running values of the ratio of annual cycle variance to total variance, for monthly SST anomalies averaged over the belt 30°N to 40°N, without corrections and with corrections to pre-1942 data assuming 0.5, 1.5 and 3 minutes' heat transfer time. The corrections are based on a model version "D9" which is similar to those used by Bottomley et al (1988). It is necessary to minimise the variance ratio, rather than the annual cycle variance itself, because there will be real interannual variability of the strength of the annual cycle as a result of oceanic and meteorological fluctuations, as a result of which the annual cycle variance of true SST anomalies will not be zero, and can be assumed to be approximately proportional to the variance at other frequencies. Note in Figure 9.13A that the uncorrected data show generally much higher values of the variance ratio before the 1940's. Application to pre-1942 data of corrections assuming progressively longer heat transfer times reduces these values until a minimum is reached, in this case at around 1.5 minutes' heat transfer time. Eventually, lengthening the heat transfer time begins to increase the variance ratio, because the corrections are now making the data too warm in winter and too cold in summer. Figure 9.13B summarises this relationship between the variance ratio and the assumed heat-transfer time for the same zonal belt for the period 1881 to 1941 as a whole.

Figures 9.14A, B show the corrections as applied up to 1900 by Bottomley et al (1988). The corrections for 1901 to 1941 were more positive by 0.02°C to 0.04°C because it was assumed (Krummel (1907)) that buckets were more often exposed to direct insolation in the 19th Century, so different versions of the model, assuming respectively 100% and 25% of climatological direct insolation, were used in the earlier and later periods respectively. Corrections based on a variety of versions of the model (assuming, for example, different sizes of bucket or different degrees of reduction of the wind speed by the ship's structure) were found to be very similar. For example, a bigger bucket, holding more water, would cool more slowly than a small bucket, but the modelled exposure time would need to be greater if the spurious annual cycles were to be removed, so the resulting corrections would be similar. Additional versions of the model are still being assessed: for example, the effect of ship's speed is being investigated further, and it may become necessary to allow for the use of, for example, some wooden or metal buckets in the 19th Century (cf Maury (1958)).

As expected, Figures 9.14A, B show generally positive corrections, especially in midlatitude winter and in the tropics. The largest corrections are in winter over the Gulf stream and the Kuroshio where the sea is much warmer than the air. The effects of the corrections on time-series of regional SST anomalies can be assessed by comparing Figures 9.15A and B. As anticipated, the corrected anomalies are made less negative, or more positive, before 1942, and the climatic trends for the different seasons are brought into closer agreement. Clearly, the uncorrected data somewhat misrepresent climatic change.

9.3.1.2 Night Marine Air Temperature

Corrections for long-term systematic increases in deck elevation were derived by Bottomley et al (1988) on the basis of typical profiles of temperature in the marine boundary layer. Because these corrections were found to be insensitive to reasonable variations in the shape of the assumed boundary layer profile, corrections based on the same globally averaged profile were chosen irrespective of location and season. This profile is superadiabatic in the relevant height range, and the corrections applied were -0.15°C up to 1900; -0.09°C for 1901-15; -0.02°C for 1916-60; 0.01°C for 1971-5 and 0.02°C thereafter. These corrections are generally smaller than those made to SST (Figure 9.14), and much smaller than those which would be required to daytime marine air temperatures to compensate for solar heating on deck, which would be of the order of -1°C (Parker (1988)). However Bottomley et al (1988) did find the need to apply additional corrections as large as -0.9°C to night marine air temperatures observed between 1940 and 1945. These data showed discontinuities in time, not shared by the daytime data which were used as a reference: the cause was probably the wartime practice of carrying the thermometers indoors to be read, to avoid showing a light to the enemy.

Marine air temperature data for years before about 1880 appear to have been affected by positive biases in windy conditions (Parker (1988)). Possibly the thermometers were read under cover: investigations are continuing, and corrections have not yet been applied to compensate.

9.3.2 The effects of variations of coverage on estimates of the course of hemispheric marine temperatures

Incomplete geographical coverage could result in biases in estimating global and hemispheric trends from marine as well as from land (Section 9.2.4) temperature data. Figure 9.16 illustrates some of the changes in coverage of SST data since the 1860's. The coverage of marine air temperature data has followed virtually identical patterns. The coverage was temporarily diminished during the World Wars and has been affected by changes in patterns of international trading, due, for example, to the opening of the Suez Canal in 1869 and the Panama Canal in 1914, which resulted in a reduction of shipping traversing the Southern Ocean. In order to assess the effects of the changes in coverage, "frozen grid" experiments were carried out. The results of one of these are shown in Figure 9.17. Firstly, SST anomalies (SSTA) for each season in the record were averaged globally using all 5° latitude x 5° longitude boxes with data: the resulting seasonal time-series was smoothed using the filter illustrated in the inset of Figure 9.17, to give the continuous time-series curve in the main part of the diagram. The computations were then repeated, but using only the heavily hatched areas of Figure 9.16A, ie those with over 90% coverage in 1861-70, throughout the time-series. Comparison of the resulting dashed curve with the continuous curve in the main part of Figure 9.17 suggests that restriction of coverage to that available in the 1860's allows adequate simulation of the subsequent course of the longest-term changes of SST averaged over the entire expanding network. Similar experiments using hemispheric SST data, or global or hemispheric marine air temperature data, yielded estimates of long-term trends which were nearly as stable as those in Figure 9.17. The reason for this insensitivity to coverage is partly that the long-term trends appear to have occurred in unison over virtually the entire globe (Bottomley et al (1988)). This is shown by the correlation of 0.92 between seasonal time series of the coefficient of the rather geographically uniform first global all-seasons covariance eigenvector of SSTA defined for 1901-80 (Figure 9.18A) and the globally averaged SST anomaly, derived using all available data, for 1856 to 1987 (Figure 9.18B). Although the long-term trends have geographically varying amplitude (Figure 9.18A), this has apparently been rather well sampled by the time-varying coverage throughout the record. However, caution is needed because the region south of 45°S, which contains about 20% of the world's ocean, has never been adequately sampled (Figure 9.16). For this reason, and because we have not proved that the characteristic patterns of SST variations, represented by the eigenvectors, are entirely stable from epoch to epoch, the above results do not absolutely prove the adequacy of the coverage for assessments of global and hemispheric marine temperature trends.

9.3.3 Summary of large-scale trends of marine temperature

Figures 9.19A and B present the hemispheric trends of SST for 1856 to 1987, subject to the above mentioned unavoidable limitations of coverage. Instrumental corrections have been applied up to 1941 as in Bottomley et al (1988). The Northern Hemisphere curves are very similar to those for the Atlantic north of 35°N (Figure 9.15B, which has a different plotting scale), and the North Atlantic as a whole and the North Pacific have also undergone similar trends (Bottomley et al (1988)). Until about 1960 the Southern Hemisphere also cooled and warmed in unison with the Northern . The worldwide nature of the century time-scale fluctuation of SST is brought out by Figure 9.20A, which shows SSTA for 1903-12 which was on a global average the coldest decade. The geographical uniformity in long-term trends has already been noted in connection with the discussion of variations of data coverage in Section 9.3.2 and illustrated by means of the geographically rather uniform, first all-seasons eigenvector of global SSTA and the hightly-correlated time-series of its coefficient and of global SSTA in Figure 9.18. However, since about 1960 there has been substantial oceanic warming of the Southern Hemisphere relative to the Northern. This differential change has not, in fact, been exactly hemispheric: the Northern Indian Ocean has warmed in phase with the Southern Hemisphere, and the trends in much of the South Pacific have been weak (Figure 9.20B). The quasi-interhemispheric changes of SST since the 1950's are discussed in Lecture 5 in connection with the drought of the last two decades in sub-Saharan Africa.

Global, hemispheric and regional trends of night marine air temperature have, as would be expected on physical grounds, been very similar to those of SST (Bottomley et al (1988): see also Figure 9.21). This similarity confirms the reality of the trends, because the measurements have been made independently, and the instrumental corrections included no attempts to constrain the series to agree.

Shorter-term variations of both SST and night marine air temperature have been superimposed on the longer-term trends. As can be seen from the time-series in Figure 9.21, many of the shorter-term variations appear to be associated with the El Nino-Southern Oscillation (ENSO): see also Lecture 6. The variations on time-scales of 2 to 6 years indicated by the power-spectra in Figure 9.11 are likely, therefore, to be associated with ENSO, but the peak near 17 years in Southern Hemisphere SST and its equivalent near 20 years in night marine air temperature are as yet unexplained. The dominant peaks at about 70 years (Northern Hemisphere) and 100 years (Southern Hemisphere) represent the century time-scale fluctuations visible in Figure 9.19.

9.4 COMPARISON OF LAND AND MARINE TEMPERATURE TRENDS

Figures 9.8 and 9.19 reveal substantial similarities, but also some contrasts, between the changes of hemispheric anomalies of land surface air temperature and SST since the mid 19th Century. The similarities are, perhaps, surprising in view of the thermal inertia of the oceans. In the Northern Hemisphere, the general trends have been very similar since 1900 (note the different scales of the graphs), but in the mid-and late 19th Century the land surface air temperature anomalies were low relative to those of SST by about 0.5°C in winter and by about 0.25°C in spring and autumn. In the Southern Hemisphere the land surface air temperature anomalies were also low relative to those of SST in the 19th Century in autumn and winter, but to a lesser extent. In addition, the very recent rise of SST in the Southern Hemisphere has been more marked than that of land surface air temperature.

There are several possible reasons for the divergences between the indications of the early data:

a) The instrumental corrections to SST could have been inadequate, as a result of the use of different types of bucket or different procedures. The close agreement between the seasons in Figure 9.19A suggests, however, that this may not have been a serious problem.

b) The early land data could be too cold relative to the 1951-80 reference period as a result of increasing urban heating, changes of instrumentation, or changes in observing times. However, Jones et al (1986) eliminated stations showing evident urban heating and other discontinuities relative to neighbouring stations. The relative warmth over Northern Hemisphere land in summer may have resulted from the limited sampling (Section 9.2.4).

c) Atmospheric circulation anomalies could have made the oceans relatively warm and the continents relatively cold, or in the Northern Hemisphere, low latitudes (mainly oceanic) relatively warm and high latitudes (mainly continental) relatively cold. Jones and Kelly (1983) and Jones et al (1988) have documented substantial geographical variations in 20th Century temperature trends.

A test of the reliability of the data was made by comparing time-series of land surface air temperature over selected islands with corresponding series of SST and night marine air temperature from the surrounding ocean within 10° of latitude and longitude, instrumentally corrected as in Bottomley et al (1988). When averaged together over the hemispheres, the series for these locations were in better agreement than the series for the hemispheres as a whole after 1870 (see eg Figure 9.22 for the Northern Hemisphere), suggesting that anomalies of atmospheric circulation may have caused the divergences between Figures 9.8 and 9.19. The portion of Figure 9.22 before 1870 should be ignored because there were fewer than 5 sites available for the comparison. The relative warmth over the island stations between the 1890's and 1940 is, however, significant because about 30 well-scattered sites were used, and may indicate that slightly larger corrections are required to the SSTs after about 1900. If, in accord with known trends in ships' performance, a ships' speed of 7 m/sec were assumed after 1900, as opposed to 4 m/sec as used by Bottomley et al (1988), the corrections would be larger, though not in general by as much as 0.1°C. However, the SSTs in Figure 9.22 are supported by the night marine air temperatures, suggesting the need for investigation into the reliability of the land surface air temperatures also. Similar results were obtained for the Southern Hemisphere.

Climatic changes of island and coastal air temperature are, as Figure 9.22 suggests, often determined by regional climatic changes of SST. An example for the British Isles is shown in Figure 9.23, in which are compared the climatic changes of SST anomalies for the Atlantic north of 35°N, Central England Temperature, and Scilly Islands temperature, on days with westerly atmospheric circulation types defined by Lamb (1972b). Knowledge of local SST has been found to be useful in the interpretation of predicted patterns of atmospheric flow in terms of temperatures in the United Kingdom on weekly to monthly time-scales.

Figures 9.15B and 9.24 suggest a possible link between the long term changes of ocean surface temperatures and the fluctuations of some European glaciers, despite the complexity of the climatic factors that influence individual glacier advances and retreats. The advance of the Swiss glaciers in the early twentieth century seems to correspond with the cool period in the midlatitude N Atlantic (and over the globe) around 1900-1915; the subsequent retreat centred around 1950 coincides with highest SST. Most convincing is the recent advance that corresponds well with the fall in midlatitude N Atlantic SST up to about 1980. The changes in SST may not of course be the direct cause of the glacier fluctuations - both may be the result of a third common factor.

9.5 CHANGES IN RAINFALL

Long-term local, regional and Northern Hemispheric series of rainfall have been constructed on the basis of land-based observations, in a manner similar, but not identical, to that employed for land surface air temperature. However, we do not yet have reliable means of estimating rainfall at sea: for this, satellite-based techniques are being developed, partly under the aegis of the Global Precipitation Climatology Project (see Lecture 1).

The climatology of local rainfall can vary substantially over short distances, especially in mountainous terrain. Furthermore, the statistical distributions of local rainfalls are not Gaussian, even on monthly and seasonal time-scales. For these reasons, composite regional series cannot be formed by simply averaging anomalies over a set of stations. Often the data are first expressed as normalised deviations from the local average (eg Nicholson (1985)), or in terms of the parameters of a gamma-distribution (eg Bradley et al (1987)). If the rainfall climatology of the region is known in detail, the resulting series can be converted back into "dimensional" units, ie millimetres.

The best-attested climatic change in a regional rainfall series is the recent dessication of sub-Saharan Africa (Figure 9.25). The associated worldwide changes of SST (Figure 9.20B) and the mechanisms possibly involved in the generation of the drought are discussed in Lecture 5. There have, however, also been accompanying changes in atmospheric circulation in the extratropical N Atlantic sector, involving a tendency to increased anticyclonicity near the British Isles in high summer (see Section 9.6 below), and a resulting reduction of rainfall. The latter can be seen as a decrease in July and August rainfall over England and Wales since the 1950's in Figure 9.26.

The most significant long-term change in the England and Wales rainfall over the period of about 200 years covered by Figure 9.26 is an increase in January rainfall. December shows a much weaker increase and February shows no change. The annual totals have not changed systematically, so the increase in January is unlikely to have resulted from instrumental or procedural changes. The series was carefully adjusted for variations in observing locations. Figure 9.26 therefore suggests a change in atmospheric circulation in January, not affecting February. This explanation is supported by the relative constancy of February's Central England Temperature (Figure 9.1). Regressions relating monthly England and Wales rainfall (EWR) to monthly patterns of mean sea level pressure (MSLP) for the period 1901-80 were applied to earlier MSLP fields in order to simulate EWR. The results verified January EWR as far back as 1873, and to some extent for earlier years for which the pressure fields had been created by different techniques. The very dry conditions in January in the early 19th Century are in agreement with the pressure fields of Lamb and Johnson (1966).

Bradley et al (1987) created the first precipitation series for the Northern Hemisphere (Figure 9.27). However both their hemispheric and their regional series are likely to be revised when full account is taken of instrumental and procedural changes. For example, the Soviet Union has introduced gauges which are more efficient collectors of snow, and has also started to apply corrections for the fact that wetting of the collector funnel must occur before the water can begin to accumulate in the receiving bottle. These changes are likely to have contributed substantially to the recent increase in rainfall in the Soviet Union reported by Bradley et al (Figure 9.28).

9.6 FLUCTUATIONS OF THE ATMOSPHERIC CIRCULATION

9.6.1 North Atlantic sector

The chief evidence for fluctuations of atmospheric circulation in the last few hundred years years comes from the North Atlantic sector and is to be found in:

(a) diaries kept by careful observers of wind direction and weather;

(b) Many measurements of pressure at station level made since the eighteenth century.

One of the most interesting and lengthy series of type (a) was put together by Lamb (1972a), of necessity rather subjectively (Fig 9.29), and shows variations in the frequency of south westerly winds in S E England. A relatively low frequency during much of the seventeenth century and a peak in the 1730's is in accord with the variations in CET outside the summer season (Figure 9.1). In summer, the level of CET is not expected to be well-related to the frequency of south westerly winds. A minimum frequency of south westerly winds has been suggested for a few years in the late 18th century by Kington (1988) who has constructed daily weather maps for the period 1781-85. At this time, due to a briefly successful interlude of international cooperation, there was a well-distributed network of pressure observations in Europe. Lamb and Johnson (1966) have constructed monthly-mean MSL pressure charts for January and July since 1750 for the N Atlantic sector, and for later years for much of the Northern Hemisphere.

Strong evidence for the changing characteristics of the atmospheric circulation in winter in the N Atlantic sector over the last century is provided by the distributions of the Azores minus Iceland monthly pressure differences in Figure 9.30. The pressure data from the two stations used are of good quality and have been carefully scrutinised. Both stations are situated near sea level. The data provide an index of circulation reflecting the strength, or location, of the mid-latitude westerlies between the Azores and Iceland. Winters in the early twentieth century were characterised by persistently strong westerlies (middle panel) whereas those in the late nineteenth century and the period since 1940 have had a greater relative frequency of weak westerlies or even easterlies, probably reflecting an increased incidence of atmospheric blocking (see Section 2.5.3.1 in Lecture 2). Within the latter-period there has been a tendency for interdecadal fluctuations with more severe (blocked) winters in the 1940's, 1960's, and late 1970's to mid 1980's, and a notable succession of mild winters in the early to mid 1970's. Figure 9.31 shows variations in the frequency of Lamb's westerly types over the British Isles (see Lamb (1972b, 1977) and Lecture 1) for the year as a whole, and again indicates a greater prevalance of westerlies in the early twentieth century. Figure

9.32 shows differences in mean sea level pressure during January over the extratropical Northern Hemisphere between 1901-30 and 1951-70, and also indicates that the N Atlantic westerlies were substantially stronger in the earlier period, by perhaps 3 or 4 m/sec over Scotland. Scrutiny of Figure 9.1, where the 20 year running average of CET is plotted against the last year of the 20 year period, shows that between 1911-30, January CET averaged about 1.2°C higher than in the latter period. 1.2°C is a large change in mean temperature; e.g. during the recent 30 year period 1951-80 a month with an anomaly of 1.2°C from the mean was just enough to place that month into the top 20% of the January temperature probability distribution. The even larger warming in October between 1890 and 1975 in Figure 9.1 was also partly due to an increase in the frequency of south westerly winds in that month. The warming was so large that a very mild month (top 20% of the ranked distribution of October temperatures) in the period 1870-1900 could easily have had the same temperature as a rather cold month (bottom but one 20% of the 30 year ranked distribution of October temperature) in the period 1951-80. The sharp cooling in April since 1961 has been associated with a strong increase in blocking and thus in east-north-east winds in that month. So (mainly) as a result, there were no very warm Aprils in Central England after 1961 until 1987.

9.6.2 Evidence of circulation variations on the global scale

A comprehensive analysis of all available quality-controlled mean sea level (MSL) pressure data on land and at sea has yet to be carried out. However, the potential value of such analyses is suggested by Figure 9.33 taken from Tan and Yasunari (TY) (1982). TY analysed July MSL pressure over much of the globe using station, including island, data but excluding the Atlantic Ocean sector 0-60°W. The data were first analysed into a grid point format. Figure 9.33 shows the first two eigenvectors of the field of 11 year running mean MSL pressure; this averaging time-scale was chosen to highlight the longer-period variations. The first eigenvector (31% of the variance) is negative north of about 20°N and positive to the south; the time series suggests a progressive reduction of MSL pressure in the Southern Hemisphere relative to the extratropical Northern Hemisphere over the last century with a temporary halt to this tendency between about 1900 and 1930. These changes do not seem to be in accord with the elementary assumption that the warmer region (relative to climatology) will have the lower MSL pressure (again relative to climatology). Although the Southern Hemisphere with the N Indian Ocean has been relatively warm, by comparison with the rest of the Northern Hemisphere, in the most recent 20 years (Figures 9.8, 9.19, 9.20B), the same applied to a lesser extent at the beginning of the twentieth century, and the opposite was true around the 1940's and 1950's when Figure 9.33B indicates reduced MSL pressure on the Southern Hemisphere. The comparison is, however, hindered by the omission of the Atlantic by TY. The second eigenvector (19%) of the variance) represents a variation of MSL pressure between the Pacific and the Indian Ocean on the one hand and the surrounding continental areas on the other. Relatively low pressure over land and high pressure over the oceans is suggested in the late nineteenth century and mid-twentieth century, with a reversed pattern around 1900-1920. The century time-scale variations are in phase with those of hemispheric temperatures in Figures 9.8 and 9.19, but the physical connections are as yet unknown.

It must be emphasised that, away from the midlatitude N Atlantic sector, most existing grid point data sets of MSL pressure must be used with great caution. There have been unrealistic changes of derived MSL pressure over some mountainous regions and over the Arctic (Williams and Van Loon (1976)).

9.6.3 Links between Sahel rainfall and extratropical atmospheric circulation

The Sahel drought has been a special theme of these lectures, and we have already repeated at Figure 9.25 the time series of Sahel rainfall anomalies shown in Lectures 1 and 5. Figures 9.34A and B show, for the extratropical N Atlantic sector, July and August MSL pressure differences between the most recent dry Sahel period (1986-87) and the wet period (1950-59). The grid-point MSL pressure data set used has been corrected for a change of data time from 12 GMT to 00 GMT in 1966. The two maps are similar and indicate higher pressure centred near northern Britain in the later period, though only in August is this locally statistically significant. For the hemisphere north of 20N as a whole 8% (July) and 7% (August) of the area is locally statistically significant. Although this indicates that the field as a whole is probably not statistically significant (Livezey and Chen (1983)), the persistence of the anticyclonic anomaly, which was also very weakly apparent in June, suggests dynamical significance. The anticyclonic anomaly has not been consistently indicated by the atmospheric general circulation model experiments with SST anomalies appropriate to Sahel drought (Lecture 5). It has, however, been associated with a significant reduction of July and August England and Wales rainfall (Figures 9.26 and 9.35), and the summers affected include 4 of the 11 driest summers (June to August) in the England and Wales rainfall series which began in 1766. 1976 was the driest and 1983 the second driest.

Another feature of the MSL pressure differences between 1968-87 and 1950-59 has been a persistently deeper Aleutian low in the later period between December and March. The strengthened westerlies over the midlatitude N Pacific are likely to have contributed to the reduced SSTs there (Figure 9.20B), by southward Ekman drift, increased vertical mixing in the ocean, and increased fluxes of heat to the atmosphere. Despite increased anticyclonicity from April to June, the reduced SSTs in the later period have been evident throughout the year, possibly because the westerlies were strengthened slightly in most of the remaining months.

9.7 TEMPERATURE CHANGES ALOFT

Series of data based on radiosondes are generally too short to indicate much about climatic change; the series are at present much more useful for studying interannual variability, especially the effects of El Nino. Radiosonde data are unfortunately subject to severe problems of changing instrumental biases, which affect particularly upper atmospheric temperature measurements; biases vary between countries and therefore may be geographically variable. This problem results from a combination of changes in instrumentation and changes in correction procedures. The main difficulty has been the need to compensate adequately for solar heating of radiosonde thermometers; the problem is acute in the lower stratosphere. For example, Parker (1985a) found, in a study covering 1958 to 1982, that cooling of the lower stratosphere, an expected result of increasing atmospheric carbon dioxide, was only evident over stations using USA Weather Bureau radiosondes. Spurious changes in tropical tropospheric radiosonde data were eliminated as far as possible in a separate stucy by Parker (1985b) by checking the spatial consistency of interannual changes of the thicknesses of the 850 to 500 mb and 500 to 200 mb layers recorded over the stations. Those interannual changes which were regarded as reliable were used to construct series of thicknesses representing the entire tropics for 1950 to 1983. After adjustment for the phase of Southern Oscillation (see also Lecture 6) these series showed no trend (Figure 9.36).

Time series of tropospheric temperatures for 1958-87, derived by Angell (1988) from data from a global network of 63 well-distributed radiosonde stations, are presented in Figure 9.37, which also includes a series of SST for part of the eastern equatorial Pacific to show the influence of the El Nino-Southern Oscillation on the interannual changes of tropospheric temperature. The longer-term relative warming of the Southern Hemisphere is in agreement with hemispheric SST trends (Figure 9.19). Angell also found a recent marked cooling in the lower stratosphere over much of the globe: see Figure 10.10 in Lecture 10, and the associated discussion.

9.8 SEA LEVEL

A worldwide warming of climate might be expected to lead to a rise of sea level as a result of the thermal expansion of sea-water and the addition of water to the oceans from melting glaciers and ice-sheets. On the other hand, if a warmer climate were to entail increased precipitation of snow onto existing ice sheets, a fall of sea level could result.

Fairbridge (1987), however, drew attention to the non-climatic influences on sea-level. For time-scales shorter than a century these include:

i) Regional glacio-isostatic changes in response to loading and unloading of the Earth's crust by ice;

ii) Local and regional sedimental loading and compaction;

iii) Seismic displacement.

Fairbridge concluded that the averages of mean-sea-level change deduced from tide-gauge measurements during the 20th Century are grossly misrepresentative of changes of global ocean volume, because of clustering of gauges in northern midlatitudes (where glacio-isostatic changes may be important) and because of siting of stations at river mouths and on estuaries and deltas where crustal loading and sedimental compaction cause subsidence.

Barnett (1984) also discussed the difficulties inherent in the estimation of global mean sea level changes, and found that the existing data set was inadequate for this purpose. He warned that interpretation of long-term changes of sea level would be difficult because of glacio-isostatic changes. Nevertheless he found a coherent rise in mean sea level since the early 1900's except near Alaska, Scandinavia and southeast Asia, and, with the above caveats, computed a global rise of 23 cm/century since the early 1900's. This rate is greater than the consensus, 10 to 15 cm, of the estimates tabulated by Ellsaesser et al (1986), who not only reviewed the difficulties in assessing global sea level change, but also drew attention to problems in confirming such changes of sea level by means of changes in the Earth's rotation rate. The latter is affected not only by the increase of the Earth's moment of inertia when polar land-ice melts, but also by Earth-moon interactions and, maybe, by rearrangements of material in the Earth's core.

Wigley and Raper (1987) used an energy-balance climate model, with separate boxes for land and ocean for each hemisphere and with oceanic upwelling and diffusion, to deduce that the greenhouse-gas-induced thermal expansion contribution to sea-level rise between 1880 and 1985 was between

2 and 5 cm. The range in their values resulted from the fact that a variety of combinations of oceanic diffusivity and equilibrium climate sensitivity to carbon dioxide increases could be inserted in the model and still give global mean sea surface temperature changes consistent with those observed: the different combinations of parameters gave different vertical profiles of sea temperature changes, and therefore different estimates of thermal expansion.

9.9 CAUSES OF CLIMATIC CHANGES ON DECADAL TO CENTURY TIMESCALES

We conclude by drawing attention to some likely reasons for the climatic changes described in this Lecture. Much of the relevant discussion of these mechanisms has already been presented in other Lectures, to which the reader is referred where necessary.

9.9.1 Variations in solar output

The most recent finding is that total solar irradiance appears to vary in phase with the 11-year sunspot cycle (Section 3.1.2 and Figure 3.5 in Lecture 3). If this relationship also holds for the longer-period changes in the number of sunspots (Figure 3.6), then the minimum in worldwide temperatures shortly after the beginning of the present century may have at least part of its origin in a reduction of the solar output; and the peak of warmth around the 1940's to 1950's may have been partly caused by increased solar irradiance. Similar considerations would apply to the climax of the "Little Ice Age" around the time of the Maunder minimum of sunspots in the 17th Century: see also Lecture 8.

9.9.2 Oceanic circulations

Changes in the thermohaline circulation of the oceans have been proposed as mechanisms of past climatic change (Section 7.5.2 in Lecture 7; Section 8.4.3 in Lecture 8). Interactions between winds and ocean currents may also be important in maintaining the present relative warmth of the Southern Hemisphere (Section 5.4.5 in Lecture 5).

9.9.3 Volcanic eruptions

Section 3.3 (Lecture 3) discusses the possibility that injections of volcanic aerosols into the stratosphere cause temporary coolings of climate. Most of the observational evidence and modelling results suggest, however, that the residence times of the aerosols are only of the order of a few years: thus, to force the sustained interdecadal climatic changes observed in the last century would require sequences of several decades with many and few powerful eruptions respectively. The volcanic indices and Antarctic sulphuric acid profile shown in Figure 3.16 do not show this and certainly do not match the observed decadal to century time-scale temperature changes. In particular, the marked early 20th century warming began about 20 years after Santa Maria (1902) and the subsequent cooling began befor Agung which was not followed by other major eruptions until El Chichon, which may not (Section 3.3.3) have interrupted the recent warming.

9.9.4 Greenhouse gases

The reader is referred to Lecture 10 for an assessment of the evidence for the influence of increasing carbon dioxide and other greenhouse gases in the atmosphere on the climate of the Earth in recent decades. The rôle of carbon dioxide in the climatic changes in the late Pleistocene is discussed in Section 7.5.3 (Lecture 7) and Section 8.4.1 (Lecture 8).

REFERENCES TO ADVANCED LECTURE NO 9

ANGELL, J K (1988) Variations and trends in tropospheric and stratospheric global temperature, 1958-1987. Submitted to J Climate.

ANGELL, J K and GRUZA, G V (1984) Climate Variability as estimated from atmospheric observations. In "The Global Climate" Ed: J T Houghton, pp 25-36. Cambridge University Press.

BARNETT, T P (1984) The estimation of "global" sea level change: a problem of uniqueness. J Geophys. Res., 89, C5 7980-7988.

BORZENKOVA, I I, VINNIKOV, K Ya SPIRINA, L P and STECHNOVSKII, P I (1976) Variations of Northern Hemisphere air temperature from 1881 to 1975. Met i Gid, 7, 27-35.

BOTTOMLEY, M, FOLLAND, C K, HSIUNG, J, NEWELL, R E and PARKER, D E (1988). Global Ocean Surface Temperature Atlas (GOSTA). Meteorological Office/Massachusetts Institute of Technology. In press.

BRADLEY, R S, DIAZ, H F, EISCHEID, J K, JONES, P D, KELLY, P M and GOODESS, C M (1987) Precipitation fluctuations over Northern Hemisphere land areas since the mid-19th Century. Science, 237, 171-175.

DETTWILLER, J (1978) L'evolution seculaire de la temperature à Paris. La Meteorologie, VI, 13, 95-130.

ELLSAESSER, H W, MacCRACKEN, M C, WALTON, J J and GROTCH, S L (1986) Global climatic trends as revealed by the recorded data. Rev Geophys, 24, 745-792.

FAIRBRIDGE, R W (1987) The spectra of sea level in a Holocene time frame. In "Climate. History, Periodicity, and Predictability", Eds. M R Rampino, J E Sanders, W S Newman and L K Königsson. Van Nostrand Reinhold Co. New York. pp 127-143.

FOLLAND, C K (1983) Regional-scale interannual variability of climate - a north-west European perspective. Met. Mag., 112, 163-183.

FOLLAND, C K, PARKER, D E and KATES, F E (1984) Worldwide marine temperature fluctuations 1856-1981. Nature 310, 670-673.

FOLLAND, C K, PARKER, D E and NEWMAN, M (1985) Worldwide marine temperature variations on the season to century timescale. Proc 9th Climate Diagnostics Conf., Corvallis, Oregon 22-26 Oct. 1984. Amer. Met. Soc., pp 70-85.

GLAHN, W (1933) False measurements of air temperatures on ships. Hamburg, D Seewarte, Der Seewart, 2, H6, 250-256. In German but English translation available in National Meteorological Library, Bracknell, UK.

GROVEMAN, B S and LANDSBERG, H E (1979) Reconstruction of Northern Hemisphere temperature: 1579-1980. Univ. Maryland Met. Program, Publ. 79-181. Data appendices in separate volume.

HANSEN J and LEBEDEFF, S (1987) Global trends of measured surface air temperature. J. Geophys. Res., 92, D11, 13345-13372.

HAYASHI, S (1974) Some problems in marine meteorological observations, particularly of pressure and temperature. Tokyo, Japan Met. Agency, J. Met. Res. 26, 84-87. In Japanese but English translation available in National Meteorological Library, Bracknell, UK.

HER MAJESTY'S STATIONERY OFFICE (1950) Marine Observers' Handbook, 7th Edition. London.

JONES, D E (1987) Daily Centrel England Temperature: recently constructed series. Weather, 42, 130-133.

JONES, P D and KELLY, P M (1983) The spatial and temporal characteristics of Northern Hemisphere surface air temperature variations. J. Climatology, 3, 243-252.

JONES, P D, RAPER, S C B, BRADLEY, R S, DIAZ, H F, KELLY P M and WIGLEY, T M L (1986) Northern Hemisphere surface air temperature variations: 1851-1984. J. Clim. Appl. Met., 25, 161-179.

JONES, P D, RAPER, S C B and WIGLEY, T M L (1986) Southern Hemisphere surface air temperature variations: 1851-1984. J. Clim. Appl. Met., 25, 1213-1230.

JONES, P D, WIGLEY, T M L, FOLLAND, C K and PARKER, D E (1988) Spatial patterns in recent worldwide temperature trends. Submitted to Nature.

KASSER, P and AELLEN, M (1981) Switzerland and her Glaciers. Swiss National Tourist Office, Kummerly and Fry, Bern, 191 pp.

KINGTON, J (1988) The weather of the 1780's over Europe. Cambridge University Press, 166 pp.

KRÜMMEL, O (1907) Handbuch der Oceanographie, Vol 1, Stuttgart, 373 pp.

LAMB, H H (1965) The early mediaeval warm epoch and its sequel. Paleogeography, Palaeoclimatology, Palaeoecology, 1, 13-37. Amsterdam (Elsevier).

LAMB, H H (1972a) Climate Present, Past and Future. Vol 1, Methuen.

LAMB, H H (1972b) British Isles weather types and register of the daily sequence of circulation patterns 1861-1971. Geophysical Memoirs No 116 (SECOND NUMBER, VOLUME XVI). London, Her Majesty's Stationery Office, 85 pp.

LAMB, H H (1977) Climate Present, Past and Future. Vol. 2, Methuen.

LAMB, H H and JOHNSON, A I (1966) Secular variations of the atmospheric circulation since 1750. Geophysical Memoirs No. 110. (FIFTH NUMBER VOLUME XIV). London, Her Majesty's Stationery Office, 125 pp..

LANDSBERG, H E (1979) Atmospheric changes in a growing community. Urban Ecology, 4, 53-82.

LIVEZEY, R E and CHEN, W Y (1983) Statistical field significance and its determination by Monte Carlo techniques. Mon. Weath. Rev., 111, 46-59.

MANLEY, G (1974) Central England temperatures: monthly means 1659-1973. Quart. J. Roy. Met. Soc., 100, 389-405.

MAURY, M F (1852) Correspondence with J Glaisher, in the Report of the Council of the British Meteorological Society, 25 May 1852, pp. 6-10. Available in National Meteorological Library, Bracknell, UK.

MAURY, M F (1858) Explanations and Sailing Directions to accompany the wind and Current Charts. Vol. 1. 383 pp + 51 plates. Printed by W A Harris, Washington D C.

NICHOLSON, S E (1985) Sub-Saharan rainfall 1981-84. J. Clim. Appl. Met., 24, 1388-1391.

OKE, T R (1982) The energetic basis of the urban heat island. Quart J Roy. Met. Soc., 108, 1-24.

PARKER, D E (1985a) On the detection of temperature changes induced by increasing atmospheric carbon dioxide. Quart. J. Roy. Met. Soc, 111, 587-601.

PARKER, D E (1985b) The influence of the Southern Oscillation and volcanic eruptions on temperature in the tropical troposphere. J. Climatology, 5, 273-282.

PARKER, D E (1988) A note on the use of voluntary observing fleet data to estimate air-sea fluxes. Long-Range Forecasting and Climate Research LRFC 17, Meteorological Office, Bracknell.

PARKER, D E and FOLLAND, C K (1988) The nature of climatic variability. Met. Mag., 117, 201-210.

SIREN, G (1961) Skogsgranstallen som indikator for klimatfluktuationerna i norra Fennoskandien under historisk tid. Communicationes Inst. Forest. Fenniae, 54 (2), Helsingfors.

TAN, C and YASUNARI, T (1982) Fluctuations of global surface pressure patterns during the past 100 years and their relation to the Asian monsoon. Part I. Northern Summer (July). J. Met. Soc. Japan, 60, 1132-1142.

UNTERSTEINER (1984) The cryosphere. In "The Global Climate" Ed: J T Houghton, pp 121-140. Cambridge Univ. Press.

WIGLEY, T M L, LOUGH, J M and JONES, P D (1984) Spatial patterns of precipitation in England and Wales and a revised homogeneous England and Wales precipitation series. J. Climatology, 4, 1-25.

WIGLEY, T M L and RAPER, S C B (1987) Thermal expansion of sea water associated with global warming. Nature, 330, 127-131.

WILLIAMS, J and VAN LOON, H (1976). An examination of the Northern Hemisphere sea level pressure data set. Mon. Weath. Rev, 104, 1354-1361.

WOODRUFF, S D, SLUTZ, R J, JENNE, R L and STEURER, P M (1987) A Comprehensive Ocean-Atmosphere Data Set. Bull. Amer. Met. Soc., 68, 1239-1250.

WRIGHT, P B (1986) Problems in the use of ship observations for the study of interdecadal climate changes. Mon. Weath. Rev., 114, 1028-1034.

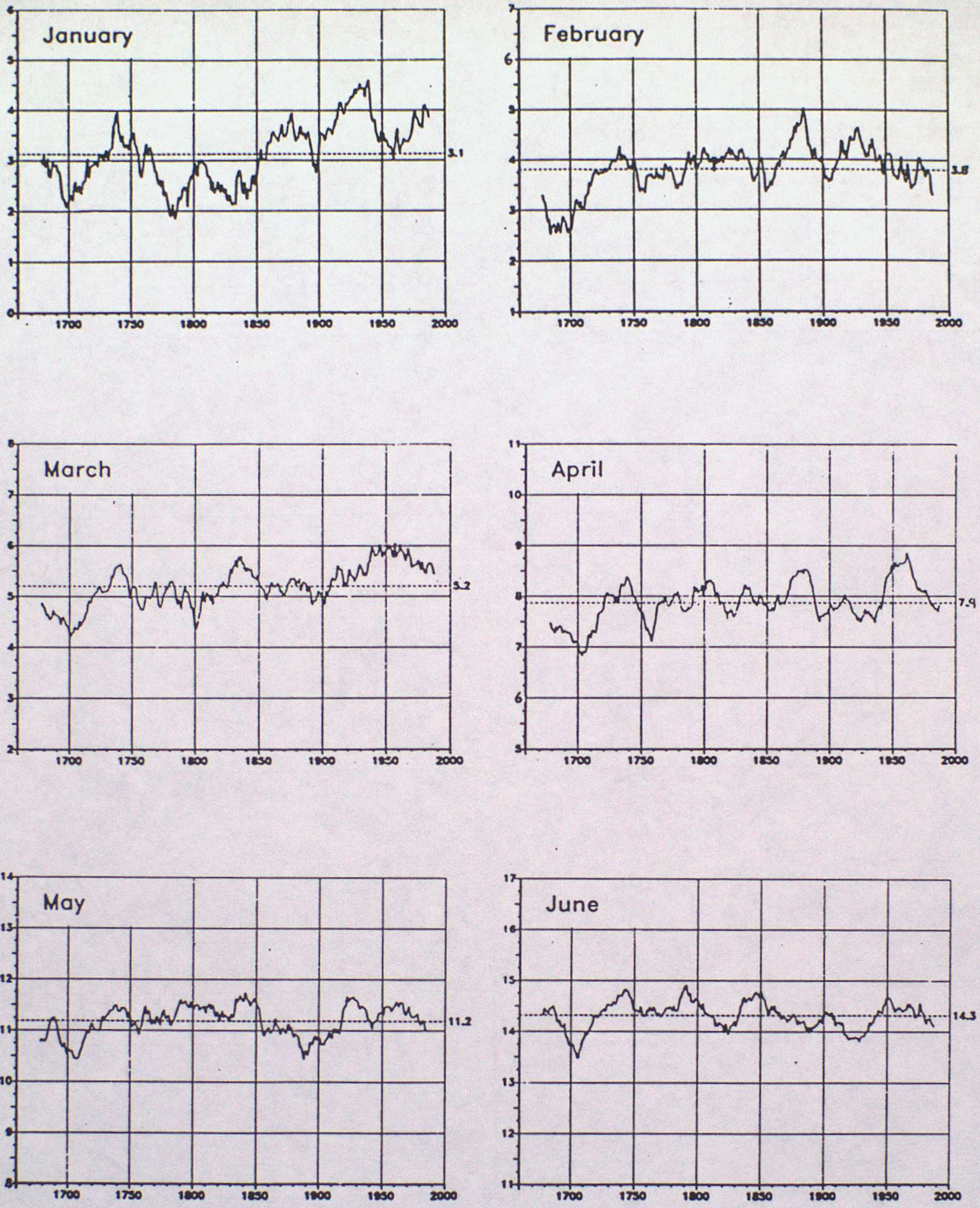

Figure 9.1. Central England Temperature (°C) , 1659 to 1987 . Values are 20-year running averages ending at the plotted date. Dashed horizontal lines are whole-period means.

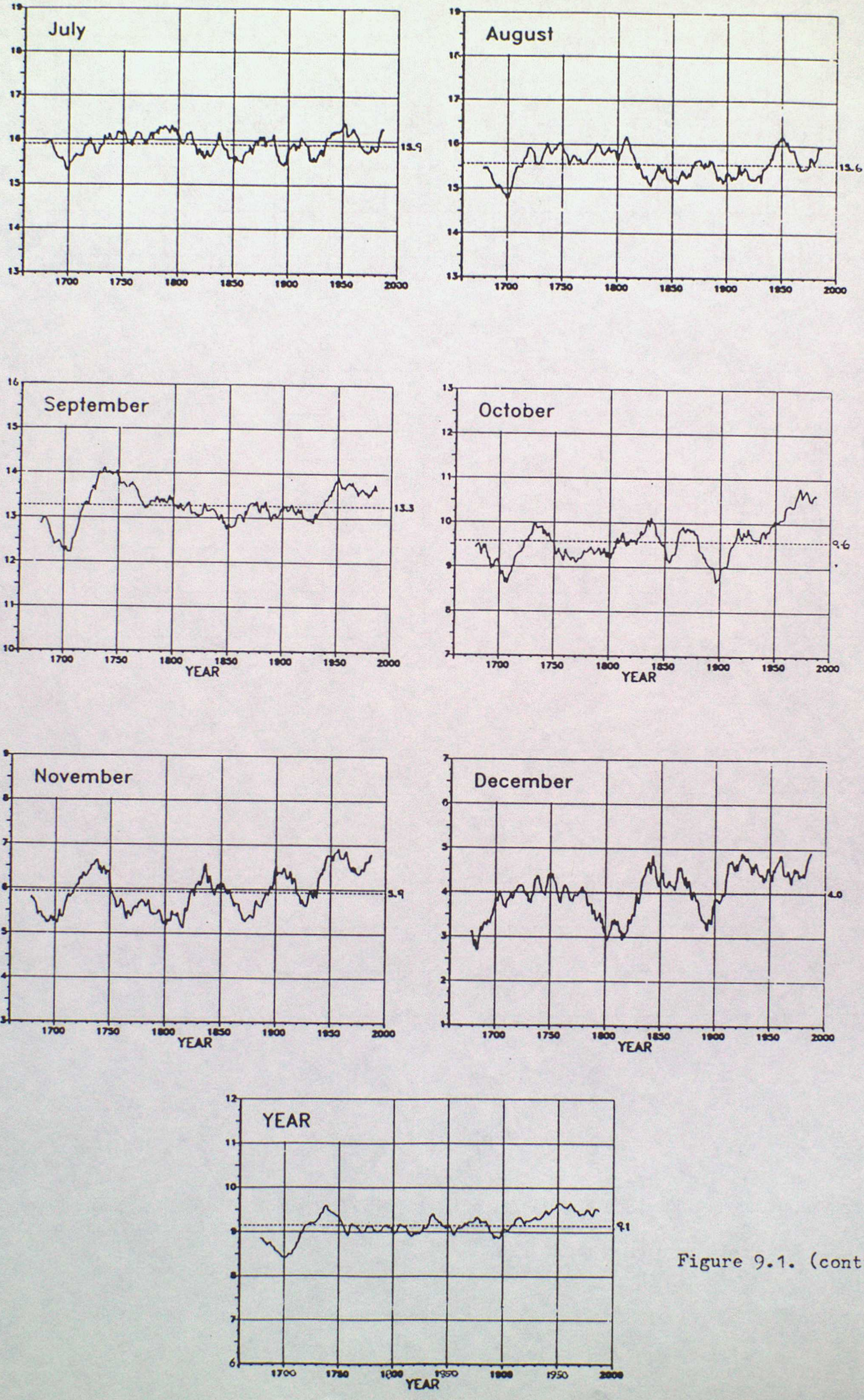

Figure 9.1. (continued)

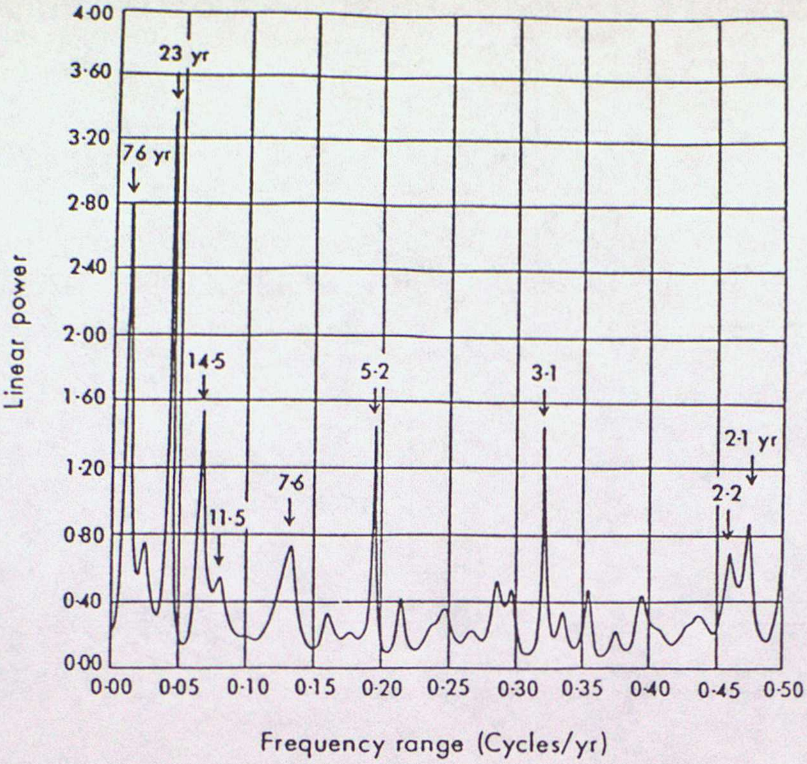

Power spectrum of the Manley record of Central England temperatures with the long-term trend removed.

Figure 9.2A.

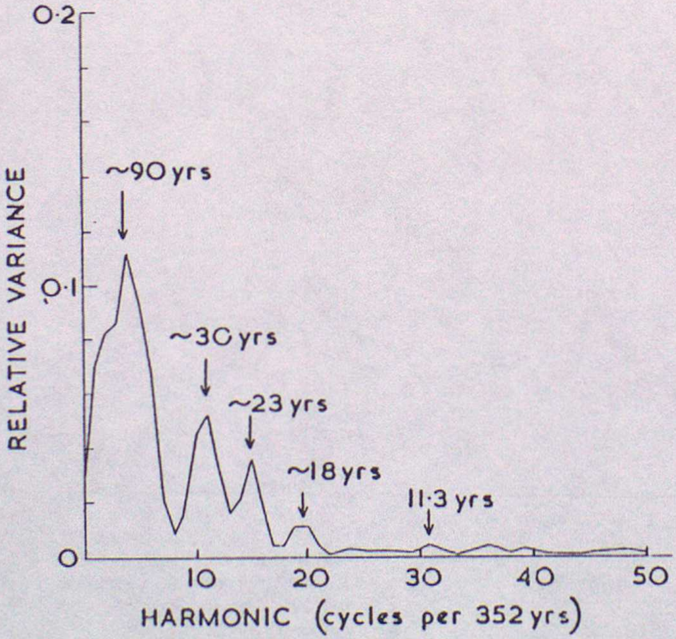

Power spectrum of SIRÉN's (1961) Lapland tree-ring index from 1463 to 1960, which is believed to register mean temperatures of the high summer period in northern Finland. (*Kindly supplied to the author by* J. M. MITCHELL *and reproduced by permission.*)

Figure 9.2B. From Lamb (1972a).

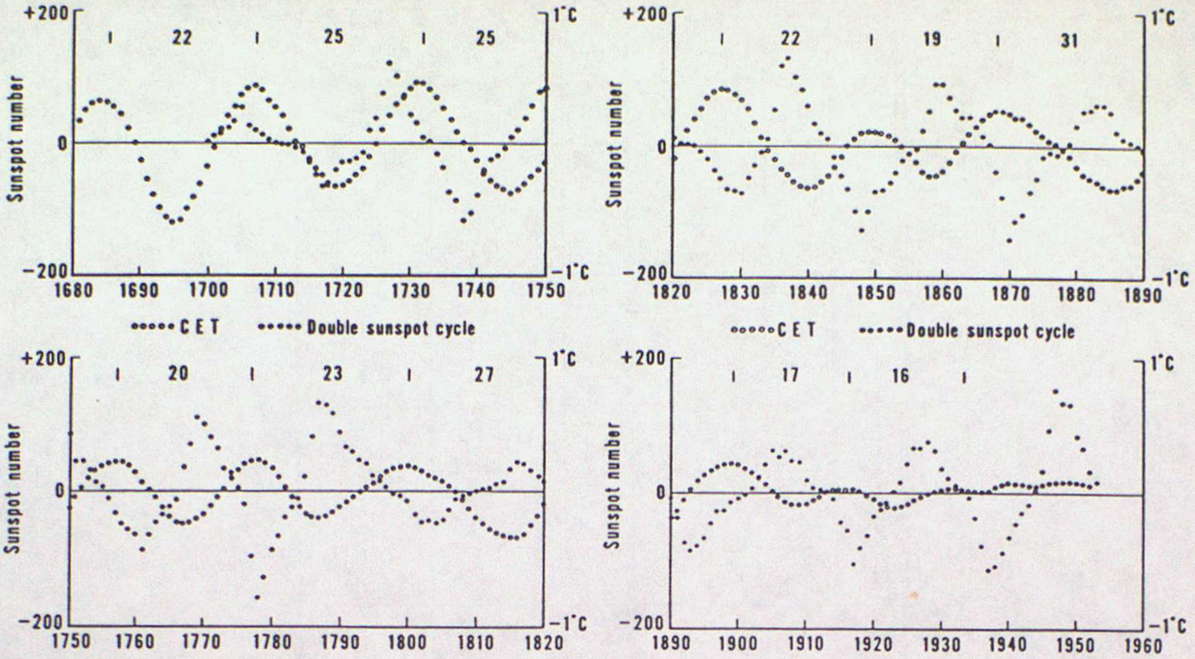

The '23-year' wavelength band-pass filtered series of annual mean Central England Temperature and the 'Hale' or double-sunspot cycle.

Figure 9.2C. From Folland (1983).

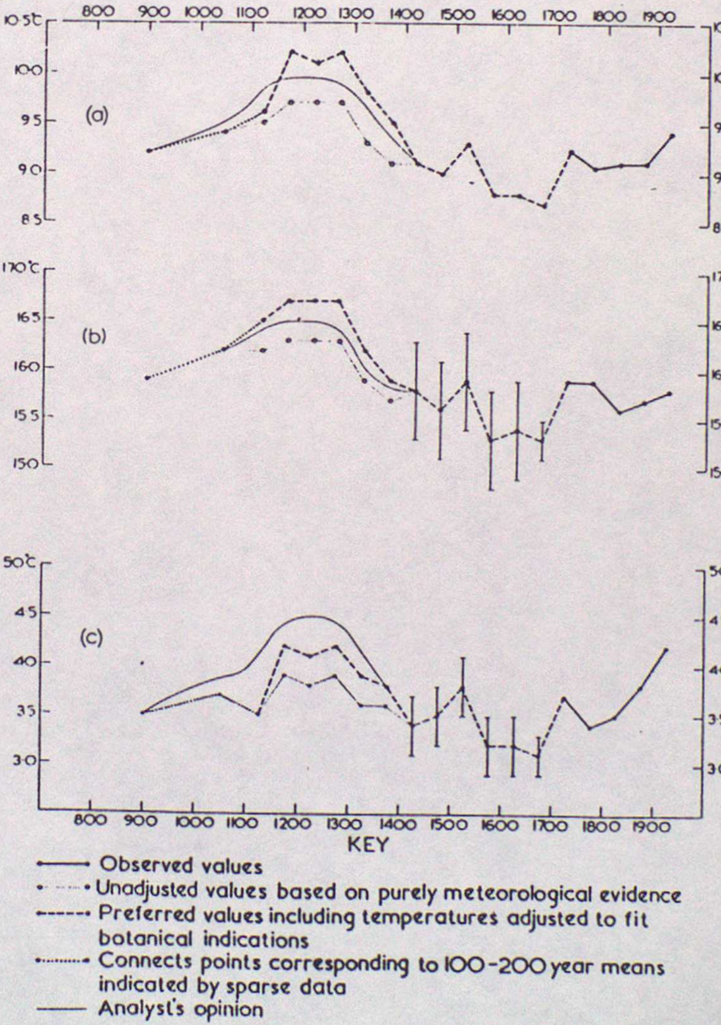

Temperatures (°C) prevailing in central England, 50-year averages:

(*a*) Year

(*b*) High summer (July and August)

(*c*) Winter (December, January and February).

Observed values from 1680, as standardized by MANLEY. Values for earlier periods as derived by LAMB (1965). The ranges indicated by the vertical bars are three times the standard error of the estimates.

Figure 9.3. From Lamb (1972a).

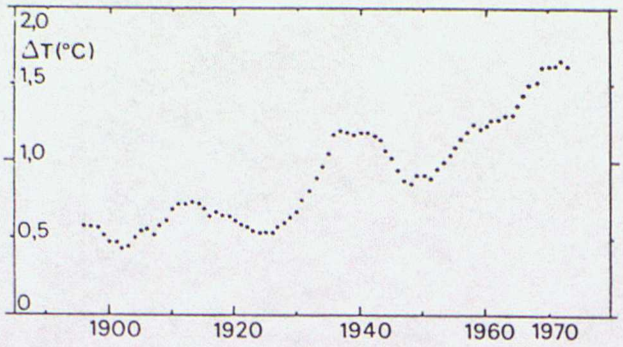

Figure 9.4A. 10-year running mean temperature difference, Paris (Montsouris) minus Besançon. The data are for 1891 to 1977 and the values are plotted at the centre of the averaging interval.

After Dettwiller (1978).

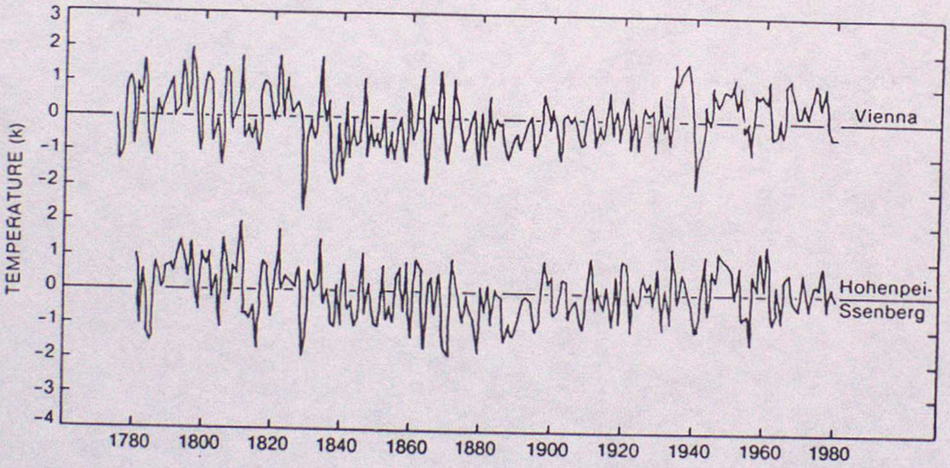

Figure 9.4B. Variation in mean annual temperature at Vienna and Hohenpeissenberg. After Angell and Gruza (1984).

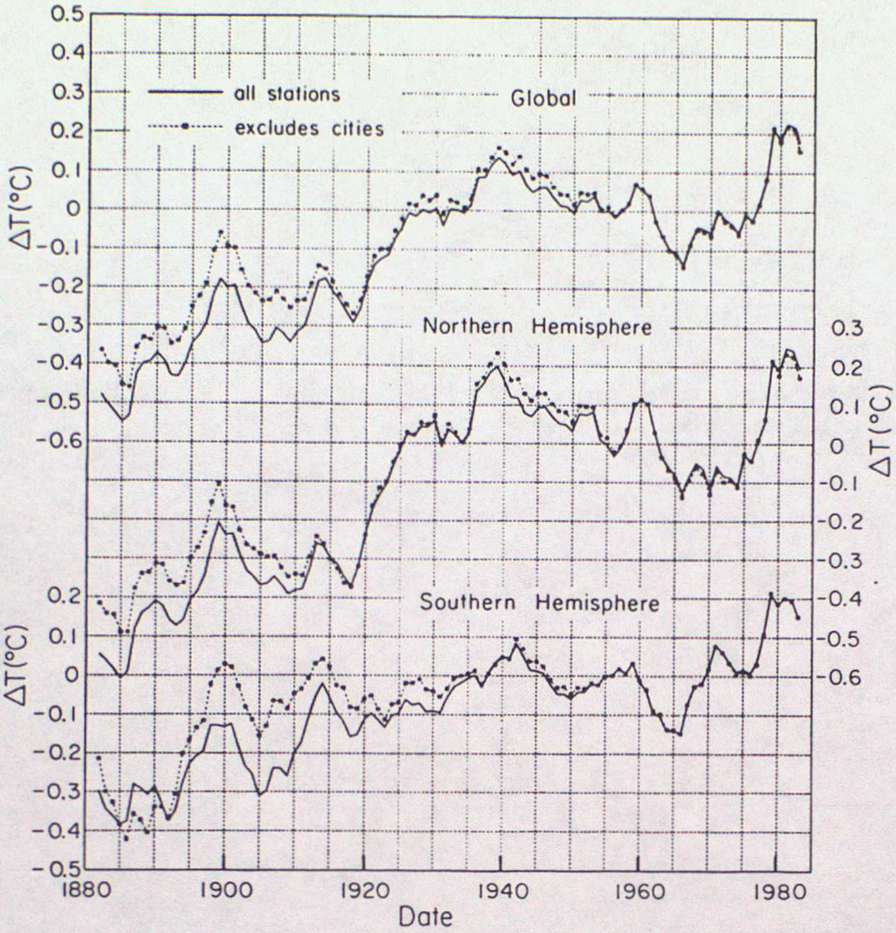

Comparison of 5-year running mean temperature change derived with and without urban stations included.

Figure 9.5. From Hansen and Lebedeff (1987).

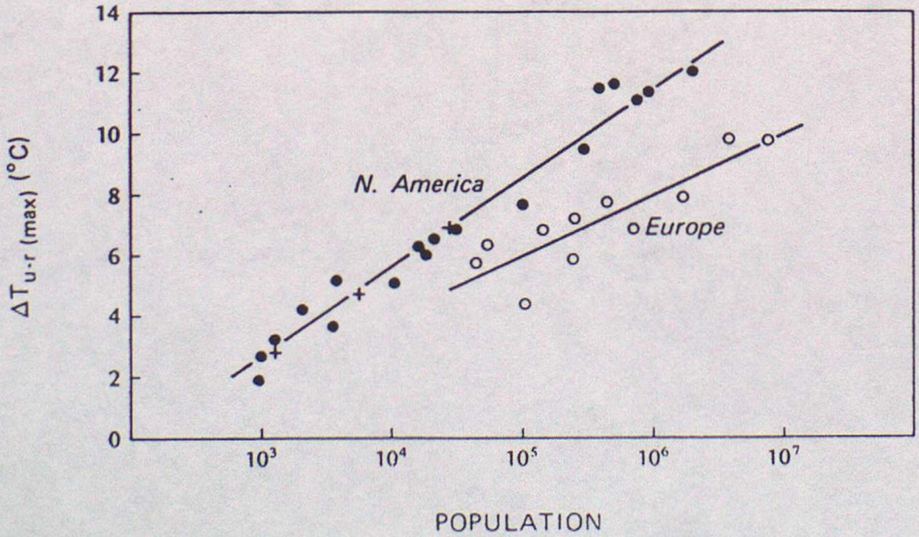

Relation between maximum heat island intensity ($\Delta T_{u-r(max)}$) and population (P) for European and North American settlements. The crosses are for the growing new town of Columbia, Maryland reported by Landsberg (1979).

Figure 9.6. From Oke (1982).

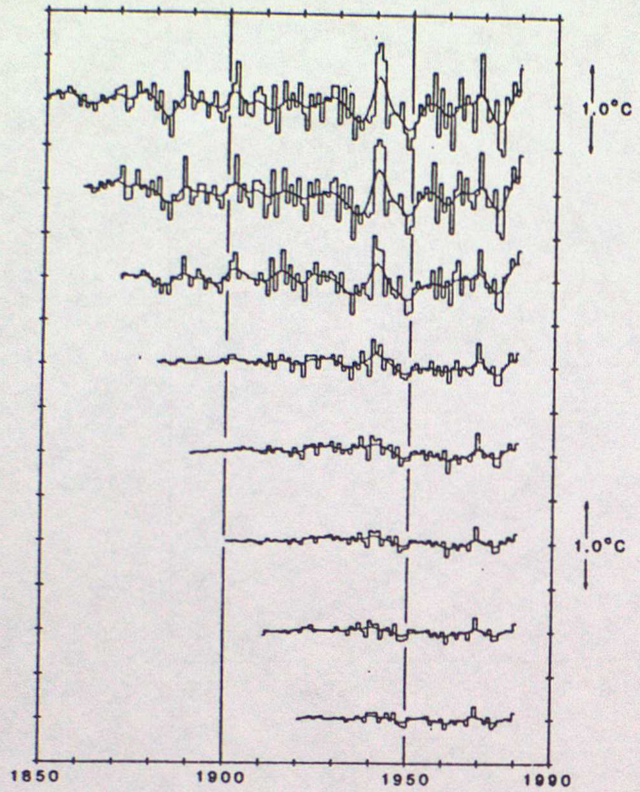

Estimating the effect of incomplete coverage during the early years. Each curve shows the difference between the result from the time-varying grid and Northern Hemisphere averages based only on grid points with data during at least 80% of the decades (top to bottom): 1850s, 1860s, 1870s, 1880s, 1890s, 1900s, 1910s and 1920s. The filtered curve is a 13-term Gaussian filter designed to suppress variations on time scales less than 10 years. In order to estimate filtered values at the ends of each curve, six extra years are used at each end with values equal to the mean of the six years at the beginning/end of each curve.

Figure 9.7A. After Jones et al (1986)

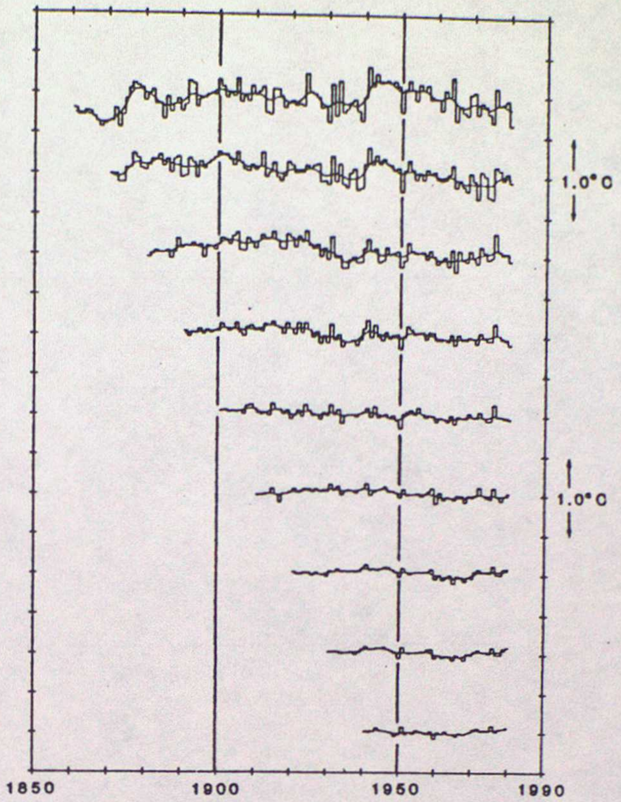

Estimating the effect of incomplete coverage during the early years. Each curve shows the difference between the result from the time-varying grid and the average based only on grid points with data during the decades (top to bottom) 1850s, 1860s, 1870s, 1880s, 1890s, 1900s, 1910s, 1920s and 1930s. The filtered curve is a 13-term Gaussian filter designed to suppress variations on time scales less than 10 yr. In order to estimate filtered values at the ends of each curve, six extra years are used at each end with values equal to the mean of the six years at the beginning/end of each curve.

Southern Hemisphere (2.5°–62.5°S).

Figure 9.7B. After Jones, Raper and Wigley (1986).

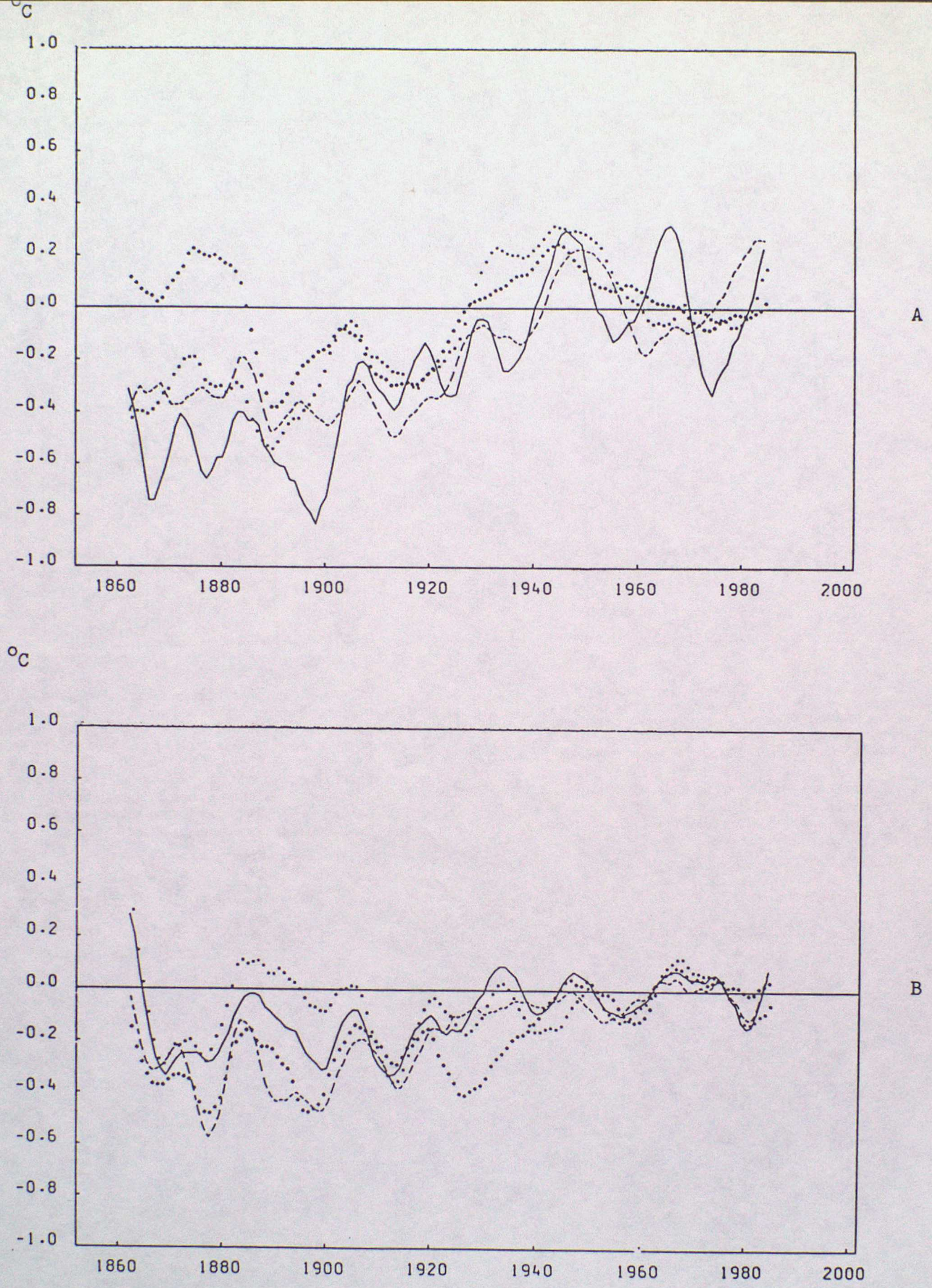

Figure 9.8. Land surface air temperature anomalies (w.r.t. 1951-80) for 1852 to 1984 averaged over the Northern Hemisphere (A) , the Southern Hemisphere north of $62\frac{1}{2}^\circ$S (B), and central and northern Europe (45°-65°N , 25°W-60°E) (C; on next page), plotted against the end-date of an 11-year triangular smoothing filter. Dec-Feb, Mar-May, June-Aug, Sept-Nov are solid line, dashed line, round dots, square dots. Data from P.D.Jones , University of East Anglia.

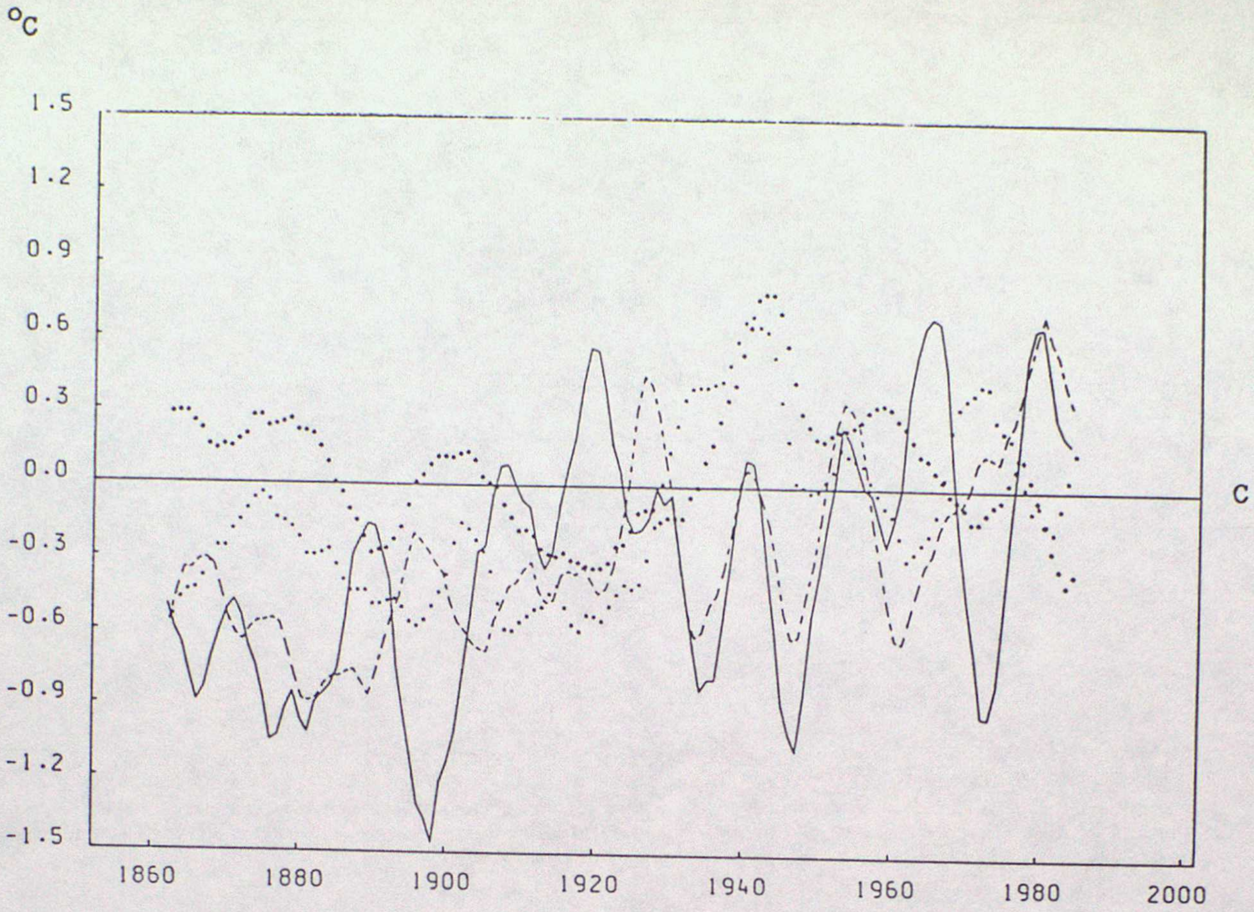

Figure 9.8. (continued). Caption is on previous page.

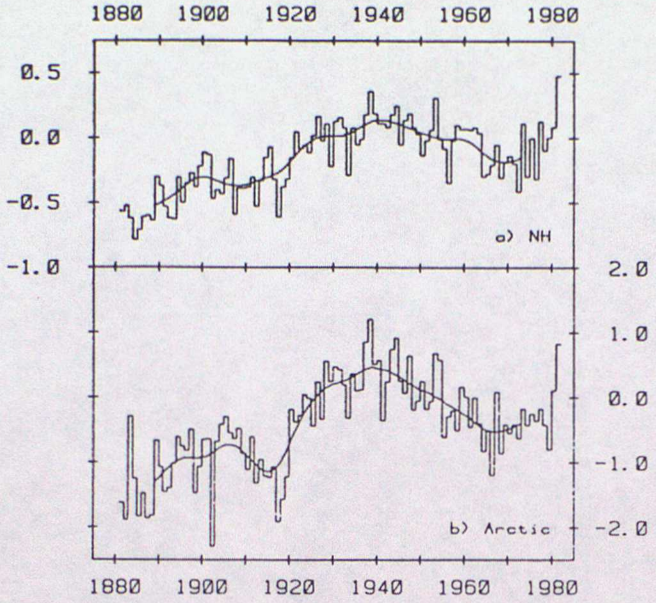

A. Annual means of surface air temperature for the Northern Hemisphere and for the Arctic (expressed as departures in °C from the 1946–1960 reference period). Data for 1981 are included in this figure but have not been analyzed. The smoothed curves show the data smoothed with a binomial filter designed to suppress variations on time scales of less than 20 years

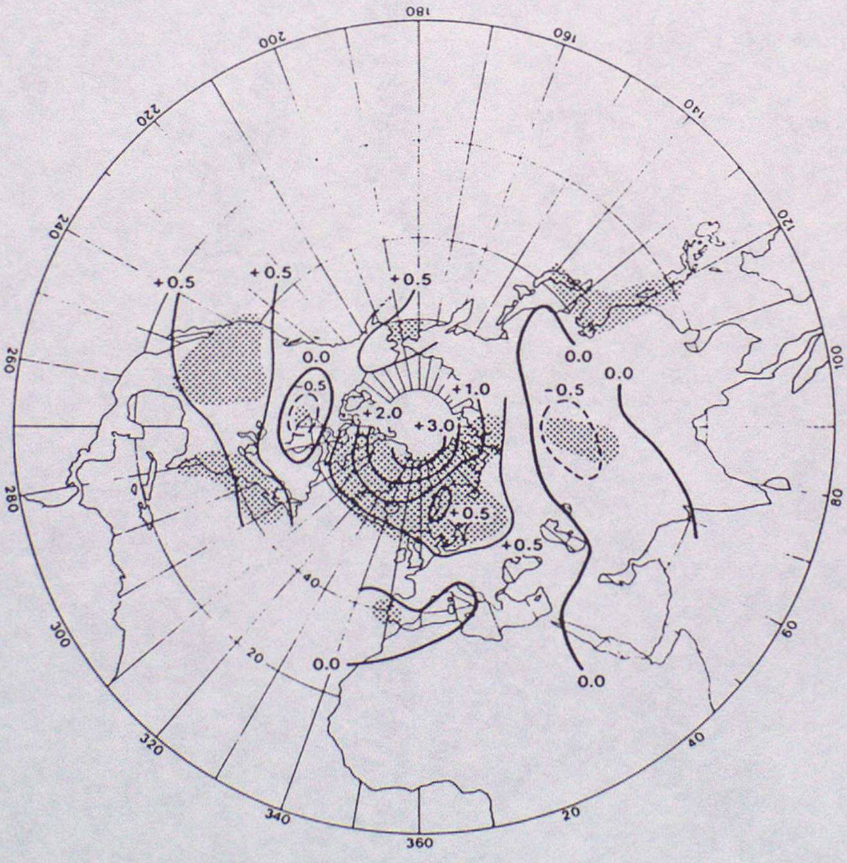
180
160
140
120
100
80
60
40
20
360
340
320
300
280
260
240
220
200
+0.5
+0.5
+0.5
0.0
-0.5
+1.0
+2.0
+3.0
+0.5
+0.5
0.0
0.0
-0.5
40
20
0.0
0.0

B. Linear trend of gridpoint temperatures over the period 1917–1939 (°C/y×10^{-1}). Shaded areas are significant at the 5 per cent level

Figure 9.9. From Jones and Kelly (1983).

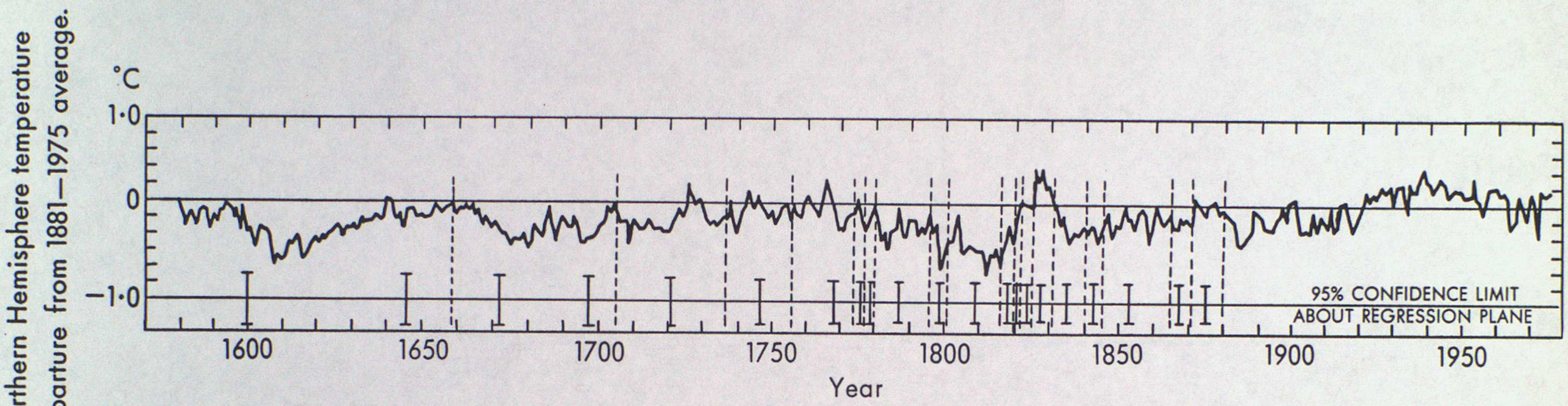

FIGURE 9.10 RECONSTRUCTED ANNUAL TEMPERATURE DEPARTURES (1579—1880) FOR THE NORTHERN HEMISPHERE FOLLOWED BY DATA OF BORZENKOVA et al., (1976). AFTER GROVEMAN AND LANDSBERG (1979). Confidence limits of regressions at bottom of graph.

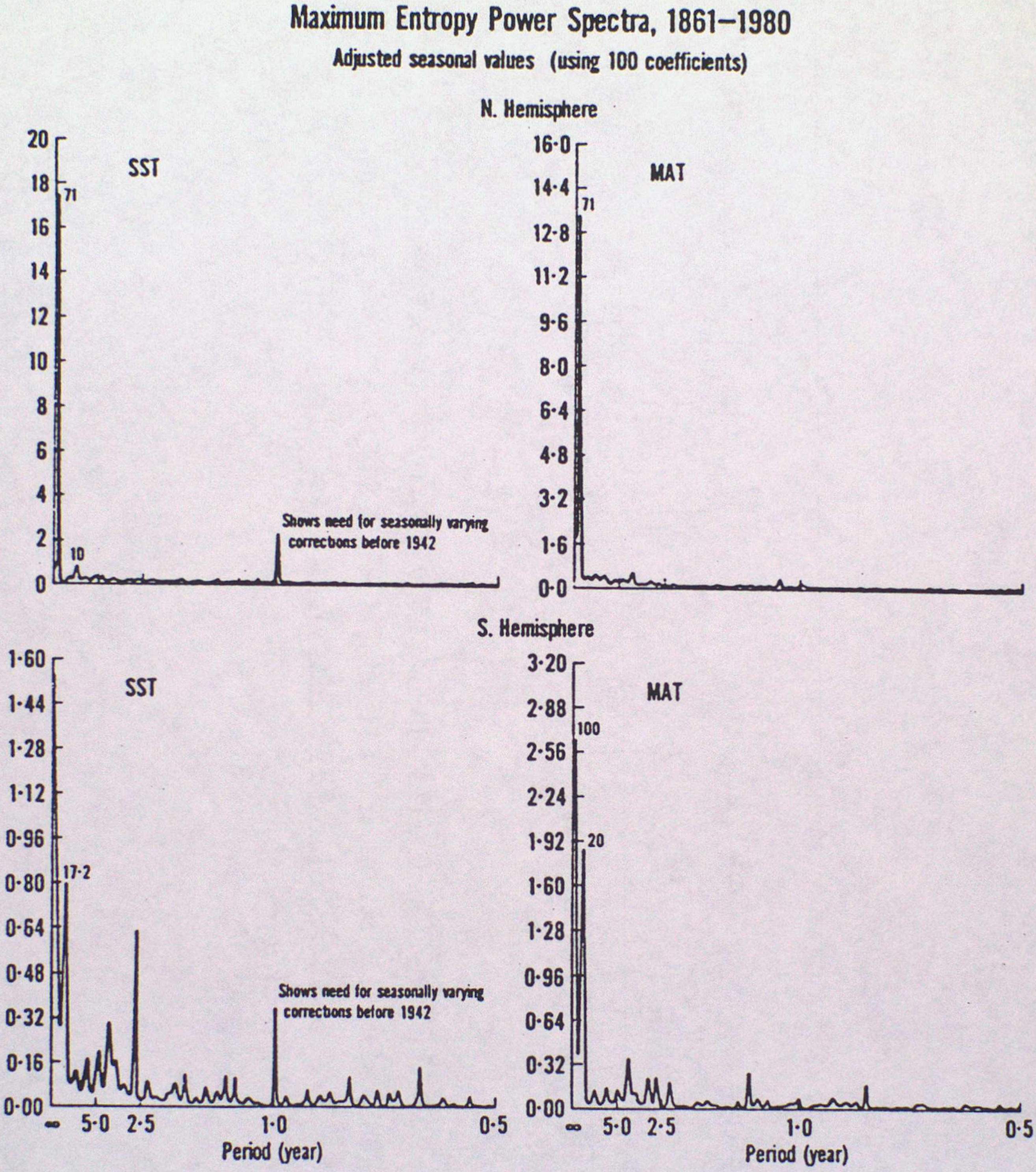

Figure 9.11. From Folland, Parker and Newman (1985).

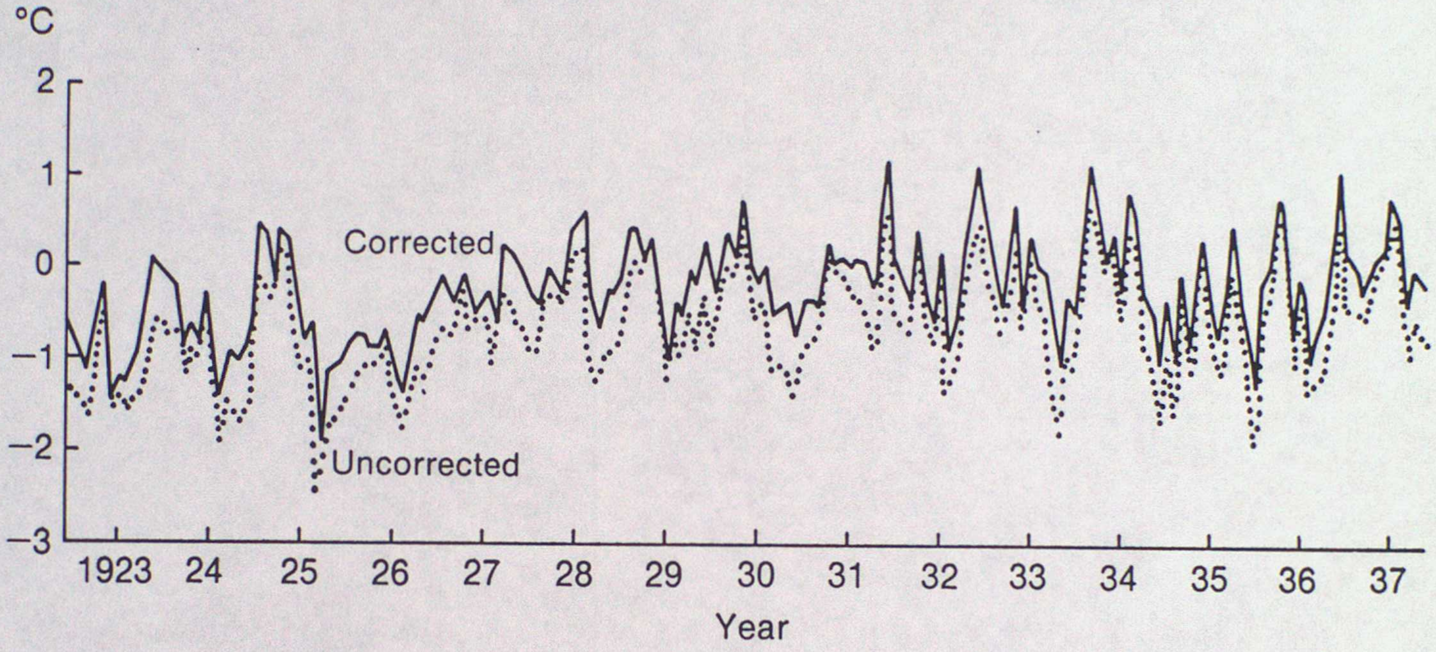

Monthly SST anomalies (relative to 1951–80) for 1923–1937, 35°–45°N; 60°–70°W, with and without corrections for the use of uninsulated buckets. Tick marks are in July of each year.

Figure 9.12. From Bottomley et al (1988).

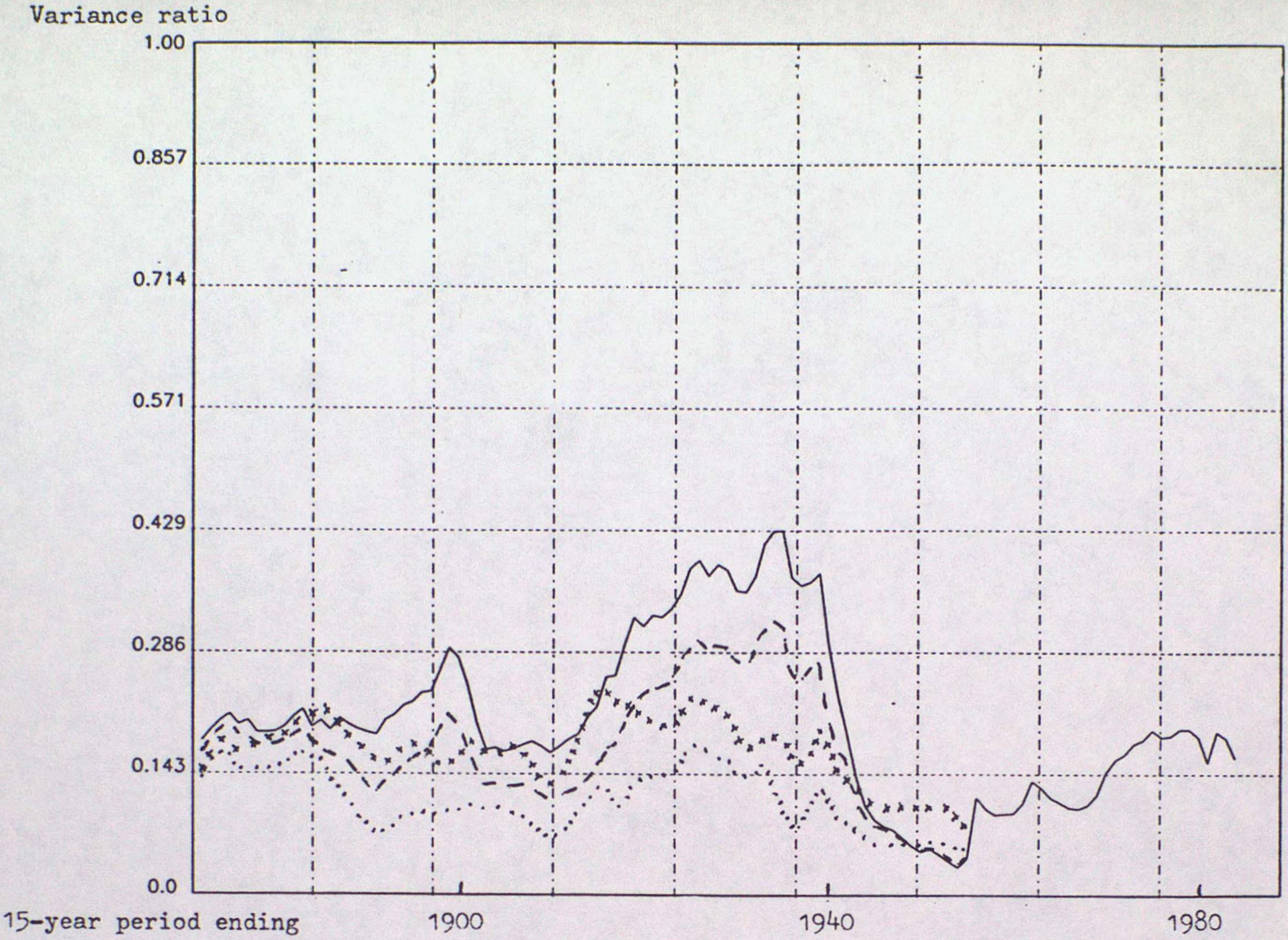

Figure 9.13A. 15-year running ratio of annual cycle variance to total variance of monthly SST anomalies (w.r.t. 1951-80 climatology) for the belt 30°N to 40°N.

KEY

———— Uncorrected

- - - - - Corrected up to 1941 assuming model D9 with 0.5 minutes' heat-transfer time.

.... Ditto but 1.5 minutes' heat-transfer time.

xxxxxxxxx Ditto but 3 minutes' heat-transfer time.

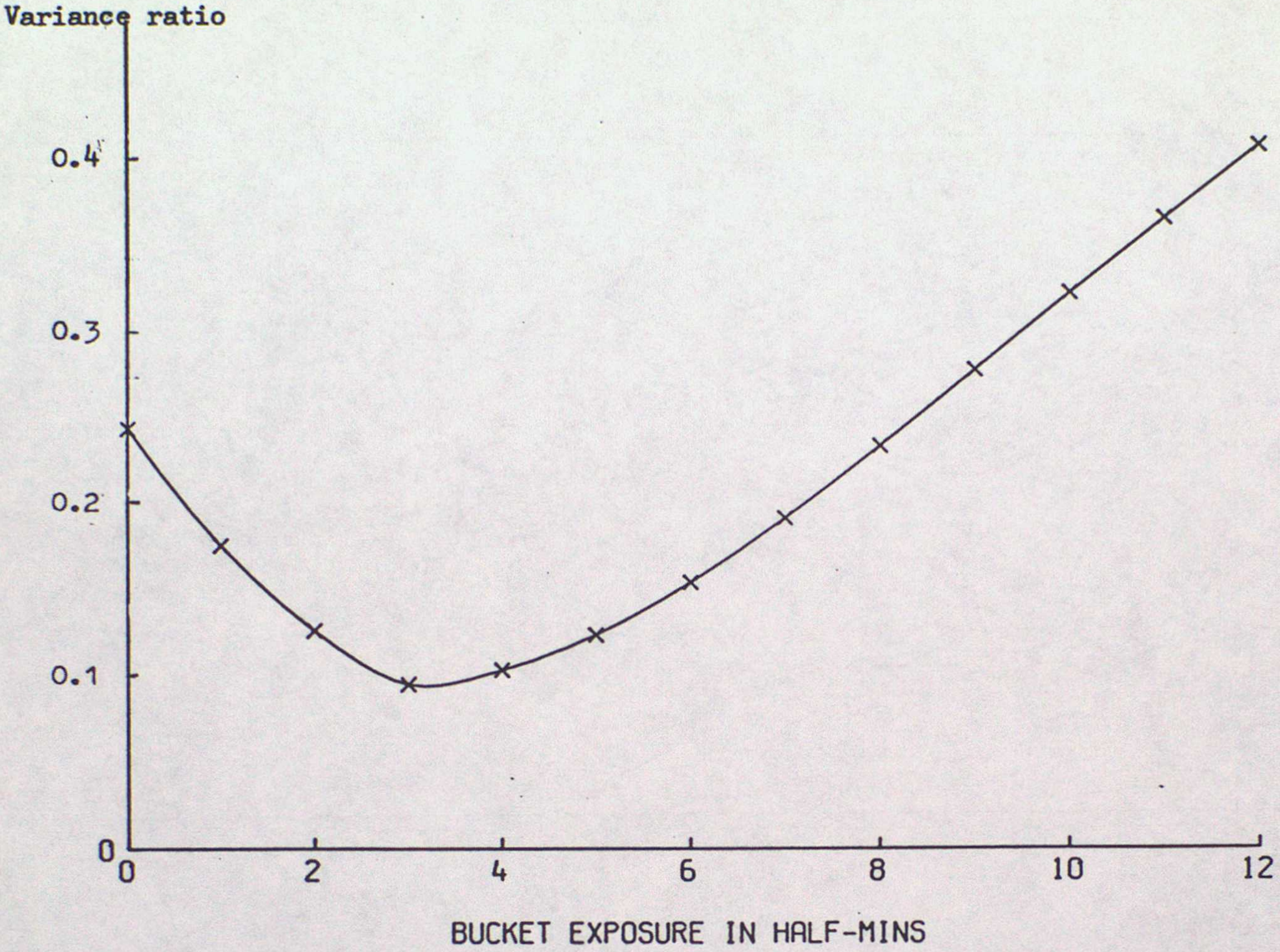

Figure 9.13B. Ratio of annual cycle variance to total variance of monthly SST anomalies (w.r.t. 1951-80 climatology) for 1881 to 1941 for the belt 30°N to 40°N, as a function of exposure time, assuming uninsulated bucket model D9 was used to compute the corrections.

(A) June

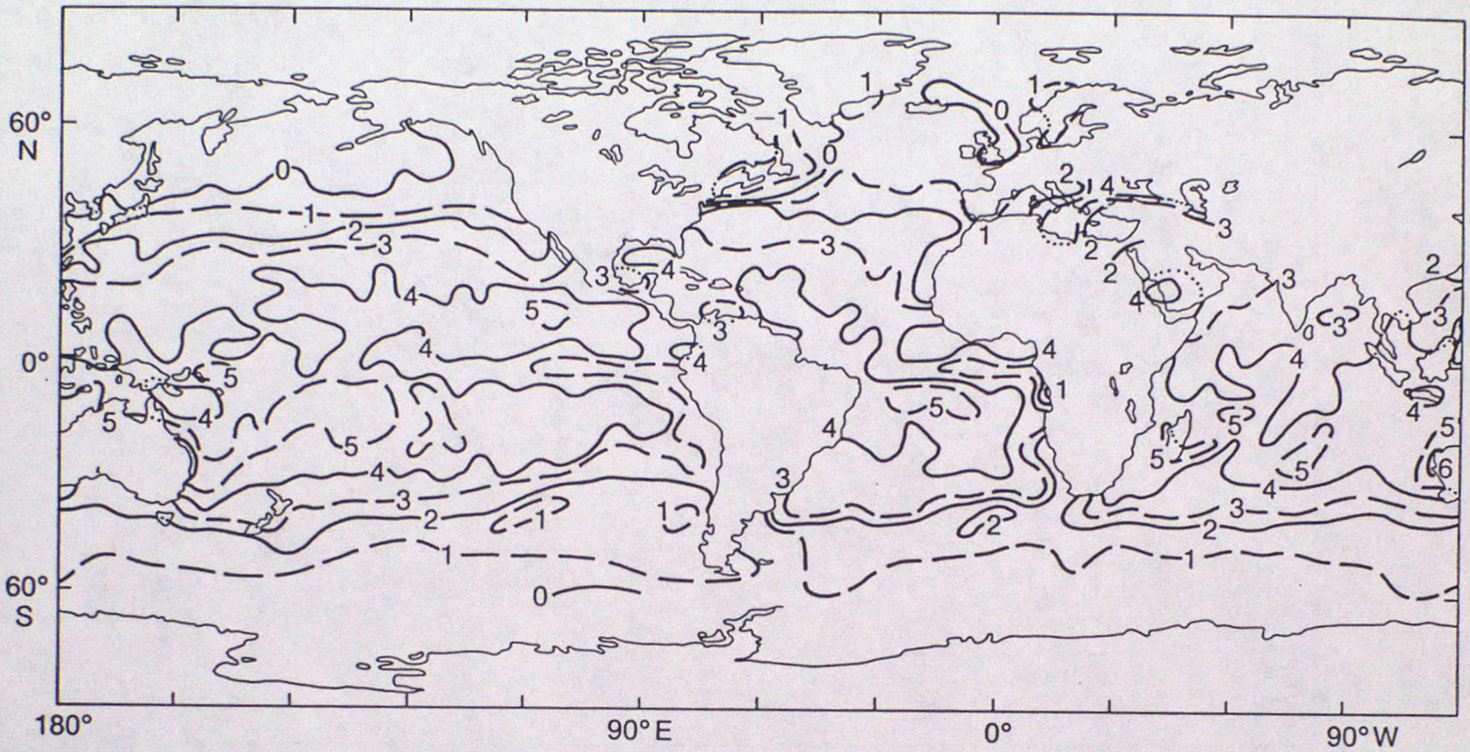
60° N
0°
60° S
180°
90° E
0°
90° W

(B) December

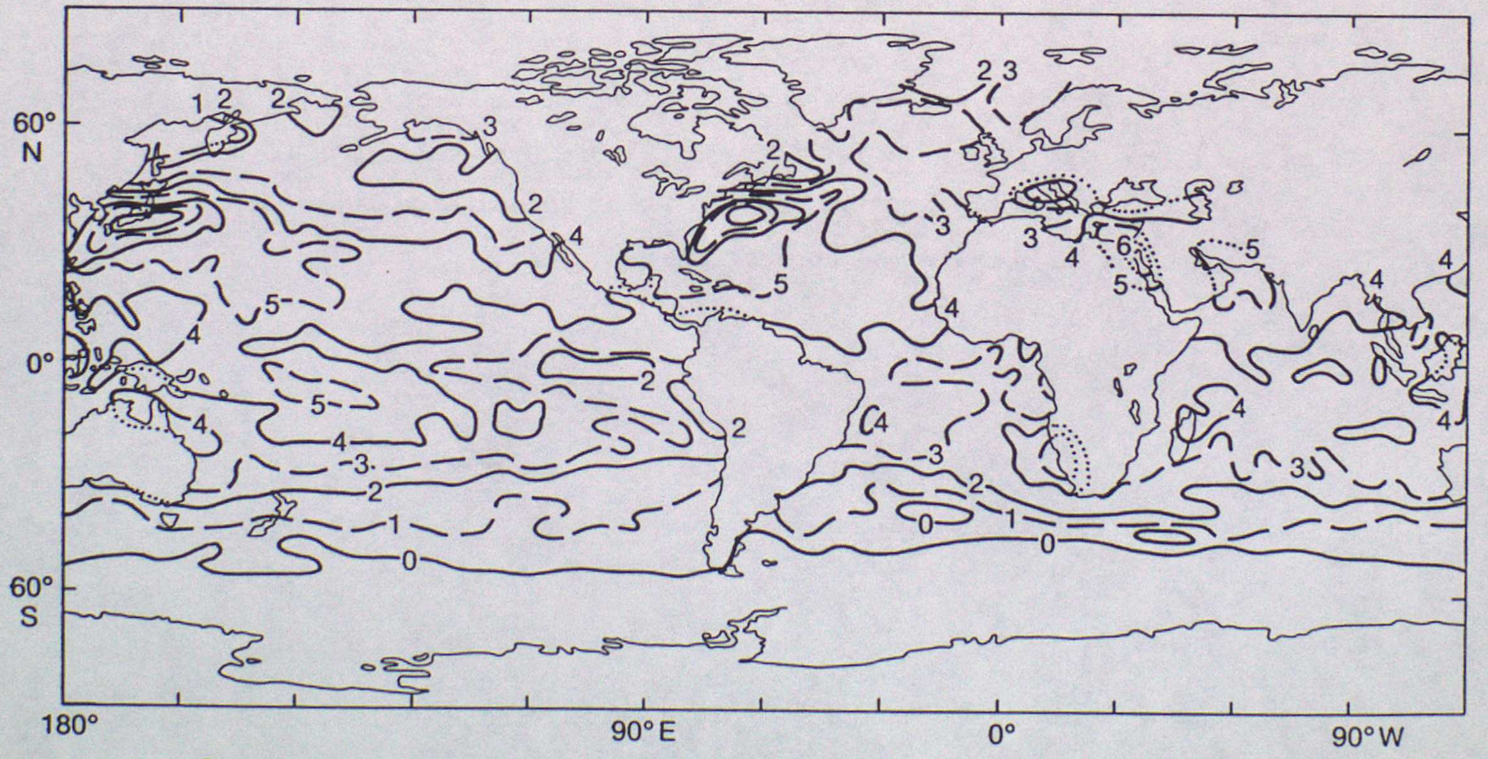
60° N
0°
60° S
180°
90° E
0°
90° W

Corrections to uninsulated bucket SST applied up to 1900 (tenths °C)

Figure 9.14. From Bottomley et al (1988).

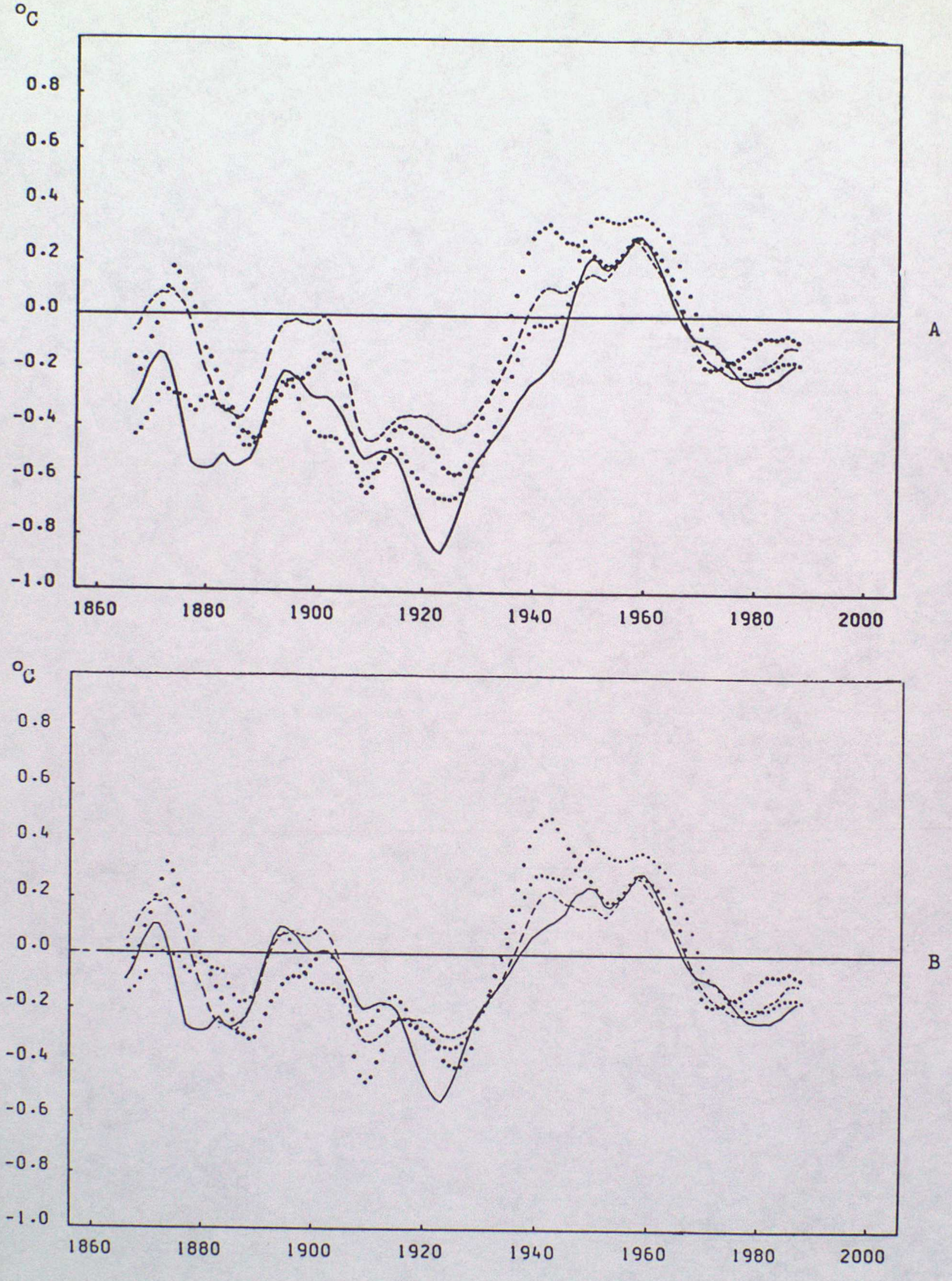

Figure 9.15. SST anomalies (w.r.t.1951-80) for 1856 to 1987 averaged over the Atlantic north of 35°N, plotted against the end-date of an 11-year triangular smoothing filter. Northern winter (JFM), spring (AMJ), summer (JAS), autumn (OND) are solid line, dashed line, round dots, square dots.

A. No instrumental corrections. B. Instrumental corrections as in Bottomley et al (1988).

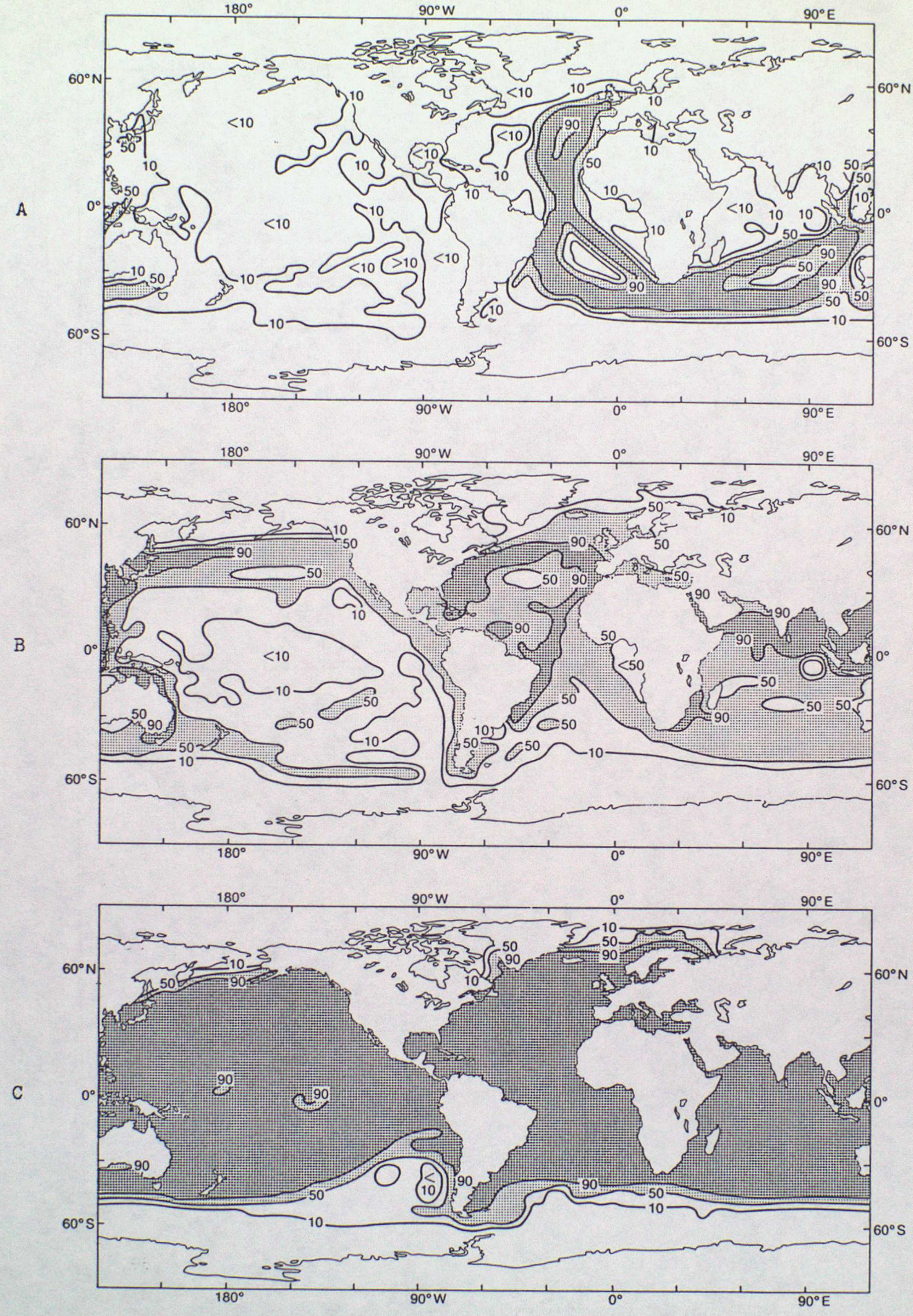
A
B
C
180°
90°W
0°
90°E
60°N
0°
60°S
<10
10
50
90
>10

Percentage of seasons with SST data (on a 5° × 5° space scale).
A) 1861–70; B) 1911–20; C) 1971–80.

▩ >90% ▨ 50–90%

Figure 9.16. From Bottomley et al (1988).

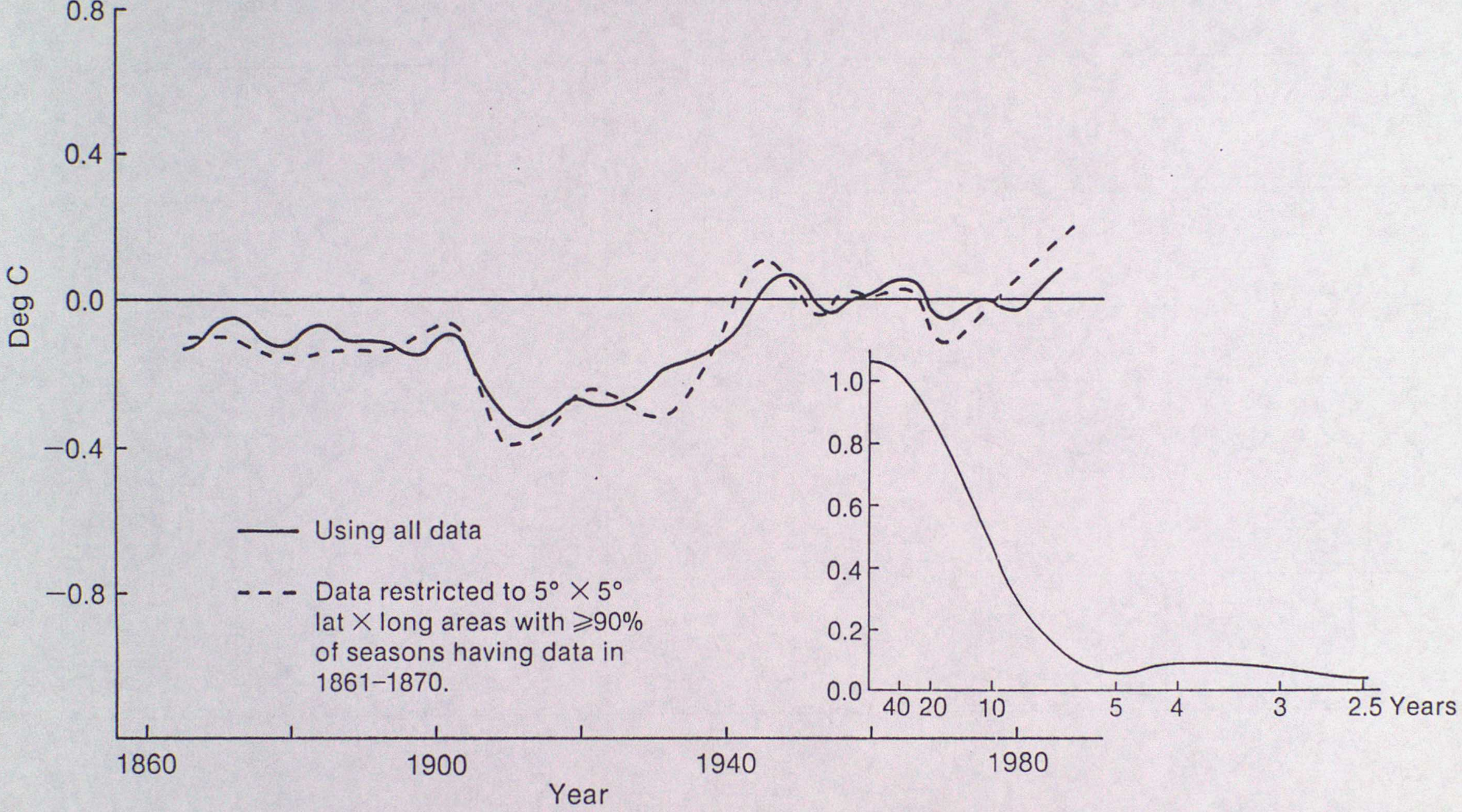

Global SST w.r.t. 1951–80. Values plotted at end date of 10.25 year triangular filter (magnification function given in inset). Bucket corrections applied to SST up to 1941.

Figure 9.17. From Bottomley et al (1988).

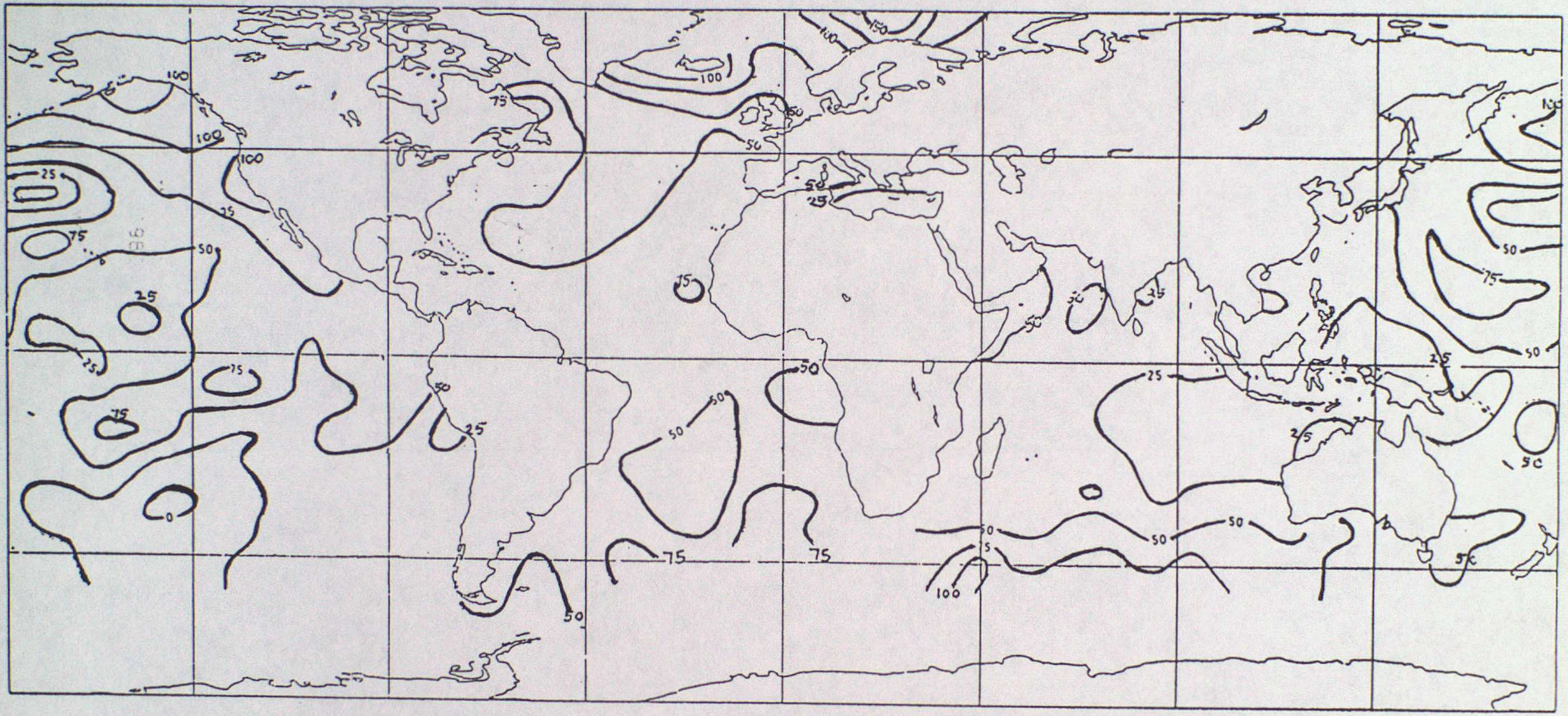

Figure 9.18A. The first all-seasons covariance eigenvector of global SSTA, 1901-80. The pattern is scaled so that the sum of squares of 10° latitude x longitude values equals 10^6. Instrumental corrections as in Bottomley et al (1988).

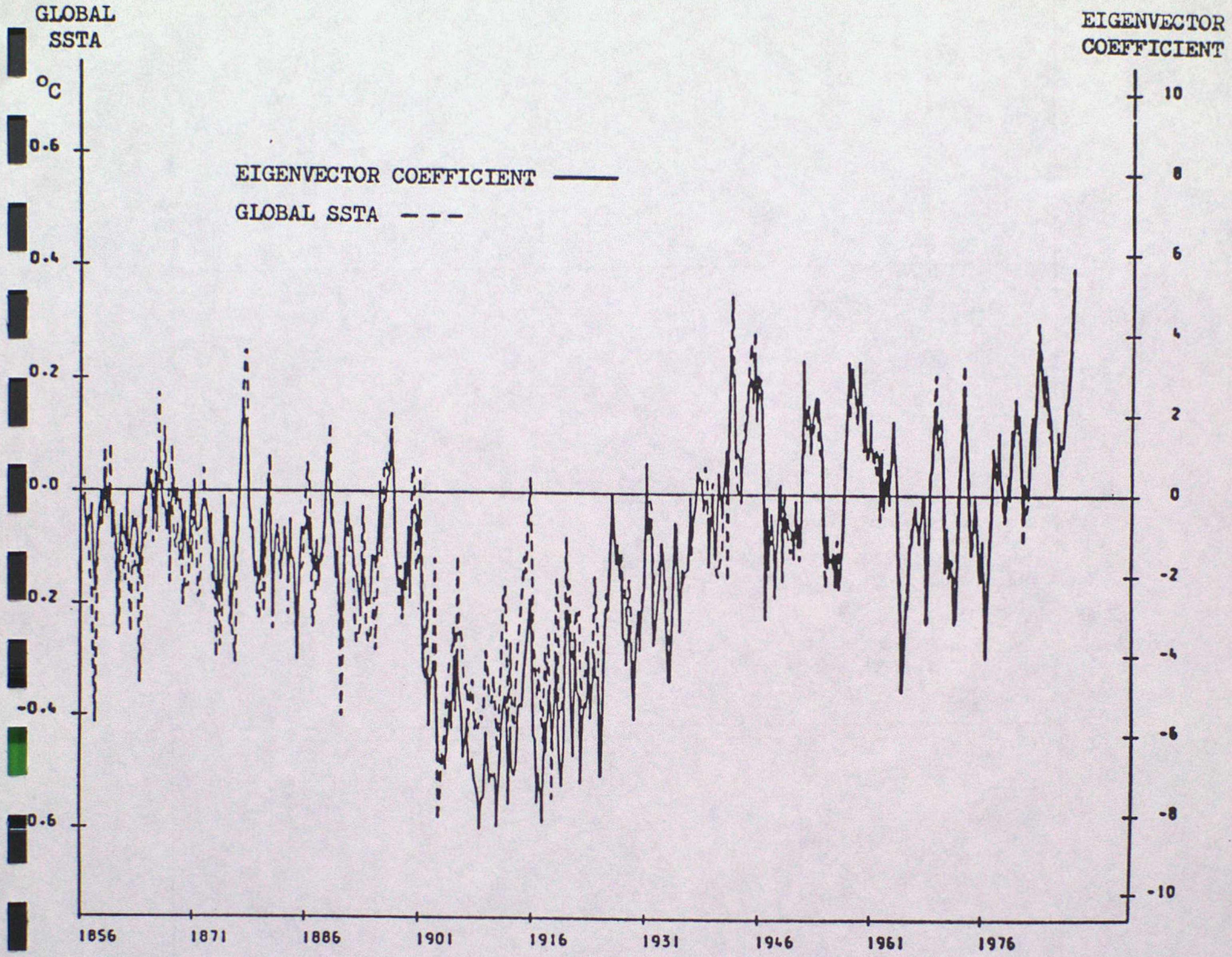

Figure 9.18B. Seasonal time series for 1856 to 1987 of the coefficient of the first all-seasons covariance eigenvector of global SSTA weighted according to the area of the appropriate 10° latitude x 10° longitude square, along with seasonal time series of global SSTA. Instrumental corrections as in Bottomley et al (1988).

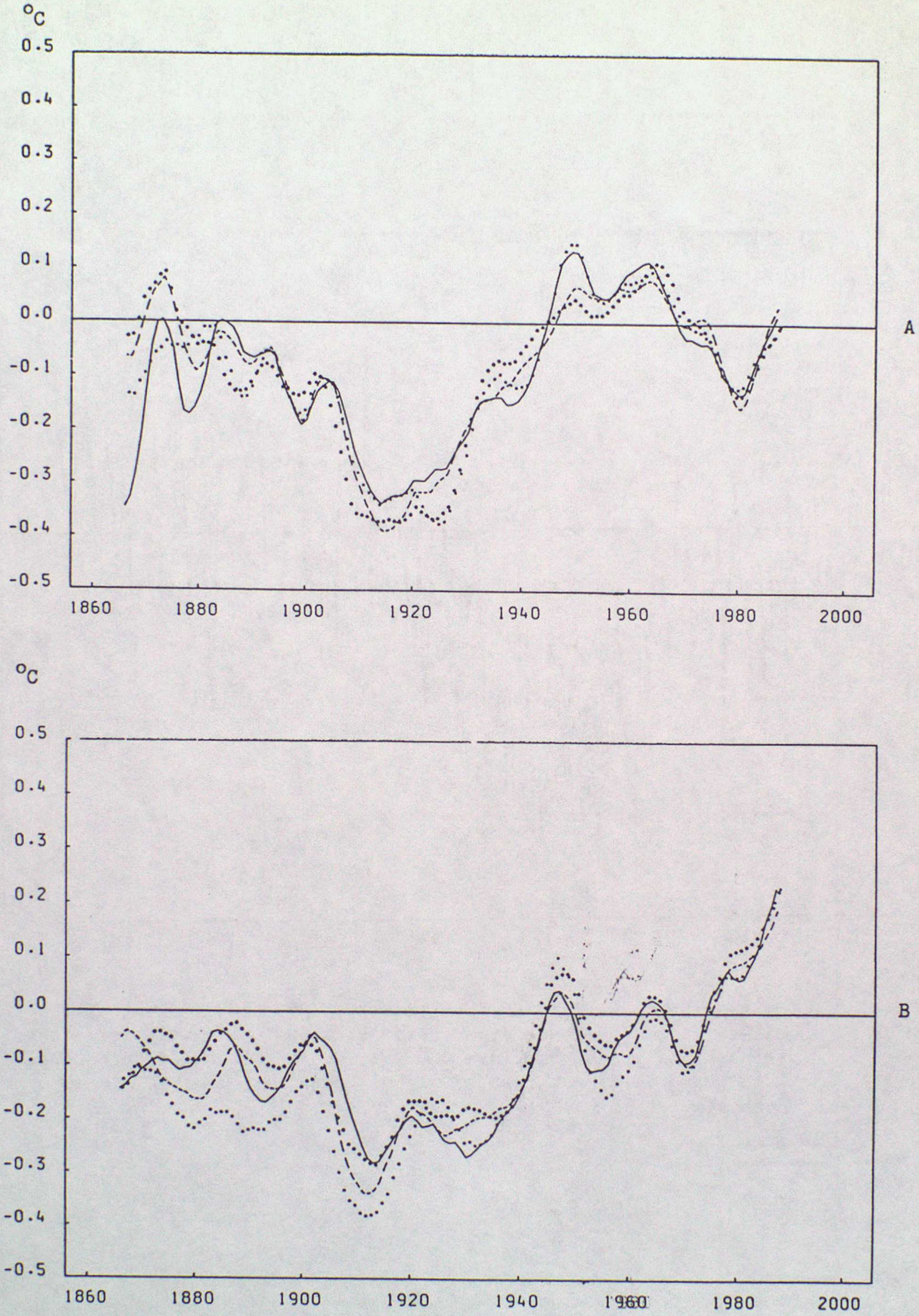

Figure 9.19. SST anomalies (w.r.t. 1951-80) for 1856 to 1987 averaged over the Northern Hemisphere (A) and the Southern Hemisphere (B), plotted against the end-date of an 11-year triangular smoothing filter. Jan-Mar, Apr-Jun, Jul-Sept, Oct-Dec are solid line, dashed line, round dots, square dots. Instrumental corrections as in Bottomley et al (1988).

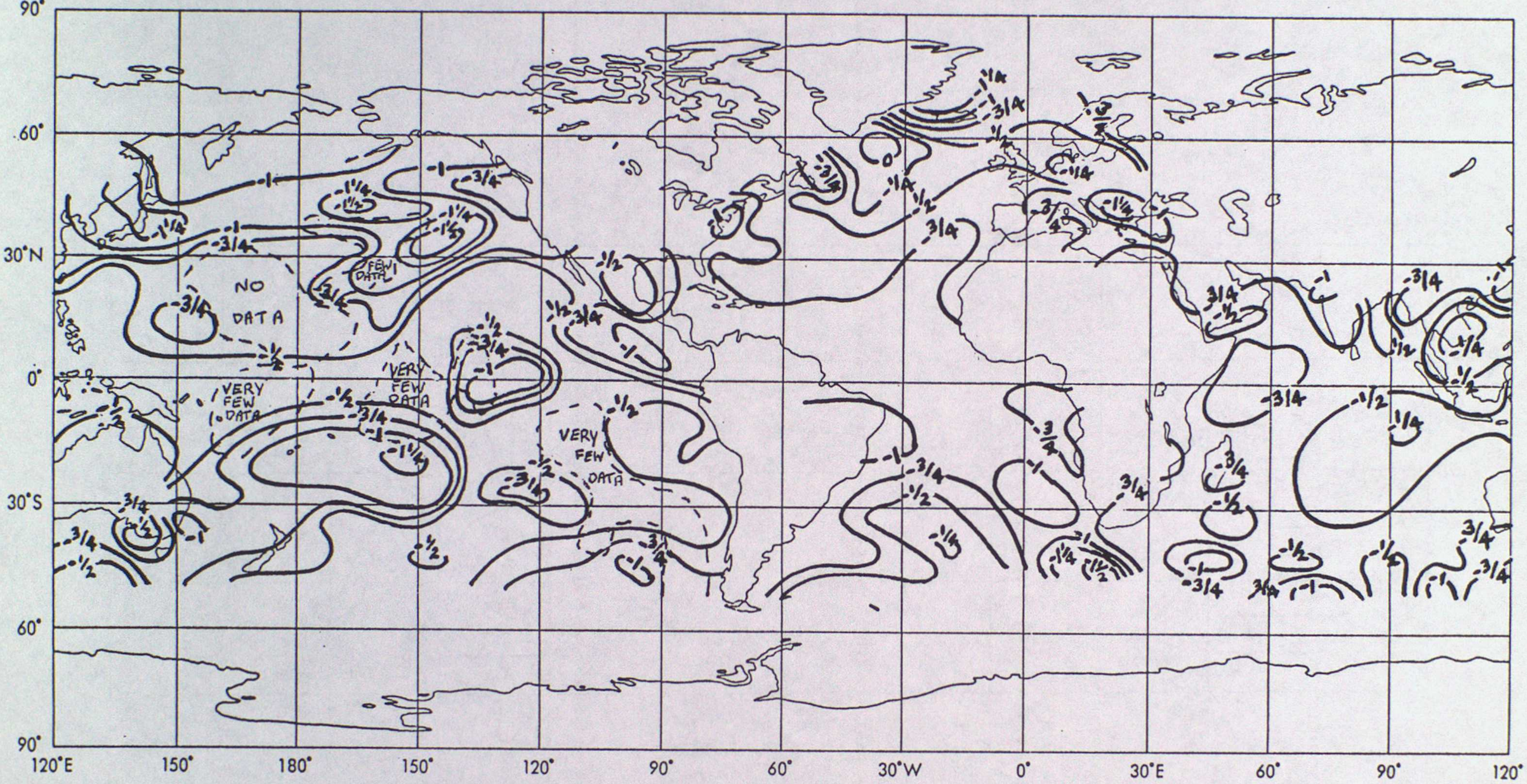

90°
60°
30°N
0°
30°S
60°
90°
120°E
150°
180°
150°
120°
90°
60°
30°W
0°
30°E
60°
90°
120°
NO DATA
VERY FEW DATA
FEW DATA
VERY FEW DATA
VERY FEW DATA
-1/4
-1/2
-3/4
-1
3/4
0

Figure 9.20A. Sea surface temperature, 1903-12, relative to 1951-80. Contours every $\frac{1}{4}^{\circ}$C. Instrumental corrections as in Bottomley et al (1988).

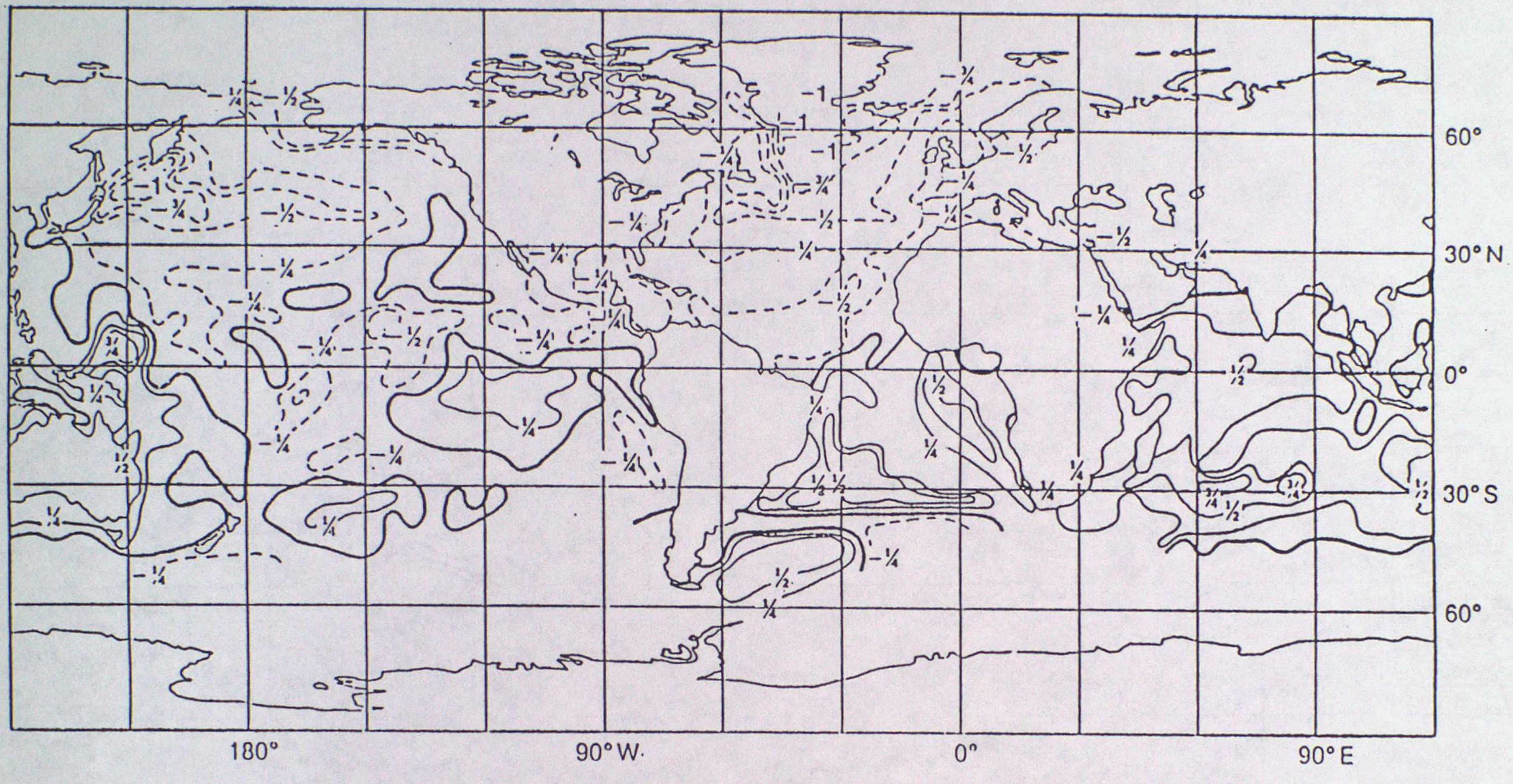
60°
30° N
0°
30° S
60°
180°
90° W
0°
90° E
-1
-3/4
-1/2
-1/4
1/4
1/2
3/4

Figure 9.20B. Sea surface temperature, 1971-87, relative to 1951-60. Contours every $\frac{1}{4}$°C. From Parker and Folland (1988).

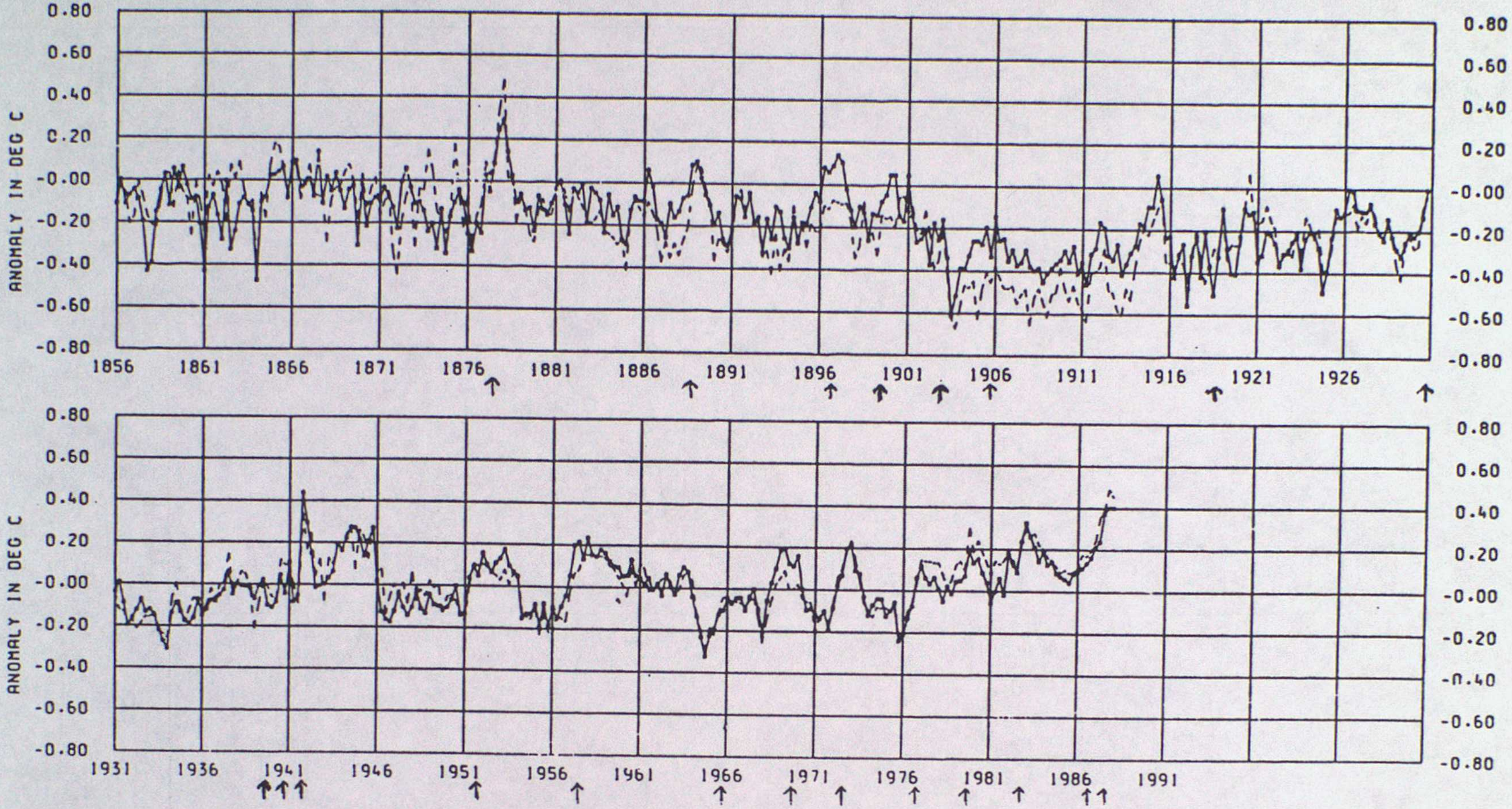

Figure 9.21. Seasonal sea surface temperature (solid) and night marine air temperature (dashed) anomalies (w.r.t. 1951-80) averaged over the globe , 1856 to 1987. Instrumental corrections as in Bottomley et al (1988). Arrows mark Oct to Dec of El Nino years.

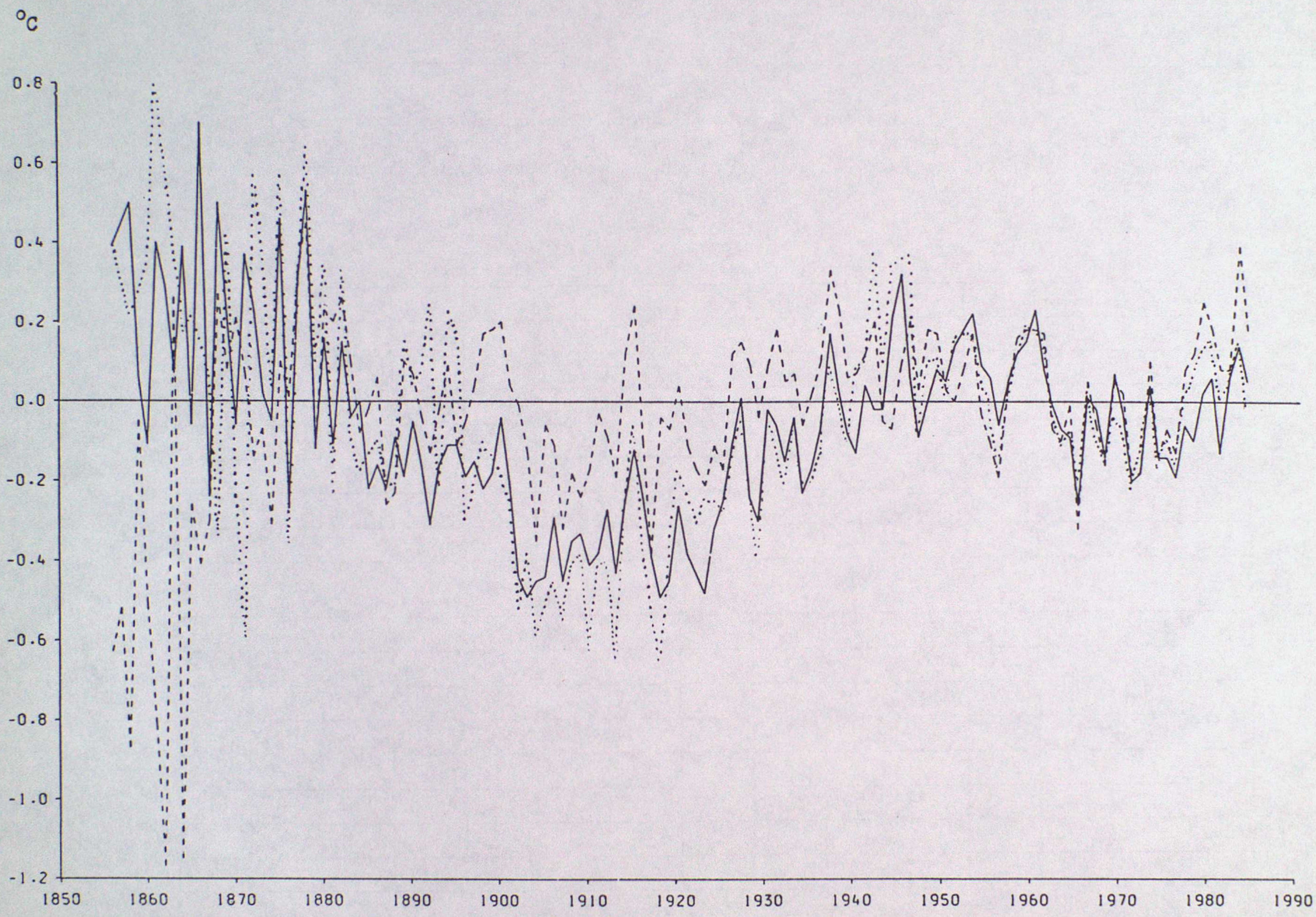

Figure 9.22. Annual land surface air temperature (----), ships' SST (——) and ships' night marine air temperature (....), w.r.t. 1951-80, averaged over selected islands in the Northern Hemisphere.

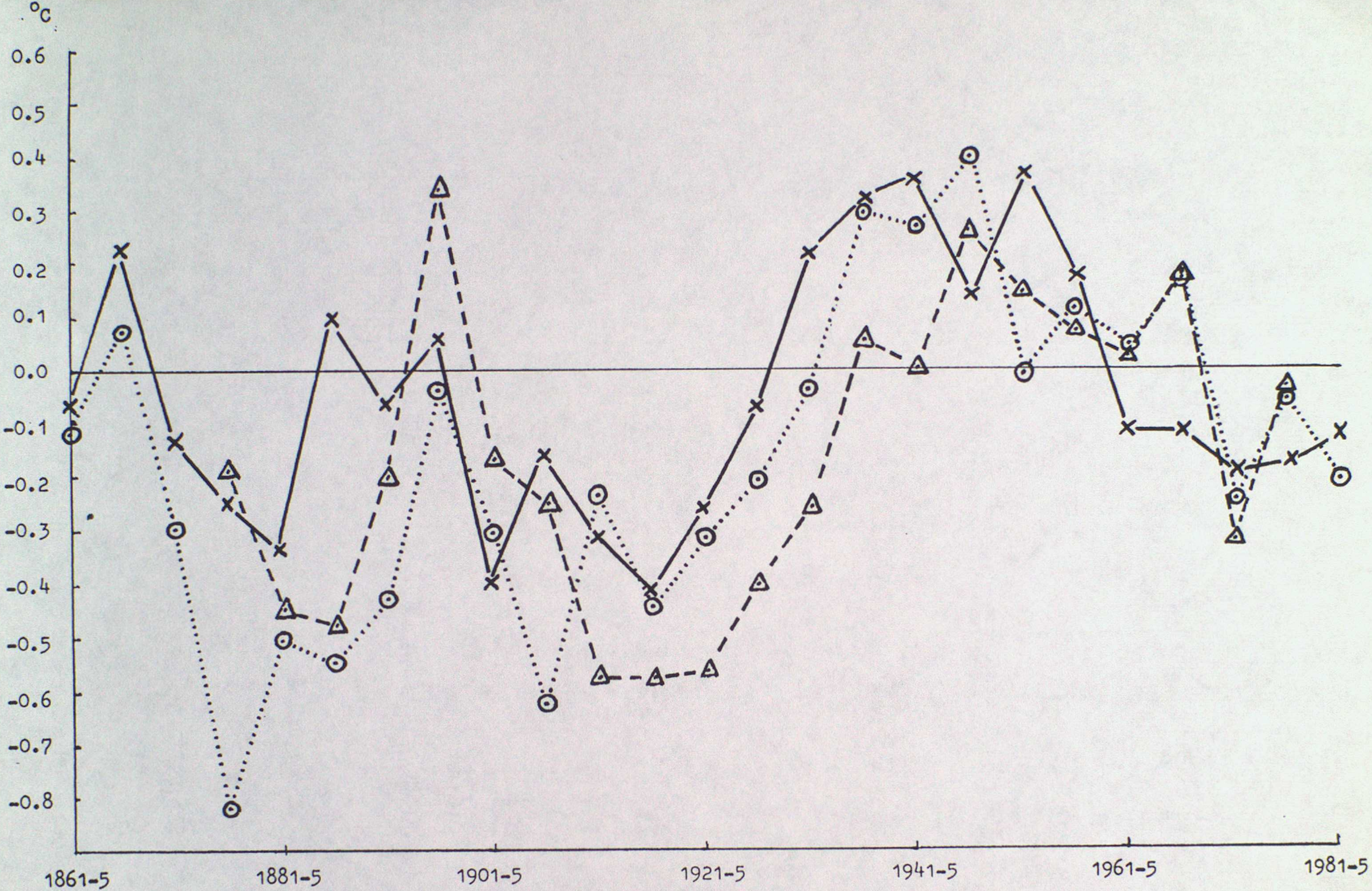

Figure 9.23. Solid line: Averages of seasonal SST anomalies w.r.t. 1951-80 for the Atlantic north of 35°N, weighted by the frequency of Lamb's circulation types NW,SW,CSW,W,CW (Lamb (1972b)), excluding isolated days and first days of spells.

Dashed line: Average temperature anomalies w.r.t. 1951-80 for the Scilly Is. on days with Lamb's circulation types NW,SW,CSW,W,CW, excluding isolated days and first days of spells.

Dotted line: Ditto but for Central England Temperature.

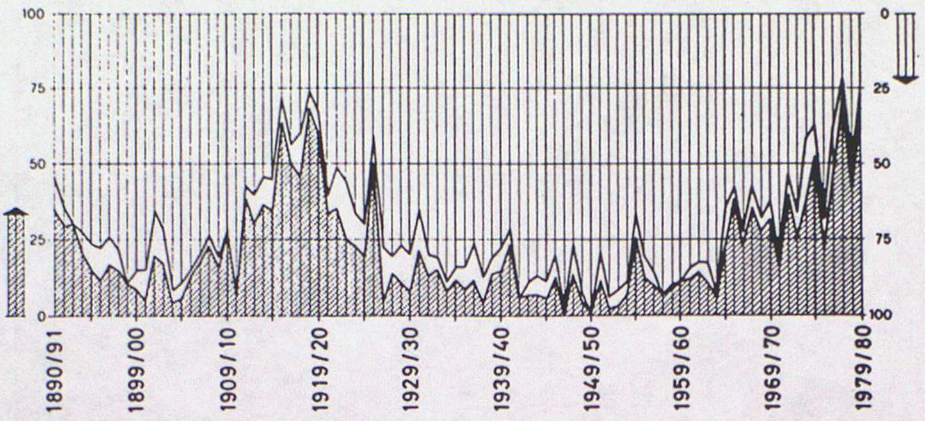

Percentage of advancing and retreating glaciers in Switzerland, 1891–1980, showing the increase of advancing glaciers since the mid-twentieth century. (From Kasser & Aellen, 1981.)

Figure 9.24. From Untersteiner (1984).

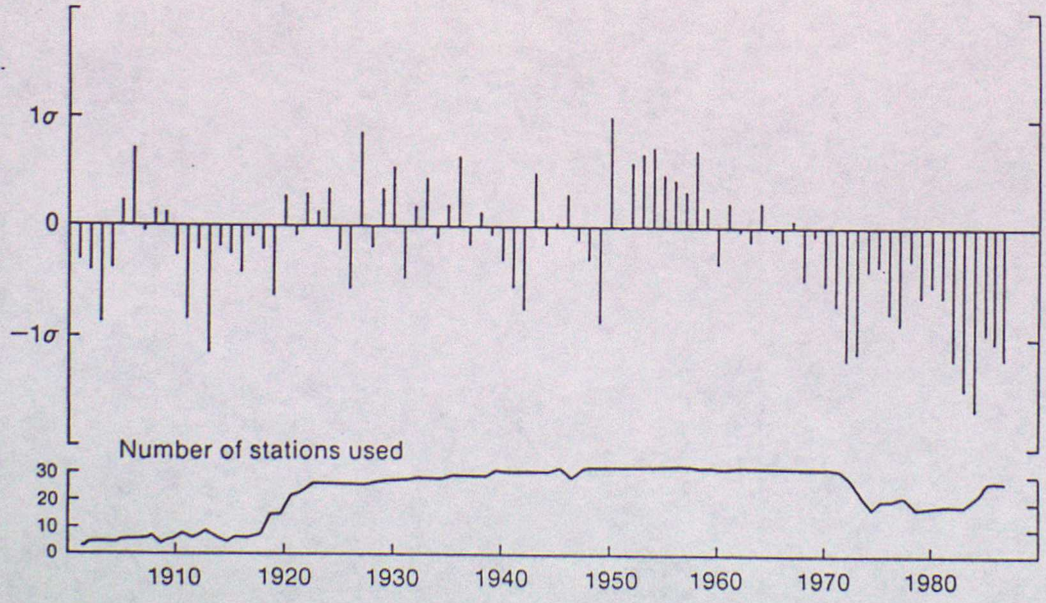

Figure 9.25. Standardised annual rainfall anomalies for the Sahel, 1901-87. Values to 1984 after Nicholson (1985): 1985-87 estimated from CLIMAT reports.

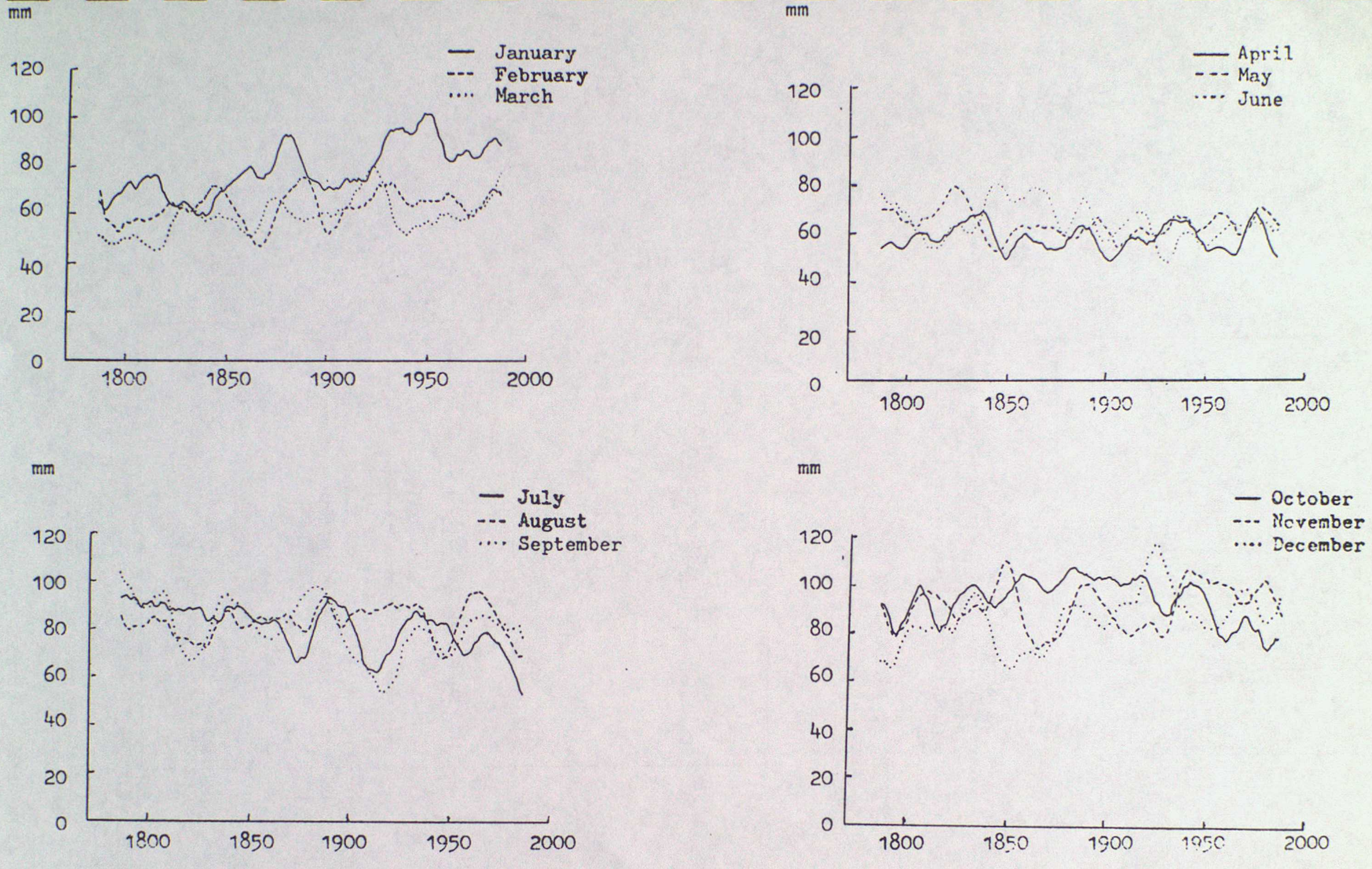

Figure 9.26. England and Wales rainfall, 1766 to 1987, plotted at the end date of a 20-year triangular smoothing filter. Data up to 1980 are from Wigley et al (1984).

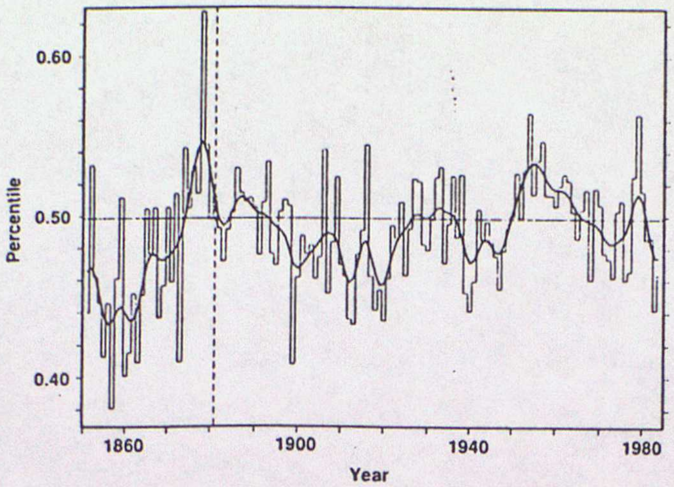

Annual precipitation index (mean of percentiles of the gamma probability distribution at all valid grid points) for Northern Hemisphere continental regions. Dashed line shows year in which 50% of grid points are available for analysis. Curved line shows the smooth trend line fitted through individual values.

Figure 9.27. From Bradley et al (1987).

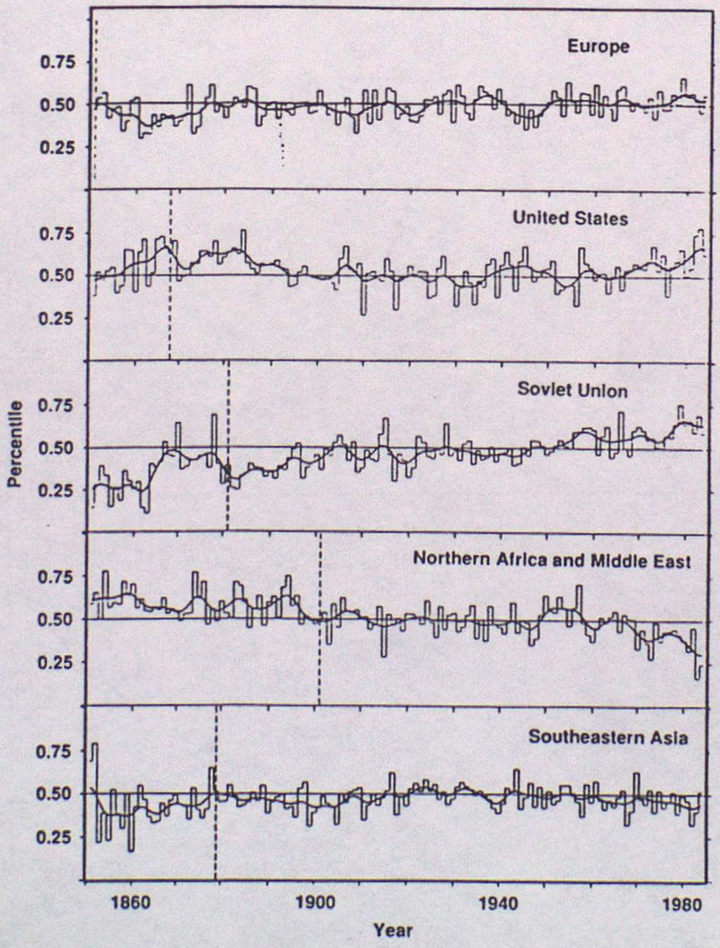

Precipitation indices for Europe, the United States, the Soviet Union, Northern Africa and the Middle East, and Southeastern Asia.

Figure 9.28. From Bradley et al (1987).

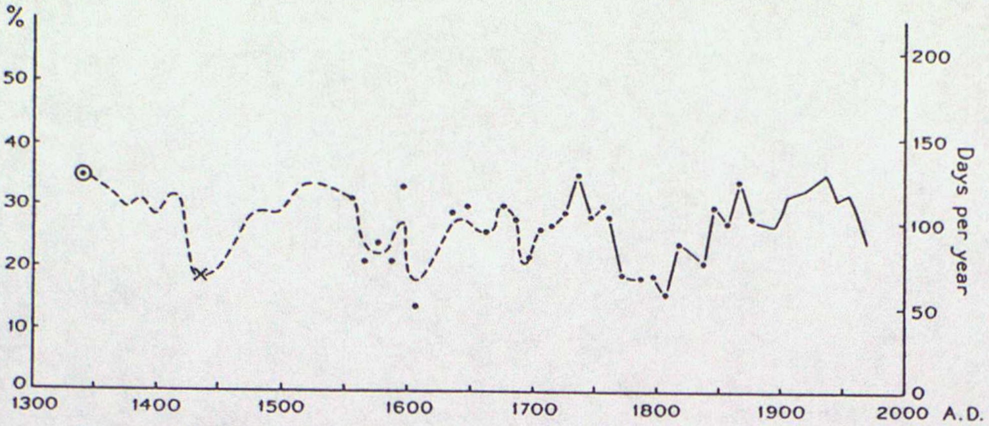

Frequency of SW'ly surface winds in southeastern England since A.D. 1340. Approximately 10-year average values and estimates.

Composite record derived directly from daily observations near London since 1670 (the earlier part worked up from manuscript sources by MANLEY, the later part since 1811 from observations in the archives of the Meteorological Office). Estimates for periods before 1670 provisionally derived from indirect evidence including weather diaries kept in various parts of England and neighbouring parts of Europe.

Figure 9.29. From Lamb (1972a).

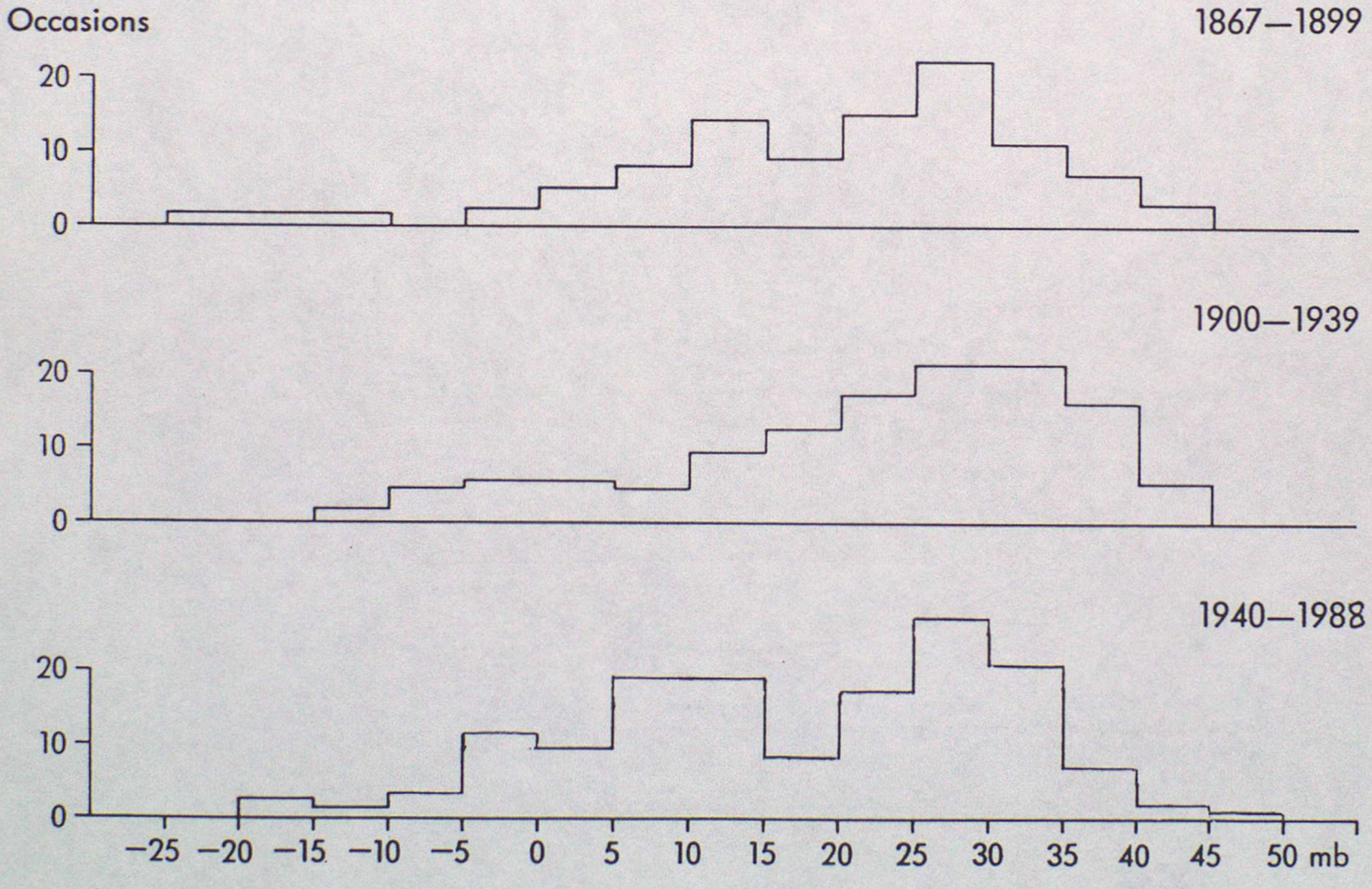

Ponta Delgada (Azores) minus Stykkisholmur (Iceland) mean sea level pressure, winter months (up to Feb. 1988).

Figure 9.30.

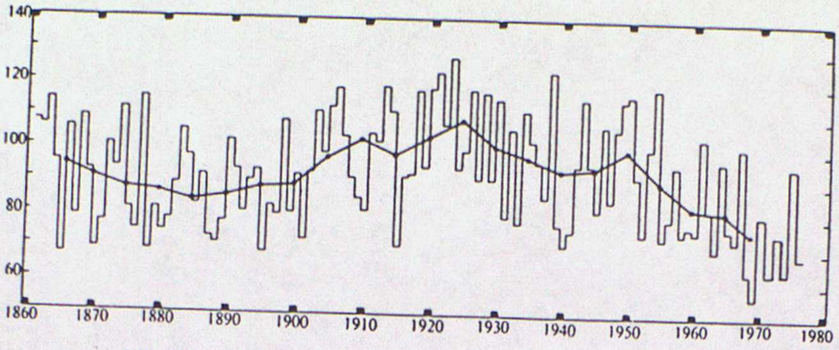

Number of days each year of general W'ly type over the British Isles: 1861 to 1975. (The number of W'ly type days in 1976 was 59.) Individual years and 10-year means at 5-year intervals.

Figure 9.31. From Lamb (1977).

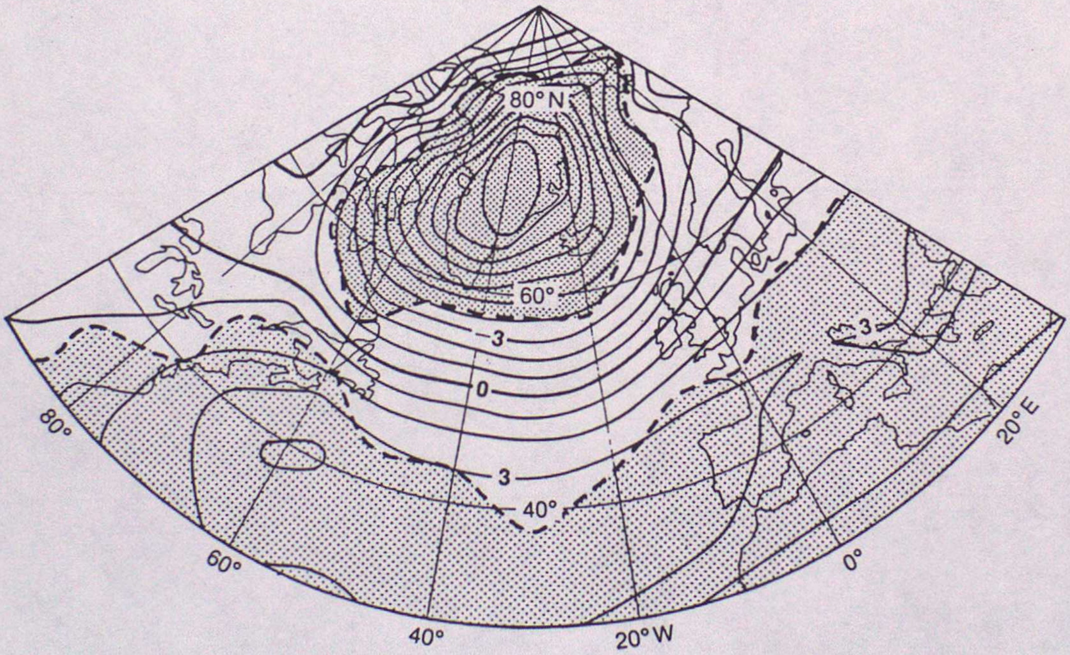

Mean-sea-level pressure difference (mb) for January 1901–30 relative to January 1951–70. Areas of 5% significant difference obtained using a Student's *t*-test (approximate assessment) are shaded: heavy shading, 1901–30 lower; light shading, 1901–30 higher.

Figure 9.32. From Parker and Folland (1988).

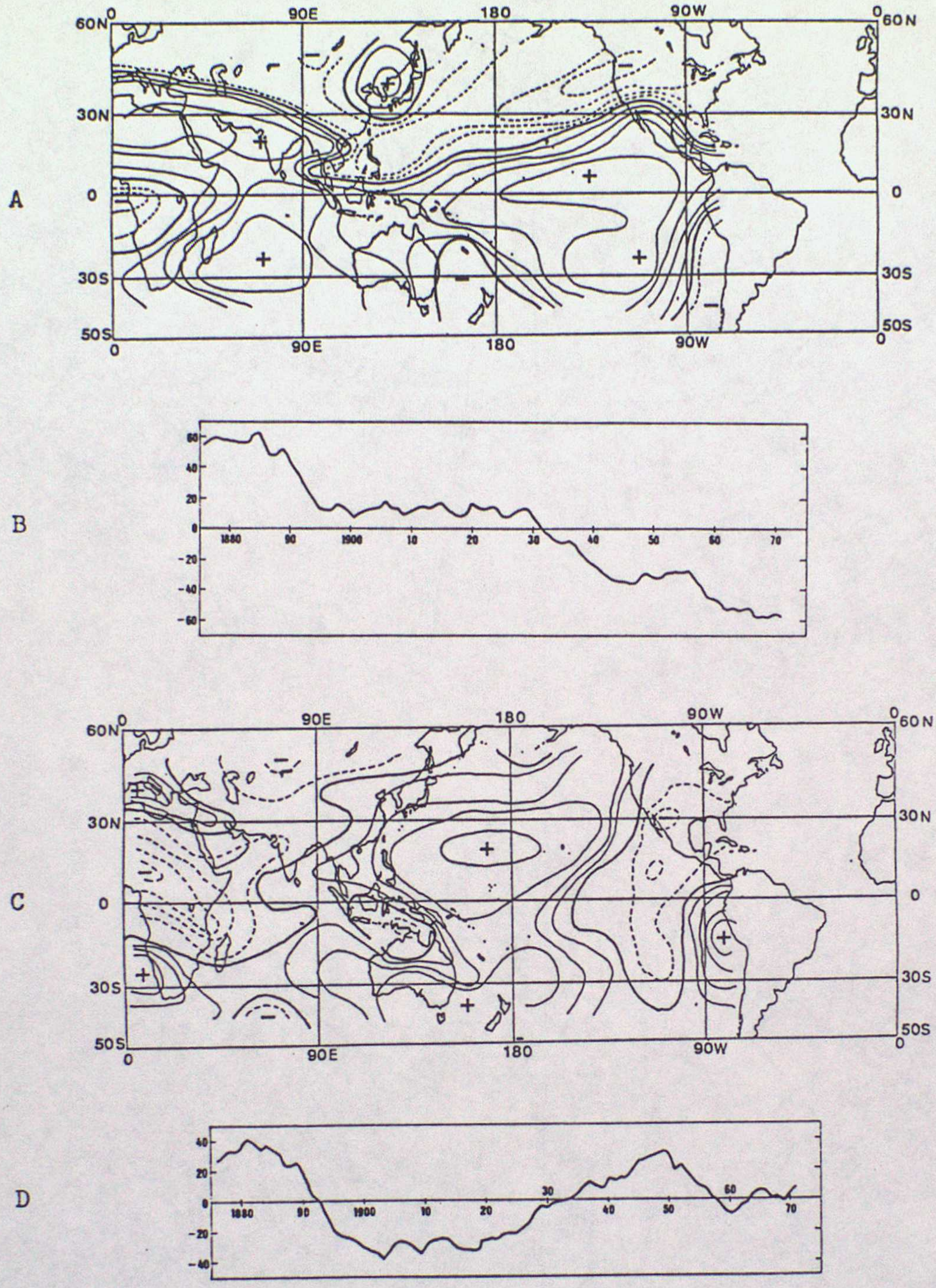

Figure 9.33. A. First eigenvector of the field of 11-year running mean MSL pressure. Dashed contours are negative values. Units are 0.2.

B. Time coefficients of the first eigenvector.

C. As A but for the second eigenvector.

D. As B but for the second eigenvector.

Data base : 1871 to 1976.

After Tan and Yasunari (1982).

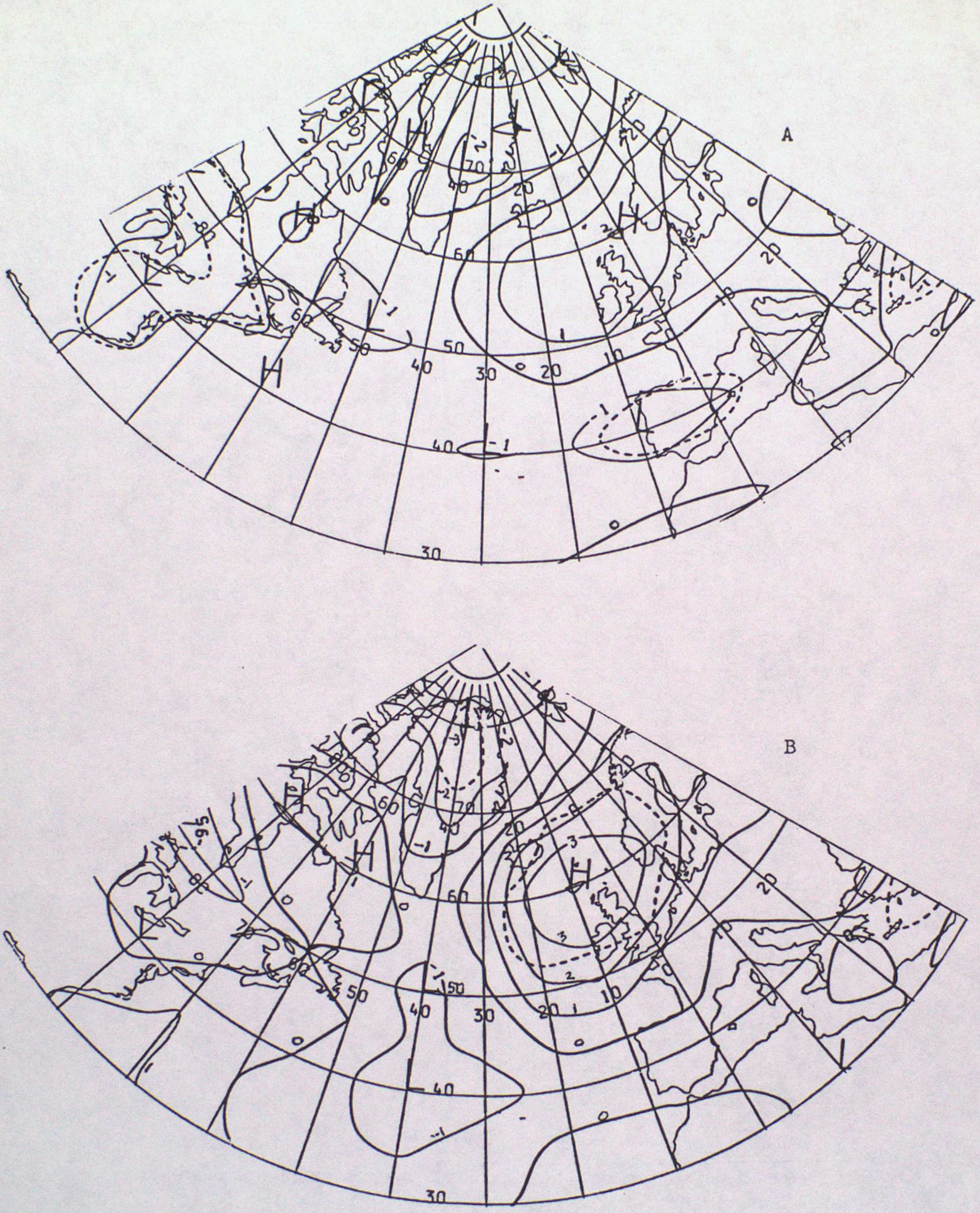
A
H
L
70
60
50
40
30
20
10
0
-1
-2
1
2
B
H
L
70
60
50
40
30
20
10
0
-1
-2
-3
1
2
3

Figure 9.34. MSL pressure (mb), 1968-87 relative to 1950-59.
A, July. B, August.

Areas of 5% significant difference obtained using a Student's t-test (approximate assessment) are enclosed by the dashed lines.

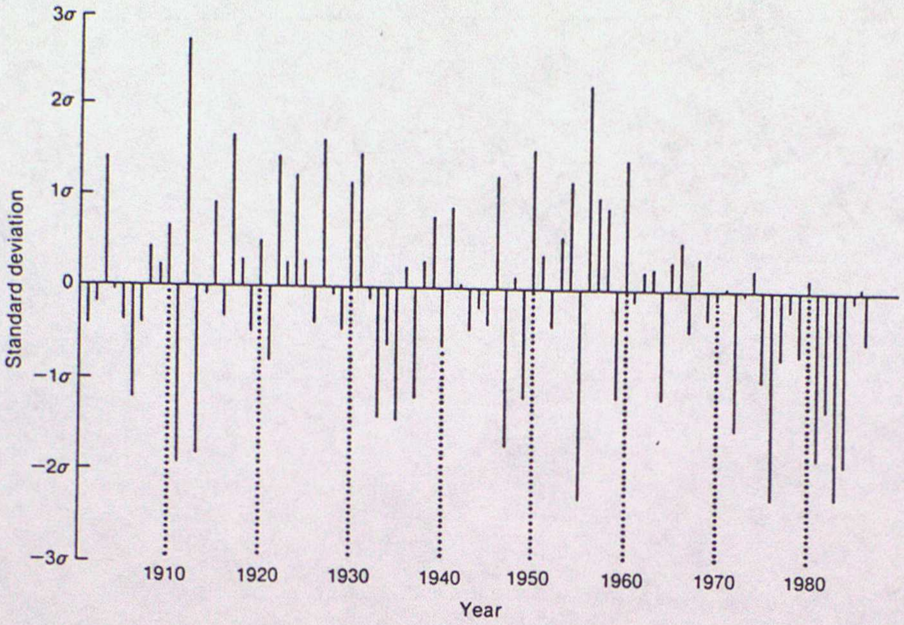

Standardized July and August total rainfall for England and Wales, 1901–87, based on the period 1901–80.

Figure 9.35. From Parker and Folland (1988). Data up to 1980 are from Wigley et al (1984)

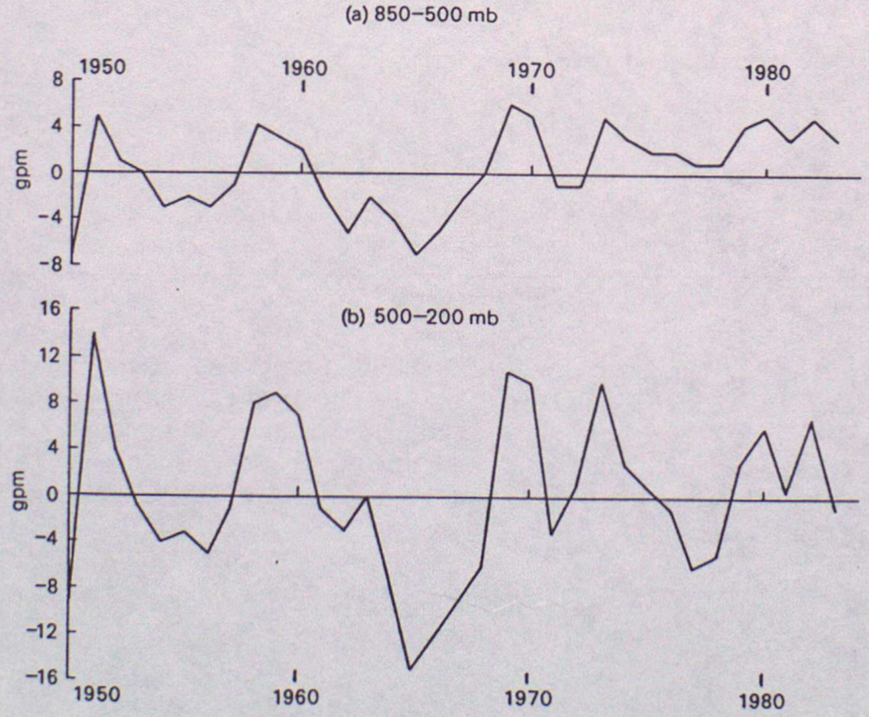

Note: The annual values are based on the seasonal residuals in Figure 5 and therefore refer to December (year minus one) to November (year)

Annual residuals of thickness for the zone 20°N to 20°S (gpm) after linear regression against optimally lagged Southern Oscillation index

Figure 9.36. From Parker (1985b).

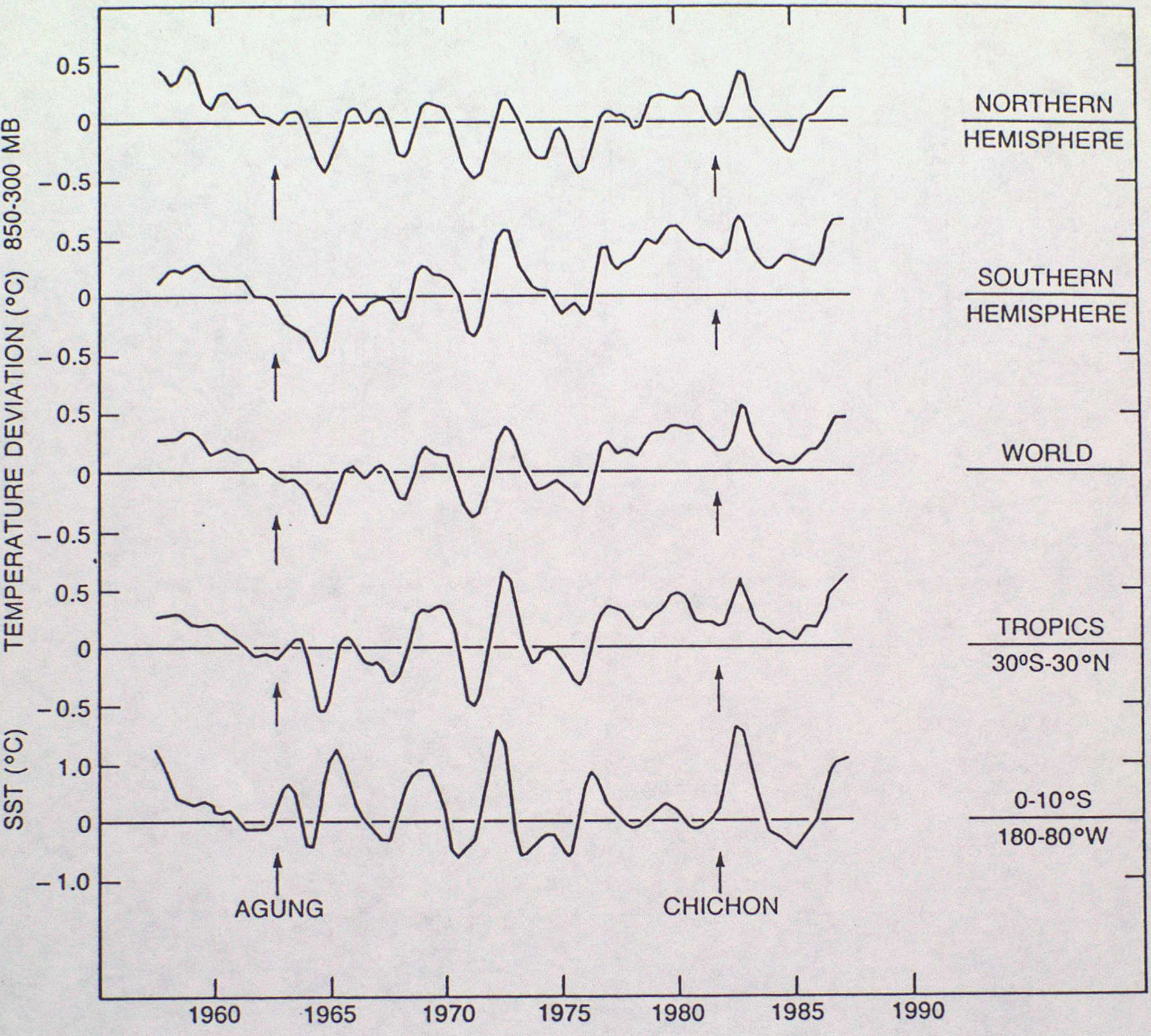

Figure 9.37. Variation in temperature in the 850-300mb layer and in part of the eastern equatorial Pacific. A 1-2-1 weighting has been applied twice to successive seasonal deviations from long-term seasonal means, with the first two and last two deviations twice averaged. Abscissa tick marks are in northern summer (June to August) of the indicated years.

After Angell (1988).

CARBON DIOXIDE AND OTHER GREENHOUSE GASES, AND CLIMATIC VARIATIONS

D E PARKER AND C K FOLLAND

MET O 13

SUMMARY

The observational and theoretical evidence is reviewed for the possible past and present impact of changing atmospheric carbon dioxide concentration on climate. The influence of other radiatively active gases is also considered, and mention is made of the "ozone hole". A strategy for detection of the impact of increasing concentration of atmospheric carbon dioxide and other greenhouse gases is presented, based on the 3-dimensional pattern ("fingerprint") of changes anticipated in the light of simulations with atmospheric general circulation models.

10.1 EVIDENCE FOR INCREASING ATMOSPHERIC CARBON DIOXIDE

Reliable direct measurements of the amount of CO_2 in the atmosphere are available only from 1958, and show (Figure 10.1) an increase from 315 parts per million (ppm) to about 350 ppm. Until the early 1980's it was generally thought, on the basis of earlier, less accurate measurements, that the pre-industrial concentration was about 290 ppm. However recent measurements of carbon-13 in tree-rings (Figure 10.2: Webster (1985) quoted in World Meteorological Organisation (1987))and of carbon dioxide concentration in air bubbles trapped in polar ice (Barnola et al (1983); Neftel et al (1985) (Figure 10.3)), yield estimates in the range 260 to 280 ppm. The basis of the carbon-13 method is that changes in the size of the biosphere, which are likely causes of past changes of atmospheric CO_2 concentration, introduce tiny changes in the atmospheric carbon-13/ carbon-12 ratio because organic materials are about 1.8% deficient in carbon-13 relative to the nominal concentration of carbon-13 in atmospheric carbon dioxide. Possible difficulties with these methods include contamination with present day air (which would cause estimates of past CO_2 concentration to be too high), and more diffusion than expected of carbon-13 in the tree rings or of carbon dioxide locked in polar ice layers.

Analysis of air bubbles in polar ice has been used to extend the record of atmospheric CO_2 concentration back for more than 100,000 years. (Barnola et al (1987)). Figures 7.20 (Lecture 7) and 8.10B (Lecture 8) show the results. Of particular note are the low concentration in both the final and the penultimate (> 140 k.y BP) glaciations; the rapid increase around the beginning of the Eemian interglacial (ca 140 k.y BP) and the decrease around 110 k.y BP, after the end of this interglacial; the rapid and possibly sudden increase around 14 k.y BP accompanying the Allerod warming; the temporary decrease accompanying the Younger Dryas readvance around 10-11 k.y BP; and the strong subsequent increase (see also Siegenthaler and Wenk (1984)). This increase is likely to have accelerated the global warming during the early Holocene (Sarmiento and Toggweiler (1984)). For further discussion of the rôle of carbon dioxide fluctuations in the climatic changes in the late Pleistocene see Section 7.5.3 (Lecture 7) and Section 8.4.1 (Lecture 8).

Estimates of CO_2 input to the atmosphere, as a result of man's activities, yield a rate of increase of atmospheric concentration around double that observed. The discrepancy can largely be accounted for by oceanic absorption processes (Broecker et al (1979)), though a small part of the difference may result from increased photosynthesis in the biosphere because of the increased atmospheric carbon dioxide concentration (Schiff (1981)). In their review of work on the uptake of carbon dioxide by the oceans, Baes et al (1985) find that most of the more detailed models of the ocean indicate that the oceans should have taken up between 30% and 40% of the excess fossil carbon released up to the present.

10.2 THE RADIATIVE EFFECTS OF INCREASING ATMOSPHERIC CARBON DIOXIDE

10.2.1 Direct Effects

In Lecture 3, a very simple explanation of the greenhouse effect was provided. Figure 10.4, along with Table 3.14 of Kondratyev (1969), illustrates the fact that CO_2 absorbs perhaps 2 to 3 times more outgoing long wave terrestrial radiation than radiation reaching the Earth from the sun: some absorption of the longer solar wavelengths occurs. There is not, at present, 100% absorption of long wave radiation in the wavelengths affected by CO_2 (Figure 10.5): therefore, as the concentration of CO_2 increases, the absorption of outgoing long-wave radiation will increase: absorption is given by

$$I_\lambda = I_{\lambda o} \exp \left(-\int_0^\infty k_\lambda \rho dz\right) \qquad (10.1)$$

at any given wavelength λ, where $I_{\lambda o}$, I_λ are the outgoing beam intensities at the surface ($z = 0$) and the top of the atmosphere ($z = \infty$) respectively; k is the absorption coefficient of the gas, ρ is its density, and integration is with respect to height z, from the surface to the top of the atmosphere. Because CO_2 is distributed throughout the depth of the atmosphere, and because there is a temperature lapse with height, the "effective" re-emission of terrestrial radiation to space will be at intensities corresponding to the temperature at the atmosphere's "centre of mass" of emission (roughly half-way up through the mass of the atmosphere) rather than at the higher intensities corresponding to the higher temperature of the surface. The level of effective re-emission will become higher as increasing CO_2 makes the atmosphere more opaque to long wave terrestrial radiation. (Figure 10.6). Lecture 3 shows that if α, the albedo of the earth-atmosphere system remains unchanged, the outgoing radiation to space from the earth-atmosphere system remains unchanged. Thus for $e = 1$ (perfectly absorbing "glass"), the outgoing radiation B is still equal to the ingoing solar radiation I. However the fluxes within the earth-atmosphere system change, giving a changed vertical temperature profile within the atmosphere (with the aid of convective and dynamical processes) and a net increase in incident radiation at the surface of the earth, because the troposphere needs to be warmer if the same outgoing radiation B is to be effectively re-emitted from a higher level (Figure 10.6).

10.2.2 Indirect Effects

Lack of radiative equilibrium at the earth's surface caused by increasing atmospheric CO_2 will cause the ocean surface, as well as the land surface, to warm. As a result, the mixing ratio of atmospheric water vapour will, on a global average, increase. This increase will enhance surface warming because of the increased absorption and downward re-emission of long-wave radiation by the extra water vapour in the troposphere (Figures 10.4 and 10.5) ie the 'glass' will become more opaque so its emissivity will increase. Radiative-convective models indicate that the effect of the additional water vapour on the long-wave flux is markedly greater than the direct effect of the additional CO_2 on the long-wave flux (see Figure 10.4 and Lal and Ramanathan (1984)).

An increase of global surface temperature might be expected to result in a decrease in the area covered by snow and ice. Since both snow and ice have a larger albedo than water or land, the amount of solar radiation reflected back into space will decrease, further enhancing the global surface warming. The temperature rises are also likely to affect atmospheric circulation and, therefore, cloud, providing further potential influences on the earth's radiation budget. Clouds both reflect insolation (encouraging cooling) and absorb terrestrial radiation (encouraging warming) and in a given situation the balance between these two depends intricately on cloud level, cloud thickness and water content, though low clouds tend to cause surface cooling and cirrus clouds surface warming. Because of the complex factors involved, and the rudimentary treatment of clouds in atmospheric general circulation models, varying results have been obtained by different modellers who have attempted to simulate the effects of changes in cloud amount when atmospheric CO_2 concentration is increased.

Not all the indirect effects of increased CO_2 need enhance surface warming. For example, Choudhury and Kukla (1979) suggest that increased atmospheric absorption of solar radiation resulting from an increase in atmospheric CO_2 concentration will hinder the melting of snow, given that the surface air temperature is low enough: snow slowly melts in bright sunshine even when air temperature is below 0°C. Also the warming of water surfaces, eg the ocean, by direct solar heating may also slightly decrease. These effects would tend to offset, to a small extent, the surface warming that would result from an increased flux of long-wave radiation.

Hansen et al (1984) used a radiative-convective model (RCM) to determine the indirect effects on global mean surface air temperature of changes of water vapour amount and profile, lapse rate, surface albedo, and cloud height and cover in a Goddard Institute for Space Studies (GISS) general circulation model (GCM) run to equilibrium with doubled atmospheric carbon dioxide. The control run of the GCM with present-day carbon dioxide was used to provide globally-averaged parameters for the control run of the RCM. The RCM was then run, without feedbacks, with doubled carbon dioxide but with all other parameters as in its control run: the change in its surface air temperature was taken to represent the direct effect of the extra carbon dioxide. Next the RCM was run with the water vapour amount at each level increased by 33%, to correspond to the increase in total water vapour in the doubled carbon dioxide run of the GCM, but with all other parameters as in its control run including present-day carbon dioxide: again there were no feedbacks, and the change in its surface air temperature from the control was taken to represent the effect of the change of water vapour amount. The difference between the surface air temperature in this run of the RCM, and a subsequent run identical except that the water vapour amount at each level was equal to the global average at that level in the doubled carbon dioxide run of the GCM, was taken to represent the effect of the change of water vapour profile. An analogous pair of RCM runs was used to differentiate the effects of changes of cloud height and cloud cover, and two single runs provided estimates of the effects of changes of lapse rate and surface albedo. The results, collated by Schlesinger and Mitchell (1987) are as follows:

Mechanism	Effect on surface air temperature (°C)
Extra carbon dioxide alone	1.20
Change of water vapour amount	1.85
Change of water vapour profile	0.90
Change of lapse rate	-1.10
Change of surface albedo	0.38
Change of cloud height	0.51
Change of cloud cover	0.42
Total	4.16

The total agrees with the GCM-simulated value. The negative feedback resulting from change of lapse rate arises because the upper troposphere in the GCM warms much more than the surface throughout the tropics, subtropics and lower midlatitudes (Section 10.5 below), so that there is greatly increased emission of radiation to space from the modelled upper troposphere.

10.2.3 A Cautionary Tale

By considering the energy balance at the surface a few authors (eg Newell and Dopplick (1979) (ND), Idso (1982)) have deduced that a doubling of atmospheric CO_2 concentration would result in a global surface warming of $^1/_4$°C or less, in conflict with the consensus range of 1.5°C to 4.5°C obtained by general circulation models and vertical profile (radiative-convective) models. Cess and Potter (1984) have demonstrated that, despite the considerable uncertainties that remain with AGCM results, the results of ND and of Idso can unfortunately be shown to be based on violations of the first law of thermodynamics. ND did not take into account the response of the depth of the atmosphere (they considered the surface in isolation), while Idso implicitly regarded the atmospheric feedbacks as part of the initial forcing.

The global annual average surface energy balance may be expressed as:-

$$F + LH + SH = Q \qquad (10.2)$$

F and Q denote the net upward terrestrial and net downward solar radiation fluxes at the surface, while LH and SH are the net upward latent and sensible heat fluxes from the surface. Let the global surface energy balance be initially perturbed by an amount ΔG resulting from a change in the radiation fluxes F and Q caused by a change in CO_2 concentration (Figure 10.4), all other terms being kept fixed and no feedbacks due to changes in cloudiness etc being initially considered. When equilibrium is later reached, the total change in the surface energy balance, allowing for the operation of feedbacks etc is:-

$$\Delta F_D + \Delta F_I + \Delta LH + \Delta SH = \Delta Q_D + \Delta Q_I \qquad (10.3)$$

where subscript D denotes direct effects in the fluxes F and Q, and I the indirect effects that result from feedback processes. ΔQ_I, for example, might result from changes in cloudiness or changes in ice cover. Now by definition $\Delta G \equiv \Delta Q_D - \Delta F_D$, the direct change in net radiation, and ΔLH and ΔSH are by definition special cases of indirect effects of the changes in net radiation. Substituting $\Delta G = \Delta Q_D - \Delta F_D$ yields:-

$$\Delta G = \Delta F_I + \Delta LH + \Delta SH - \Delta Q_I \qquad (10.4)$$

ie the indirect changes in energy flux at the surface are balanced by the direct change in net radiation at the surface when equilibrium is attained. So ΔG is a measure of either change.

Let $\lambda(T_s)$ be a surface temperature function defined by

$$\frac{dT_s}{dG} = \lambda(T_s)$$

So $\lambda(T_s)$ is the sensitivity of surface temperature either (a) to the directly imposed change of radiation flux or (b) to the total of the changes in indirect radiative and surface energy fluxes.

From (10.4):-

$$\frac{1}{\lambda(T_s)} = \frac{dF_I}{dT_s} + \frac{d(LH)}{dT_s} + \frac{d(SH)}{dT_s} - \frac{dQ_I}{dT_s} \qquad (10.5)$$

T_s is surface temperature, not air temperature. Equation (10.5) describes the sensitivity of T_s to the terms of the surface energy balance. These terms are forced to change by ΔF_I, ΔLH, ΔSH and $-\Delta Q_I$ respectively when CO_2 increases. If a surface temperature change ΔT_s occurs then from (10.4)

$$\frac{1}{\lambda(T_s)} = \frac{\Delta F_I}{\Delta T_s} + \frac{\Delta LH}{\Delta T_s} + \frac{\Delta SH}{\Delta T_s} - \frac{\Delta Q_I}{\Delta T_s}$$

or $$\Delta T_s = \lambda(T_s) \times \Delta G \qquad (10.6)$$

Equations (10.4), (10.5) and (10.6) are statements of the first law of thermodynamics: total change in surface heating = total change in internal energy of the surface layer + total of work done by the surface. Note that the definition of λ refers to the equilibrium response of each part of the climate system including all feedbacks and so is a sum of total derivatives of the fluxes.

Now ND ignored indirect changes in Q, (ΔQ_I) and also assumed a constant atmospheric temperature-height and water vapour content-height profile during the response of the climate system. This latter assumption corresponds to replacing the total derivatives of LH and SH within equation

(10.5) by their partial derivatives. They also, for the same reason, effectively used the direct effect F_D in their balance equation. Thus ND's surface temperature response function, (λ_{ND}), is given by

$$\frac{1}{\lambda_{ND}(T_s)} = \frac{dF_D}{dT_s} + \frac{\delta(LH)}{\delta T_s} + \frac{\delta(SH)}{\delta T_s} \qquad (10.7)$$

Since the total derivatives $d(LH)/dT_s$ and $d(SH)/dT_s$ include the inhibiting effects on the upward surface energy flux of the moistening and warming of the overlying atmosphere (Figure 10.6) whereas $\delta(LH)/\delta T_s$ and $\delta(SH)/\delta T_s$ do not, the total derivatives of LH and SH imply reduced rates of change of the upward fluxes, compared with the partial derivatives, ie

$$\frac{d(LH)}{dT_s} < \frac{\delta(LH)}{\delta T_s} \qquad (10.8a)$$

and

$$\frac{d(SH)}{dT_s} < \frac{\delta(SH)}{\delta T_s} \qquad (10.8b)$$

In fact many models give $d(SH)/dT_s < 0$ whereas the partial derivative is strongly positive. In addition,

$$\frac{dF_I}{dT_S} < \frac{dF_D}{dT_s}$$

because the former includes increased back-radiation from increased atmospheric water-vapour: remember F is positive upwards. Thus equation (10.7) tends to give a value of λ smaller than does the thermodynamically-consistent equation (10.5), and ND's calculated surface temperature response is expected to be too small. Of course if ΔQ_I were sufficiently negative, eg due to increased cloudiness reducing the solar radiation input to the ground by a substantial amount, and ΔF_I were larger (more positive) than expected, then small values of λ would be possible -but not for the reasons implied by ND. The essential point is that one cannot consider the surface in isolation: the whole troposphere - surface system must be taken into account. In summary, the troposphere will tend to warm and moisten, and equilibrium will be maintained by reduced convection of heat and reduced net radiation from the surface. These reductions will tend to increase surface temperature. The changes in moist convection are also likely to affect surface relative humidity, air-sea temperature difference, surface wind speed etc. Table 10.1 summarises Cess and Potter's analysis of ND's results.

The absorption by H_2O already in the atmosphere of longwave radiation in the absorption lines and bands of CO_2 has sometimes been cited in support of argurments that the "greenhouse" effect caused by increasing CO_2 will be very weak. This "overlap" effect is potentially important in the 12-18 µm region of the spectrum. However, Kiehl and Ramanathan (1982) used a 1-dimensional radiative model to show that the mitigating effect of the overlap on the direct CO_2 - induced change of radiation balance for the surface-troposphere as a whole is much smaller than its mitigating effect on the corresponding change of radiation balance at the surface alone. The enhancement of downward longwave radiation at the surface when CO_2 was doubled in their model was reduced from 3.65 to 0.55 Wm^{-2} by the overlap, but that at the tropopause was only reduced from 4.69 to 3.99 Wm^{-2}. The reduction in the CO_2 -induced surface heating was mostly compensated by a simultaneous increase in lower tropospheric heating, ie, enhanced H_2O absorption of the increased CO_2 emission. The overall result was that the vertical distribution of radiative heating was significantly affected, but the total heating of the surface-tropopause system was not. In the real atmosphere such a change in heat balance would again be compensated by reduced convection of heat from the surface, and this reduction would again play an important rôle in increasing surface temperature.

Idso (1982) carried out a very simple calculation: proceeding from one assumed equilibrium state (a 254.4K earth surface with no atmosphere) to a second equilibrium state (the present earth-atmosphere system), he calculated a change of downward infrared surface flux from an initial value of zero to 348 Wm^{-2} for a 33.6°C surface temperature increase. He equated the 348 Wm^{-2} to the forcing ΔG, ie the DIRECT change in net radiation, whereas the downwards flux at the surface of 348 Wm^{-2} in fact includes the net effect of both forcing and response (feedback), ie the sum of the direct and indirect changes. Thus Idso's λ, (about 0.1), calculated using equation (10.6) with ΔT_s = 33.6°C, was much too small.

10.3 EFFECTS OF OTHER RADIATIVELY ACTIVE GASES ON ATMOSPHERIC TEMPERATURE

The trace gases of interest include nitrous oxide (N_2O), methane (CH_4), chlorofluorocarbons ($CFCl_3$ and CF_2Cl_2), sulphur dioxide (SO_2), tropospheric ozone (O_3), and stratospheric water vapour from aircraft. The probable effects on surface temperature of changes in the concentrations of these gases are summarised by Mitchell (1984) and discussed in detail by Ramanathan et al (1987): for recently observed and likely future changes, the total effect of these gases on surface air temperature is likely to be comparable to that resulting from increasing carbon dioxide. Lacis et al (1981) find that, between 1970-1980, the combined equilibrium warming for the measured increments of CH_4, chlorofluorocarbons and N_2O was probably between 50% and 100% of that for carbon dioxide for the same period. Volz and Kley (1988) find that tropospheric ozone over Europe may have doubled since the late 19th Centruy. According to the compilation of WMO (1982) (Table 10.2), a doubling of tropospheric ozone for the globe would result in equilibrium globally-averaged surface warming of 0.9°C. Note that Table 10.2, which includes a wide range of trace gases, suggests that uncertainties in the values quoted for the effects of individual trace gases are analogous to the uncertainties for carbon dioxide. Table 10.2 quotes an equilibrium globally-averaged surface warming of 2.0°C for a doubling of atmospheric carbon dioxide: this is towards the lower end of the range (1.5°C to 4.5°C) now suggested by the results of numerical model experiments (Section 10.5 below).

10.4 THE "OZONE HOLE"

Observations from satellites and surface-based stations have revealed a marked diminution of stratospheric ozone over Antarctica in the southern spring since the late 1970's. A major cause of this ozone depletion appears to be the increased concentrations of chlorine compounds in the stratosphere, largely as a result of anthropogenic releases of chlorofluorocarbons but possibly also partly as a consequence of the injection of chlorine into the stratosphere by the eruption of El Chichon in 1982. The phenomenon is complicated further by dynamical processes, by changes in solar emission in the ultraviolet through the sunspot cycle, and possibly by variations in stratospheric water vapour. The dynamics of the Antarctic stratosphere include interactions with the troposphere, which itself interacts with the ocean in a manner influenced, inter alia, by the El Nino-Southern Oscillation. Variations in horizontal and vertical motion can result in regional changes in ozone concentration. In addition, deceased (increased) concentration of ozone results in decreased (increased) absorption of solar radiation in the stratosphere, and the resulting cooling (warming) affects the stratospheric circulation (Kiehl et al (1988)).

Heath (1988) has shown that stratospheric ozone depletion has in fact affected most of the globe during the 1980s, though to a much lesser extent than Antarctica. The degree of depletion has been debated by Rodgers (1988) on the grounds of instrumental drifts, but Rodgers still finds a global decrease of over $2^1/_2$% since 1978. The depletion has been accompanied by an almost worldwide lower stratospheric cooling, which was most intense in the south polar zone in the southern spring, the season affected by the ozone hole (Angell (1988)). The expected effects of increasing atmospheric concentrations of carbon dioxide include stratospheric cooling (Section 10.5 below), so it is necessary to take the ozone depletion into account when assessing the impact which increasing concentrations of carbon dioxide may have had on stratospheric temperatures.

10.5 GCM INDICATIONS OF THE EFFECTS OF INCREASING ATMOSPHERIC CARBON DIOXIDE

Schlesinger and Mitchell (1987) have reviewed climate model simulations of the equilibrium climatic response to increased atmospheric carbon dioxide. Their collation of a wide range of earlier published results indicated that a global mean equilibrium surface warming of between 1.3°C and 3.9°C resulted when atmospheric carbon dioxide was doubled in GCMs with annual mean insolation coupled with a "swamp" ocean of zero heat capacity but with an unlimited supply of moisture for evaporation. These results included indications that warming at the surface would be greatest in high latitudes; that in the tropics the upper troposphere would warm more than the surface, because of enhanced release of latent heat; and that the stratosphere would cool (eg Manabe and Wetherald (1975, 1980)). Early simulations with seasonally varying insolation and a mixed layer ocean (eg Manabe and Stouffer (1980)) suggested similar patterns of equilibrium temperature change but with the enhanced warming at the surface in high latitudes restricted to the winter half year. So did the results of Mitchell and Lupton (1984) with seasonally varying insolation and sea surface temperatures constrained to maintain present-day meridional convergence of heat by the oceans at low latitudes and taken from Manabe and Stouffer (1980) at high latitudes. More recent simulations of the equilibrium effects of doubled atmospheric carbon dioxide by Hansen et al (1984) at GISS, Washington and Meehl (1984) at the National Center for Atmospheric Research (NCAR) and Wetherald and Manabe (1986) at the Geophysical Fluid Dynamics Laboratory (GFDL) were compared in detail by Schlesinger and Mitchell (1987). Their comparisons for December to February (DJF) and June to August (JJA) zonal mean temperature changes are shown in Figures 10.7A and B. All three models showed a global mean equilibrium surface warming of about 4°C when atmospheric carbon dioxide was doubled. Each model shows enhanced warming at the surface in high latitudes in winter, an increase in warming with height in the tropical troposphere, and cooling in the stratosphere. The latter feature varies least in intensity from model to model because it is largely a direct result of the increased emission from the stratosphere to space of longwave radiation from the excess carbon dioxide, and is not directly affected by tropospheric and oceanic heat-transfers and interactions which vary from model to model. The GISS model shows a much greater warming in the tropical upper troposphere than the GFDL and NCAR models. This is likely to be because the GISS model incorporates a penetrative convection scheme that is more efficient in transporting heat and moisture into the upper troposphere (Schlesinger and Mitchell (1987)). Recent results from a Meteorological Office model with a penetrative convection scheme (Wilson and Mitchell (1987)) are similar to those of the GISS model in Figures 10.7A and B, with a warming of over 7°C in the tropical upper troposphere for doubled atmospheric carbon dioxide. On the other hand, when a version of the GISS model was constrained to have a sea-surface temperature change in general accord with that predicted by the GFDL model with doubled atmospheric carbon dioxide, the tropical upper tropospheric warming was reduced to about that obtained by the GFDL model (Rind (1987)). Thus the modelled sea surface temperature change is also a controlling factor on the tropical upper troposphere, as would be expected from, for example, studies of the El Nino-Southern Oscillation (Lecture 6). The sea surface temperature change in interactive integrations will not, of course, be independent of the choice of convection scheme. The third common feature in Figure 10.7, enhanced warming at the surface in high latitudes in winter, also varies in strength from model to model, because it is sensitive to features such as changes of sea ice coverage and thickness, and of snow cover, which are parameterized differently in the different models. The control runs of the different models have, as a result of the parametrizations, differing "climatologies" of sea ice: a model with, for example, a larger coverage of sea ice in its control run has greater potential for high-latitude warming through albedo reductions and ocean-atmosphere heat flux increases when the ice melts.

The effects of enhanced atmospheric carbon dioxide on precipitation in the GFDL, GISS and NCAR models were also compared by Schlesinger and Mitchell (1987) (Figure 10.8). On a zonal average, all three models give enhanced equatorial precipitation throughout the year, with decreases in adjacent latitudes at some times of the year. The GISS model gives the greatest enhancement near the equator. At middle and high latitudes all three models indicate slight increases of precipitation on a zonal average.

Schlesinger and Mitchell also show geographical distributions of surface air temperature and precipitation changes for the three models. The temperature change fields show significant differences, resulting from different changes in atmospheric circulation, sea ice, and snow cover; and the precipitation change fields show major qualitative differences as a result of different changes in atmospheric circulation and sea surface temperature. Precipitation changes may also be sensitive to the models' soil moisture changes (Lecture 4) and these in turn are likely to depend on the soil parameterizations used (Mitchell and Warrilow (1987)). Thus it is not yet possible to specify what regional changes are to be expected as a consequence of increased atmospheric carbon dioxide.

In summary, GCMs indicate that, in equilibrium with doubled atmospheric carbon dioxide, the following broadscale changes of climate are likely.

a) A global mean surface warming of about 4°C, and in any case of between 1.5°C and 4.5°C: the larger warmings are obtained by the more recent models and are likely to have resulted from the more comprehensive treatment of clouds which appear to induce positive feedbacks (Section 10.2.2);

b) Stratospheric cooling of between 3°C and 5°C;

c) Increase in warming with height in the tropical troposphere: the magnitude of this feature is uncertain;

d) Enhanced warming at the surface in high latitudes in winter: again the magnitude of this phenomenon is uncertain;

e) Generally greater precipitation in equatorial regions and in middle and high latitudes: regional details are very uncertain;

f) A tendency to decreased precipitation in the tropics away from the equator: regional details are very uncertain.

10.6 A STRATEGY FOR DETECTION OF THE IMPACT OF INCREASING GREENHOUSE GASES

Increases of carbon dioxide (Section 10.5) and of other radiatively active gases (Section 10.3) are expected to contribute to similar patterns of climatic change as the physical mechanisms will be similar, though there will be differing impacts on stratospheric photochemistry (Ramanathan et al (1987)). However, if we are to establish that increases of radiatively active gases, including carbon dioxide, have been responsible for climatic changes we must:

a) Take account of the disequilibrium which is likely to exist at present because of the delaying role of the oceans resulting from their high thermal capacity: as a result, observed changes are likely to be smaller than the equilibrium changes and may show patterns which differ from them;

b) Establish that a pattern or "fingerprint" of changes corresponding to those listed in Section 10.5 has actually been observed, with a statistically significant magnitude;

c) Assess whether the above-mentioned observed pattern, or parts of it, could have arisen through other, natural, causes.

10.6.1 The Delaying Role of the Oceans

The necessarily over-rudimentary treatment of the oceans by modellers highlights the need to develop fully interactive ocean-atmosphere-cryosphere models, despite their computational expense. Initial attempts have been made by Spelman and Manabe (1984) and others, which indicate that the oceans should produce a delay of several decades in CO_2-induced warming as a result of their thermal capacity. In reality, the magnitude of the delay depends on the extent to which the deep and abyssal waters are connected with surface waters. Figure 2.5, Lecture 2, shows that in the tropics the regions of cool ocean water that result from large-scale upwelling are quite extensive. So, the effect of upwelling ocean waters is likely to be important in the transient response of the climate system to changes in CO_2 concentration. Further observational and modelling studies are required to clarify this important point.

The increase of atmospheric greenhouse gases during the past century has been radiatively equivalent to at least a 40% increase in carbon dioxide. Section 10.1 implies a 25% increase of carbon dioxide itself: multiplication by 1.6 results from a conservative assessment of the material on other gases presented in Section 10.3. But an ocean-induced lag of, say, 30 years would effectively reduce the present-day effects to correspond in average magnitude to those expected in equilibrium with concentrations of greenhouse gases in the late 1950s, which were radiatively equivalent to perhaps a 20% increase in carbon dioxide since the 19th Century. The expected global mean surface warming to date would not, in that case, exceed 1°C and might be less than 0.5°C, the warming being proportional to log (concentration). A greater ocean-induced lag would result in an even smaller expected warming to date. Conversely, a longer ocean-induced lag implies that the ultimate warming will be a larger multiple of the warming observed to date.

10.6.2 Observed Climatic Changes and their Possible Causes

a) Measurements of surface air temperature over land, and of sea surface temperature, indicate that, on a global average, there has been a warming of about 0.5°C since the beginning of the century (Figure 10.9, from Jones et al (1988)). However, the late 19th Century appears to have been somewhat warmer than the period 1900-1920, at last over the oceans, though the reliability of this result remains a matter of continuing research (Lecture 9). Figure 10.9 illustrates the "noise" against which the "signal" of greenhouse gas - induced global warming needs to be detected. This "noise" includes short-term fluctuations related to the El Nino

-Southern Oscillation (Lecture 6) and maybe to volcanic activity and to changes in the solar "constant" (Lectures 3 and 9). Between 1940 and 1970 there was a halt in the warming trend (Figure 10.9): it is therefore likely that even the long-term changes in global surface temperature in Figure 10.9 are not solely a result of the continuously increasing concentrations of greenhouse gases in the atmosphere, but are partly a result of ocean-atmosphere interactions or even of long-term changes in the solar constant.

b) Parker (1985a) was unable to find significant lower stratospheric cooling relative to the upper troposphere since the late 1950s using a network of 27 radiosonde stations. Changes in instrumentation were taken into account. Labitzke et al (1986) found a global cooling trend at 30 mb, amounting to between -0.3°C and -0.4°C for the period 1966 to 1980, but warming then followed as a result of volcanic activity. Angell (1988) has documented recent marked cooling in the lower stratosphere (Figure 10.10) but this may be at least partly connected with the recent depletion of stratospheric ozone (Section 10.4).

c) Temperatures in the tropical troposphere are strongly modulated by the El Nino-Southern Oscillation (ENSO) (Lecture 6). The sequences of tropical upper tropospheric temperatures for 1949 to 1983 presented by Parker (1985b) after compensation for ENSO show no evidence of a warming trend.

d) Warmings and coolings of natural origin on decadal and longer time-scales are strongest in high latitudes in winter (Hansen and Lebebeff (1987)). The enhanced warming at the surface in high latitudes in winter suggested by GCMs as a consequence of increasing concentrations of greenhouse gases may, therefore, be difficult to detect.

e) Bradley et al (1987) suggest that there have been increasing trends of rainfall at 35°-70°N since the early 20th Century, with little change near the equator. However, the rainfall data probably contain biases resulting from changes in instrumentation and observing procedures, and research is continuing. See also Lecture 9.

f) Decreases in precipitation at 5°-35°N since the 1950s also reported by Bradley et al (1987) partly arise through decreases in sub-Saharan Africa which have been shown to result from patterns of mainly interhemispheric change of sea surface temperature (Lecture 5 and Folland et al (1986)).

10.7 CONCLUSION

There is growing evidence for the importance of the rôle of variations of atmospheric carbon dioxide concentration in the climatic changes of the late Pleistocene and early Holocene. The atmospheric effects to be expected as a result of the recent anthropogenic increase of atmospheric greenhouse gases are becoming more clearly understood as a result of increasingly sophisticated studies with climate models, but uncertainty remains as to the response of the oceans. As a result, the timing of the expected atmospheric changes is still uncertain. Observational evidence corroborating the anticipated climatic changes is beginning to accumulate, but may yet be ascribed to other, natural causes.

REFERENCES

ANGELL, J K	(1988)	Variations and trends in tropospheric and stratospheric global temperatures, 1958-1987. Submitted to J Climate.
BAES, C F Jr, BJORKSTROM, A and MULHOLLAND, P J	(1985)	Uptake of carbon dioxide by the oceans. "Atmospheric carbon dioxide and the global carbon cycle", US Dept of Energy Report No DOE/ER-0239, Washington DC, 81-111.
BARNOLA, J M, RAYNAUD, D KOROTKEVICH, Y S and LORIUS, C	(1987)	Vostok ice core provides 160,000-year record of atmospheric CO_2. Nature, 329, 408-414
BARNOLA, J.M., RAYNAUD, D., NEFTEL, A and OESCHGER, H	(1983)	Comparison of CO_2 measurements by two laboratories on air from bubbles in polar ice. Nature, 303, 410-413.
BRADLEY, R S, DIAZ, H F, EISCHEID, J K, JONES, P D KELLY, P M and GOODESS, C M	(1987)	Precipitation fluctuations over Northern Hemisphere land areas since the mid 19th Century. Science, 237, 171-175
BROECKER, W S, TAKAHASHI,T., SIMPSON, H J, and PENG, T-H	(1979)	Fate of fossil fuel carbon dioxide and the global carbon budget. Science, 206, 409-418.

CESS, R.D. and POTTER, G L (1984) A commentary on the recent CO_2 climate controversy. Climatic Change 6, 365-376.

CHOUDHURY B. and KUKLA, G. (1979) Impact of CO_2 on cooling of snow and water surfaces. Nature, 280, 668-671.

DONNER, L and RAMANATHAN V, (1980) Methane and nitrous oxide: their effects on the terrestrial climate. J. Atm. Sci., 37, 119-124.

FISHMAN J, RAMANATHAN V, CRUTZEN P J and LIU, S C (1979) Tropospheric ozone and climate. Nature, 282, 818-820.

FOLLAND, C K, PALMER, T N and PARKER, D E (1986) Sahel rainfall and worldwide sea temperatures, 1901-85. Nature, 320, 602-607.

HAMEED, S, CESS R D and HOGAN J (1980) Response of the global climate to changes in atmospheric chemical composition due to fossil fuel burning. J. Geophys. Res., 85, 7537-7545.

HANSEN J, LACIS A, RIND, D, RUSSELL, G, STONE, P, FUNG, I, RUEDY, R, and LERNER, J (1984) Climate sensitivity: analysis of feedback mechanisms. In 'Climate Processes and Climate Sensitivity' (J.E. Hansen and T. Takahashi, Eds.), Maurice Ewing Series 5, 368 pp. Amer. Geoph. Union, Washington, DC.

HANSEN, J, and LEBEDEFF, S (1987) Global trends of measured surface air temperature. J Geophys. Res, 92, D11, 13345-13372.

HEATH, D F (1988) Non-seasonal changes in total column ozone from satellite observations, 1970-86. Nature, 332, 219-227.

HOUGHTON, J T (1979) Greenhouse effects of some atmospheric constituents. Phil. Trans. R. Soc. Lond. A.290, 515-521.

HUMMEL, J R and RECK, R A (1981) The direct thermal effects of $CHClF_2$, CH_3CCl_3 and CH_2Cl_2 on atmospheric surface temperatures. Atmos. Environ., 15, 379-382.

IDSO, S B (1982) A surface air temperature response function for Earth's atmosphere. Boundary Layer Met., 22, 227-232.

JONES, P D, WIGLEY, T M L, FOLLAND, C K, PARKER, D E, ANGELL, J K, LEBEDEFF, S and HANSEN, J E (1988) Evidence for global warming in the past decade. Nature, 322, 790.

KIEHL, J T, BOVILLE, B A and BRIEGLEB, B P (1988) Response of a general circulation model to a prescribed Antarctic ozone hole. Nature, 332, 501-504.

KIEHL, J T and RAMANATHAN, V (1982) Radiative heating due to increased CO_2: the role of H_2O continuum absorption in the 12-18 µm region. J. Atm. Sci., 39, 2923-2926.

KONDRATYEV, K Ya (1969) Radiation in the atmosphere. International Geophysics series, Vol. 12. Academic Press, New York and London. 912 pp.

LABITZKE, K, BRASSEUR, G, NAUJOKAT, B and DE RUDDER, A (1986) Long-term temperature trends in the stratosphere: possible influence of anthropogenic gases. Geophys. Res. Lett, 13, 52-55.

LACIS, A, HANSEN, J, LEE, P., MITCHELL, T , and LEBEDEFF, S (1981) Greenhouse effect of trace gases, 1970-1980. Geophys. Res. Lett., 8, 1035-1038.

LAL, M and RAMANATHAN V (1984) The effects of moist convection and water vapour radiative processes on climate sensitivity. J. Atm. Sci., 41, 2238-2249.

MANABE, S and STOUFFER, R J (1980) Sensitivity of a global climate model to an increase of CO_2 concentration in the atmosphere. J. Geophys. Res., 85, 5529-5554.

MANABE, S and WETHERALD, R T (1975) The effects of doubling the CO_2 concentration on the climate of a general circulation model. J. Atm. Sci., 32, 3-15.

MANABE, S and WETHERALD, R T (1980) On the distribution of climate change resulting from an increase in CO_2 content of the atmosphere. J. Atm. Sci., 37, 99-118.

MITCHELL J F B (1984) The effects of pollutants on global climate. Met. Mag., 113, 1-16.

MITCHELL, J F B and LUPTON, G (1984) A 4 x CO_2 experiment with prescribed changes in sea surface temperatures. Progress in Biometeorology, 3, 353-374

MITCHELL, J F B and WARRILOW, D A (1987) Summer dryness in northern mid-latitudes due to increased CO_2. Nature, 330, 238-240.

NATIONAL ACADEMY OF SCIENCES (NAS) (WASHINGTON) (1979) Carbon dioxide and climate: a scientific assessment. Pp xi + 22.

NATIONAL ACADEMY OF SCIENCES (NAS) (WASHINGTON) (1982) Carbon dioxide and climate: a second assessment. Nat. Acad. Press. Pp xx + 72.

NEFTEL, A, MOOR, E, OESCHGER, H and STAUFFER, B (1985) Evidence from polar ice cores for the increase in atmospheric CO_2 in the past two centuries. Nature, 315, 45-47.

NEWELL R E and DOPPLICK, T G (1979) Questions concerning the possible influence of anthropogenic CO_2 on atmospheric temperature. J. Appl. Met., 18, 822-825.

NEWELL, R E, KIDSON, J W, VINCENT, D G and BOER, G J (1974) The General Circulation of the Tropical Atmosphere and Interactions with Extratropical Latitudes. 2 Vols. MIT.

PARKER, D E (1985a) On the detection of temperature changes induced by increasing atmospheric carbon dioxide. Quart. J. Roy. Met. Soc, 111 587-601.

PARKER, D E (1985b) The influence of the Southern Oscillation and volcanic eruptions on temperature in the tropical troposphere. J Climatology, 5, 273-282.

RAMANATHAN, V (1975) Greenhouse effect due to chlorofluorocarbons: climatic implications. Science, 190, 50-52.

RAMANATHAN, V (1982) Commentary on "Climate effects of minor atmospheric constituents". Carbon Dioxide Review, Oxford Univ Press, New York, pp 278-283.

RAMANATHAN, V, CALLIS, L CESS, R, HANSEN J, ISAKSEN, I, KUHN, W, LACIS, A, LUTHER, F, MAHLMAN, J, RECK R, and SCHLESINGER, M (1987) Climate-chemical interactions and effects of changing atmospheric trace gases. Rev. Geophys., 25, 1441-1482.

RIND, D (1987) The doubled CO_2 climate: impact of the sea surface temperature gradient. J Atm Sci, 44, 3235-3268.

RODGERS, C (1988) Global ozone trends reassessed. Nature, 332, 201.

SARMIENTO, J L and TOGGWEILER, J R (1984) A new model for the role of the oceans in determining atmospheric P_{CO2}. Nature, 308, 621-624.

SCHIFF, H I (1981) A review of the carbon dioxide greenhouse problem. Planet. Space Sci., 29, 935-950.

SCHLESINGER, M E and MITCHELL, J F B (1987) Climate model simulations of the equilibrium climatic response to increased carbon dioxide. Rev Geophys, 25, 760-798.

SIEGENTHALER, U and WENK, Th (1984) Rapid atmospheric CO_2 variations and ocean circulation. Nature, 308, 624-626.

SPELMAN, M J and MANABE, S	(1984)	Influence of oceanic heat transport upon the sensitivity of a model climate. J. Geophys. Res., 89, C1, 571-586.
VOLZ, A and KLEY, D	(1988)	Evalution of the Montsouris series of ozone measurements made in the nineteenth century. Nature, 332, 240-242.
WANG W C, YUNG, Y L LACIS, A A, MO, T and HANSEN, J E	(1976)	Greenhouse effects due to man-made perturbations of trace gases. Science, 194, 685-690.
WANG W C, PINTO J P and YUNG, Y L	(1980)	Climatic effect due to halogenated compounds in the earth's atmosphere. J. Atm. Sci., 37, 333-338.
WASHINGTON, W M and MEEHL, G A	(1984)	Sessonal cycle experiment on the climate sensitivity due to a doubling of CO_2 with an atmospheric general circulation model coupled to a simple mixed-layer. J Geophys. Res, 89, 9475-9503.
WEBSTER, P J	(1985)	Great events, grand experiments: man's study of the variable climate - Part II: Prospects of a warming Earth. Earth and Mineral Sciences, 55, 21-24.
WETHERALD, R T and MANABE, S	(1986)	An investigation of cloud cover change in response to thermal forcing. Clim. Change, 8, 5-23.

WILLIAMS W J, KOSTERS, J J, GOLDMAN, A and MURCRAY, D G (1976) Measurements of stratopsheric halocarbon distributions using infrared techniques. Geophys. Res. Lett, 3, 379-382.

WILSON, C A and MITCHELL, J F B (1987) A doubled CO_2 climate sensitivity experiment with a global climate model including a simple ocean. J Geophys. Res., 92, 13315-13343.

WORLD METEOROLOGICAL ORGANISATION (WMO) (1982) Report of the Meeting of Experts on Potential Climatic Effects of Ozone and other Minor Trace Gases, Boulder, Colorado, 13-17 September 1982.
WMO Global Ozone Research and Monitoring Project, Report No. 14.

WORLD METEOROLOGICAL ORGANISATION (WMO) (1987) The global climate system autumn 1984-spring 1986. CSM R84/86. 87 pp.

WMO/UNEP/ICSU (1981a) On the assessment of the role of CO_2 on climate variations and their impact. WMO, Geneva 33 pp. Joint WMO/ICSU/UNEP meeting of experts, Villach. Nov. 1980. WCP-3, Geneva.

Table 10.1. Effects of a doubling of atmospheric CO_2 (from the 2-dimensional model of Cess and Potter (1984))

Quantity		Value
ΔT_s		1.87°C
ΔG		1.69 Wm^{-2}
$\frac{dF\downarrow}{dT_s}$	($F\downarrow$ is downward component of terrestrial radiation at the surface)	5.87 Wm^{-2} $°C^{-1}$
$\frac{dF}{dT_s}$		-0.24 Wm^{-2} $°C^{-1}$
$\frac{dQ}{dT_s}$		-0.39 Wm^{-2} $°C^{-1}$
$\frac{d(LH)}{dT_s}$		1.11 Wm^{-2} $°C^{-1}$
$\frac{d(SH)}{dT_s}$		-0.35 Wm^{-2} $°C^{-1}$
$\frac{\delta(LH)}{\delta T_s}$		51.64 Wm^{-2} $°C^{-1}$
$\frac{\delta(SH)}{\delta T_s}$		18.26 Wm^{-2} $°C^{-1}$

Table 10.2. From WMO (1982)

Compilation of the climatic effects of trace gas increase. The change in net flux at the tropopause is the reduction in the net (up-down) outgoing longwave flux at the tropopause.

Trace Gas	Band Center cm^{-1}	Reference Mixing Ratio[1] (ppb)	Perturbed Mixing Ratio in Trace Gas (ppb)	Change in Net Flux at Tropopause (W/m^2)	Change in Surface Temperature[5] (°K)	Source[6]
CO_2	667	330×10^3	660×10^3	4.0	2.0	NAS
N_2O	589, 1168, 1285	300	600	0.65	0.3 - 0.4	DR, W1
CH_4	1306, 1534	1500	3000	0.61	0.3	DR, H
O_3(T)	1041, 1103	F(ϕ, Z)[2]	2 F(ϕ, Z)	1.24[8]	0.9[4]	H, F
$CFCl_3$(CFC11)	846, 1085, 2144	0	1	0.31	0.15[7]	R, W1[9]
CF_2Cl_2 (CFC12)	915, 1095, 1152	0	1	0.26	0.13[7]	R, W1[9]
CF_4	632, 1241, 1261, 1283	0	1		0.07	W2
CF_2HCl (CFC22)	1117, 1311	0	1		0.04	HR
CCl_4	776	0	1		0.14[4]	R, W1[9]
$CHCl_3$	774, 1220	0	1		0.1[4]	R, W1[9]
CH_2Cl_2	714, 736, 1236	0	1		0.05[4]	R, W1[9]
CH_3Cl	732, 1015, 1400	0	1		0.013[4]	R, W1[9]
CH_3CCl_3	707, 1084	0	1		0.02	HR
C_2H_4	949	0.2	0.4		0.01	W1
SO_2	518, 1151, 1361	2	4		0.02	W1
NH_3	950	6	12		0.09	W1
HNO_3	1695, 1333, 850, 459	F(Z)[3]	2 F(Z)		0.06	W1
H_2O	0-2000	3×10^3 [10]	6×10^3		0.6	W1

---

[1] Unless specified, refers to volume mixing ratio. Many of these mixing ratios are chosen for the convenience of sensitivity studies; for realistic values and trends see the previous section. Whenever possible, we have chosen the reference mixing ratio for minor trace gases to be zero, since the effects of these gases are linearly proportional to the mixing ratio, the change in surface temperature reflects the surface warming per ppb of the gases for which the reference mixing ratio is zero.

[2] Ozone distribution varies with latitude and altitude. The doubling applies primarily to tropospheric O_3.

[3] Profile varies with altitude.

[4] These results are for a fixed cloud-top temperature model. All other results are for a fixed cloud-top altitude model.

[5] Global mean surface temperature change. The problem of uncertainties in these values is analogous to CO_2 uncertainties. WMO CO_2 (1981).

[6] DR = Donner and Ramanathan (1980); F = Fishman et al. (1979); H = Hameed et al. (1980); HR = Hummel and Reck (1981); NAS = NAS (1979, 1982); R = Ramanathan (1975); W1 = Wang et al. (1976); W2 = Wang et al. (1980).

[7] Temperature changes were obtained with a fixed cloud altitude model as described in Ramanathan (1982). The flux changes were obtained from Ramanathan (1975).

[8] The flux change is from H but the surface temperature change is from F.

[9] These results are from R, which are larger than W1 values by about 30%. However, recent estimates by Wang (private communication) are in very good agreement with R.

[10] Stratospheric mass mixing ratio.

CARBON DIOXIDE CONCENTRATIONS AT MAUNA LOA

DATA FROM C.D.KEELING (SCRIPPS) VIA CARBON DIOXIDE INFORMATION ANALYSIS CENTRE (OAK RIDGE.CAL.)

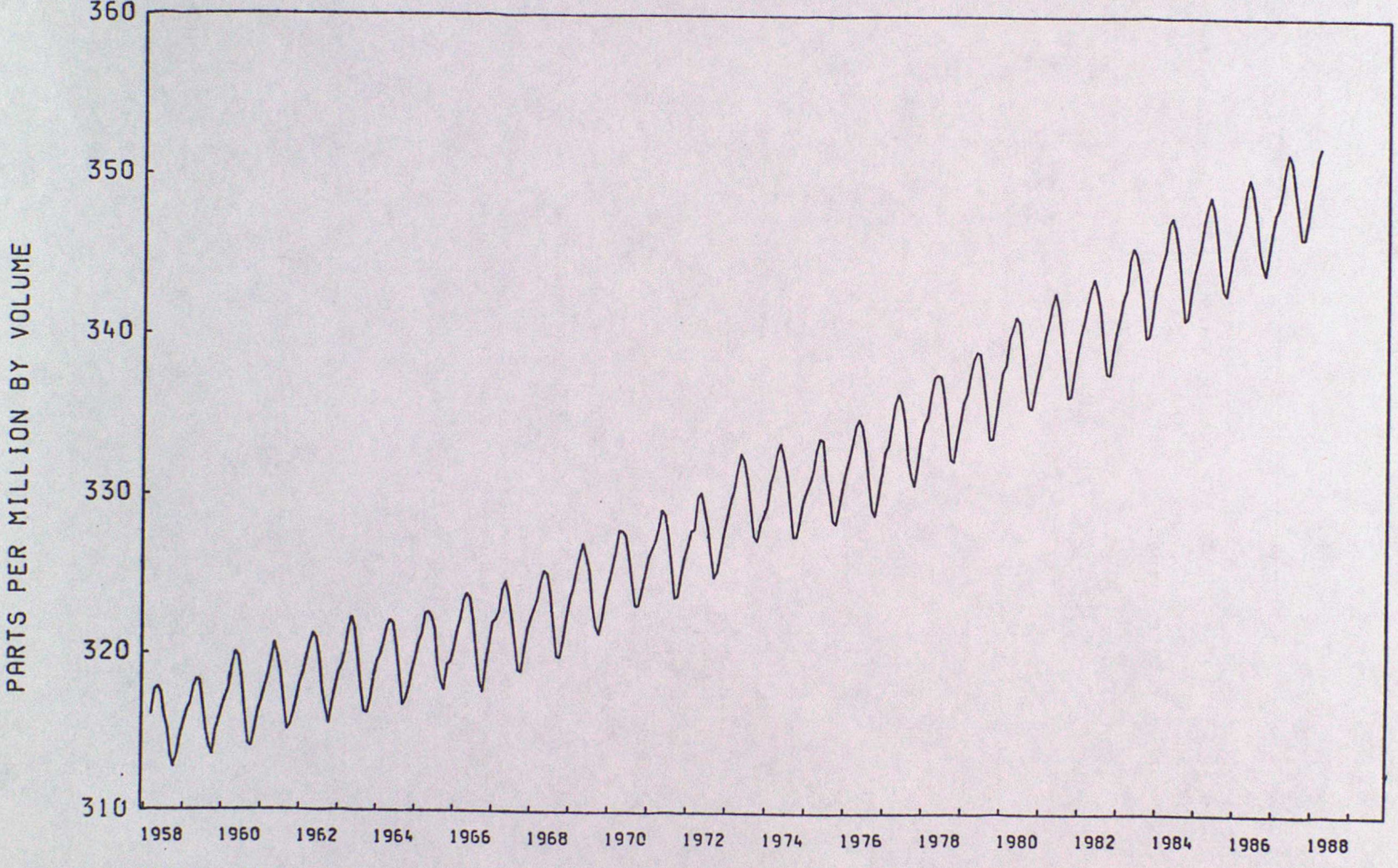

Figure 10.1.

PLOTTED 27 7 1988

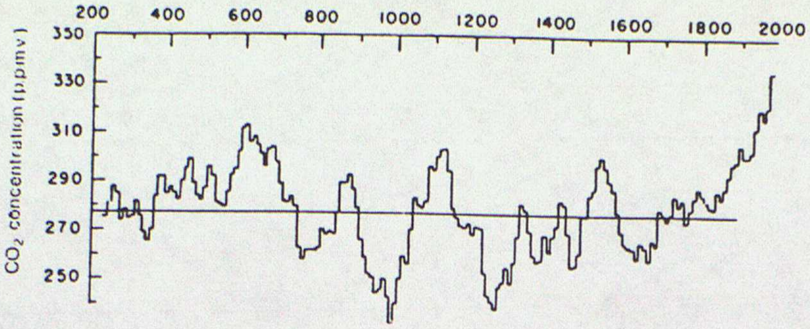

Figure 10.2 Variation in atmospheric carbon dioxide concentration between A D 200 and the present, as determined from the carbon-13 content of tree rings. From Webster (1985)

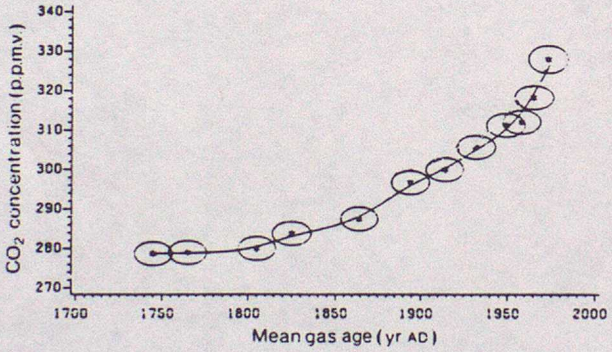

Figure 10.3. Measured mean CO_2 concentration plotted against the estimated mean gas age. The horizontal axis of the ellipses indicates the close-off time interval of 22 yr. The uncertainties of the concentration measurements are twice the standard deviation of the mean value, but not lower than the precision of 1% of the measurement.
Adapted from Neftel et al (1985).

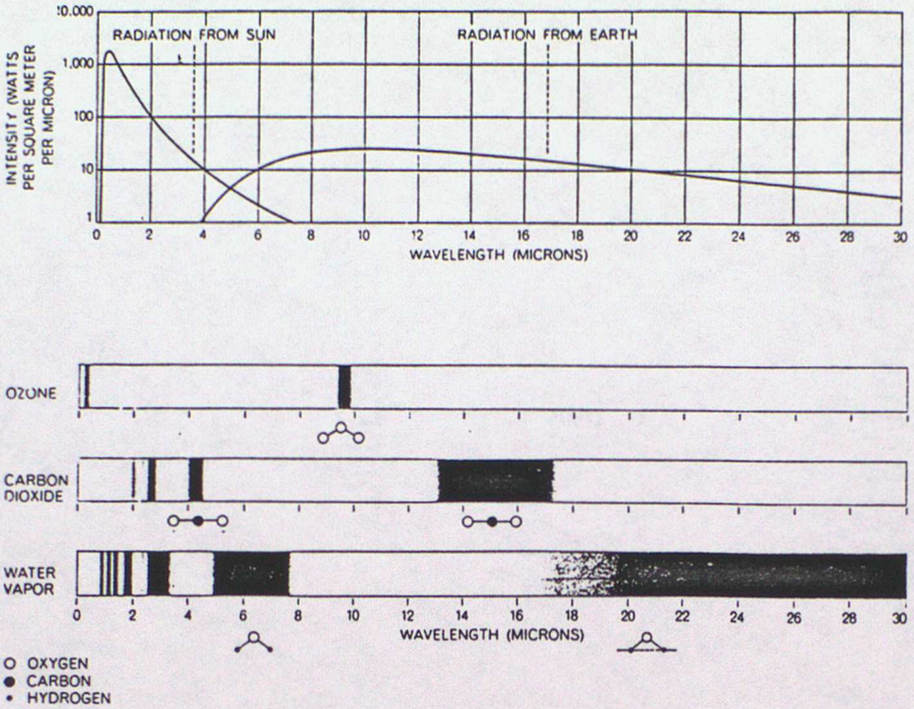

Schematic representation of the solar and thermal radiation spectrum and of the absorption lines and bands of ozone, carbon dioxide, and water vapor. (From *Scientific American* 210, no. 3:68.)

Figure 10.4. From Newell et al (1974).

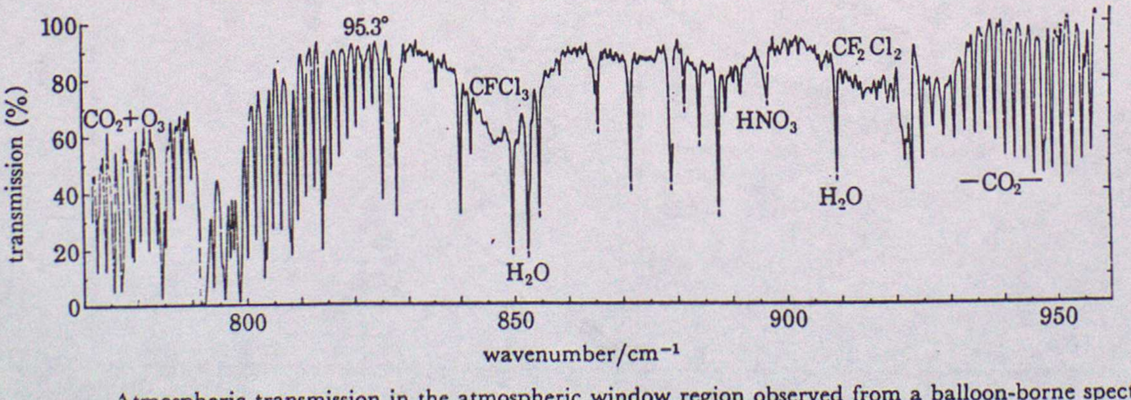

Atmospheric transmission in the atmospheric window region observed from a balloon-borne spectrometer from a height of 30 km along a limb path at 95.3° to the zenith by Williams *et al.* (1976). Notice the absorption bands of $CFCl_3$ and CF_2Cl_2. Resolution is 0.2 cm^{-1}.

Figure 10.5. From Houghton (1979).

Figure 10.6

Effect of increasing CO_2 on the vertical profile of temperature (schematic)

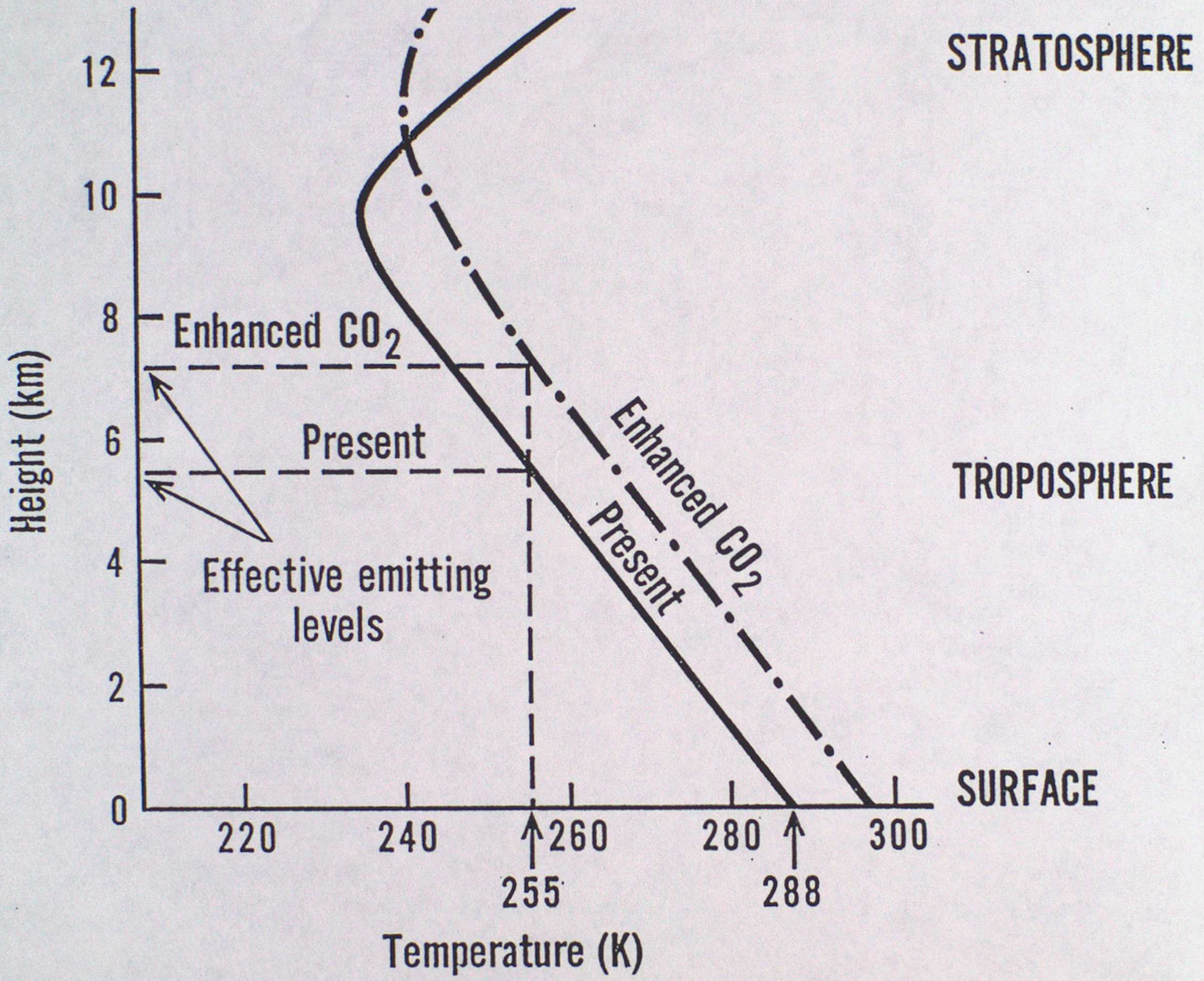

Figure 10.7A.

F om Schlesinger and Mitchell (1987).

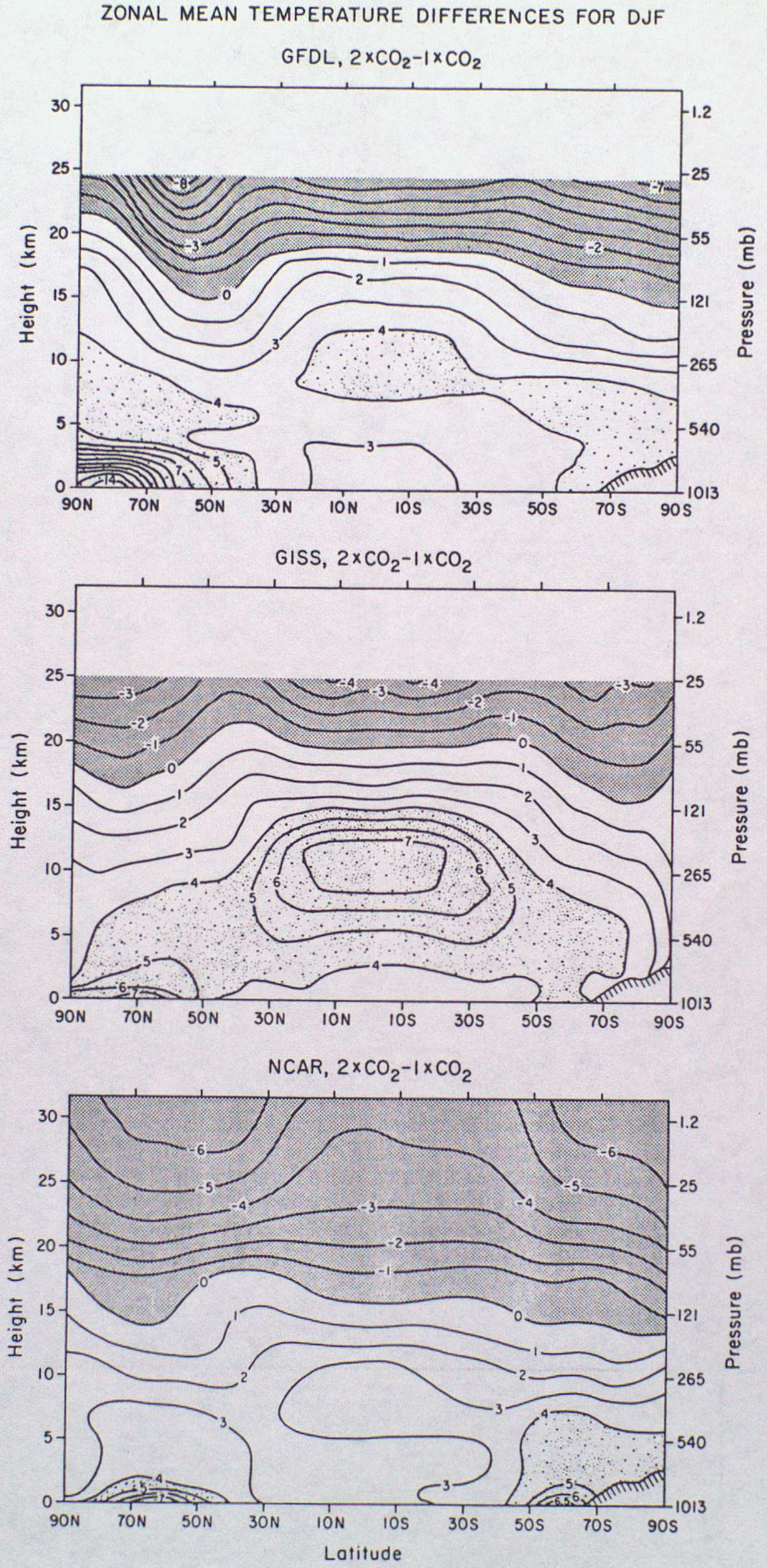

ZONAL MEAN TEMPERATURE DIFFERENCES FOR DJF

GFDL, 2×CO$_2$-1×CO$_2$

GISS, 2×CO$_2$-1×CO$_2$

NCAR, 2×CO$_2$-1×CO$_2$

Latitude-altitude cross section of the change in zonal mean air temperature (in degrees Celsius), (2 × CO$_2$) – (1 × CO$_2$), for DJF simulated with (top) the GFDL GCM by *Wetherald and Manabe* [1986], (middle) the GISS GCM by *Hansen et al.* [1984], and (bottom) the NCAR GCM by *Washington and Meehl* [1984]. Dense stippling indicates a temperature decrease and sparse stippling an increase larger than 4°C.

ZONAL MEAN TEMPERATURE DIFFERENCES FOR JJA

GFDL, $2\times CO_2 - 1\times CO_2$

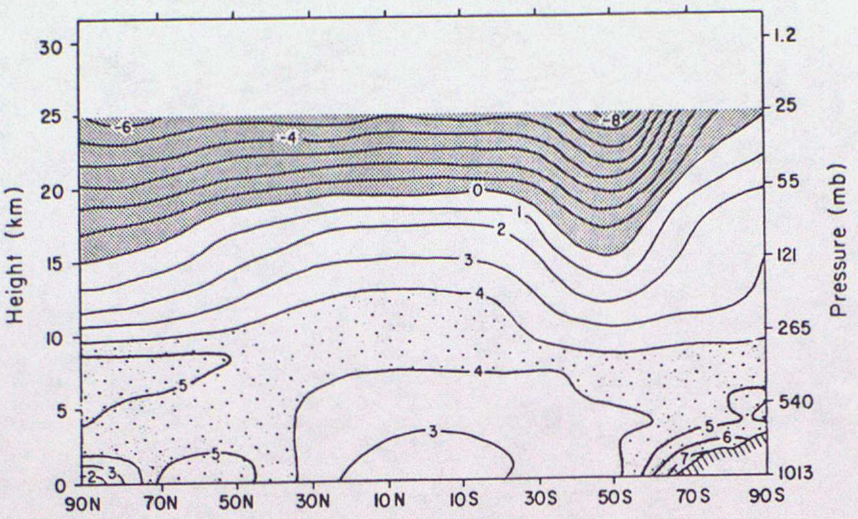

Figure 10.7B.

As Fig. 10.7A but for June to August.

From Schlesinger and Mitchell (1987).

GISS, $2\times CO_2 - 1\times CO_2$

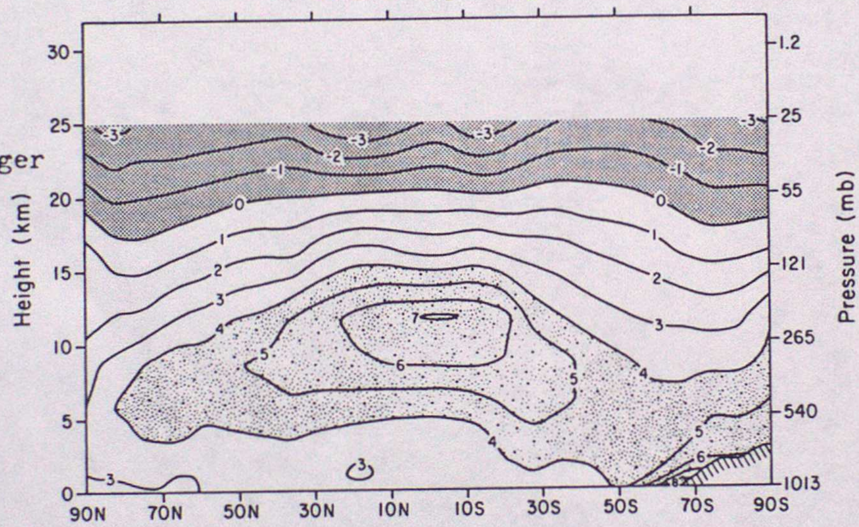

NCAR, $2\times CO_2 - 1\times CO_2$

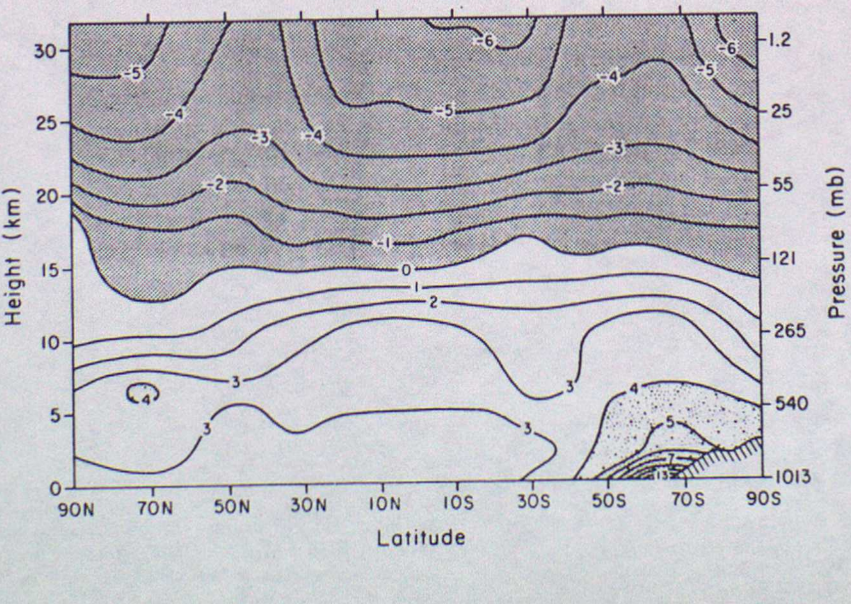

Figure 10.8.

'rom Schlesinger and
Mitchell (1987).

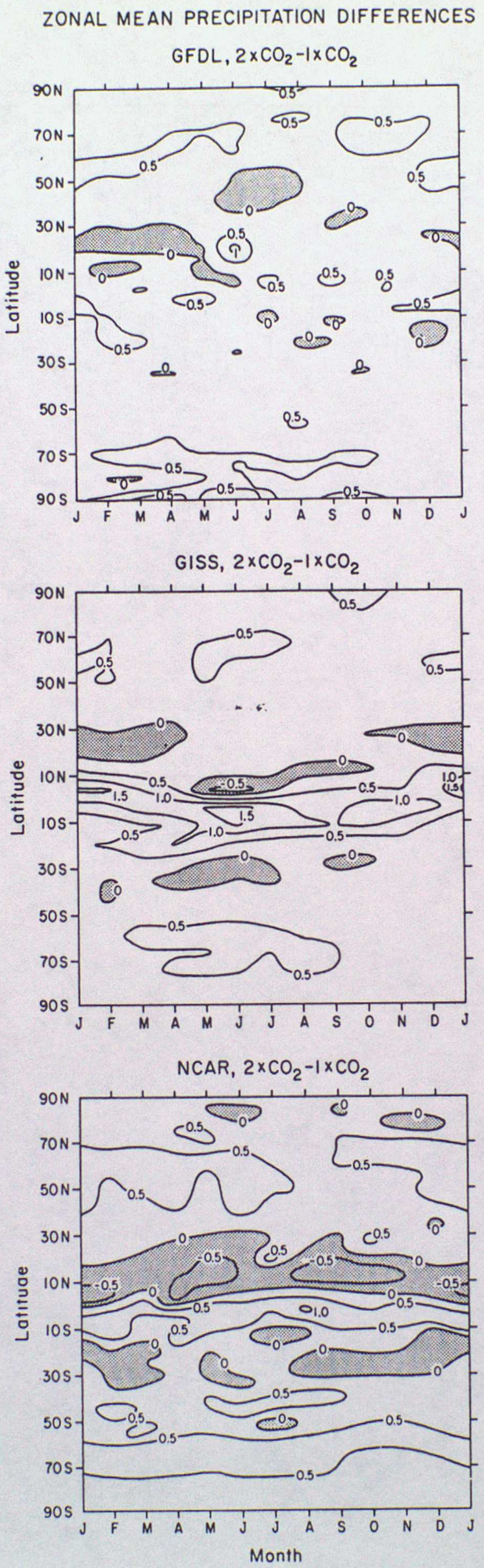

Latitude-time cross section of the zonal mean precipitation rate change (in millimeters per day), $(2 \times CO_2) - (1 \times CO_2)$, simulated with (top) the GFDL GCM by *Wetherald and Manabe* [1986], (middle) the GISS GCM by *Hansen et al.* [1984], and (bottom) the NCAR GCM by *Washington and Meehl* [1984]. Stippling indicates a decrease in precipitation rate.

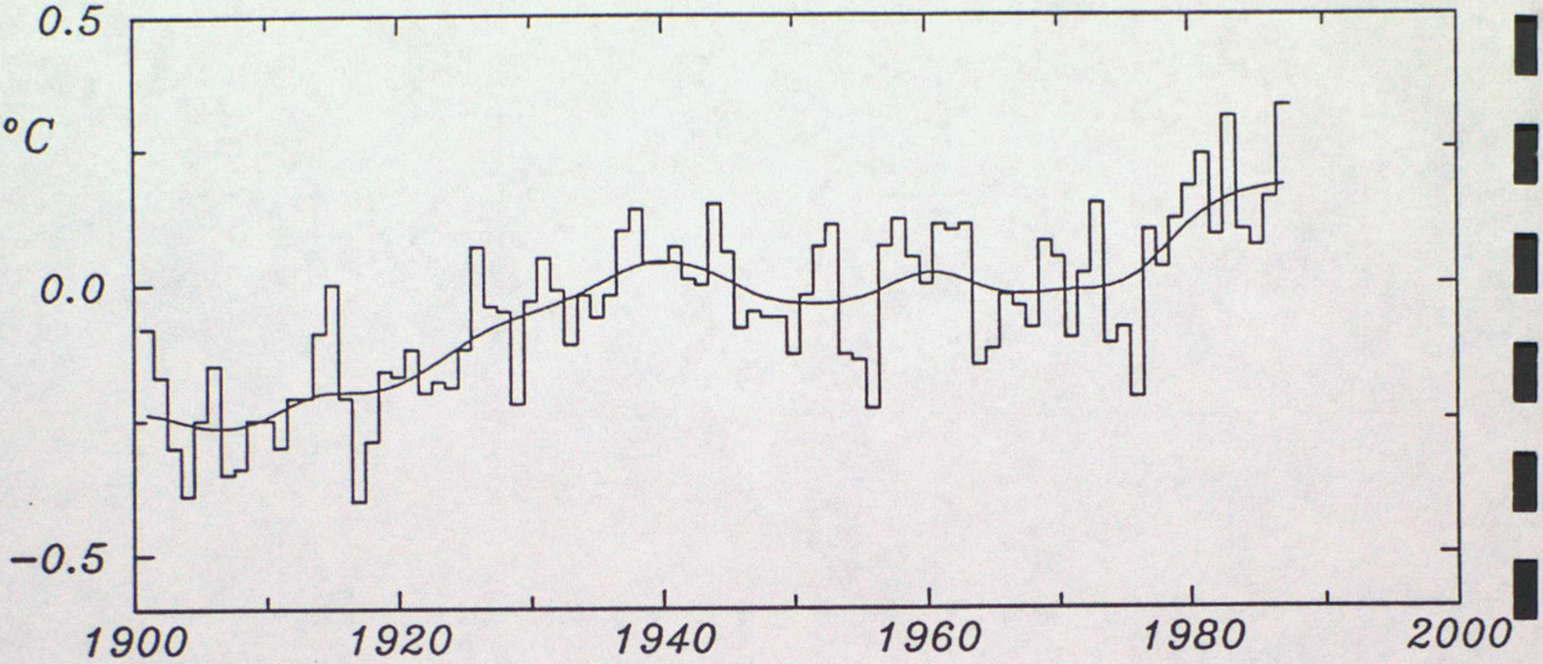

Figure 10.9. Changes of global surface temperature, 1901–87.

After Jones et al (1988), with minor amendments to the data for the 1980's.

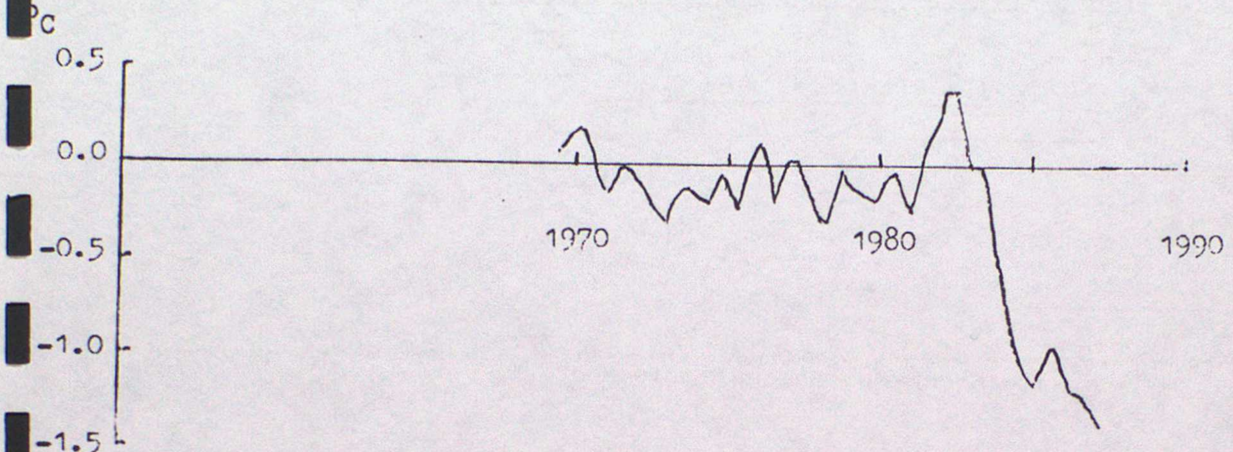

Figure 10.10. Changes of global temperature in the 100-50mb layer, 1969-87.
Data from Angell (1988).

VS

APPENDIX I

TO 1988 ADVANCED LECTURES ON THE CLIMATE OF THE WORLD

METEOROLOGICAL OFFICE - ADVANCED LECTURES 1982

THE CLIMATE OF THE WORLD

Lecture 5

Simple Energy-balance Climate Models

by

D J Carson

Met O 13

March 1982

10-40

Simple Energy - balance Climate Models

by

D J Carson

A10.1. Introduction

An increasing awareness of man's vulnerability to climate variations and a growing belief that his activities may have a significant influence on the climate have led, over the past decade, to the World Climate Conference in 1979 (WMO, 1979) and to the formulation of the World Climate Programme (WMO, 1980), one component of which is the programme for research on climate change and variability, the World Climate Research Programme (WCRP). One of the main elements in the WCRP is the development and evaluation of climate models to be used for the study of climate predictability and climate sensitivity.

There is as yet no comprehensive theory of climate to explain its variability, nor are there, at this juncture physical-dynamical models which can simulate adequately the subtleties and complexities of the full climate system. Indeed there exists an almost continuous spectrum of types of so-called climate model, ranging from simple, one-dimensional, equilibrium representations of the vertical radiative processes in the atmosphere to the full complexity of the three-dimensional, time-dependent, global general circulation models. The latter, in which the effects of large-scale disturbances in the atmosphere are included explicitly, are sometimes referred to as comprehensive models in contrast to the simple models in which many more dynamical and physical processes have to be parametrized. There is of course debate about the advantages and deficiencies of each class of model but at present it is probably fair to claim that each type has a rôle to play in furthering our understanding of the real climate system. It should be obvious, for example, that some of the time scales of interest in climate modelling make it both economically and practically impossible to apply the fully comprehensive models in many studies and so the simpler, usually less realistic, models have to be used.

The Meteorological Office has a major commitment to develop its atmospheric general circulation models to produce, ultimately, a comprehensive, coupled atmosphere - land - ocean - cryosphere climate model. The structure and performance of such general circulation models have been discussed, for example, by Dr A Slingo in the complementary lecture series on The General Circulation of the Atmosphere. The aim of this lecture is not to review the state of the art of simple climate modelling (there exists too large a body of literature!) but rather it is to introduce the reader to the concept of such models and to the assumptions made in the simplest examples. Their application to climate-related problems and the somewhat surprising properties of their solutions will also be discussed.

Before describing the models it is worth introducing some terms which are likely to be encountered, increasingly without being explained, in the literature concerned with the design of climate models and their application to sensitivity and predictability studies.

Predictability of Different Kinds

Consider the two questions:

(1) Is climate predictable in some sense or another and at some time range ?

(2) Are man's activities influencing the climate in any way ?

Different modelling methodologies are required to tackle the two, generally distinct, aspects of climate predictability embodied in these questions. Lorenz (1975) recognised these as questions of predictability of the first and second kind, respectively.

Predictability of the First Kind

This is defined as the prediction of the natural variations of the climate system i.e. it is effectively long-range forecasting using the present state of the climate system as an initial condition.

In principle this includes variations from the synoptic scale limit of predictability of a few weeks up to the epochs of glaciations. The nature of climate predictability of the first kind is not understood anywhere in its range. Indeed, a major open question is whether there are any characteristics of the circulation that retain predictability in the range of several weeks to several years. Even if climate predictability of the first kind is possible in principle it remains to be determined how the problem can be approached. The long-range forecasting for a month to a season ahead, which is being researched in the Synoptic Climatology branch (Met O 13), comes into this category at the short-period end of the range. Because such relatively short periods (in climate terms) of prediction are involved at present in such studies, then fully comprehensive general circulation models can be used.

Predictability of the Second Kind

This is defined as the determination of the response of the climate system to changing external influences which might be prescribed or predicted in terms of other dynamical and physical considerations. Such predictions are not concerned directly with the chronological order of occurrence of atmospheric states, but rather with the long-term average statistical properties of the climate (or model).

Most applications of atmospheric general circulation models to climate problems are necessarily predictability studies of the second kind i.e. the typical set of control and perturbation integrations to determine the sensitivity of a simulated climate to prescribed changes in external forcing. A topical example is the study of the impact on the simulated climate of doubling the amount of CO_2 in the atmosphere (see, for example, Mitchell (1981)). It is still an unresolved question whether predictability of the second kind is a meaningful concept or not.

Transitivity, Intransitivity and Almost Intransitivity

An important issue of climate theory is whether the causes of most climate fluctuations are external to the climate system or internal to it, i.e. have past changes been caused, for example, by fluctuations in solar emissions or changes in the earth's orbital parameters (the so-called Milankovich Theory of climate change), or can these changes be explained to a large extent by the intrinsic internal variability within the system, which needs only an external trigger ? This question has been given a more precise mathematical formulation by Lorenz (1968, 1970, 1975) who introduced the concepts of transitivity, intransitivity and almost intransitivity, taken from ergodic theory.

Transitivity. If the very long-term averaged statistics of a climate system (or climate model) are independent of the initial state, then that climate (or model) is said to be transitive.

Intransitivity. If no unique set of such equilibrium climate statistics exists then the climate (or model) is called intransitive, i.e. there are two or more sets of statistical properties and some initial states lead to one set while others lead to another.

Almost Intransitivity. If the climate system (or model) is transitive for statistics taken over an infinite period and yet contains shorter-period self-fluctuations that might be interpreted as climate changes indicative of an intransitive climate system, then it is called almost intransitive. An almost intransitive system could be mistaken for a truly intransitive one if the statistics over long but finite times were identified as those over an infinite period. For example, the existence of glacial and interglacial periods raises the possibility that the climate system is almost intransitive.

There exists the possibility that for fixed external conditions, very different climate states may be implied by finite-interval time averages owing solely to intransitivity or almost intransitivity. The association of a particular climate with a given external state requires an assumption (as yet unfounded) of transitivity of the climate. With any climate model it is very important to determine the sensitivity of its equilibrium state statistics to variations of internal (e.g. initial) conditions. It will be discussed below that some of the simplest climate models are intransitive and do in fact support two steady state solutions corresponding to glacial and interglacial climates.

A10.2. Radiative-convective Thermal Equilibrium Models (Vertical Column Energy-balance Models)

A10.2.1 Introduction

This class of one-dimensional models computes the annually and horizontally averaged, global, surface and atmospheric temperatures. The temperature profile is determined essentially from a balance between the incoming short-wave (or solar) and the outgoing long-wave (alternatively called terrestrial, infrared or thermal) radiative fluxes, which, in turn, depend upon specified surface properties and vertical distributions and optical properties of clouds, aerosols and of the most important of the optically active gases such as water vapour, carbon dioxide and ozone. A method of convective adjustment is used to ensure that realistic vertical temperature profiles are obtained.

The first radiative-convective models for the earth's atmosphere were developed by Manabe and Strickler (1964) and Manabe and Wetherald (1967). Further variations of the approach have also been developed and are discussed in the comprehensive review by Ramanathan and Coakley (1978). Radiative-convective modelling is a technique commonly employed in studies of stellar and planetary atmospheres.

The paper by Manabe and Wetherald (1967) is to some extent a repeat of the computation of radiative-convective equilibrium of the atmosphere which was discussed in the earlier paper by Manabe and Strickler (1964). The main difference is that Manabe and Wetherald specify a given distribution of relative humidity instead of a given distribution of absolute humidity as used in Manabe and Strickler. The former assumption is thought to be the more realistic. The prime objective in both cases was to formulate and test a method to incorporate radiative transfer into a general circulation model.

Note that with respect to the formulation of the radiative transfer processes in the single column the radiative-convective models are not necessarily simple. Because so much else is parametrized in such a simple way the combination of high vertical resolution and the small demand made on computing resources enables the radiative processes to be modelled in a very detailed fashion. It is not the purpose of this lecture to examine the subtleties and complexities of the actual schemes used by Manabe and his colleagues; for this information the reader is referred to the original papers.

Further objectives of such modelling were:

(1) To determine the influence of various factors such as the solar constant, cloudiness, surface albedo and the various atmospheric absorbers in maintaining the existing thermal structure of the atmosphere.

(2) To determine the rôles of the above factors in maintaining the observed climate at the earth's surface.

A10.2.2 Model assumptions and structure

a. Pure radiative equilibrium

In order to prepare for the study of thermal equilibrium with convective adjustment, calculations were first done for the simple case of purely radiative equilibrium, in which the equilibrium state was approached as an asymptotic steady state of an initial value problem. Equilibrium is considered to have been reached when the temperature change at each level over the time-step used in the model is less than a specified small value.

The following constraints are also satisfied in the equilibrium state:

(1) At the earth's surface, the net upward flux of long-wave radiation is equal to the net downward flux of solar radiation. This guarantees radiative equilibrium at the surface.

(2) At the top of the atmosphere the net upward flux of long-wave radiation is equal to the net downward solar radiation. This guarantees the radiative equilibrium of both the atmosphere and the earth as a whole.

The unrealistic temperature profiles which result when radiation alone is acting have been described by Dr A Slingo in the complementary lecture series on the General Circulation of the Atmosphere and so there is no need to discuss them further here.

b. Radiative-convective equilibrium

The procedure of convective adjustment is to modify the lapse rate to the critical lapse rate whenever that critical lapse rate is exceeded in the course of the integration. The critical lapse rate generally adopted is 6.5 K km^{-1} which was assumed to be a reasonably realistic value for the observed tropospheric lapse rate of temperature. The process of convective adjustment will transfer heat energy from the surface into the atmosphere and thereby permit more realistic temperatures to occur throughout the troposphere.

The requirements for radiative-convective equilibrium are:

1. (1) **At the top of the atmosphere, the net incoming solar radiation should be equal to the net outgoing long-wave radiation.**

(2) No temperature discontinuity should exist.

(3) Free and forced convection, and mixing by large-scale eddies, prevent the lapse rate exceeding a critical value of 6.5 K km^{-1}.

(4) Whenever the lapse rate is subcritical, the condition of local radiative equilibrium is satisfied.

(5) The heat capacity of the earth's surface is zero.

(6) The atmosphere maintains the given distribution of relative humidity. (This is a requirement introduced in Manabe and Wetherald (1967)).

Figure A10.1 gives a simple schematic representation of the iterative procedure used to obtain the state of radiative-convective equilibrium. Both 18 and 9 atmospheric levels were used in the computations such that the pressure thickness of the layer is thin both near the surface and near the top of the atmosphere.

Mathematical Note: r (the humidity mixing ratio) = $\dfrac{0.622\,e}{p-e}$

where e is the water vapour pressure, p is the atmospheric pressure.

h (the relative humidity) = $\dfrac{e}{e_s}$

where e_s is the saturation water vapour pressure.

Therefore, r can be written

$$r = \frac{0.622\,h\,e_s(T)}{p - h\,e_s(T)}$$

where e_s as a function of temperature, T, can be evaluated from the Clausius-Clapeyron relationship,

$$\frac{de_s}{dT} = \frac{0.622\,L\,e_s}{R_d T^2}$$

where L is the latent heat of evaporation and Rd is the specific gas constant for dry air.

c. Details of the radiation scheme

The reader is referred to Manabe and Strickler (1964) for details of:

(1) The computation of the flux of long-wave radiation.

(2) The computation of the depletion of solar radiation.

(3) The determination of mean absorptivity and emissivity.

d. Assumptions made about standard distributions of atmospheric absorbers

The following constituents and their vertical distributions are adopted unless otherwise specified.

Water vapour	The relative humidity is assumed to be a linear function of pressure throughout most of the atmosphere, as illustrated in Figure A10.2. The line was chosen to fit the data quoted in the Figure legend and a constraint of a minimum value of the humidity mixing ratio of 3×10^{-6} is enforced.
Carbon dioxide	The mixing ratio of carbon dioxide in the atmosphere is assumed constant at 0.0456 % by weight (300 ppm by volume).
Ozone	The adopted vertical distribution of ozone is shown in Figure A10.3.

The vertical distributions of gaseous absorbers are those appropriate for 35°N in April. Insolation is assumed to be the annual mean value for the hemisphere.

Clouds The characteristics of the clouds implied in the model are listed in Table A10.1. The albedo of the earth's surface is assumed to be 0.102.

Cloud	Height (km)	Amount	Albedo
High	10.0	0.228	0.20
Middle	4.1	0.090	0.48
Low: Top	2.7	0.313	0.69
Bottom	1.7		

Table A10.1. Cloud characteristics used in the radiative-convective equilibrium model of Manabe and Wetherald (1967).

A10.2.3 Some results from radiative-convective equilibrium models

Figure A10.4, from Manabe and Wetherald, shows the purely radiative equilibrium profile obtained with the assumption of fixed absolute humidity (as used by Manabe and Strickler) and that obtained with the assumption of fixed relative humidity. Note that with fixed relative humidity there is a very sharp decrease with height near the surface and that the temperature of the troposphere is generally much lower than that obtained with fixed absolute humidity. The radiative-convective equilibrium profile for the case with fixed relative humidity is also shown and demonstrates quite clearly the role of convective adjustment in establishing and maintaining the existing distribution of atmospheric temperature (Cf. Figure 6 of Slingo (1982)).

Figure A10.5, from Manabe and Strickler, shows the approach to pure radiative equilibrium and radiative-convective equilibrium from both initially warm and initially cold isothermal states, respectively. This figure indicates that the final states may be regarded as steady states.

A wide range of experiments has been done to examine the sensitivity of the radiative-convective equilibrium temperature profiles obtained, for example, with different values of the solar constant and the surface albedo and different combinations and vertical distributions of the main atmospheric absorbers such as water vapour, CO_2, O_3 and clouds. Of particular, topical interest are the experiments of Manabe and Wetherald which examined the response of the surface temperature to changes in the atmospheric CO_2 content.

Figure A10.6, from Manabe and Wetherald, shows the vertical distributions of equilibrium temperature corresponding to three different CO_2 contents, viz. 150, 300 and 600 ppm. Note:

(1) The larger the mixing ratio of CO_2 the warmer is the equilibrium temperature of the earth's surface and troposphere. This results primarily from an enhanced absorption of the surface long-wave radiation by the tropospheric CO_2 but is also partly due to the effective increase in downward radiation emitted by stratospheric CO_2.

(2) The larger the mixing ratio of CO_2, the colder is the equilibrium temperature of the stratosphere. This results from the increase in long-wave radiation emitted to space by CO_2 in the stratosphere.

(3) Relatively speaking, the dependence of the equilibrium temperature of the stratosphere on CO_2 content is much larger than that of the tropospheric temperature.

Tables A10.2 and A10.3 show the equilibrium temperature of the earth's surface corresponding to different CO_2 contents and also the change of the equilibrium surface temperature corresponding to the specified changes in CO_2. Values for both fixed absolute humidity and fixed relative humidity cases are given. Note that the equilibrium temperature of the latter is almost twice as sensitive to the change in CO_2 as that of the former due to the adjustment of water vapour content to the temperature variation of the atmosphere. The changes resulting from doubling the CO_2 content are in reasonable agreement with those obtained in subsequent experiments with general circulation models. Table A10.4, from Mitchell (1981), gives a comparison of estimates of the change in global mean surface temperature obtained for specified changes in the CO_2 content from single-column, radiative-convective equilibrium models (including the results of Manabe and Wetherald (1967)) with the changes obtained from corresponding general circulation model integrations.

	Average cloudiness		Clear	
CO_2 content (ppm)	Fixed absolute humidity	Fixed relative humidity	Fixed absolute humidity	Fixed relative humidity
150	289.80	286.11	298.75	304.40
300	291.05	288.39	300.05	307.20
600	292.38	290.75	301.41	310.12

Table A10.2. Equilibrium temperature of the earth's surface (K) for different values of the CO_2 content of the atmosphere, from Manabe and Wetherald (1967).

Change of CO_2 content (ppm)	Fixed absolute humidity		Fixed relative humidity	
	Average cloudiness	Clear	Average cloudiness	Clear
300 ⟶ 150	-1.25	-1.30	-2.28	-2.80
300 ⟶ 600	+1.33	+1.36	+2.36	+2.92

Table A10.3. Change of equilibrium temperature of the earth's surface corresponding to various changes of CO_2 content of the atmosphere, from Manabe and Wetherald (1967).

A10. 2.4 Limitations of the radiative-convective equilibrium models

(1) The most important limitation is that results from these models are mostly of academic interest, since they do not give any information about regional and latitudinal temperature changes.

(2) Many of the model parameters (cloud amounts, surface albedo, relative humidity, critical lapse rates, etc) are prescribed on the basis of present day conditions which may not apply for large departures from present day conditions. Radiative-convective models cannot be applied for large perturbations from present conditions.

(3) The model results depend very critically on the details of the parametrizations. Also like many other models, particularly the simpler models, these models are probably too deterministic.

It is of course very important that the limitations of all the models, especially the simpler, cruder models, be borne in mind when their results are being interpreted.

A10.3. Horizontally Varying Energy-balance Models

A10.3.1 Introduction

In contrast to the radiative-convective equilibrium models of the previous section, this class of one-dimensional, energy-balance models treats the vertical structure with much less detail than the horizontal structure. There exist many types of model of varying degrees of complexity within this class but here we shall concentrate on those which presume to compute the zonally-averaged surface temperature as a function of latitude only, obtained effectively as a balance between incoming solar and outgoing terrestrial radiation. Budyko (1969) and Sellers (1969) are generally acknowledged as having proposed independently the first such models and it is now common practice to refer to the class of derivatives and extensions of their approaches as Budyko - Sellers type models.

Table A10.4. Estimates of global mean changes in temperature and precipitation due to increasing atmospheric carbon dioxide.

Source	3-dimensional model							
	Topography	Solar Radiation	Cloud	Ocean	CO_2	PPTN	T*	1-D model T*
Manabe and Wetherald, 1975	Idealized	Annual mean	Fixed	Swamp	2	7%	2.93	2.36 †
Manabe and Wetherald, 1980	Idealized	Annual mean	Model Dependent	Swamp	2	7%	3.0	2.0
					4	12%	5.9	4.1
Manabe and Stouffer, 1980	Realistic	Seasonal	Fixed	Fixed depth	4	6.7%	4.1	
Present work								
(a) 2 x CO_2 + 2K	Realistic	Seasonal	Fixed	Present day + 2K	2	5%	2.25	
(b) Estimate assuming no change in global mean net surface heat balance				Present day + 1.65K	2	3.5%	1.9	1.7

† Manabe and Wetherald(1967)

This table is taken from Mitchell (1981).

There is incontrovertible evidence of the existence of large fluctuations in past climate. There is also debate that the impact of man's activities may possibly initiate a significant response in the climate system. Therefore there is concern about and interest in the question of the stability of the global climate to small perturbations of any sort. This led Budyko (1969) and Sellers (1969) to develop their simple models of the earth's climate, based on the mean annual balance of heat entering and leaving latitudinal strips of the earth-atmosphere system, for the purpose of testing the sensitivity of the equilibrium state of the climate to changes in the solar radiative heating.

Schematically, the heat balance for the i-th strip in equilibrium may be written:

$$\left\{\begin{matrix}\text{Absorbed solar}\\ \text{radiation}\end{matrix}\right\}_i - \left\{\begin{matrix}\text{Outgoing infrared}\\ \text{radiation}\end{matrix}\right\}_i = \left\{\begin{matrix}\text{Horizontal divergence of}\\ \text{thermal energy flux}\end{matrix}\right\}_i$$

Each of the above terms is parametrized by some theoretical or semi-empirical formula, usually in terms of the sea-level temperature field. All of the equations are then solved simultaneously to give the surface temperature field. Note that the balance equation assumes that there is no heat or moisture storage in the oceans, land or atmosphere and hence no long-term climatic trend. There is also the gross assumption that the character of the climate of the whole column of the earth-atmosphere system is embodied in a single variable, the surface temperature. Although the various particular studies differ in the exact details of their parametrizations of the above components of the balance it is generally believed that they are at least qualitatively equivalent.

Although these models are highly simplified their solutions to particular problems have a rather complicated structure. Indeed it will be shown that a multiplicity of solutions is obtained for the present value of the solar constant. The interesting and, arguably, unexpected character of such solutions, their mathematical stability properties and the consequent implications for our appreciation of climate are the main reasons why an increasingly large amount of study has been devoted to this class of simple climate model since the appearance of the papers by Budyko (1969) and Sellers (1969).

A10.3.2 The model of Budyko (1969)

In the first instance let us consider the model and results of Budyko (1969). The simplified, integrated thermodynamic energy equation for the whole earth-atmosphere system is represented in terms of annually and zonally averaged variables and equations, thus

$$R + \text{div}\,\underset{\sim}{F} = 0 \qquad (A10.1)$$

where R is the net radiation for a column of the earth-atmosphere system at a given latitude and div $\underset{\sim}{F}$ represents the net gain or loss of heat, i.e. it represents the divergence of the net energy flux, as a result of the atmospheric and hydrospheric circulations for that latitude

The net radiation is expressed as

$$R = Q\,(1-\alpha) - I \qquad (A10.2)$$

where Q is the annual mean solar radiation at the outer boundary of the atmosphere, α is the planetary albedo (or reflectivity) and I is the net terrestrial radiation to space, all for a given latitude.

An analysis of radiation and temperature data led Budyko to propose and use the empirical formula

$$I = a + BT_o - (a_1 + B_1 T_o) n \qquad \text{(A10.3)}$$

where I is the outgoing radiation in kcal cm^{-2} month^{-1},
T_o is the temperature at the earth's surface in ^{o}C,
n is the cloudiness in fractions of unit, and
a, B, a_1, B_1 are dimensional coefficients with values
$a = 14.0$, $B = 0.14$, $a_1 = 3.0$ and $B_1 = 0.10$.

For the earth as a whole (i.e. with div $\underset{\sim}{F} \equiv 0$) Budyko found that with $n = 0.50$ and constant $\alpha = 0.33$, a change of solar radiation by 1% results in a temperature change of 1.5K. He cites a corresponding estimate from Manabe and Wetherald (1967) as giving a 1.2K change in surface temperature as a result of a solar radiation change of 1%. Budyko argues that the long time-scales involved in any climate response resulting from radiation variations require that changes in the earth's albedo should be taken into account which are due to the expansion or reduction of the ice-cover at the surface. The parametric coupling that results between α and T_o provides a strong positive feedback between ice-cover and temperature and we shall see later that it is this empiricism which is responsible for many of the surprising results.

The flux divergence term in Equation (A10.1) is also specified empirically. Budyko derived a relationship which enabled him to represent this term quite simply in terms of the difference between the local zonal mean and the planetary mean temperature, thus

$$\text{div}\, \underset{\sim}{F} = -\beta (T_o - T_p) \qquad \text{(A10.4)}$$

where T_p is the globally averaged, annual mean surface temperature and β is an empirically derived coefficient equal to 0.235 kcal cm^{-2} month^{-1} K^{-1}.

From (A10.1) - (A10.4) we obtain the following equations:

$$T_o = \frac{Q(1-\alpha) - a + a_1 n + \beta T_p}{\beta + B - B_1 n} \qquad \text{(A10.5)}$$

$$T_p = \frac{Q_p(1-\alpha_p) - a + a_1 n}{B - B_1 n} \qquad \text{(A10.6)}$$

where Q_p, α_p are the corresponding planetary values of incident radiation and albedo, respectively. Budyko used these to derive the average latitudinal annual mean temperatures corresponding to present climatic conditions for the Northern Hemisphere. Q and Q_p were computed corresponding to a solar constant of 1.92 cal cm^{-2} min^{-1}. In the calculation, the influence on the temperatures of deviations of cloudiness values from the mean planetary value of 0.50 is neglected.

Based on observational data Budyko chose the following specification of albedo:

$$\alpha = \begin{cases} 0.32 & 0 \leq \varphi \leq 60^\circ \quad (\varphi \text{ is latitude}) \\ 0.50 & \varphi = 70^\circ \\ 0.62 & \varphi = 80^\circ \end{cases}$$

Budyko's calculation of contemporary average latitudinal distribution of temperature is shown in Figure A10.7. The computed values of T_o are in good agreement with the observed values, T, and this encouraged Budyko to use his model to study the effects of variations in the radiation on the Earth's thermal regime and glaciations.

Budyko asserts that the southern boundary of the Arctic ice corresponds to a mean latitude of 72°N and adopts an ice-albedo-temperature coupling such that the ice-cap expands or contracts to coincide with the surface whose temperature is less than or equal to the temperature observed now at 72°N i.e. about -10°C. The -10°C isotherm therefore determines the extent of the ice-covered area which is given an albedo of 0.62 with a discontinuity and drop to 0.50 at its southern boundary. Budyko then computed the zonal mean temperatures and hence the position of the edge of the ice-sheet for effectively different values of the solar constant. The results are shown in Figure A10.8 where the lines $T_{1.0}$ and $T_{1.5}$ correspond to the temperature distributions for a 1% and a 1.5% decrease in the incoming solar radiation. It is assumed that the relative decrease in radiation is the same at all latitudes. Figure A10.9 shows the values obtained for the mean planetary temperature, T_p and the mean latitude to which glaciation extends, φ_o, as a function of the relative radiation changes.

The most striking feature of Figure A10.9 is the implication that only a small per cent (about 1.6%) drop in the solar constant is required for the earth to ice over completely. When radiation decreases by 1.6% the ice-cover reaches the mean latitude of about 50°N after which it starts shifting towards lower latitudes up to the equator as a result of self-development. Simultaneously, T_p drops sharply to values several tens of degrees below zero.

A10·3.3 The model of Sellers (1969)

Sellers' starting point is also the integrated energy-balance equation for the earth-atmosphere system for a given latitude belt. His dependent variable is the average annual sea-level temperature, T_s, in each 10° latitude belt. Again, as in Budyko (1969), several empirical and relatively crude relationships are involved in the model. Using the same definitions and notation as was used above for Budyko's model, the components of Sellers' model can be expressed as follows:

Net terrestrial radiation to space:

$$I = \sigma T_s^4 \left[1 - m \tanh\left(19 T_s^6 \times 10^{-16}\right)\right] \qquad \text{(A10.7)}$$

where σ is the Stefan-Boltzmann constant $(1.356 \times 10^{-12}\ ly\ s^{-1}\ K^{-4})$, and m is an atmospheric attenuation coeffient, taken to be 0.5 for present conditions. Equation (A10.7) is based on an empirical fit to data.

Albedo:

$$\alpha = \begin{cases} b - 0.009\, T_o & T_o < 283.16\text{K} \qquad \text{(A10-8a)} \\ \alpha_d = b - 2.548 & T_o \geqslant 283.16\text{K} \qquad \text{(A10-8b)} \end{cases}$$

with the constraint that $0.25 \leq \alpha \leq 0.85$ for all T_o,

where $T_o = T_s - 0.0065Z$ is the average surface temperature, Z is the average surface elevation in metres, and b is an empirical coefficient. Values of Z and b are tabulated by Sellers for each latitude belt of 10° latitudinal span.

As in Budyko's model, it is assumed that variations in α are associated mainly with variations in surface snow cover and Equation (A10.8a) is valid only as long as $T_o < 10°C$ and $\alpha < 0.85$. The planetary albedo α_d of (A10.8b) is used for higher temperatures i.e. in the absence of snow or ice cover. Equation (A10.8a) implies an increase in α by 0.009 for every 1K drop in T_o. The coefficient b was selected so that the equation would fit observed data. The effects of variations in cloud cover on albedo were ignored.

The flux-divergence term:

Sellers identifies three separate components making up the total net flux of heat out of the belt at a given latitude. They are due to, respectively, the net fluxes of water vapour and sensible heat by the atmospheric circulation and sensible heat by ocean currents.

Let F_o be the meridional sensible heat transport due to ocean currents,
F_A the corresponding sensible heat transport due to atmospheric motion,
and F_q the meridional transport of latent heat energy (q is specific humidity),

then Sellers adopts a parametrization which relates these fluxes to the horizontal mixing by large-scale eddies and to a vertically integrated mean meridional wind $\langle v \rangle$ which, in turn, is parametrized as an empirically determined function of the North-South temperature gradient, thus

$$F_o \propto -K_o \frac{\partial T_s}{\partial y} \qquad \text{(A10. 9a)}$$

$$F_A \propto -K_A \frac{\partial T_s}{\partial y} + \langle v \rangle T_s \qquad \text{(A10. 9b)}$$

$$F_q \propto -K_q \frac{\partial q(T_s)}{\partial y} + \langle v \rangle q(T_s) \qquad \text{(A10. 9c)}$$

where K_o, K_A and K_q are effective eddy diffusion coefficients.

An implicit important assumption here is that average atmospheric temperatures and specific humidities and ocean temperatures are proportional to their respective sea-level values. Further the actual specific humidity is replaced by the saturation specific humidity which enables it to be related to the temperature through the Clausius-Clapeyron relationship (see, for reference, the Mathematical Note of Section A10.2.2b). The poleward transport of water vapour and sensible heat (equations (A10.9b) and (A10.9c)) are assumed to consist of two parts, one associated with a mean meridional motion and the other with large-scale eddies or cyclones and anticyclones. The inclusion of the mean meridional motion is necessary in order to avoid having to deal with negative diffusivities. Values of the K's are tabulated by Sellers at 10° intervals for each latitude circle.

Sellers' system of equations leads to a second-order equation, effectively in T_o , with only one of the roots giving realistic temperatures. The model was first used to reconstruct the present state of the earth-atmosphere system. The reader is referred to Sellers (1969) to verify that the model specifies present conditions very well. Sellers then applied his model to several different problems, two of which are considered here.

a. Modification of the polar ice caps

A number of different combinations of albedo were used, with α at one or both poles (70 - 90°) being set equal to and held fixed at either 0.50 or 0.40 (with the exception of 70 - 80°S where a minimum value of 0.44 was imposed). The results, shown in Figure A10.10, have a number of interesting features, viz,

(1) Cases 1 and 2. Removal of north polar ice results in an increase in temperature poleward of 70°N by at most about 7K. Temperature would rise by about 1K in the tropics and 1-3K near the South Pole.

(2) Cases 3 and 4. Removal of antarctic ice produces a temperature increase there of 12-15K with a rise in the Arctic of about 4K.

(3) Cases 5 and 6. Removal of both polar ice-caps yields temperature increases of 7-10K in the Arctic and 13-17K in the Antarctic. Tropical warming does not exceed 2K.

Therefore albedo changes at either pole have global repercussions. An interesting result, comparing the curves for Cases 1 and 3, is that reducing the albedo south of 70°S to 0.50 would, according to this model, produce a larger temperature rise in the Arctic than would a reduction of the albedo north of 70°N to 0.50. The greater effects of changes to the albedo in the Antarctic than in the Arctic are simply the result of the Antarctic's higher initial albedo. Others have argued that the extent of sea-ice in the Southern Hemisphere has a much more significant effect on the global circulation than the extent of sea-ice in the Northern Hemisphere.

b. Variations in the solar constant

Sellers examined the sensitivity of his models to variations in the solar constant and his calculations corroborate, qualitatively at least, the implications from Budyko's model that a slight reduction in the solar constant (or, for example, increase in global dust contamination) would be sufficient to initiate another ice age. In Figure A10.11 the global mean sea-level temperature, T_{sp} , is plotted as a function of the solar constant, S., currently assumed to be 2.00 ly min^{-1} (cf. Budyko used 1.92 ly min^{-1} as the current value !) The present value of T_{sp} is about 14.0°C. Three analyses were carried out, two with α allowed to vary according to $\alpha = b - 0.009\, T_o$ and $\alpha = b - 0.005\, T_o$, respectively, and the other with α held fixed at its assumed current values. There are no very dramatic events when α is kept fixed at the present values and S allowed to vary. However with a realistic albedo-temperature coupling a decrease of about 2% in the solar constant is sufficient to create another ice-age with ice-caps extending equatorward to 50° (i.e. where $T_o = -10°C$). Any further drop in the solar constant is accompanied in the model by a rapid transition to an ice-covered earth with albedo of 0.85 (cf. Equation (A10.8a)) and an equilibrium temperature of -100°C. With the weaker dependence of α on surface temperature and ice-cover (i.e. 0.005 used in place of 0.009 and b adjusted accordingly) a severe ice-age would not occur until the solar constant decreased by about 5 - 6%.

Sellers also reports a few sensitivity studies where he has kept the solar constant fixed but has increased or decreased the effective diffusion coefficients in his model. He concludes that a relatively small change in the ability of the system to transfer heat poleward could conceivably offset any increase or decrease in the intensity of solar radiation. Hence the obvious caution about allowing only one variable to change without being able to allow for consequent changes in the others. Nevertheless Sellers' model implies quite conclusively that a decrease in the solar constant of less than 5% would be sufficient to start another ice-age.

A10.3.4 The sensitivity of time-dependent Budyko-Sellers type models

Schneider and Gal-Chen (1973) examined the sensitivity of time-dependent models of the Budyko-Sellers type to changes in initial as well as external conditions. The problem is then formulated as an initial value problem in which the basic equations are integrated from a given initial state until a final asymptotic equilibrium state is obtained.

The time-dependent version of the zonally averaged, vertically integrated heat balance equation for the earth-atmosphere system is

$$C \frac{\partial T_0}{\partial t} = R + \mathrm{div}\, \underset{\sim}{F} \qquad (A10.10)$$

where C is a prescribed thermal inertia coefficient for a zonal column through the land-ocean-atmosphere system. R is defined as in Equation (A10.2) with I the net infra-red cooling to space given by

$$I = c(\varphi)\, \sigma T_0^4 \left[1 - m \tanh\left(19 T_0^6 \times 10^{-16}\right)\right] \qquad (A10.11)$$

with $m = 0.5$. Note that with $c(\varphi) = 1$ (and ignoring the distinction between T_0 and T_s) this formula is identical to that used by Sellers (1969). Scheider and Gal-Chen claim to be using the zonally averaged 1000-mb temperature which has been written here as T_0, the notation used previously for the surface temperature. Their numerical scheme requires that the 'consistency factor' $c(\varphi)$ be adjustable over a small range of values close to unity.

Schneider and Gal-Chen examined four different versions of the model, defined by different formulations of $\mathrm{div}\, \underset{\sim}{F}$ and α.

(1) Labelled (S), is the formulation of Sellers (1969) with respect to $\mathrm{div}\, \underset{\sim}{F}$ and α.

(2) Labelled (SV), is exactly as (S) but with $\langle v \rangle \equiv 0$.

(3) Labelled (B), uses α as defined in (S) but has the Budyko (1969) formulation for $\mathrm{div}\, \underset{\sim}{F}$ as in Equation (A10.4).

(4) Labelled (FG), is as (S) with respect to $\mathrm{div}\, \underset{\sim}{F}$ but uses a formulation for α attributed to Faegre (1972) such that

$$\alpha = 0.4860 - 0.0092\,(T_0 - 273)$$

$$0.25 \leq \alpha \leq 0.85 \qquad \text{for all values of } T_0$$

ie. α is a function of temperature everywhere.

The asymptotic equilibrium climate from the time-dependent version was shown to exhibit the same sensitivity to small changes in the solar constant as experienced with the steady-state models. Figure A10.12 shows the results of Schneider and Gal-Chen for their version (S) of the Sellers (1969) approach. Again with a decrease in solar constant of more than 1.6% a planetary mean temperature of 174.65K was obtained corresponding to an entirely ice-covered earth. Calculations for a 1% decrease in solar constant and Sellers-type energy fluxes with, (S), or without, (SV), mean meridional motion gave quite similar results both in the global average amount of temperature decrease and in the latitudinal distribution of the temperature decrease. The results for the Budyko parametrization, (B), are qualitatively similar to those of (S) and (SV) for the global average. However the corresponding latitudinal distribution of temperature decrease differs significantly from that of Sellers. The particular form used for div F does appear to be significant for determining the details of the latitudinal distribution of temperature.

The stability of the (B) and (S) solutions to various perturbations of the initial temperatures were examined and the results are summarised in Table A10. 5. It was found in both cases that the respective steady-state control climates could be recovered exactly if the temperature perturbation was positive. Perturbations of 2K and 16K were tried and in both energy-balance requirements alone produced a return to the control climate ie. the control climates appear to be unique, fully stable and transitive. For an initial temperature decrease of magnitude not exceeding 18.3K the apparent slight intransitivity in the equilibrium climates has been attributed to computer rounding errors. The models then show that the asymptotic equilibrium climate is extremely insensitive to changes in the initial conditions. However for initial temperature decreases greater than about -18.3K both models lead to an ice-covered earth solution similar to curve D in Figure A10.12. Thus it takes a very large negative perturbation to the initial temperatures to lead to the highly intransitive alternative ice-covered earth regime of these models. The insensitivity of the model to decreases in the initial temperature conditions of less than 18K follows from an unchanged albedo in equatorial latitudes.

Initial Temperature Perturbation (K)	Mean Planetary Temperature (K)	
	Sellers (S)	Budyko (B)
0	287.06	287.09
$0 < P < 16$ for all φ	287.06	287.09
$-18.3 < P \leq 0$ for all φ	286.67	286.87
$P < -18.3$ for all φ	175.58	175.44
-22 for $\lvert\varphi\rvert \geq 20^\circ$ 0 for $\lvert\varphi\rvert < 20^\circ$	286.67	286.87

Table A10.5. Asymptotic steady-state global average temperatures resulting from various perturbations to the initial temperature distributions for two of Schneider and Gal-Chen's (1973) parametrizations. This table is taken from the review of climate modelling by Schneider and Dickinson (1974).

The implication from these experiments is that even when ice-cover exists down to temperate latitudes, if the solar constant and the tropical albedos are unaltered then there is still sufficient energy available to the tropics to provide a poleward heat transport to melt the ice and restore the equilibrium climate to near the present-day value. If the equatorial temperature is reduced into the range of the positive feedback temperature-albedo coupling then climate instability is triggered, and an ice-covered earth results. This hypothesis was tested (see Table A10.5) by introducing a very large negative perturbation in the initial temperatures, viz. -22K, for all $|\varphi| \geqslant 20^\circ$ only. In both models there was a return to near the present-day climate.

The model, (FG), which adopts Faegre's (1972) formulation for α is very sensitive to negative perturbations in both solar constant and initial conditions. The interpretation is that, with the temperature-albedo coupling for all temperatures and at all latitudes, a slight negative perturbation in either initial temperature or solar constant can cause a decrease in energy input to the tropics thereby enhancing the albedo-temperature positive feedback at all latitudes. Experiments with such energy-balance models suggest that the stability of the climate may be quite dependent on the functional relationship between the albedo and the surface temperature.

A10-3.5 Multiple solutions and their stability

We have seen from the numerical perturbation studies of Schneider and Gal-Chen (1973) that more than one solution is admissable in the Budyko-Sellers models with the present value of the solar constant ie. the system appears to be intransitive. North (1975) studied the latitude of the ice-line as a function of the solar constant by using a model, described as intermediate between that of Budyko and that of Sellers, which yielded exact analytical solutions. His results, summarised in Figure A10.13, show a multiplicity of solutions for the present-day value of the solar constant; indeed, there are no less than five solutions for the present value of the solar constant! Other studies with models of this type, but with different formulations for the individual terms, give results qualitatively similar to these. Lowering the solar constant by a few per cent leads to a catastrophic plunge to an ice-covered planet but more than a 30% increase is needed to yield an ice-free earth as the only solution.

North (1975) performed a linear stability analysis about the equilibrium solutions on branches I, II and III and confirmed that the present climate (I) and the ice-covered earth (III) solutions are stable (shown numerically by Schneider and Gal-Chen (1973)) while the intermediate solution (II) with the earth about two-thirds covered with ice is unstable and therefore of no physical significance.

Several other authors, including Held and Suarez (1974), Su and Hsieh (1976), Ghil (1976), Drazin and Griffel (1977), North (1977) and Cahalan and North (1978), have established a general stability theorem applicable to a wide variety of specific models within the general class. The slope stability theorem states that

$$\frac{dx_s}{ds} > 0 \quad \Longrightarrow \quad \text{Stability},$$

$$\frac{dx_s}{ds} < 0 \quad \Longrightarrow \quad \text{Instability},$$

where x_s is the sine of the latitude of the ice-line.

The validity of this theorem for a large class of models is important, since it has implications for those branches of the solutions nearest to that corresponding to the present climate, viz. they are unstable and therefore unphysical. Their instability also explains why they were not located by the earlier approaches of Budyko, Sellers and Schneider and Gal-Chen.

One interesting point is that the slope stability theorem implies that if a cusp near $x_s = 1$ exists in a model solution (as, for example, in Figure A10.13) then small ice-caps are unstable. However the existence of such a cusp appears to depend very crucially on the details of the parametrizations adopted. Budyko-Sellers type models may be too simple to examine such a point. This is unfortunate since whether small ice-caps are stable or not is an important issue if one recalls the concern over rising levels of CO_2 in the atmosphere and the possible effects of melting ice on the sea-level.

A10.3.6 Further studies with Budyko-Sellers type models

The basic concept of the Budyko-Sellers type models has been extended and made more realistic and much more complicated in a great variety of ways. The comprehensive review by Schneider and Dickinson (1974) and the more recent reviews by North (1979), North et al (1980) and Hunt (1980) are recommended as sources for further study.

REFERENCES TO APPENDIX

BUDYKO, M I (1969) The effect of solar radiation variations on the climate of the Earth. Tellus, 21, 611-619.

CAHALAN, R F and NORTH G R (1978) A stability theorem for energy-balance climate models. J. Atm. Sci., 36, 1178-1188.

DRAZIN, P G and GRIFFEL, D H (1977) On the branching structure of diffusive climatological models. J. Atm. Sci., 34, 1696-1706.

FAEGRE, A (1972) An intransitive model of the earth-atmosphere-ocean system. J. Appl. Meteorol., 11, 4-6.

GHIL, M (1976) Climate stability for a Sellers-type model. J. Atm. Sci., 33, 3-20.

HELD, I M and SUAREZ, M J (1974) Simple albedo feedback models of the ice caps. Tellus, 26, 613-629.

HERRING, W S and BORDEN, T R Jr. (1965) Mean distributions of ozone density over North America, 1963-1964. Environmental Research Papers, No. 162, AFCRL-65-913, Air Force Cambridge Research Laboratories, Bedford, Mass., 19 pp.

HUNT, B G (1980) Numerical modelling of climate. Aust. J. Phys., 33, 897-910.

LONDON, J (1962) Mesospheric dynamics, Part III. Final Report, Contract No. AF19(604)-5492, Dept. of Meteorology and Oceanography, New York Univ., 99 pp.

LORENZ, E N (1968) Climatic determinism. Meteorol. Monogr., 5, 1-3.

LORENZ, E N (1970) Climatic change as a mathematical problem. J. Appl. Meteorol., 9, 325-329.

LORENZ, E N (1975) Climate predictability. Report of the Intl. Study. Conf. on the Physical Basis of Climate and Climate Modelling, App. 2.1, pp 132-136, GARP Publications Series No. 16, WMO-ICSU.

MANABE, S and STOUFFER, R J (1980) Sensitivity of a global climate model to an increase of CO_2 concentration in the atmosphere. J. Geophys Res., 85, 5529-5554.

MANABE, S and STRICKLER, R F (1964) Thermal equilibrium of the atmosphere with a convective adjustment. J. Atm. Sci., 21, 361-385.

MANABE, S and WETHERALD, R T (1967) Thermal equilibrium of the atmosphere with a given distribution of relative humidity. J. Atm. Sci., 24, 241-259.

MANABE, S and WETHERALD, R T (1975) The effects of doubling the CO_2 concentration on the climate of a general circulation model. J. Atm. Sci., 32, 3-15.

MANABE, S and WETHERALD, R T (1980) On the distribution of climate change resulting from an increase in CO_2 content of the atmsophere. J. Atm. Sci., 37, 99-118.

MASTENBROOK, H J (1963) Frost-point hygrometer measurement in the stratosphere and the problem of moistue contamination. Humidity and Moisture, Vol. 2, New York, Reinhold Publ. Co., pp 480-485.

MITCHELL, J F B (1981) The seasonal response of a general circulation model to changes in CO_2 and sea temperatures. Unpublished Met Office Report, Met O 20 Tech. Note No. II/171.

MURGATROYD, R J (1960) Some recent measurements by aircraft of humidity up to 50,000 ft in the tropics and their relationship to meridional circulation. Proc. Symp. Atmos. Ozone, Oxford, 20-25 July 1959, IUGG Monogr. No. 3, Paris, p.30.

NORTH, G R (1975) Analytical solution to a simple climate model with diffusive heat transport. J. Atm. Sci., 32, 1301-1307.

NORTH, G R (1977) Analytical models of the earth's macroclimate. Proc. First. Intl. Conf. on Mathematical Modelling, Vol. IV, Univ. of Missouri, Rolla, Missouri, pp 2291-2302.

NORTH, G R (1979) Recent work on heat balance models. Report on the JOC Study Conference on Climate Models: Performance, Intercomparison and Sensitivity Studies, Vol II, 752-765, GARP Publications Series No. 22, WMO-ICSU.

NORTH, G R, CAHALAN, R F and COAKLEY, J A (1980) Energy-balance climate models. Washington, NASA, Tech. Memo. 82047.

RAMANATHAN, V and COAKLEY, J A (1978) Climate modelling through radiative-convective models. Rev. Geophys. Space Phys., 16, 465-489.

SCHNEIDER, S H and DICKINSON, R E (1974) Climate modelling. Rev. Geophys. Space Phys., 12, 447-493.

SCHNEIDER, S H and GAL-CHEN, T (1973) Numerical experiments in climate. J. Geophys. Res., 78, 6182-6194.

SELLERS, W D (1969) A global climatic model based on the nergy balance of the earth-atmosphere system. J. Appl. Meteorol., 8, 392-400.

SLINGO, A (1982) Introduction and radiative heat balance. Lecture on The General Circulation of the Atmosphere, Lecture Notes, Met O 20.

SU, C H and HSIEH, D Y (1976) Stability of the Budyko climate model. J. Atm. Sci., 33, 2273-2275.

TELEGADAS, K and LONDON, J (1954) A physical model of Northern Hemisphere troposphere for winter and summer. Sci. Rep. No. 1, Contract AF19(122)-165, Research, Div., College of Engineering, New York Univ., 55 pp.

WMO (1979) World Climate Conference. A Conference of Experts on Climate and Mankind, Geneva, Feb 1979, WMO.

WMO (1980) Outline Plan and Basis for the World Climate Programme, 1980-1983. WMO-No. 540.

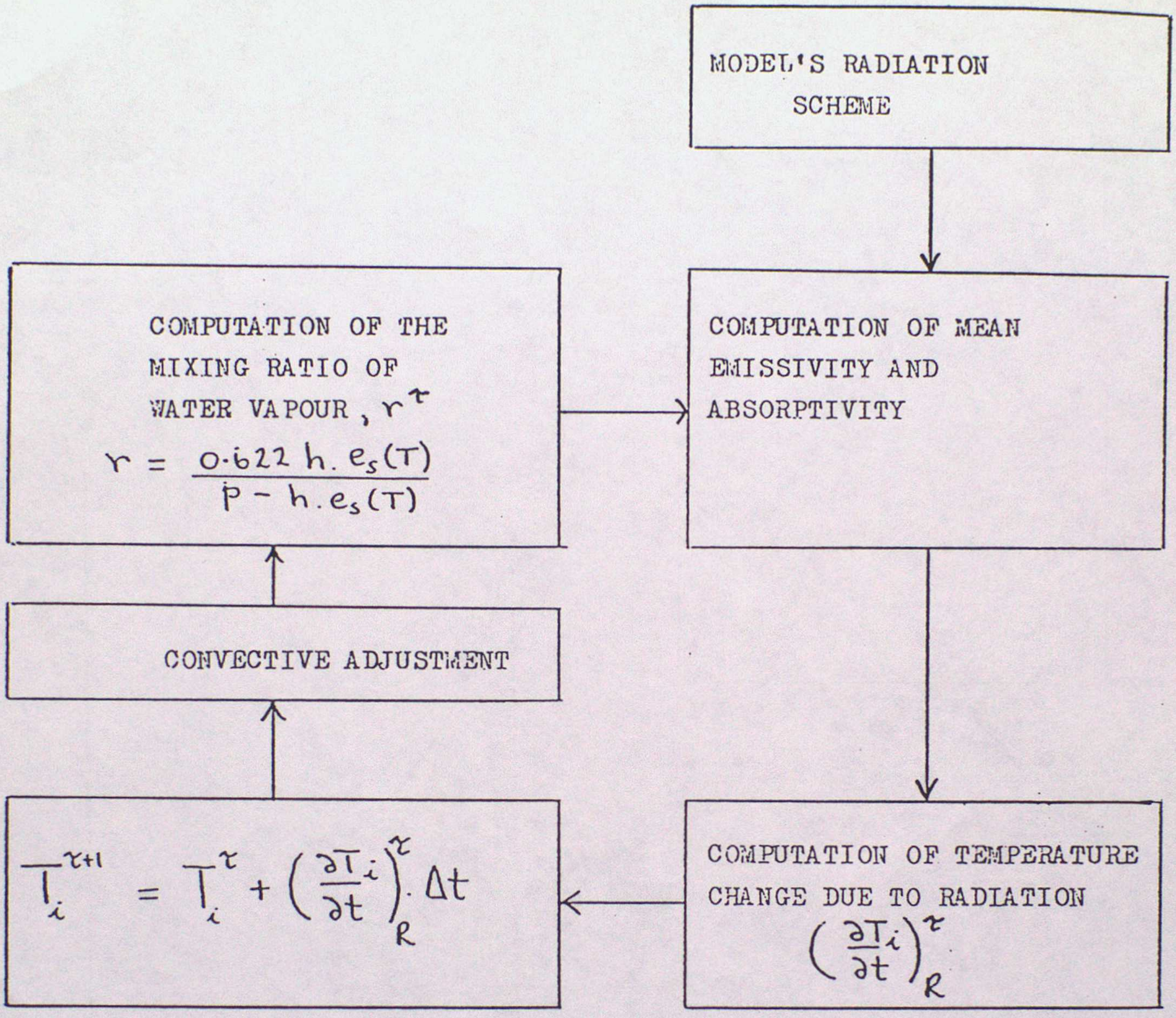
MODEL'S RADIATION SCHEME
COMPUTATION OF MEAN EMISSIVITY AND ABSORPTIVITY
COMPUTATION OF TEMPERATURE CHANGE DUE TO RADIATION $\left(\frac{\partial T_i}{\partial t}\right)_R^{\tau}$
$T_i^{\tau+1} = T_i^{\tau} + \left(\frac{\partial T_i}{\partial t}\right)_R^{\tau} \cdot \Delta t$
CONVECTIVE ADJUSTMENT
COMPUTATION OF THE MIXING RATIO OF WATER VAPOUR, r^{τ}
$r = \frac{0.622\, h.\, e_s(T)}{p - h.\, e_s(T)}$

Figure A10.1.

Schematic representation of the iterative procedure used to obtain the state of radiative-convective equilibrium, as described by Manabe and Wetherald (1967).
τ is the number of the time-step of the numerical integration.
i is the index for the finite-differencing in the vertical.

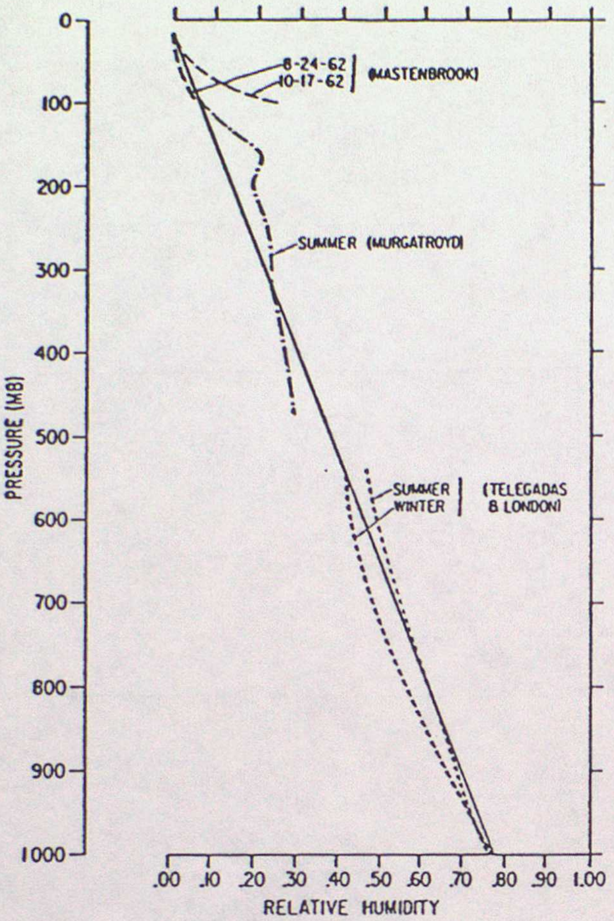

. Vertical distribution of relative humidity (Mastenbrook, 1963; Murgatroyd, 1960; Telegadas and London, 1954).

Figure A10.2.

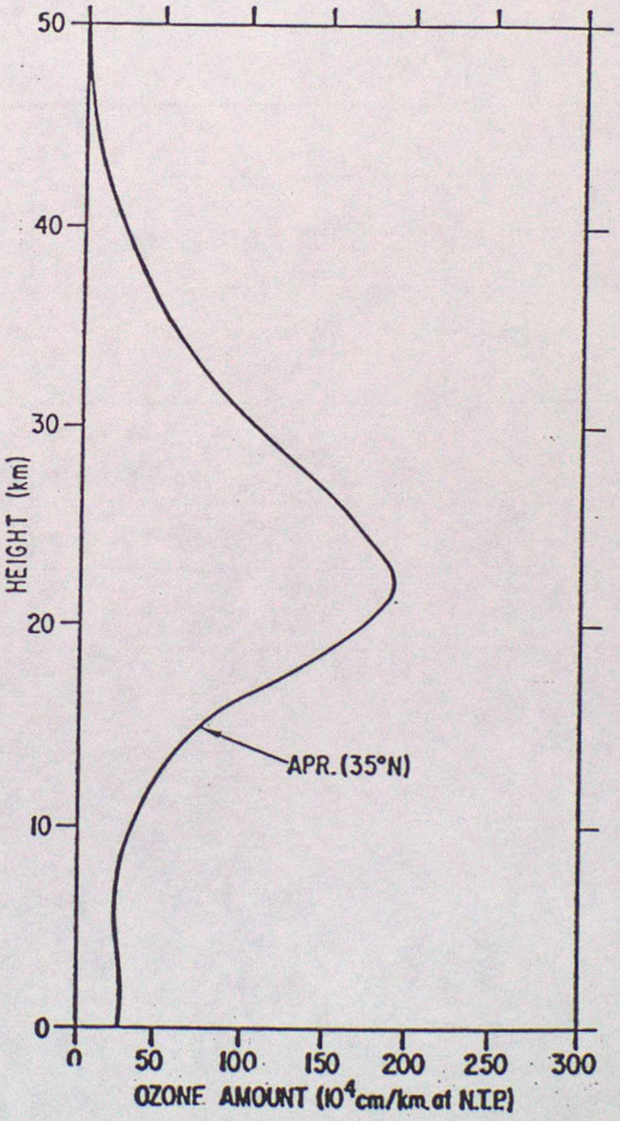

Vertical distribution of ozone at 35N, April (Herring and Borden, 1965), normalized by the total amount from London (1962).

Figure A10.3.

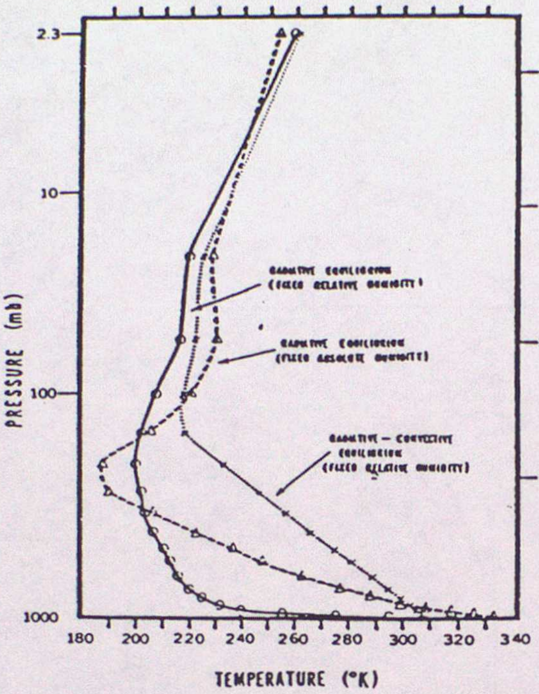

Solid line, radiative equilibrium of the clear atmosphere with the given distribution of relative humidity; dashed line, radiative equilibrium of the clear atmosphere with the given distribution of absolute humidity; dotted line, radiative convective equilibrium of the atmosphere with the given distribution of relative humidity.

Figure A10.4.

From Manabe and Wetherald(1967).

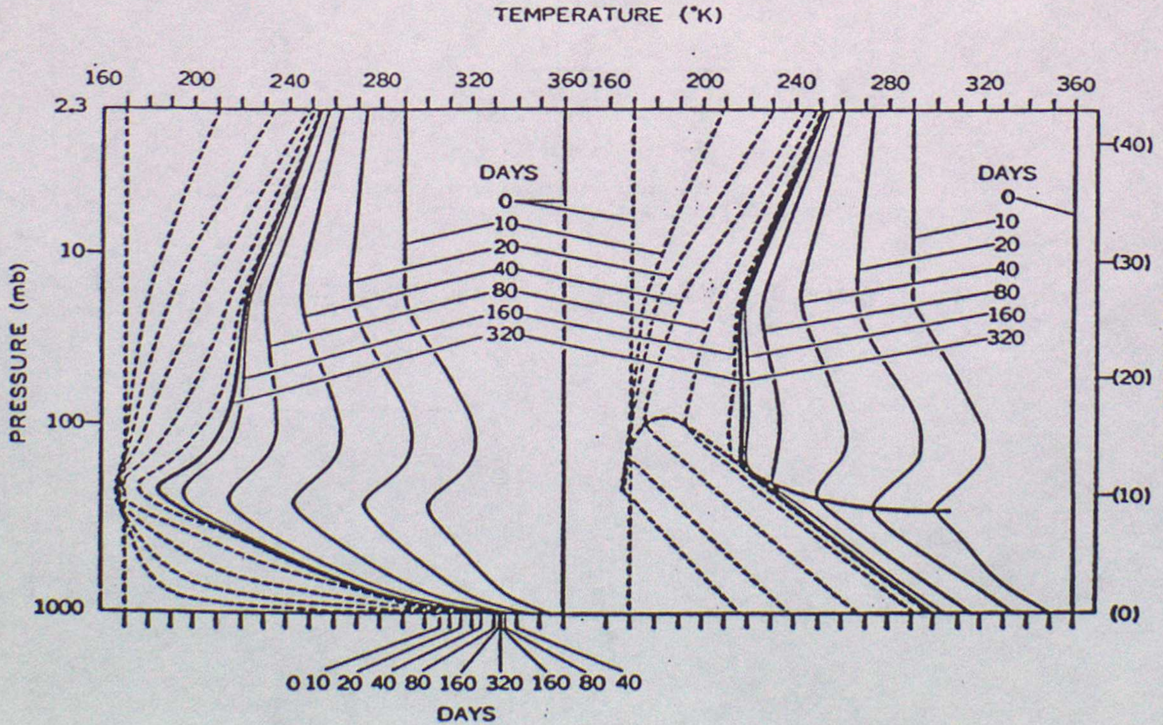

The left and right hand sides of the figure, respectively, show the approach to states of pure radiative and thermal equilibrium. The solid and dashed lines show the approach from a warm and cold isothermal atmosphere.

Figure A10.5.

From Manabe and Strickler (1964).

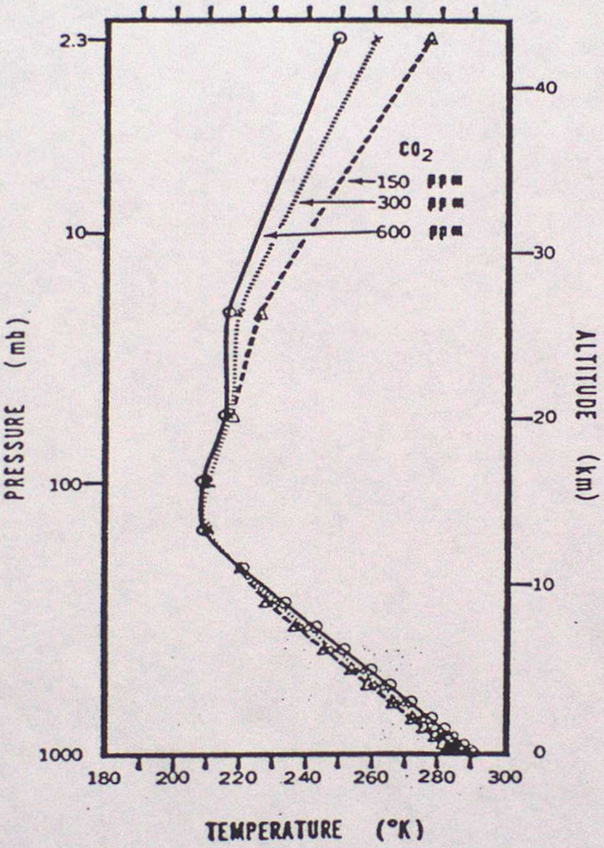

Vertical distributions of temperature in radiative convective equilibrium for various values of CO_2 content.

Figure A10.6. From Manabe and Wetherald (1967).

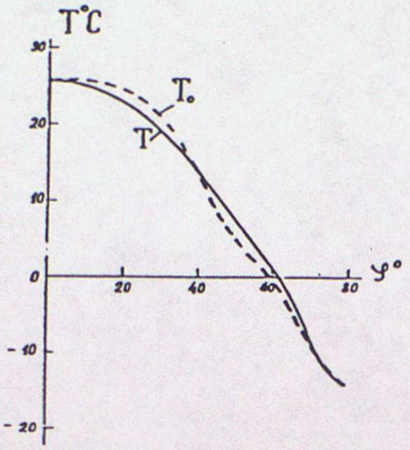

The average latitudinal temperature distribution.

Figure A10.7.
From Budyko(1969).

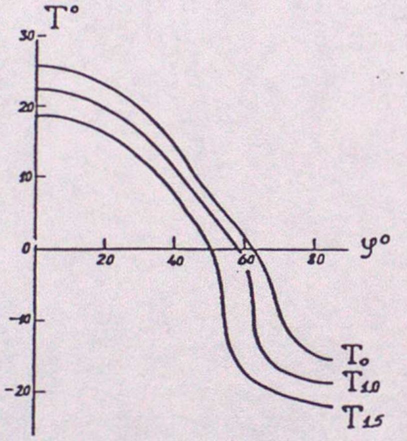

The dependence of temperature distribution on radiation amount.

Figure A10.8.
From Budyko(1969).

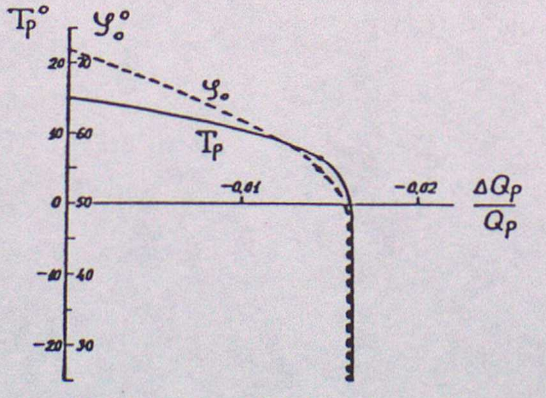

The dependence of the Earth's temperature and ice cover boundary on radiation variations.

Figure A10.9.
From Budyko(1969).

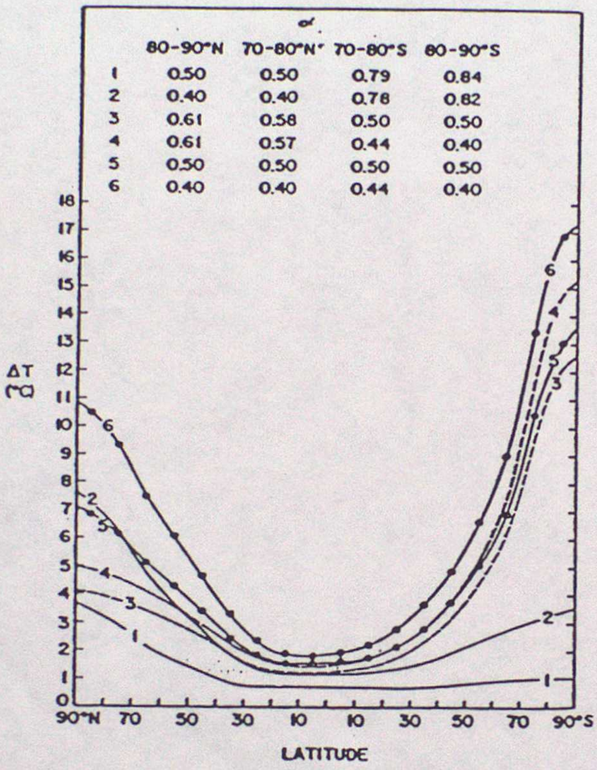

	α			
	80-90°N	70-80°N	70-80°S	80-90°S
1	0.50	0.50	0.79	0.84
2	0.40	0.40	0.78	0.82
3	0.61	0.58	0.50	0.50
4	0.61	0.57	0.44	0.40
5	0.50	0.50	0.50	0.50
6	0.40	0.40	0.44	0.40

Predicted latitudinal distribution of the mean annual temperature rise associated with albedo manipulation at one or both poles.

Figure A10.10. From Sellers(1969).

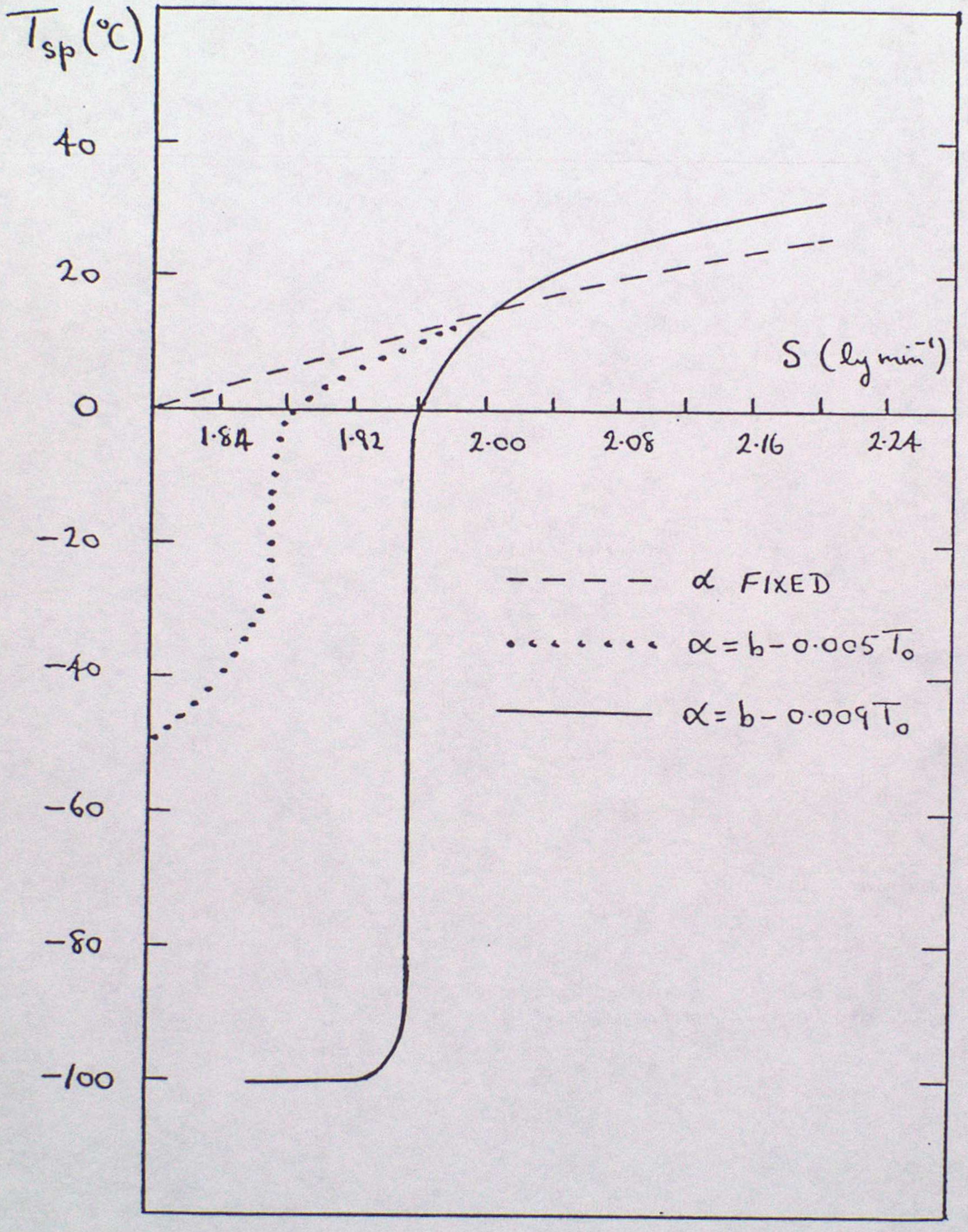

Figure A10.11. The mean global sea level temperature, T_{sp}, as a function of the solar constant, S, for different specifications of the planetary albedo, α. This figure is based on the results of Sellers(1969).

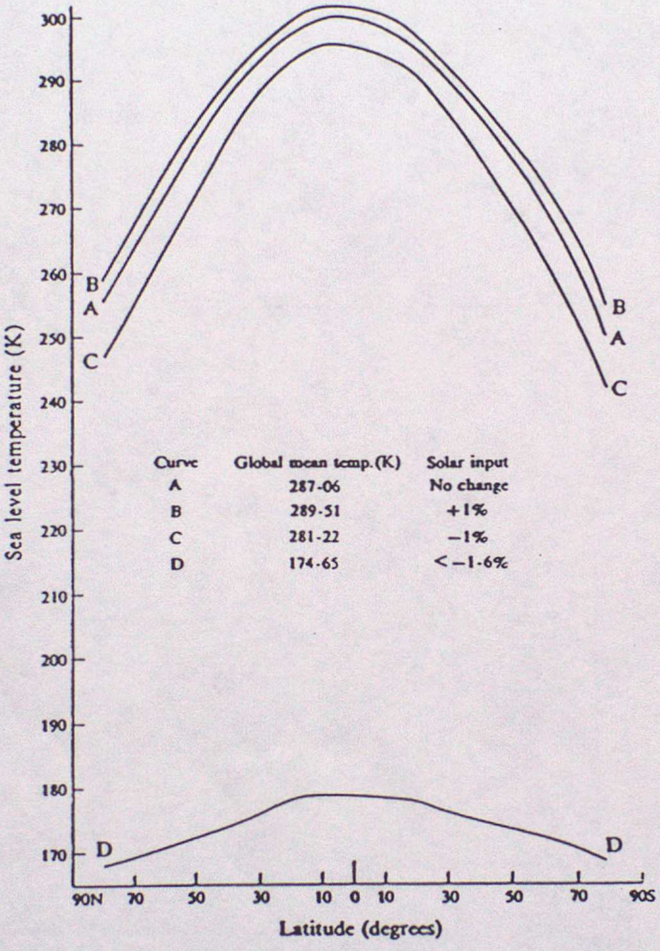

Curve	Global mean temp. (K)	Solar input
A	287·06	No change
B	289·51	+1%
C	281·22	−1%
D	174·65	< −1·6%

Latitudinal temperature distribution calculated for various solar constant values. [From Schneider and Gal-Chen (1973).]

Figure A10.12.

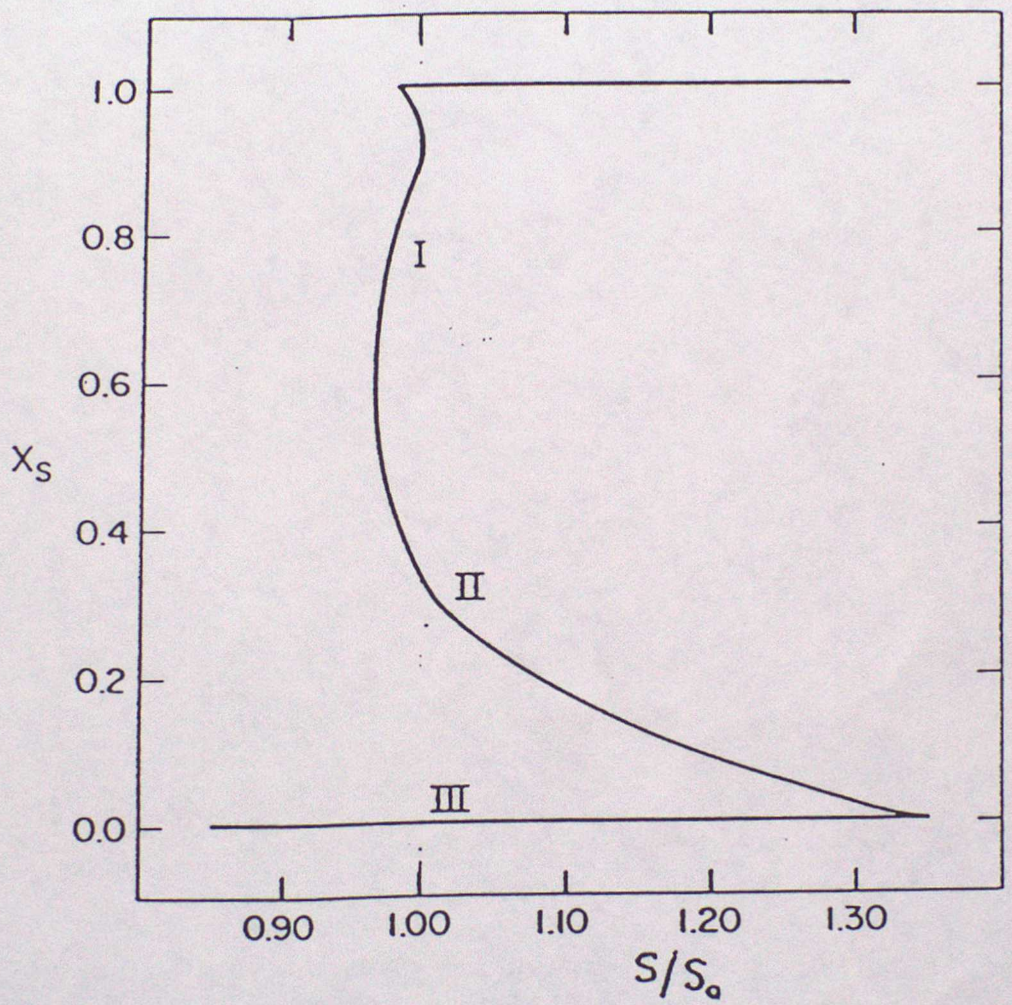

Figure A10.13. A typical plot of the sine of the latitude of the ice line (X_S) versus the solar constant S/S_o normalized to its present value. This curve is for an exact solution of a model with constant diffusion coefficient and discontinuous albedo at the ice line.

This figure is taken from North(1975).